U.S. DEPARTMENT OF COMMERCE
National Technical Information Service
PB-281 596

Annual Report of Contract Research for the Metallurgy and Materials Research Branch, Division of Reactor Safety Research, Fiscal Year 1977

Nuclear Regulatory Commission, Washington, D.C.

May 78

7908170452

815 001

PB 281 596
NUREG-0351

ANNUAL REPORT OF CONTRACT RESEARCH FOR THE METALLURGY AND MATERIALS RESEARCH BRANCH, DIVISION OF REACTOR SAFETY RESEARCH, FISCAL YEAR 1977

Office of Nuclear Regulatory Research
U. S. Nuclear Regulatory Commission

815 002

NRC FORM 335 (7-77) U.S. NUCLEAR REGULATORY COMMISSION

BIBLIOGRAPHIC DATA SHEET

1. REPORT NUMBER (Assigned by DDC)	NUREG-0351
4. TITLE AND SUBTITLE (Add Volume No., if appropriate)	Annual Report of Contract Research for the Metallurgy & Materials Research Branch, Division of Reactor Safety Research, Fiscal Year 1977
2. (Leave blank)	
3. RECIPIENT'S ACCESSION NO.	PB281596
7. AUTHOR(S)	None
5. DATE REPORT COMPLETED	MONTH April / YEAR 1978
9. PERFORMING ORGANIZATION NAME AND MAILING ADDRESS (Include Zip Code)	Contractors of Metallurgy & Materials Research Branch
DATE REPORT ISSUED	MONTH April / YEAR 1978
6. (Leave blank)	
8. (Leave blank)	
12. SPONSORING ORGANIZATION NAME AND MAILING ADDRESS (Include Zip Code)	Metallurgy & Materials Research Branch Division of Reactor Safety Research U.S.N.R.C. Washington, D.C. 20555
10. PROJECT/TASK/WORK UNIT NO.	
11. CONTRACT NO.	
13. TYPE OF REPORT	Annual Report
PERIOD COVERED (Inclusive dates)	FY 1977
15. SUPPLEMENTARY NOTES	
14. (Leave blank)	

16. ABSTRACT (200 words or less)

Annual Report of Contract Research for the Metallurgy & Materials Research Branch, Division of Reactor Safety Research, Fiscal Year 1977.

17. KEY WORDS AND DOCUMENT ANALYSIS	17a. DESCRIPTORS
17b. IDENTIFIERS/OPEN-ENDED TERMS	

18. AVAILABILITY STATEMENT	19. SECURITY CLASS (This report)	21. NO. OF PAGES
Open	unclassified	357
	20. SECURITY CLASS (This page)	22. PRICE
	unclassified	A16- A01

NRC FORM 335 (7-77)

815 003

NUREG-0351

ANNUAL REPORT OF CONTRACT RESEARCH FOR THE METALLURGY AND MATERIALS RESEARCH BRANCH, DIVISION OF REACTOR SAFETY RESEARCH, FISCAL YEAR 1977

Manuscript Completed: April 1978
Date Published: May 1978

Division of Reactor Safety Research
Office of Nuclear Regulatory Research
U. S. Nuclear Regulatory Commission
Washington, D. C. 20555

1a'

815 004

TABLE OF CONTENTS

FY 1977 ANNUAL REPORT OF CONTRACT RESEARCH
METALLURGY & MATERIALS RESEARCH BRANCH

815 005

815 006

HEAVY-SECTION STEEL TECHNOLOGY PROGRAM

Oak Ridge National Laboratory
Oak Ridge, Tennessee 37830

G. D. Whitman

OBJECTIVE

The Heavy-Section Steel Technology Program is providing data which are used in the prediction of thick-section vessel fracture characteristics to include a realistic evaluation of the fracture potential and the development of fracture prevention criteria. Flaw growth mechanisms, crack propagation and arrest including the effects of irradiation in both design and accident loading conditions are being considered. The significance of cracks residing in weld repair regions and in low shelf toughness material are being quantified. The program includes tests on pressure vessels and specimens up to 152 mm (6 in.) thick. Results from these efforts contribute to the needs of regulatory and safety bodies, code writing bodies, and the nuclear power industry.

FY 77 SCOPE

Three-dimensional photoelastic studies were performed on nozzle corner flaws to obtain data from models which represented BWR feedwater nozzle geometry. A report was issued summarizing the results of the two intermediate vessels tested with nozzle corner flaws. Data were generated on fatigue crack growth of pressure vessel steels in water reactor environment to study rise time and hold time effects to provide input for establishing ASME Section XI code rules. Irradiations were completed in a second 4T-CT project to irradiate weld metal having a low upper shelf Charpy energy fracture toughness. Methods for obtaining ductile fracture toughness of these irradiated specimens continued to be developed and evaluated. A third 4T-CT irradiation series again incorporating specimens made from low upper shelf weld metal was encapsulated for insertion in the Bulk Shielding Reactor at ORNL. The evaluation of the half-bead inservice weld repair method was expanded to include two additional simulated repairs in intermediate vessels V-7B and V-8. Extensive studies were made on residual stress and material properties of half-bead weld repair weldments and intermediate vessel V-7B was tested. Three crack arrest models were fabricated and tested over a range of fracture modes to evaluate the feasibility of performing thick-section structural tests. A fourth thermal shock experiment was performed to successfully demonstrate the applicability of LEFM in cracked sections of reactor vessel geometry under thermal shock loads. A report was issued on the significance of reheat cracks on pressure vessel integrity. An analysis-before-test document was issued on the potential corrosion problems in PCRV tendons. Foreign research reports and programs were identified to determine their applicability to NRC interests and needs.

1. FRACTURE MECHANICS AND ANALYSES

The determination of stress intensity factors (SIF) for flaws located at pressure vessel nozzle corners has been a problem for many years due to the complex and widely varying geometries involved. As a result of the degree of analytical intractability of the problem and the need for additional experimental correlation of approximate analytical methods, three-dimensional photoelastic analysis of flawed models was initiated approximately two years ago.*

Having verified the Derby[1] residual static strength technique, the photoelastic technique entered a second phase to obtain data on the feedwater nozzle geometry of a typical boiling water reactor (BWR) vessel. Models were constructed with two nozzles located at diametrically opposite positions in each model. Starter cracks were introduced into the inner surface of the juncture of the vessel wall and nozzle. The vessels were heated to a critical temperature then pressurized to cause the flaws to grow to desired dimensions. The models were cooled, freezing in the deformation fields, and then sliced for optical analysis.

The results shown in Fig. 1.1 have the same trends as the earlier results and indicate that for flaws enveloping the inner nozzle fillet, the maximum SIF occurs near the center of the flaw border for moderate to deep flaws. For

---

*Work sponsored by HSST Program under UCCND Subcontract 7015 between Union Carbide Corporation and Virginia Polytechnic Institute and State University.

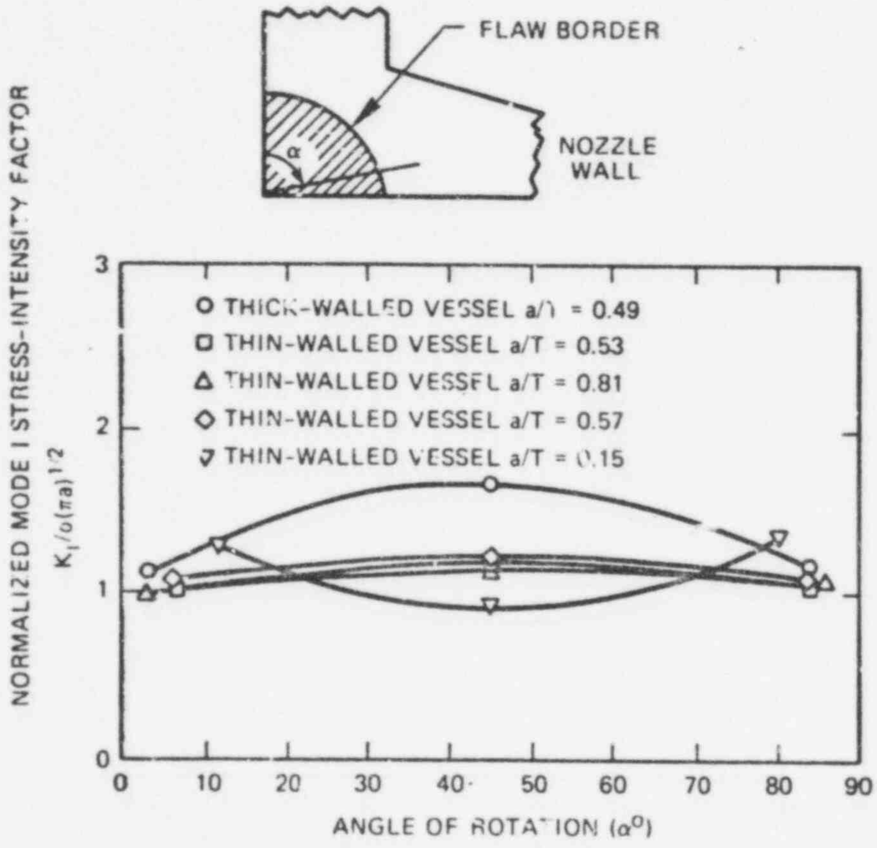

Fig. 1.1. Stress intensity factors for nozzle corner flaws.

small flaws for which the flaw border is contained within the inner fillet radius, the flaw shape is different from the deep flaws and the SIF distribution peaks near the vessel surfaces. The results imply that very small flaws are quite different from those large enough to have grown away from the inner fillet and the variation in SIF around the flaw tip may be significant. These results also indicate that the data obtained on HSST vessel tests are conservative (larger shape factors) relative to actual light water reactor pressure vessels.

A report[2] was issued summarizing the results of intermediate test vessels V-5 and V-9 with inside nozzle corner cracks. Numerous pretest and posttest fracture analyses were made for both vessels. All the estimated nozzle corner strains at failure were low (most by a wide margin), especially those based on LEFM and the assumption of full transverse restraint. The two most accurate estimates avoided assuming a plane strain constraint condition along the leading edge of the flaw, a condition that experimental strain data imply does not exist for a crack at the inside nozzle corner. Subsequent calculations made by both the method of LEFM based on strain and the tangent modulus method, using the Irwin β_{Ic} correction to estimate the increase in the effective fracture toughness due to less than full transverse restraint, provided estimates of fracture toughness that agreed well with the pretest measured values. Two simple empirical equations were found to fit the measured inside nozzle corner pressure-strain curves quite accurately. Both equations were based on the estimated value of the elastic stress concentration factor and the cylinder gross yield pressure. The report contains detailed tabulations and plots of material property, small model and test vessel strain data, and discussions of acoustic emission results.

2. FATIGUE CRACK GROWTH STUDIES

Data are being generated to characterize the fatigue crack growth rates of ferritic vessel steels exposed to light water reactor coolant environments.* Five environmental chambers continue to be used to obtain these data.

---

*Work sponsored by the HSST Program under UCCND Subcontract 3290 between Union Carbide Corporation and Westinghouse Electric Corporation.

Testing has continued to study ramp and hold time effects using trapezoidal loading forms as summarized in Table 2.1. A principal objective of the tests in this matrix which are being performed cooperatively with the Naval Research Laboratory is to determine whether or not hold time has a significant effect on crack growth rates, an important question since reactor vessel operational loadings often involve such hold times. It is also of interest to determine if crack growth rates obtained with trapezoidal loading forms are equivalent to those from sinusoidal loading forms which have been used to generate most of the previously available data. Series "a" tests have been completed and series "b" tests are nearing completion.

Table 2.1. Projected ramp and hold time tests of 2T-WOL specimens in PWR environment, A508 class 2 forging material

Test	Ramp time (min)	Hold time (min)	Crack growth (mm)
2a1	Rapid	1	10
2a2	Rapid	3	10
2a3	Rapid	6	10
2a4	Rapid	12	10
2b1	1	1	10
2b2	1	3	10
2b3	1	4	10
2b4	1	12	10
2c1	5	1	10
2c2	5	3	10
2c3	5	6	10
2c4	5	12	10

The results of the "a" series as previously reported showed that hold time had no significant effect on crack growth rate. Also, data generated in a low pressure, 0.14 MPa (20 psi), low temperature, 93°C (200°F) chamber agreed very closely with the data for a PWR water environment of 14 MPa (2000 psi) and 288°C (550°F). Unfortunately the results of these tests need further evaluation pending concerns over the potential effect of starting ΔK on crack growth behavior. All of the tests were performed with initial ΔK values greater than 30 MPa $\sqrt{m}$ (27 ksi $\sqrt{in.}$) which was equivalent to the initial loading of a 4T-CT specimen test designed to study crack growth rates at higher ΔK values. Results of this first large specimen test revealed a surprising behavior as shown in Fig. 2.1. The crack growth rate was found to be significantly lower than the data produced on smaller specimens at similar R ratio [illegible] clic frequency. This behavior appears to be caused by the high value of the initially applied ΔK. Further testing is now being performed with another 4T-CT specimen under identical conditions except for a lower starting ΔK to see if the earlier small specimen data which were developed with lower starting ΔKs can be reproduced.

The most likely locations for cracks to be produced during the manufacture of a reactor pressure vessel are in the weld region. It is thus very important to characterize the fatigue crack growth rate properties of weldments which typify vessel construction. Tests have been performed on 2T-WOL specimens made from production submerged arc weldments of A533B class 1 plate material. Data that have been developed for R ratios of 0.2 and frequencies between 1 and 5 cpm on four specimens show similar behavior. There are a number of small reversals in crack growth rate while the general upward trend continues as ΔK increases. However, the growth rates are equal to or generally less than those obtained in plate material tested under similar conditions. A fifth weld specimen is still under test to obtain data at an R ratio of 0.7.

For constant amplitude sinusoidally applied loading it is well known that crack growth rates increase as the test frequency is decreased. Tests have been conducted at frequencies of 5, 1, 0.5 and 0.1 cpm, and indicate that the maximum growth rate appears to occur in the 0.5 to 1 cpm range with specimens tested at an R ratio of 0.2. Similar behavior occurs for higher R ratios, as evidenced by a series of tests conducted at an R ratio of 0.7. Further evidence of this saturation effect in crack growth rate is provided by results

ORNL-DWG 77 18090

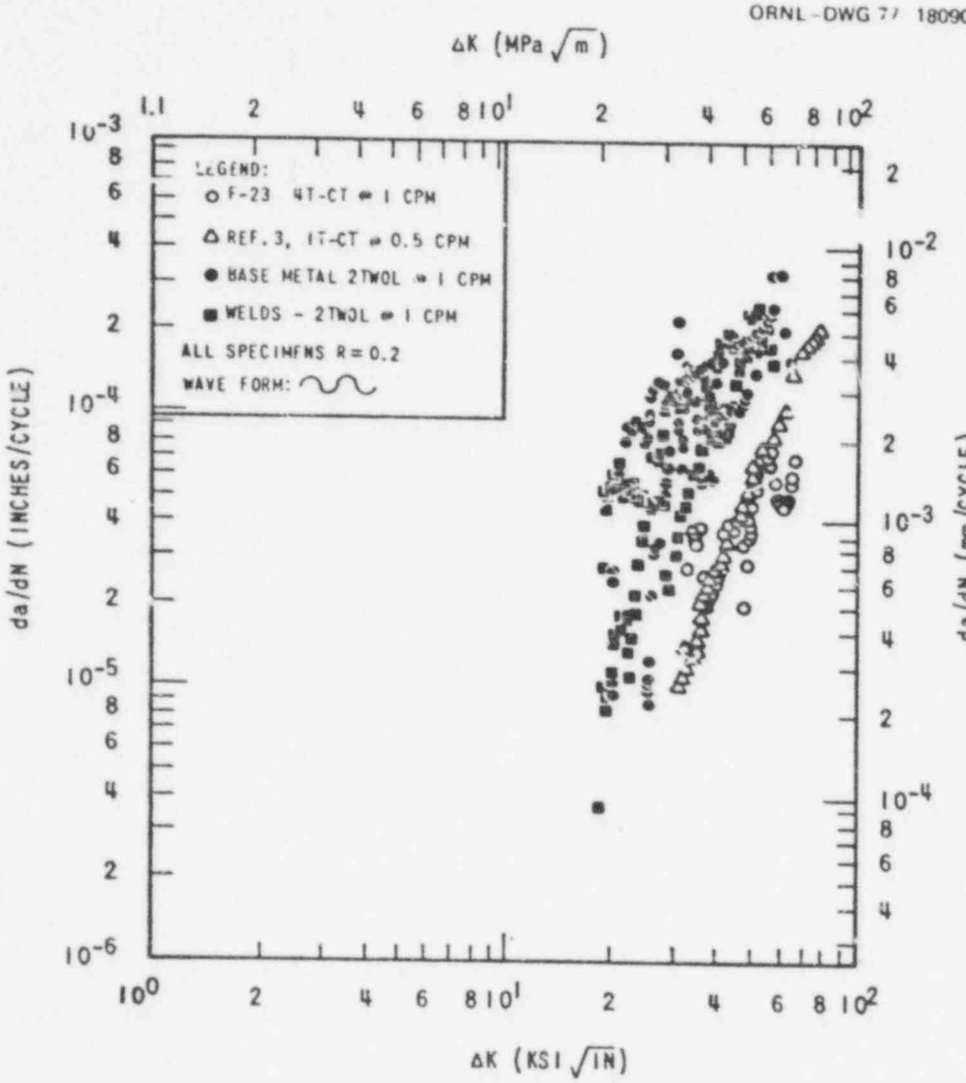

Fig. 2.1. Effect of starting ΔK value on fatigue crack growth in PWR environment (R = 0.2).

from static load stress corrosion tests which indicate that these materials do not crack under constantly applied loading in a PWR environment.

3. INVESTIGATION OF IRRADIATED MATERIALS

The irradiation of three capsules containing submerged-arc weldments in a second 4T-CT series was completed in March 1977. These weldments contain high levels of copper which increase their sensitivity to radiation damage to the extent that the ductile shelf toughness will fall below minimum specified values before the end of design life. The primary purpose of this program is to obtain ductile fracture properties which can be used to predict flawed vessel behavior and to evaluate the capability of small specimens to measure fracture properties that can be used in such an assessment.

Each capsule contains two 4T-CT specimens, smaller compact specimens ranging in size from 1.6T to 0.5T, precracked Charpy specimens, standard Charpy specimens, and tensile specimens.

Considering the limited number of specimens which may be available for surveillance in operating reactors, emphasis has been placed on developing single specimen techniques for determining ductile fracture properties.* The unloading compliance method as a single-specimen $J_{Ic}-J_R$ technique has received major attention. Comparisons are being made between crack lengths determined by multi-specimen heat tinting and those estimated on the basis of unloading compliance, using A533, grade B, class 1 and A533 quench only materials with compact specimens up to 100 mm (4 in.) thick. The data produced to date by unloading compliance agrees favorably with measured values. The results of one such comparison with Charpy thickness compact specimens is shown in Table 3.1.

The thermal history and dosimetry for the second 4T-CT series has been completed and the testing of standard Charpy unirradiated reference and irradiated specimens was initiated. The fast neutron fluences at the fatigue crack tip of the 4T compact tension specimens is shown in Table 3.2.

---

*Work sponsored by HSST Program under Purchase Order 11Y-50917V between Union Carbide Corporation and Hanford Engineering Development Laboratory.

Table 3.1. Comparison of measured and calculated crack lengths from unloading compliance J-R curve test

Material: ASTM A533, grade B, class 1
Test temperature: 121°C (250°F)
Specimen size: 0.394T CT

	Specimen 51-1	Specimen 51-2
Crack length [mm (in.)]		
Calculated		
Initial	11.51 (0.453)	11.63 (0.458)
Final	11.68 (0.460)	12.34 (0.486)
Change	0.18 (0.007)	0.71 (0.028)
Measured		
Initial	11.91 (0.469)	11.99 (0.472)
Final	12.06 (0.475)	12.75 (0.502)
Change	0.15 (0.006)	0.76 (0.030)
Percent error		
Initial	−3.4	−3.0
Final	−3.2	−3.2
Change	+17	−6.7
Crack length change [mm (in.)]		
After Clarke et al.[a]	0.22 (0.0086)	0.78 (0.031)
After Tada et al.[b]	0.19 (0.0074)	0.68 (0.027)

[a]G. A. Clarke et al., "Single Specimen Tests for J_{Ic} Determination," *Mechanics of Crack Growth*, ASTM STP 590, American Society for Testing and Materials, 1976, pp. 27–42.

[b]H. Tada et al., *The Stress Analysis Handbook*, Del Research Corp., Hellerton, Pa., 1973.

Table 3.2. Estimated fast-neutron fluence at fatigue crack tip of 4T compact tension specimens

	Fluence (neutrons/cm², E > 1 MeV)	
	Center of crack	1 in. from surfaces
Weld 61W		
Top specimen	9.4×10^{18}	1.03×10^{19}
Bottom specimen	1.30×10^{19}	1.53×10^{19}
Weld 62W		
Top specimen	1.33×10^{19}	1.43×10^{19}
Bottom specimen	1.86×10^{19}	2.00×10^{19}
Weld 63W		
Top specimen	9.7×10^{18}	1.05×10^{19}
Bottom specimen	1.35×10^{19}	1.49×10^{19}

4. PRESSURE VESSEL INVESTIGATIONS

The inservice weld repair of a nuclear reactor pressure vessel presents potentially difficult problems considering the complexity of the operations involved to effect a satisfactory procedure. A thermal stress relief would normally be required to reduce stresses induced by welding and to temper the weld heat-affected zone which might have reduced toughness properties. A thermal stress relief performed at temperatures significantly above the normal operating temperature of the system would be difficult to accomplish and could lead to warpage of the vessel. Section XI of the American Society of Mechanical Engineers Boiler and Pressure Vessel Code contains guidelines for making major repairs without thermal stress relief by the temper-bead technique.

Intermediate test vessel V-7 in the HSST program series was weld repaired using these recommendations so that another test designated as V-7A could be performed using the same vessel and flaw configuration under pneumatic loading.[4] After the successful completion of this vessel test additional work was planned to more completely evaluate the welding method.

Two additional repairs were performed on intermediate vessels this fiscal year. One of these was a second repair of intermediate vessel V-7 designated as V-7B and the other was a simulated repair of the vessel fabrication weld in intermediate vessel V-8. The objectives of this phase of the project were to obtain information on the repair weld material properties, on residual stress states, and on the structural integrity of flawed intermediate vessels in the transition and ductile temperature regimes. The tests on vessel V-7 were performed on the ductile upper shelf and the V-8 test is planned to be in the transition temperature regime to more completely evaluate residual stress effects.

Each of the vessel welds was extensively characterized by performing geometrically similar welds on cylindrical prolongations of the vessels. These prolongations provided information on surface residual stresses after the welding, and they were destructively examined to obtain data on residual stresses and material properties throughout the volume of the weld region. It was determined that residual tensile stresses approaching the yield strength of the material were present; however, the maximum stress occurred in the parent metal outside the repair weld. Circumferential stress in the region of a weld repair volume in ITV-7B is shown in Fig. 4.1. The tensile properties of the deposited weld metal were closely matched with the A533, grade B, class 1 plate from which the vessels were fabricated. The fracture toughnesses of the weld metal and heat-affected zone were determined using precracked Charpy specimens. These regions were equivalent or superior in toughness to the plate and vessel fabrication welds. The fracture toughness of the weld metal is shown in Fig. 4.2.

Pressure testing of the weld repair vessels in the V-7 series has been completed. The last test, V-7B, was performed with a very large flaw in the heat-affected zone of the repair weld.[5] This vessel sustained an overload by a factor of two over design pressure, as predicted. Destructive examination of the flaw region is under way to verify posttest ultrasonic examinations which indicated that more extensive stable cracking occurred than was observed in the previous tests.

Planning for intermediate vessel test V-8 is continuing with the determination of material toughness properties and residual stresses throughout the weld repair volume. At this time it appears that a flaw placed in the original vessel fabrication weld near the repair weld will produce the optimum combination of high residual stress and low toughness for a transition temperature test.

The work performed to date indicates that the material properties of the weld repair performed by the temper-bead technique are quite adequate. The extent and magnitude of the residual stress is significant; however, for the geometries examined peak stresses lie outside the repair weld. Additional analyses and another vessel test are planned to obtain more information on the effect of residual stress on flawed vessel behavior.

5. CRACK ARREST STUDIES

Three small pressure vessel models were tested this fiscal year to investigate the feasibility of performing a crack-arrest test with an intermediate size pressure vessel. All of the models had the configuration shown in Fig. 5.1.

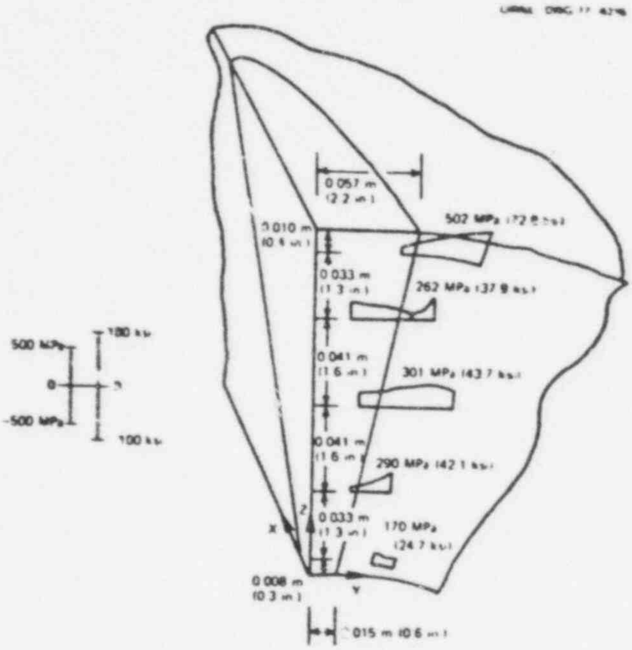

Fig. 4.1. Circumferential residual stresses measured on specimen A.

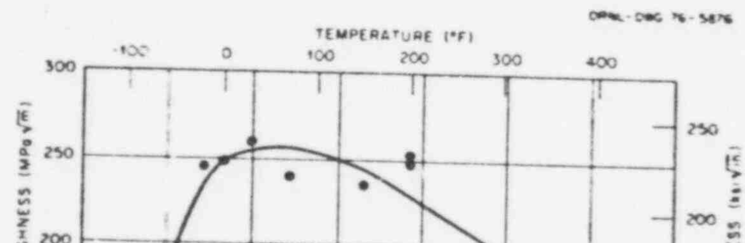

Fig. 4.2. Variation of static fracture toughness with temperature for shielded metal-arc weldment W-1.

POOR ORIGINAL

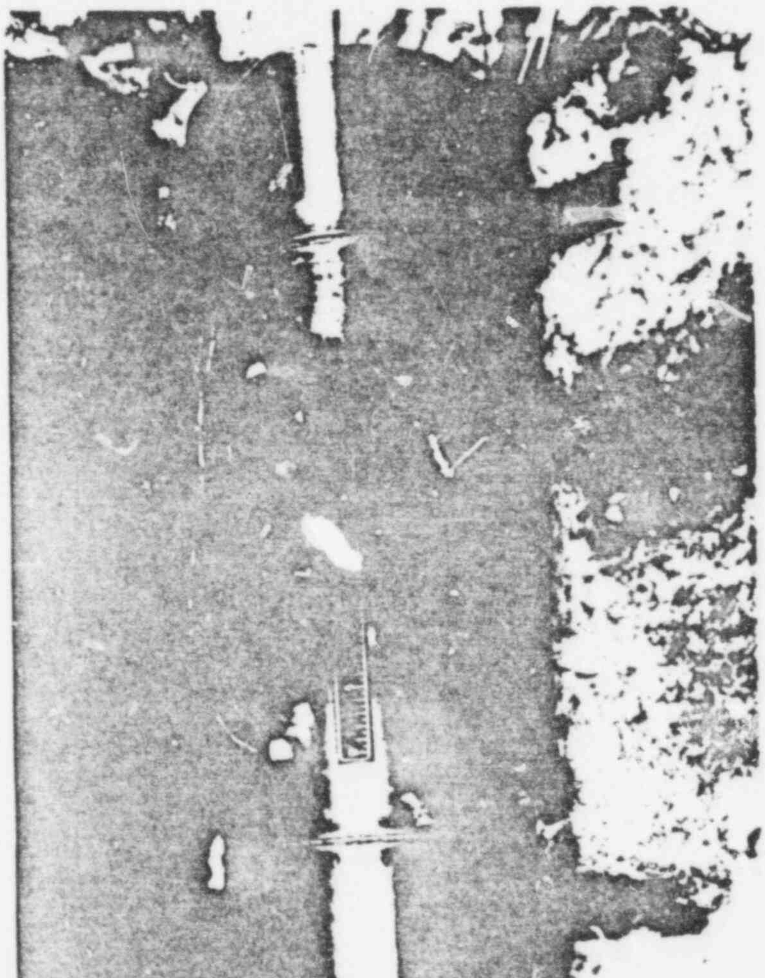

Fig. 5.1. First crack-arrest model with instrumentation.

The wall thickness and diameter of the central section were chosen to provide an approximately 1/4-scale representation of a typical intermediate test vessel. The wall thickness of the models was 38.1 mm (1.5 in.) and the outside diameter was 254 mm (10 in.). The models consisted of five cylindrical sections (including the two flat-head caps) that were joined by EB welding. This modular approach to fabrication facilitated the inclusion of a well-defined brittle starter section (i.e., the centermost cylinder) with tougher or arrest material attached to both ends as shown in Fig. [illegible] Axial slots were machined near the center of the models and an electron beam was passed along the periphery of the slot to create a sharp flaw. In effect, a through crack was present and crack advance could be arrested in the tough material. A stainless steel liner was installed to maintain pressure loading during the cracking event.

The first model test was conducted at 91°C (196°F) and slow stable crack extension occurred in the brittle section with arrest at the brittle-to-tough material interface. The second model was tested at 4°C (40°F) and exhibited substa[illegible]lly the same response as the first model with the exception of two fast crack extension events, each followed by arrest. The third model was fabricated with a brittle material having inferior fracture toughness relative to the first two models. This model was initially tested at −22°C (−8°F) and crack extension was indicated at 91 MPa (13,000 psi) comparable to the other models except that pressurization up to 103 MPa (15,000 psi) produced no further crack growth. The model was retested at −47°C (−53°F) and produced unstable crack extension and no arrest in the tougher material as predicted.

Although fast fracture and arrest did occur the results of these tests indicate that side grooves will probably be required with through-cracks to achieve the plane strain needed to reliably obtain fast fracture. The presence of side grooves would complicate to some degree the application and extension of an test results relative to actual thick vessel sections. Further, the pressure needed to achieve crack propagation and arrest is determined by the conditions at initiation and therefore subject to the same scatter or inherent uncertainty that applies to the toughness at initiation. In order to achieve a meaningful test, i.e., propagation and arrest, the test pressure would have

815 020

ORNL-DWG 77-11534

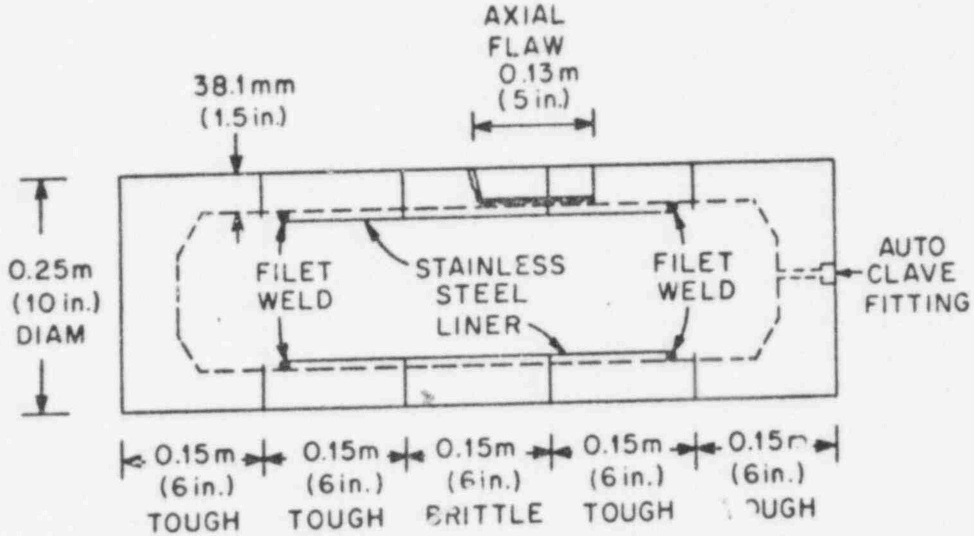

Fig. 5.2. Cross section of the crack-arrest model configuration. The center section was quenched only A533 (plate 03); the other four sections were quenched and tempered A533 (plate 57).

to fall within a narrow band and therefore, in that sense, this test configuration involves some inherent risk.

Considering the limitations discussed above two additional concepts for studying crack arrest in thick sections are being evaluated. One is a pop-in type experiment where a part through defect is caused to propagate by hydrogen charging an electron beam weld under load, and the other involves loading flawed cylindrical sections by means of thermal shock. In each of these cases the initiating load can be more accurately controlled and/or the arrest condition be achieved with greater certainty. It is however more difficult to obtain crack tip velocity measurements but in principle the velocity could be inferred from crack opening displacement measurements.

Each of these methods is being given additional study and review so that a large scale concept can have a greater certainty of meeting the project objectives.

6. THERMAL SHOCK

The HSST Thermal Shock Program at ORNL was established for the purpose of investigating the behavior of flaws in pressure vessel walls subjected to thermal shock. This type of loading in a PWR vessel introduces some unique features (equal biaxial stresses and steep gradients in stress intensity factor and fracture toughness) with regard to the application of linear elastic fracture mechanics, and thus an experimental verification of the proposed methods of analysis was in order.

For the purpose of scoping the experimental program, a specific thermal shock situation was defined (LOCA-ECC) and corresponding calculations were made for typical PWRs. The results of these calculations indicated that a PWR vessel fabricated with low-copper-impurity steel would not experience crack propagation under LOCA-ECC conditions. On the other hand, near the end of its otherwise normal life (~40 years) a high-copper vessel could experience propagation of preexisting flaws beneath the cladding. However, it appears at this time that warm prestressing effects would prevent hypothetical long axial and continuous circumferential cracks deeper than ~20% from initiating and thus would be instrumental in limiting the maximum penetration to ~35%.

Assuming that warm prestressing would indeed be this effective, the experimental program was limited to the study of shallow flaws. Four shallow-crack experiments have been completed, using 533-mm-OD × 152-mm-wall (21-in. × 6-in.) cylindrical steel test specimens. To simulate PWR fracture mechanics parameters as closely as possible, the test specimens were fabricated from PWR pressure vessel material (A508), were given a quench-only heat treatment to reduce the toughness, and were subjected to thermal shocks more severe than those imposed on PWR vessels in order to further reduce the toughness (K_{Ic}) and to enhance the stress intensity factor (K_I). These latter two measures were necessary because the test specimen material, even in the quench-only condition, was tougher than the irradiated material.

The fourth experiment in the series was conducted this fiscal year with a test specimen that contained a long axial flaw, and a specified maximum K ratio of 1.3 was achieved. The test conditions are summarized in Table 6.1. Initiation occurred in essentially a single event, as expected, at a time of 150 sec. The arrest depth was 23 mm (0.9 in.), corresponding to an arrest toughness (K_{Ia}) of 127 $MNm^{-3/2}$ (116 ksi $\sqrt{in.}$) at 126°C (258°F). The calculated K ratio at 150 sec was 1.10 (based on a nominal value of K_{Ic}), which is in good agreement with the experimental results. The interior of the test specimen after the test is shown in Fig. 6.1.

Based upon the results from TSE-4 and to a lesser extent from TSE-1 in which the flaw did not propagate, and upon the fact that no significant anomalies were encountered in any of the four experiments, it appears that linear elastic fracture mechanics is valid for thermal shock loadings. Furthermore, the results of TSE-2 indicate that under thermal shock conditions, short cracks will not grow to become extremely long and then grow radially.

The possibility of demonstrating warm prestressing with a cylindrical test specimen under thermal shock conditions is being considered. It appears that such an experiment can be conducted at a reasonable cost using liquid nitrogen under pool boiling conditions. To prevent excessive film blanketing, a thin insulating layer of rubber cement type material is applied to the surface to be quenched. Recent heat transfer experiments at ORNL and corresponding fracture mechanics analyses indicate that appropriate conditions can be achieved in this

Table 6.1. Test conditions for TSE-4

Experiment	TSE-4
Test specimen	TSV-2
Test specimen dimensions, m (in.)	
OD	0.53 (21)
ID	0.24 (9.5)
Length	0.91 (36)
Test specimen material	A508 class 2
Heat treatment	Quench only from 871°C (1600°F)
Flaw	Long axial crack, a = 11 mm (0.42 in.)
Temperature, °C (°F)	
Wall (initial)	291 (555)
Sink (initial)	−25 (−13)
Sink (final)	−19 (−2)
Coolant	40 wt % methyl alcohol, 60 wt % water
Coolant flow rate m^3/hr (gpm)	114 (500)
Coolant pressure in test section, kPa (psi)	1020 (148)
Back pressure orifice diameter, mm (in.)	43.18 (1.700)
Heat transfer coefficient, $W \cdot m^{-2} \cdot K^{-1}$ (Btu hr^{-1} ft^{-2} $°F^{-1}$)	∿5700 (∿10^3)
$(K_I/K_{Ic})_{max}$	1.29
Time of occurrence of $(K_I/K_{Ic})_{max}$, min	∿5
Duration of experiment, min	30

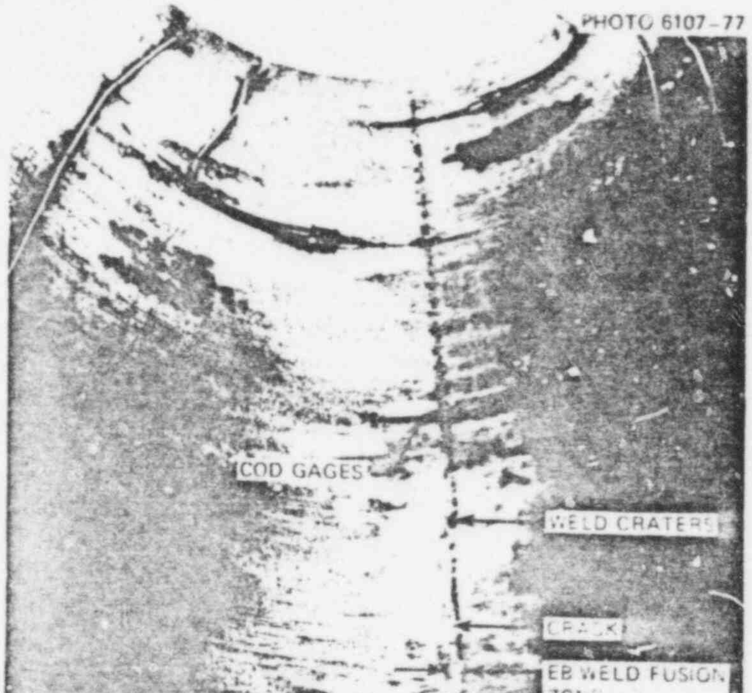

Fig. 6.1. View of inner surface of TSV-2 following TSE-4, showing EB-weld flaw and COD gages. Gages buckled during experiment.

manner for demonstrating warm prestressing in a 991-mm-OD × 152-mm-wall (39-in. × 6 in.) A508 cylinder in the normal tempered condition.

7. PLAN OF RESEARCH FOR FUTURE YEARS

The behavior of nozzle corner flaws will be evaluated with additional photoelastic studies and analyses culminating with the test of intermediate vessel V-10 to verify fracture prediction methods. Fatigue crack growth studies will be continued to develop realistically conservative bounds for inclusion in ASME codes that are applicable to assessments of pressure vessel integrity. Low upper shelf weld metal will continue to be irradiated and tested to obtain ductile fracture toughness properties, J_{Ic}-J_R, to be used in assessments of operating pressure vessel integrity when flaws are present. Recommendations for minimum specimen size in surveillance programs will be made. Inservice weld repair methods will be evaluated through the analysis and testing of weld repaired intermediate pressure vessels. Recommendations will be made on the welding procedures and practices to obtain acceptable properties, minimize residual stresses and increase welding efficiency. A crack arrest experiment using thick section geometry will be planned and a test conducted to validate predictive methods. The feasibility of performing additional thermal shock experiments to demonstrate warm prestressing will be established. Safety analyses will be performed using a reference calculational model to determine the effects of various breaks in main coolant lines and steam lines on the behavior of a flawed pressure vessel to establish the significance of this class of accidents on nuclear power plant safety. Cognizance will be maintained of foreign research applicable to the safety of light-water reactor primary systems.

References

1. R. W. Derby, "Shape Factors for Nozzle-Corner Cracks," *J. Exp. Mech.*, Vol. 12, No. 12, pp. 580–584, December 1972.

2. J. G. Merkle et al., *Test of 6-in.-Thick Pressure Vessels. Series 4: Intermediate Test Vessels V-5 and V-9 with Inside Nozzle Corner Cracks*, ORNL/NUREG-7, August 1977.

3. H. E. Watson et al., "Fatigue Crack Propagation in LWR Materials," *Structural Integrity of Water Reactor Pressure Boundary Components — Progress Report Ending May 31, 1971*, Naval Research Laboratory, Washington, D. C.

4. *Weld Repair of Heavy Section Steel Technology Program Vessel V-7*, EPRI NP-179, ORNL/SUB/88-242-76/1, August 1976.

5. R. H. Bryan, *Quick Look Report of Intermediate Test Vessel V-7B — Sustained Load Test of Flaw in Weld Repair*, SST-2, Oak Ridge National Laboratory, Aug. 3, 1977.

815 027

CONTRACT TITLE: Structural Integrity of Water Reactor Pressure Boundary Components

CONTRACTOR AND LOCATION: Naval Research Laboratory, Washington, DC 20375

PRINCIPAL INVESTIGATOR: F. J. Loss

OBJECTIVE:

Assess materials behavior in relation to structural safety and reliability for pressure boundary components of light water reactors. Develop an understanding of fracture and fatigue crack propagation phenomena in terms of continuum mechanics, metallurgical factors, and neutron irradiation. Identify metallurgical factors and evolve guidelines for radiation resistant steels. Investigate procedures for postirradiation properties recovery. Evolve engineering criteria for reliable structural performance and long-term operation.

FY-77 SCOPE

Task A - Fracture Toughness

Develop a single specimen J-R curve methodology for the purpose of characterizing the toughness of irradiated pressure vessel steels. Compare the heat tint and unloading compliance techniques to define the J-integral toughness of a low upper shelf A302-B steel.

Task B - Fatigue Crack Propagation

Characterize the cyclic crack growth data in LWR materials in a reactor water environment at elevated temperature. Investigate the factors of loading rate, waveform and temperature in the framework of the NRC preliminary matrix. Install new autoclave chambers and perform an irradiation of 2TCT crack propagation specimens.

Task C - Irradiation Sensitivity and Postirradiation Recovery

Investigate the degradation in notch ductility and fracture toughness with irradiation, define properties recovery with postirradiation heat treatment, and characterize the potential benefits to long-term service of cyclic irradiation-anneal-reirradiation procedures for reactor steels and welds with emphasis on upper shelf toughness. Determine metallurgical variables, including residual element content, and radiation variables governing property trends. Develop guidelines for projecting property changes as functions of metallurgical and reactor service variables and for improving radiation characteristics. Conduct special radiation investigations in support of other NRC research programs.

Task D - Thermal Shock-Related Investigations

Experimentally characterize the warm prestress phenomenon that can occur in a flawed reactor vessel following a LOCA and operation of the ECCS. Assess the added margin against fracture provided by warm prestress. Report on initial program; initiate and complete second-phase program involving a small ΔT and issue a topical report.

815 028

SUMMARY OF RESEARCH

Task A - Fracture Toughness

I. J-Integral Characterization of Low Upper Shelf Steel

F. J. Loss, B. H. Menke, and R. A. Gray, Jr.

A program is being conducted to characterize the fracture toughness of pressure vessel steels that exhibit a low upper shelf energy. This investigation has been motivated by the projected drop in the Charpy-V (C_v) energy to levels less than 68J (50 ft-lb), caused by irradiation of steels used in the construction of certain older LWR pressure vessels. It is necessary to characterize the toughness in terms of fracture mechanics to permit an assessment to be made of the margin of safety against fracture associated with a given C_v upper shelf energy. It is not possible to measure the toughness of these irradiated steels with linear elastic fracture mechanics (LEFM) techniques because of the large sizes of irradiated specimens that would be required. In thin sections, e.g., 25 mm, these steels are expected to exhibit an elastic-plastic behavior. For tests of this type, the J integral-R curve approach is being applied to characterize the low shelf alloys and also to permit an assessment to be made of full-section behavior.

The current ASTM-recommended method for J_{Ic} measurement requires several specimens to be tested in which the crack extension (Δa) may be determined by "heat tinting" and measuring the fracture surface. Because of the difficulties in obtaining and testing irradiated specimens, it is necessary to develop a single specimen technique for the assessment of both J_{Ic} and the R curve. The emphasis in FY-77 has been to assess the unloading compliance method (UCM) as a viable single specimen J technique for application to irradiated CT specimens.

Investigations have centered on an A302-B steel having an upper shelf energy of approximately 68J (50 ft-lb). The primary objective is to develop the UCM to a point where it could be used to predict the J-R curve obtained from the multispecimen, heat-tint technique. Additional objectives are (a) to assess the effect of specimen size, and (b) to characterize the effect of face grooves on the J-R curve. In addition, a cooperative program was initiated between CISE (Italy) and NRL. The objectives of that program are

(a) to obtain a comparison of the J-R curves for this steel using the heat tint technique, and (b) to investigate size effects with CT specimens of 12.5, 25, and 50-mm thickness.

The success of the UCM rests in the elimination of frictional effects in the mechanical apparatus so as to minimize the hysteresis obtained in the record of load vs load-line deflection. The high signal amplification employed also requires minimization of the electronic noise. In FY-77 the UCM was developed to produce signals capable of detecting a 0.12 mm (5 mil)change in effective crack length with a 25 mm CT specimen. Figure 1 illustrates the J-R curve obtained from the subject A302-B steel using the UCM. Also shown is the value of crack extension determined optically from the heat tinted fracture face. The "error" is unacceptable and was thought to be the result of crack front curvature or tunneling (Fig. 2). The same phenomenon has been observed by other laboratories.

It was found that face grooving of the specimen can effectively eliminate the crack front curvature (Fig. 3). The J-R curve for this specimen is illustrated in Fig. 4. Note that the UCM still underestimates the value of crack extension measured from the heat tinted surface. Consequently, the difference between measured and predicted values of crack extension cannot be attributed to crack front curvature. Another possible explanation for the difference in the two methods for determining crack extension rests in the crack front irregularities. This fact may introduce optical measurement errors that could lead to differences in predicted vs measured values of crack extension. Nevertheless, until this discrepancy is satisfactorily resolved, further research is required before the UCM can be applied, exclusively, for the assessment of irradiated materials.

The J_{Ic} values shown in Figs. 1 and 4 are approximately 61 kJ/m^2 (348 in.lb/in.^{2}) at 200°C. This corresponds to a K_{Jc} value of approximately 112 MPa$\sqrt{}$in. (102 ksi$\sqrt{}$in.) where K_{Jc} is a K_{Ic} value computed from J_{Ic}. However, the preceding values may not be typical since other tests at 200°C have indicated a large scatter in J_{Ic} with values in excess of 87 kJ/m^2 (500 in.lb/in.^{2}). This scatter is believed due to metallurgical inhomogeneities in this steel plate.

Over the near term it is believed that plant safety requirements can be met provided the vessel material exhibits a toughness level of approximately 165 MPa$\sqrt{}$in. (150 ksi$\sqrt{}$in.). Results from subject heat of A302-B steel suggest a 68J (50 ft-lb)

815 030

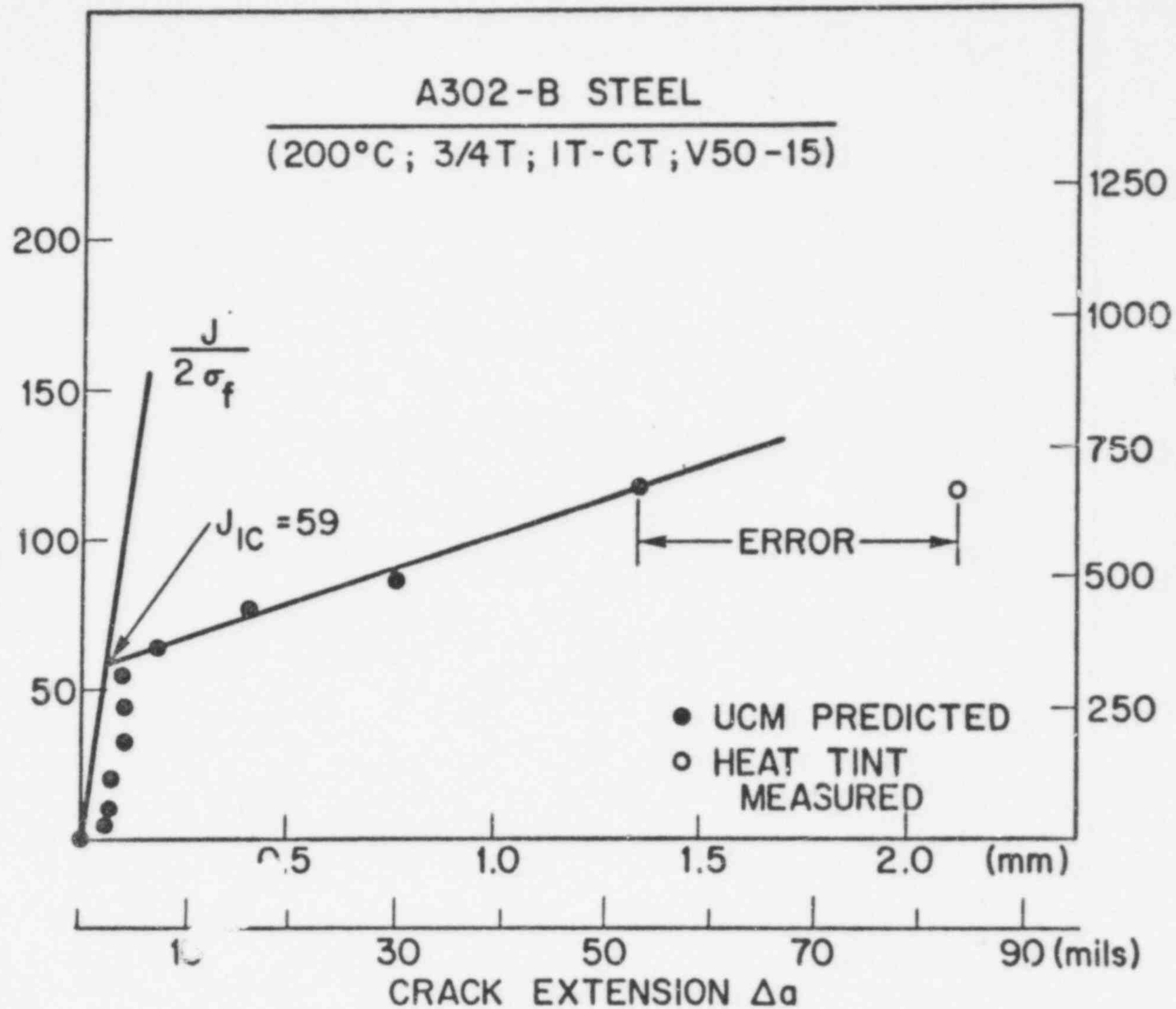

Fig. 1. Illustration of the J-R curve obtained by the UCM. The test was conducted in the upper shelf region and the crack extension occurred in a ductile manner. The "measured" value of Δa was determined optically from the heat tinted fracture surface.

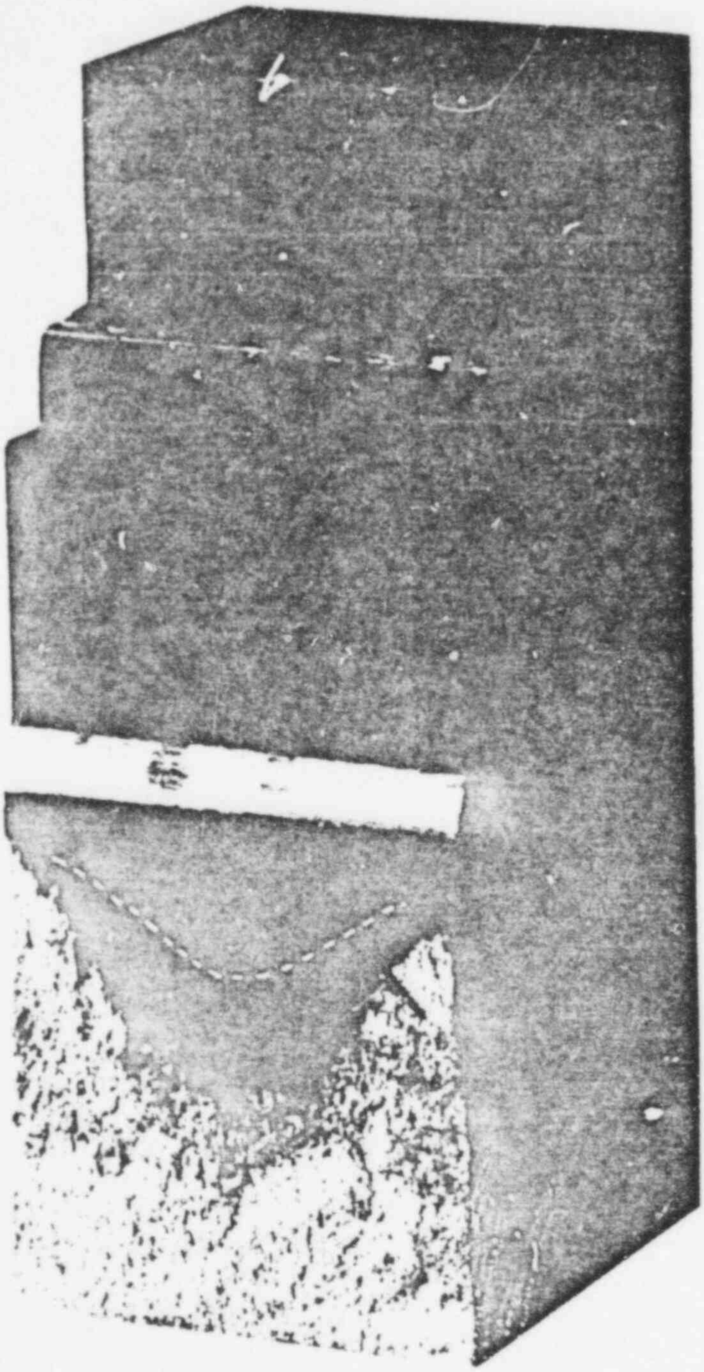

Fig. 2. Fracture surface associated with the J-R curve in Fig. 1. The heat tinted crack extension defined by the "measured" point in Fig. 1 has been outlined. The larger thumbnail marking of the fracture surface was produced by a second loading of the specimen.

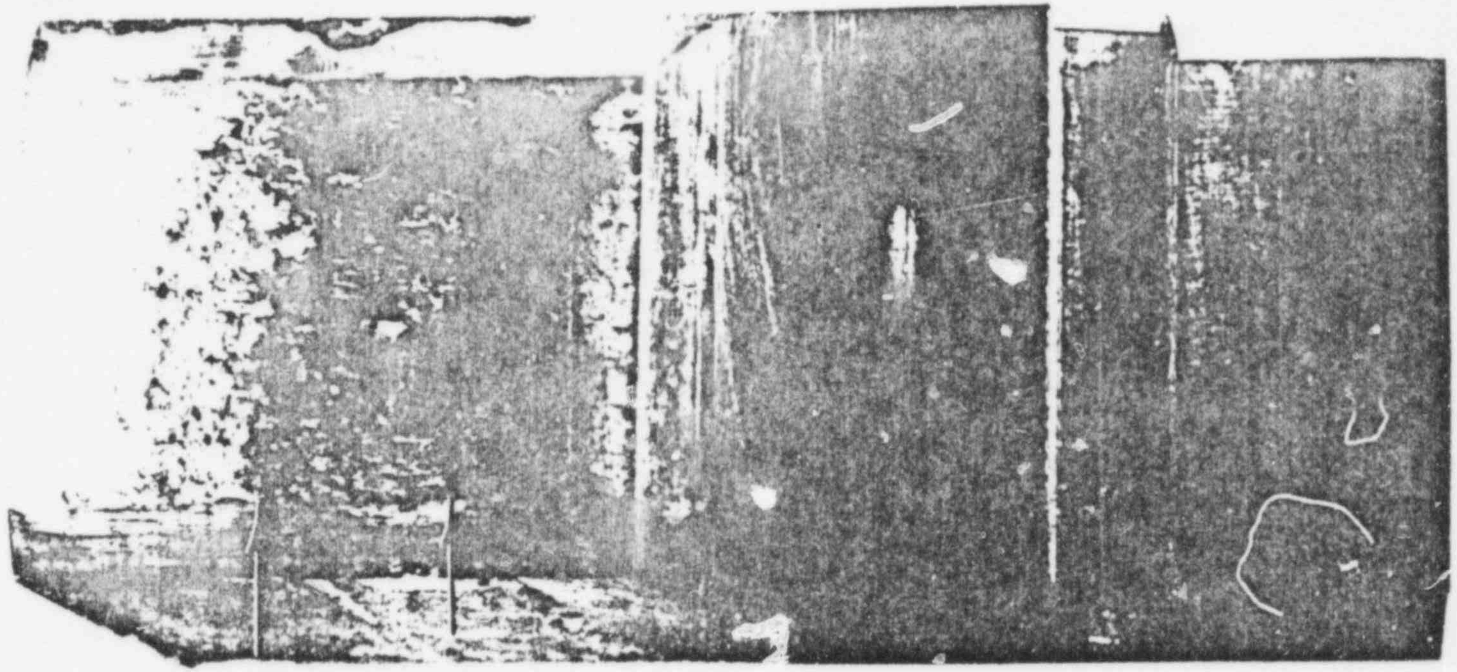

Fig. 3. Fracture surface of a specimen which has been face-grooved. This specimen illustrates the crack front shape at two points in the loading history (indicated by arrows). Face grooving effectively eliminates the crack-front curvature that was illustrated in Fig. 2.

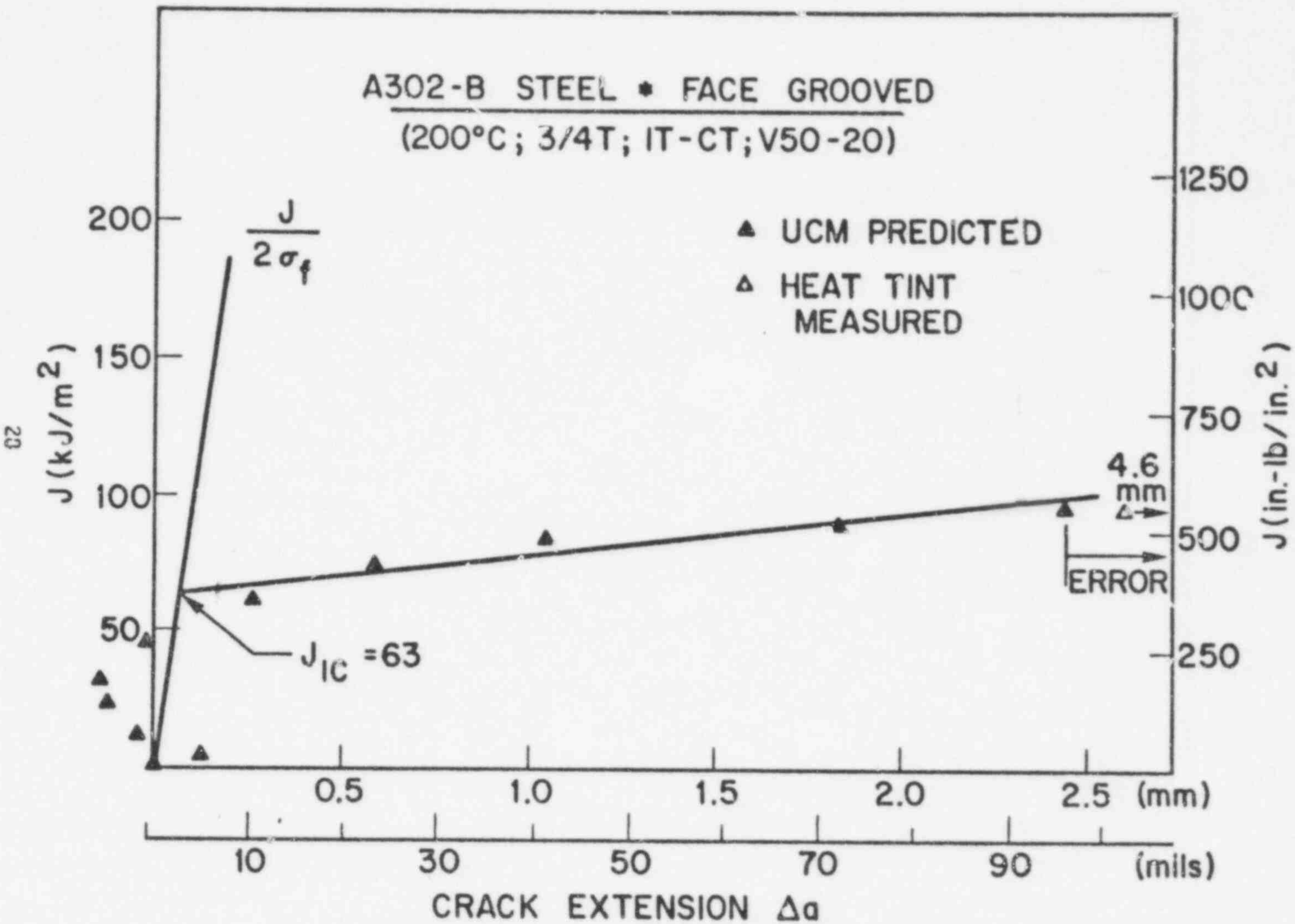

Fig. 4. J-R curve obtained from a face-grooved specimen. Note that the measured value of crack extension from the heat tinted surface does not agree with the value predicted by the UCM.

815 034

upper shelf energy will project a K_{Jc} level less than that required. Consequently, assessment methods other than J_{Ic} may be needed to define the margin of safety associated with steels of low upper shelf toughness. For example, the tearing instability model developed by Paris and others (1) projects an alternate means of assessing structural reliability for steels of low shelf toughness.

Task B - Fatigue Crack Propagation

H. E. Watson, F. J. Loss, B. H. Menke, and R. A. Gray, Jr.

An experimental program is underway to characterize the cyclic fatigue crack propagation (FCP) rates for steels used in LWR pressure vessel construction. A primary objective is to develop a conservative data base to permit assessment of the structural reliability of vessels containing flaws discovered during in-service inspection, e.g., to augment Section XI, ASME Boiler and Pressure Vessel Code. Tests are being conducted in accord with a preliminary test matrix designed to define the primary variables. Detailed investigation of these variables will be undertaken in the main program. The preliminary matrix was developed to simulate (a) the hydro and leak transient, (b) the heat-up and cool-down transient, and (c) the steady state of operation of a nuclear pressure vessel.

During FY-77, tests were conducted to evaluate the effect of rise time, hold time, temperature, reactor water, and starting ΔK on FCP. These tests were conducted with A508-2 forging material using 25-mm (1-in.) CT specimens. The crack growth rates (da/dN) were investigated in terms of the stress intensity factor, K_I. The FCP tests were conducted using both autoclave (288°C, 14 MPa) and water pot (93°C, 0.14 MPa) fatigue test equipment. In all cases, water chemistry was carefully controlled to simulate PWR conditions. Crack length measurements were obtained from specimen compliance changes referenced to the crack mouth opening and FCP rates were determined by computer analysis using the incremental polynominal technique recommended by the ASTM.

All test data reported this year have been generated using a single autoclave and water pot. The autoclave is adapted for irradiated tests which will begin when the preliminary matrix is completed. A new autoclave, capable of testing a 100-mm (4-in.) thick WOL specimen, has been designed for hot cel peration and is in the process of being activated for this program. In addition, three autoclaves, designed to simultaneously test two 100-mm WOL specimens each, are undergoing final acceptance tests.

The data shown in Fig. 5 summarize the results from the preliminary matrix. The figure illustrates the effect of (a) varying the hold time from 1 to 3 min, (b) varying the rise time from 1 sec to 1 min, (c) combining test variables (1 min rise, 3 min hold), and (d) testing at temperatures of 93 and 288°C. An analysis of the data presented in Fig. 5 indicates that the highest fatigue crack growth rate was obtained with a loading waveform consisting of a 1-min rise time combined with a 3-min hold time. Nevertheless, a comparison of these results with the crack growth rate for a water environment given in ASME Section XI (illustrated in Fig. 5) shows that the Section XI water line is conservative with respect to the NRL data. However, further investigation of the significant variables is required before a definitive conclusion can be drawn concerning a conservative upper bound to the FCP trends.

Another phenomenon, associated with the starting level of ΔK, was identified by Westinghouse during the past year (2). Results from FCP experiments from the same steel appear to exhibit a trend in growth rates that is proportional to the level of ΔK at which the test was initiated. To verify this phenomenon, two tests on the same material used by Westinghouse were conducted with starting K levels of 28 and 45 MPa$\sqrt{m}$ (25 and 41 ksi$\sqrt{in.}$), respectively. The results, shown in Fig. 6, do not conclusively show an effect of starting ΔK. However, it has been speculated that a lower threshold may exist and additional tests are being conducted with a lower starting ΔK to assess this possibility.

During FY-78 testing will continue, as defined by the preliminary matrix, using newly activated environmental chambers. When the matrix is completed, the main program tests will be initiated.

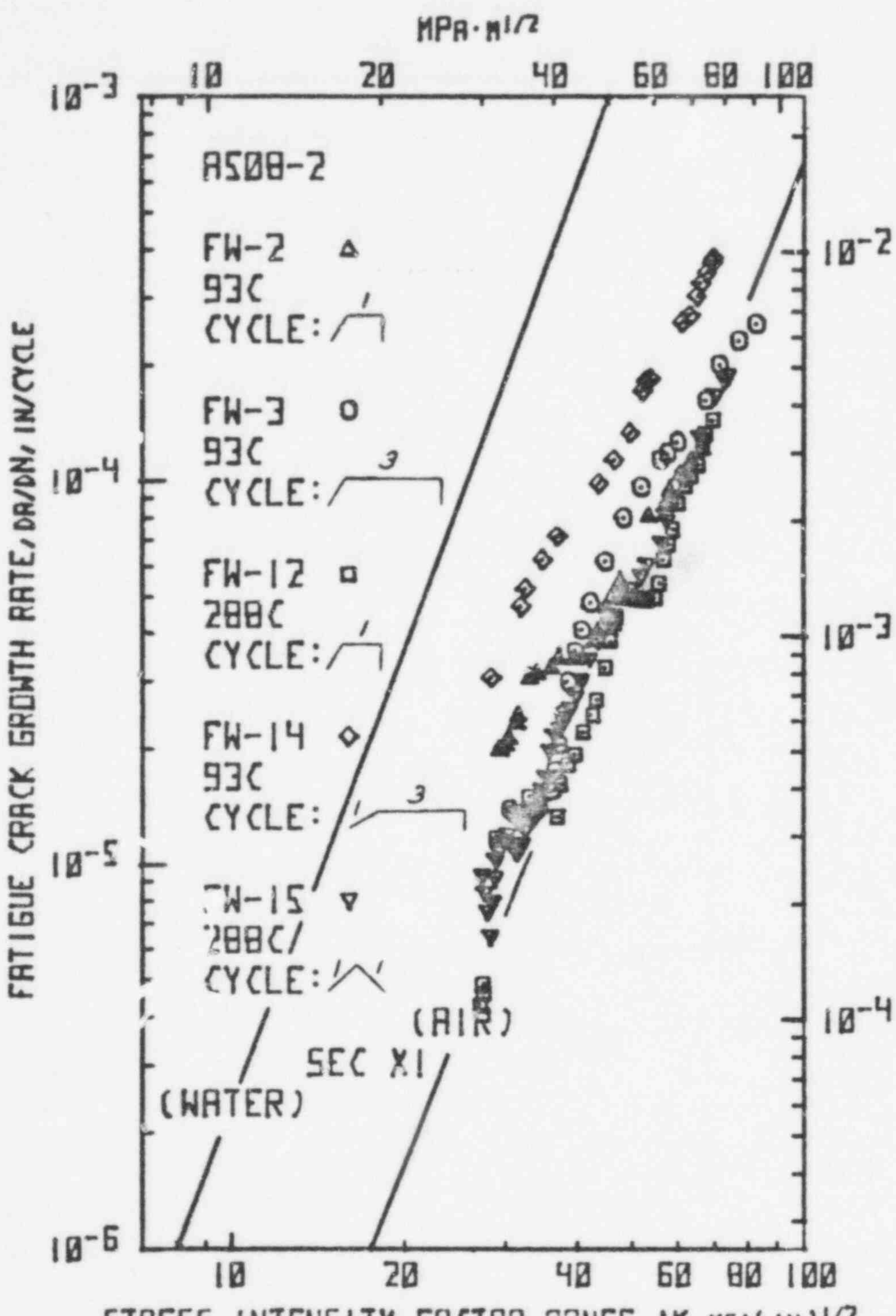

Fig. 5. Summary of FCP tests in a PWR water environment. The data were produced with 1TCT specimens cycled at an R-ratio of 0.1.

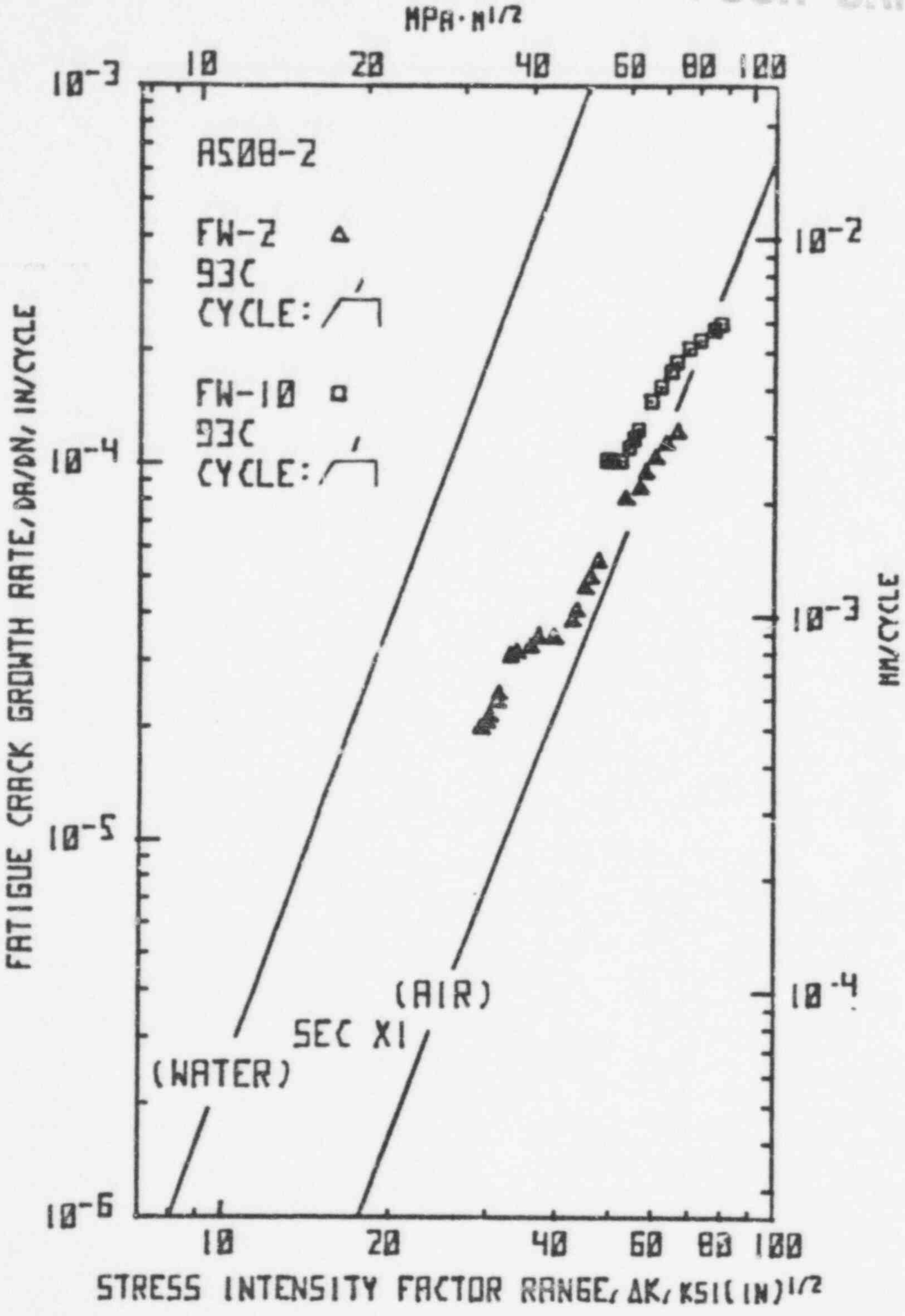

Fig. 6. Data from identical tests, except for starting ΔK (28 vs 45 MPa√m) are compared.

Task C - Radiation Sensitivity and Postirradiation Properties Recovery

The NRL radiation effects studies on the notch toughness of reactor vessel materials presently focus on the degradation of upper shelf toughness with 288°C (550°F) irradiation and on notch toughness recovery with 343 to 427°C (650 to 800°F) postirradiation heat treatment (annealing). Within these two areas, several subtasks are underway with the aim of developing key information for projecting radiation behavior and cyclic radiation and annealing behavior as a function of metallurgical and service variables. The investigations are proceeding with plates, weld deposits, weld heat affected zones (HAZ) and forgings produced commercially and in the laboratory. A summary of five specific subtasks investigated in FY-77 is given below.

I. IAR Program

J. R. Hawthorne, H. E. Watson, and F. J. Loss

The objective of the IAR program is to explore the cyclic irradiation and annealing behavior of older production (high impurities) reactor vessel welds and plates to assess the potential of periodic in-service heat treatments for reducing radiation embrittlement in vessels. At present, reactor vessel steels must exhibit a minimum Charpy-V (C_v) upper shelf energy of 68J (50 ft-lb) to satisfy the ASME Code (Section III) and the Code of Federal Regulations (10CFR50). In the case of certain older vessels, it has been projected that this minimum energy level will not be retained over the full life of the vessel because of a combination of high radiation sensitivity and a low initial upper shelf.

The IAR program is exploring material behavior under two full cycles of annealing and reirradiation. Additional features of the experimental plan are: (a) the development of material performance data at the end of each phase of the irradiation-annealing sequence; (b) an irradiation temperature of 288°C (550°F); and (c) investigation of two postirradiation heat treatment options: 343°C (650°F) annealing and 399°C (750°F) annealing. The first heat treatment option of 343°C annealing represents the use of nuclear or pump heating to attain the requisite temperature on the vessel. The second option of 399°C annealing represents the use of auxiliary heaters to bring the vessel (or selected components thereof) to temperature. While the latter option has the capability for achieving greater embrittlement relief by virtue of a higher temperature, the removal of core internals (as well as the coolant) would be necessary.

Two A533-B submerged arc welds and an A302-B modified steel plate produced commercially were obtained for the investigation. Copper contents of the materials are 0.35, 0.35, and 0.22% Cu, respectively. The welds were additionally selected for their differences in C_v upper shelf energy levels (145 vs 98J or 107 vs 72 ft-lb). The difference stems largely from the use of different welding fluxes. The program plan is to establish notch ductility and fracture toughness properties (K_J) using standard C_v specimens and 2.5-cm (1-in.) thick compact tension (CT) specimens, respectively. Primary attention will be directed to upper shelf behavior under IAR conditions; transition temperature trends will be explored as specimen numbers permit.

The radiation experiment test matrix for the program is shown in Table I

TABLE I

RADIATION EXPERIMENT MATRIX

288°C (550°F) IRRADIATION

Experiment Number	Specimen Types	Designation	Objective
1	C_v	IA	Explore recovery by 343 and 399°C (650 and 750°F) annealing.
2A, B, C	C_v	IAR	Explore reirradiation response of all three materials.
3A through 3E	CT, C_v	I through IARAR	Determine IARAR performance of Weld 1.
4A through 4E	CT, C_v	I through IARAR	Determine IARAR performance of Weld 2.

The matrix will provide full information on both A533-B welds; information for the A302-B modified plate will be developed only through Experiment No. 2. For the first phase radiation exposure, the target fluence has been set at 1×10^{19} n/cm^2 >1 MeV and was chosen for its approximate correspondence to the knee of the radiation trend curve of transition temperature increase versus fluence at 288°C (3). Fluences chosen for re-irradiation exposures were not as high as the initial value, since full recovery was not expected for either the 343°C or 399°C postirradiation heat treatments.

Program progress includes the completion of all irradiation, annealing, and re-irradiation operations for Experiments 1 and 2; examples of experimental results are presented and discussed in Figs 7-9. Reported fluences are

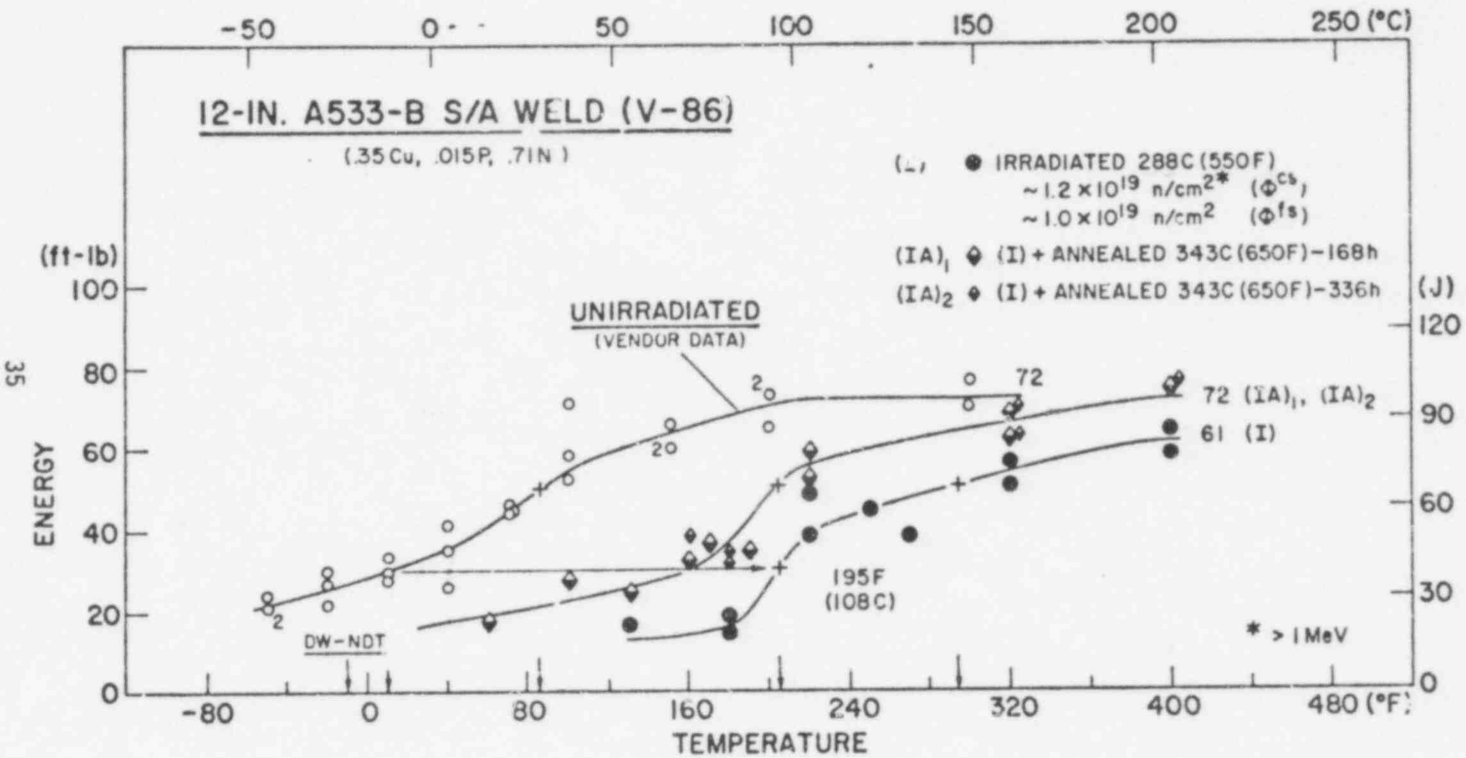

Fig. 7. Notch ductility recovery of weld V86 by 343°C (650°F) annealing heat treatment for two different times following fire cycle irradiation. Full upper shelf recovery but only 22 percent transition temperature recovery (41J ft-lb index) are observed. No difference in recovery is found between 168 hour and 336 hour heat tments.

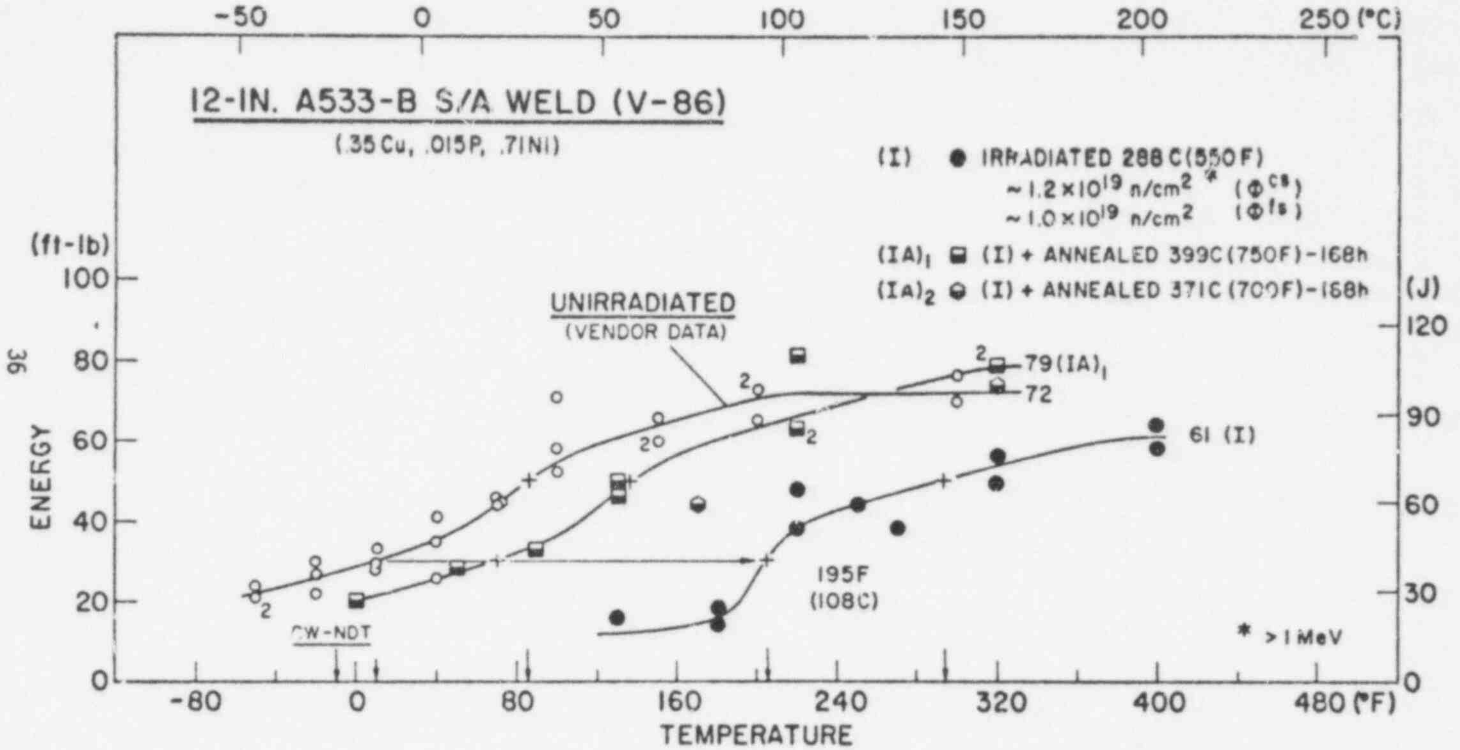

Fig. 8. Notch ductility recovery of weld V86 by 399°C (750°F) heat treatment following first cycle irradiation. Full upper shelf recovery and 69 percent transition temperature recovery (41J, 30 ft-lb index) are observed. Limited data for the 371°C (700°F) postirradiation heat treated condition are also shown.

815 042

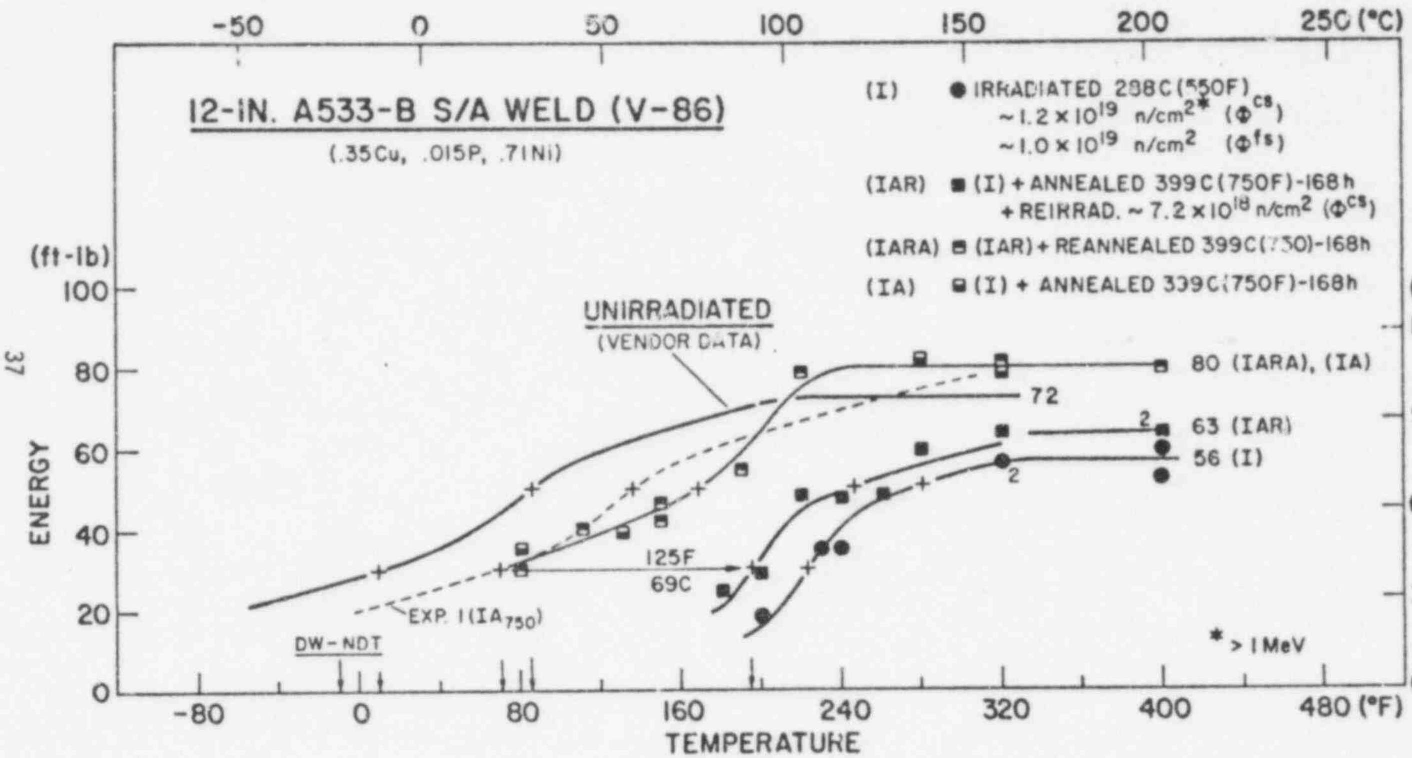

Fig. 9. Notch ductility of weld V86 after (1) reirradiation following a midcycle 399°C (750°F) annealing heat treatment (curve IAR), and (2) after reirradiation and re-heat treatment at 399°C (750°F) (curve IARA). Weld notch ductility after first cycle irradiation (curve I) and after first cycle heat treatment (data points IA) are also shown. The notch ductility after reirradiation is better than after the first cycle irradiation. However, the rate of re-embrittlement is greater than that for non-heat treated material when its fluence is increased from 1.2×10^{19} to 1.92×10^{19} n/cm^2 >1 MeV. The amount of re-embrittlement is about equal to that for virgin material at 7.2×10^{18}.

preliminary values. Additional progress includes the recent completion of radiation exposures on Experiments 3A through 3C and Experiments 4A through 4C.

Three primary observations evolved from the experimental results to date:

1. The effectiveness of a 343°C (650°F) postirradiation heat treatment appears to be limited for control of radiation embrittlement in that a high frequency of annealing would be required for reactors, i.e., at alternate refueling outages.

2. A 399°C (750°F) postirradiation heat treatment does appear to be an effective method for control of radiation embrittlement in the context of the present irradiation and heat treatment conditions. Because of the high overall recovery achieved, only infrequent annealing would appear necessary for embrittlement control.

3. Full upper shelf recovery but not full transition temperature recovery was developed by 399°C (750°F) postirradiation heat treatment for both welds following first cycle and second cycle radiation exposure.

II. Low Fluence Radiation Effects Studies

J. R. Hawthorne

Studies on the effects of low fluence irradiation on notch toughness were continued in FY-77 in recognition of the limited data available for judging changes in this property early in the life of reactor vessels. Data acquisitions were carefully planned to help establish the degree of conservatism in NRC Regulatory Guide 1.99 projections of embrittlement at low fluence, and alternately, to reveal areas of possible Guide refinement.

Several commercial production materials (plates, welds) were evaluated. Impurity copper contents ranged from 0.10 to 0.35 percent copper and were chosen to provide a range of radiation sensitivities. Experiments focused on two fluence levels: $\sim 1 \times 10^{18}$ and $\sim 6 \times 10^{18}$ n/cm^2 >1 MeV. An example of notch ductility changes noted for one weld at successively higher fluence levels is given in Fig.10. Experimental observations are compared to Guide projections in Figs. 11 and 12.

The investigations have determined that (a) the adjustment to the reference temperature (i.e., transition temperature elevation) increases very sharply with fluence in the interval of 1×10^{18} to 6×10^{18} n/cm^2; (b) the transition temperature

815 044

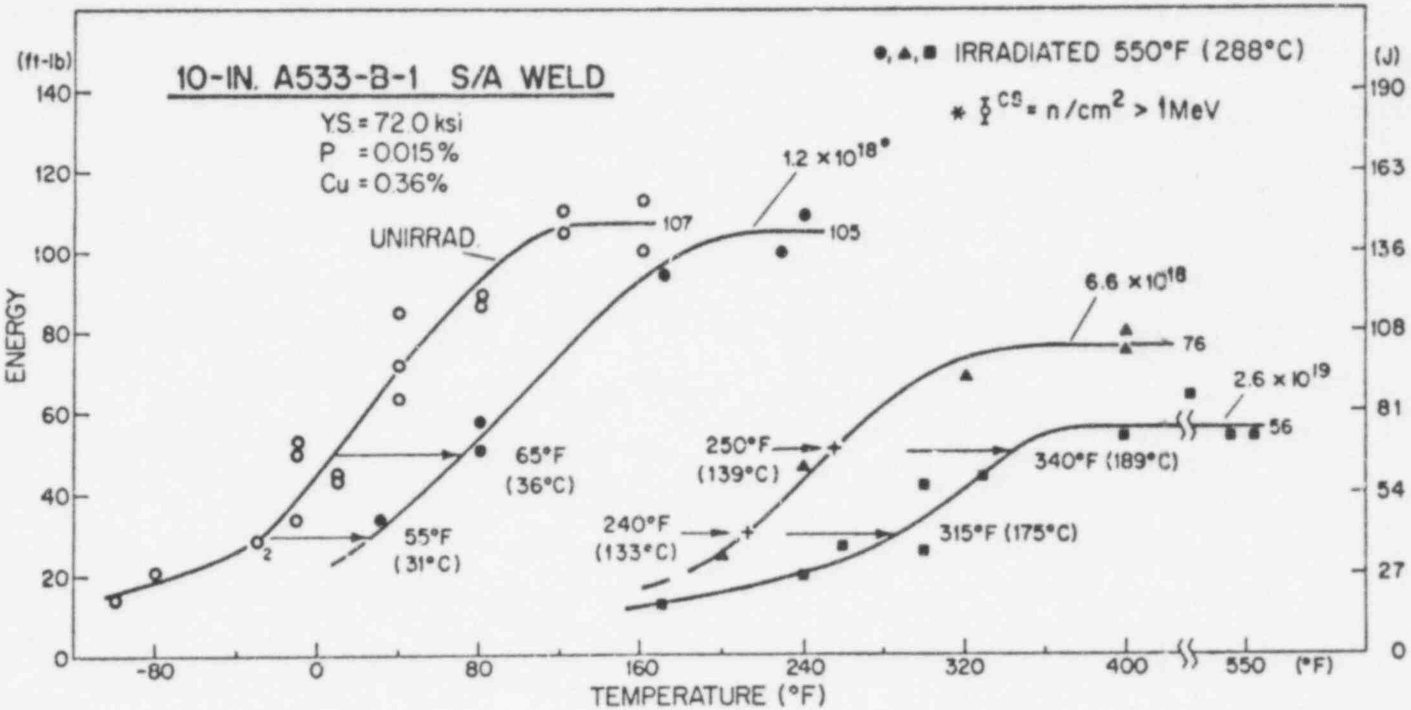

39

Fig. 10. Charpy-V notch ductility of a 0.36 percent copper content A533-B steel weld deposit before and after irradiation to three fluence levels. Note the significant elevation in transition temperature and absence of an upper shelf energy reduction with a low fluence of ~1.2 x 10¹⁸ n/cm >1 MeV.

815 045

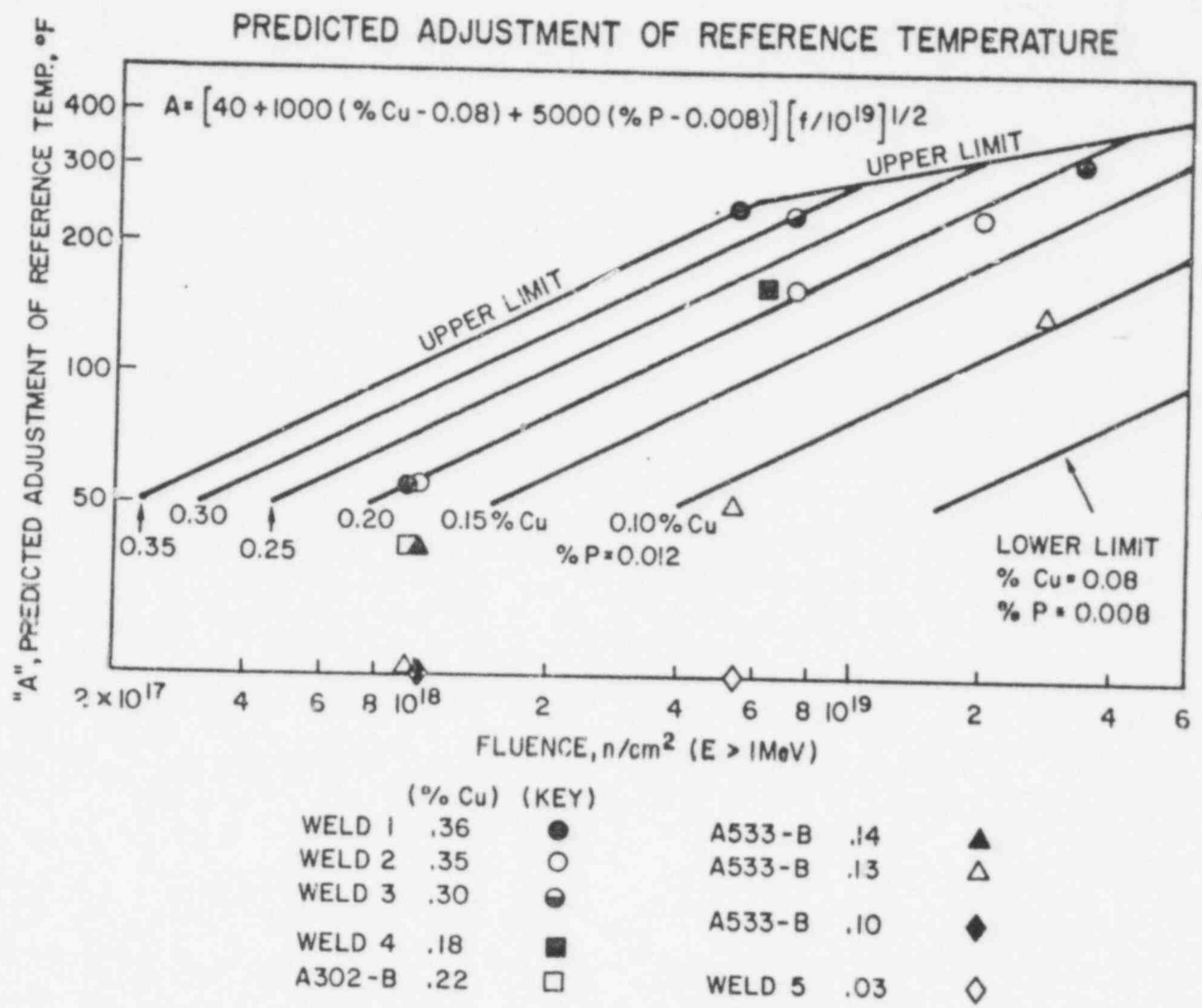

Fig. 11. Measured transition temperature elevations (C_v 41J, 30 ft-lb index) for several A533-B materials entered on Regulatory Guide 1.99 graph for projecting postirradiation transition temperature behavior.

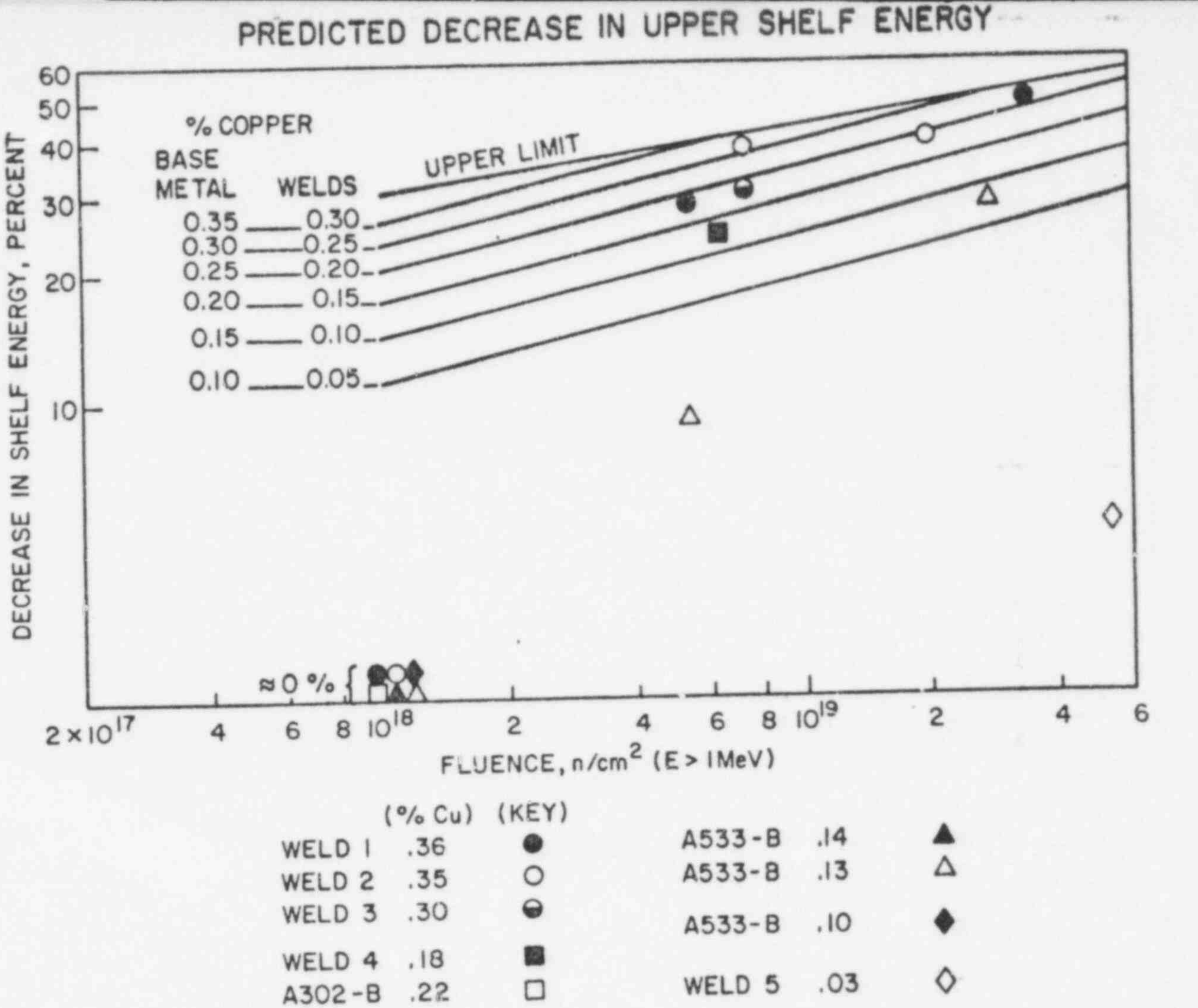

Fig. 12. Measured upper shelf energy degradations for several A533-B materials entered on Regulatory Guide 1.99 graph for projecting postirradiation upper shelf energy behavior. Note the apparent over-conservatism in Guide projections for low fluence exposure ($<1 \times 10^{18}$ n/cm^2).

is more readily affected by low fluence exposure compared to the change in the upper shelf; (c) measured upper shelf reductions are in good agreement with Guide projections at $\sim 6x10^{18}$ but not at $\sim 1x10^{18}$ n/cm^2. More importantly, the upper shelf reductions observed for test reactor irradiations (small) appear inconsistent with those by power reactor irradiations (4) (large) at $\sim 1x10^{18}$ n/cm^2. The inconsistency of test vs power reactor radiation effects revealed by the studies is considered to be an important area for future investigation.

III. NRC-CE-NRL Cooperative Program

J. R. Hawthorne

The NRC-CE-NRL Cooperative Program was established to complete the transfer to commercial practice of laboratory and demonstration test findings on the effects of steel impurities on radiation resistance. A specific objective was to establish trends in radiation resistance for A533-B materials representing progressive reductions in allowable copper content. Three series of materials were used: Series 1 (normal copper content, $\geq$0.15% Cu); Series 2 (low copper content, 0.10% Cu max); and Series 3 (extra low copper content, 0.06% Cu max).

Series 3 vs Series 2 investigations on relative notch ductility degradation have now been completed. The objective was to establish whether or not a greater degree of radiation resistance is obtained with a very low copper content (optimum steelmaking practice) compared to a low copper content (improved practice only). Figure 13 compares the results for the Series 3 materials to the trend observed for Series 2 materials. The trend for Series 1 materials is also shown. From these results, it is now established that a further reductuion in maximum allowable copper content from 0.10% Cu (new ASTM specifications) to 0.06% Cu (best steelmaking practice) will not substantially improve 288°C (550°F) radiation resistance for this type steel. It can also be concluded that, for most projected applications and fluence levels, the new ASTM (and AWS) specifications will serve the needs of industry well for radiation resistant vessel materials.

IV. 4TCT Program Support Studies

J. R. Hawthorne

Radiation assessments of NRC 4TCT program materials are being conducted to develop advance information on material upper shelf reduction vs fluence trends. The assessments, accomplished with Charpy-V specimens, were required to help establish proper exposure levels for the main (large 4TCT specimen) experiments.

815 049

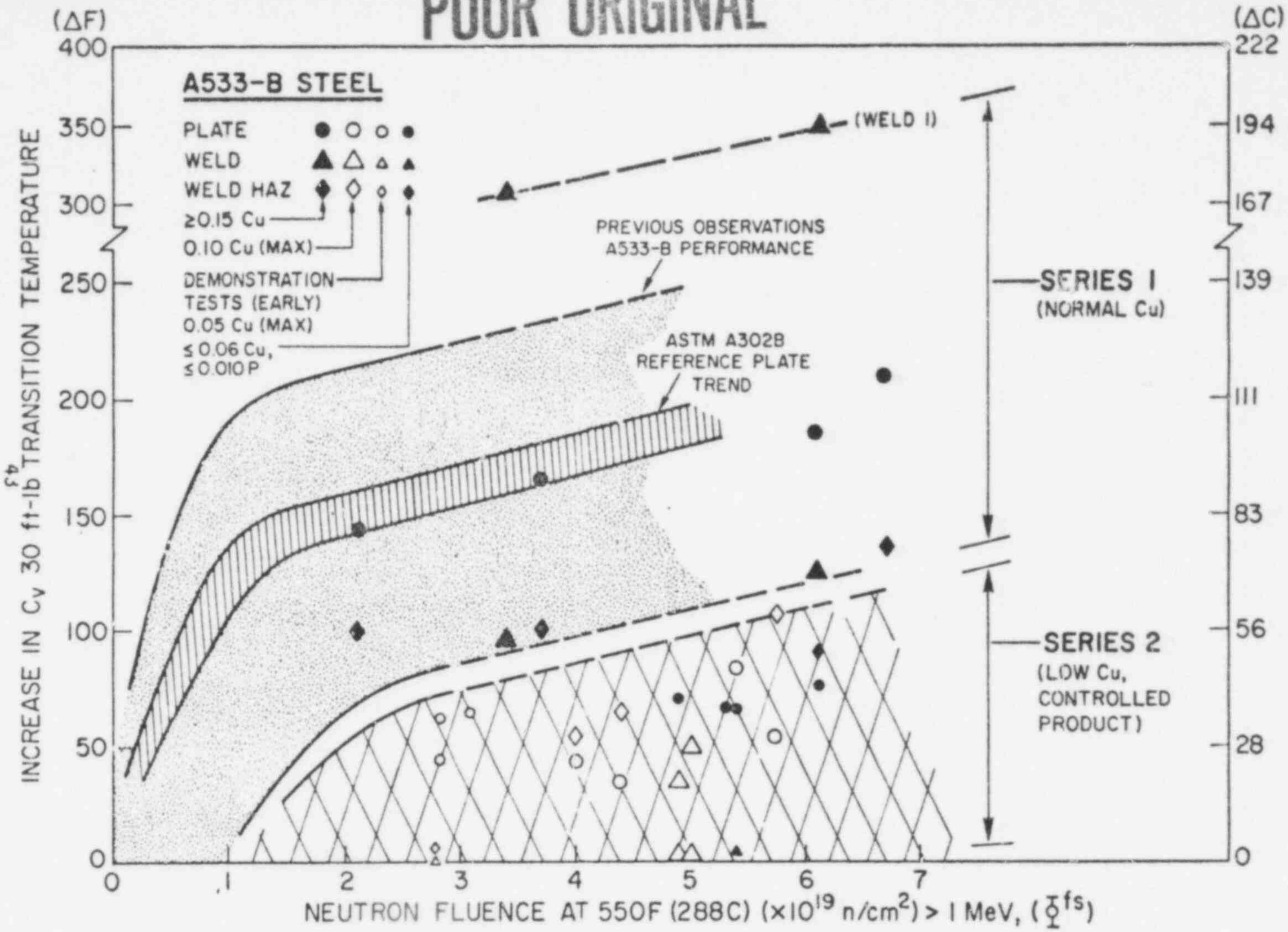

Fig. 13. Charpy-V transition temperature observations for Series 3 materials (small filled symbols) vs observations for Series 1 (large filled symbols) and Series 2 (large open symbols). Earlier determinations for extra-low copper content A533-B materials from commercial-scale demonstration tests are also shown. The Series 3 vs Series 2 results demonstrate comparable radiation resistance with 0.06% and 0.10% copper maximum, respectively representing best steelmaking practice vs improved practice to new ASTM and AWS supplement specifications.

815 049

Three radiation experiments were conducted in support of the 4TCT program this year. These experiments involved five welds from operating reactor plants that are expected to exhibit a high sensitivity to irradiation embrittlement. An example of the results from the NRL experiments is shown in Fig. 14 in which the upper shelf toughness has dropped to 49J (36 ft-lb) after irradiation to a relatively low fluence of 6.4×10^{18} n/cm^2 >1 MeV. The significance of this low upper shelf energy is being assessed in terms of fracture mechanics by the 4TCT specimens as part of the HSST program.

V. Influence of Metallurgical Variables on Upper Shelf Radiation-Anneal Behavior
J. R. Hawthorne

Systematic studies of metallurgical factors governing or contributing to the degree of upper-shelf degradation by irradiation and the extent of upper-shelf recovery by postirradiation heat treatment have been undertaken. As part of this effort, two exploratory investigations were initiated in FY-77. One focuses on the significance of initial (pre-irradiation) upper-shelf level to postirradiation upper shelf trends; the second was designed to explore the individual and joint contributions of sulfur, copper, and phosphorus impurities to steel behavior and involved specially prepared laboratory melts (Table II).

TABLE II

LABORATORY MELTS PREPARED FOR INVESTIGATION OF SULFUR, COPPER, AND PHOSPHORUS CONTENT EFFECTS ON POSTIRRADIATION UPPER SHELF

Melt*	Modification	Composition (Wt%)		
		S	P	Cu
1	A	.015	.003	.15
	B	.015	.015	.15
	C	.015	.025	.15
	D	.015	.025	.30
2	A	.025	.015	.03
	B	.025	.015	.15
	C	.025	.015	.30
	D	.025	.025	.30

*ASTM A302-B base composition.

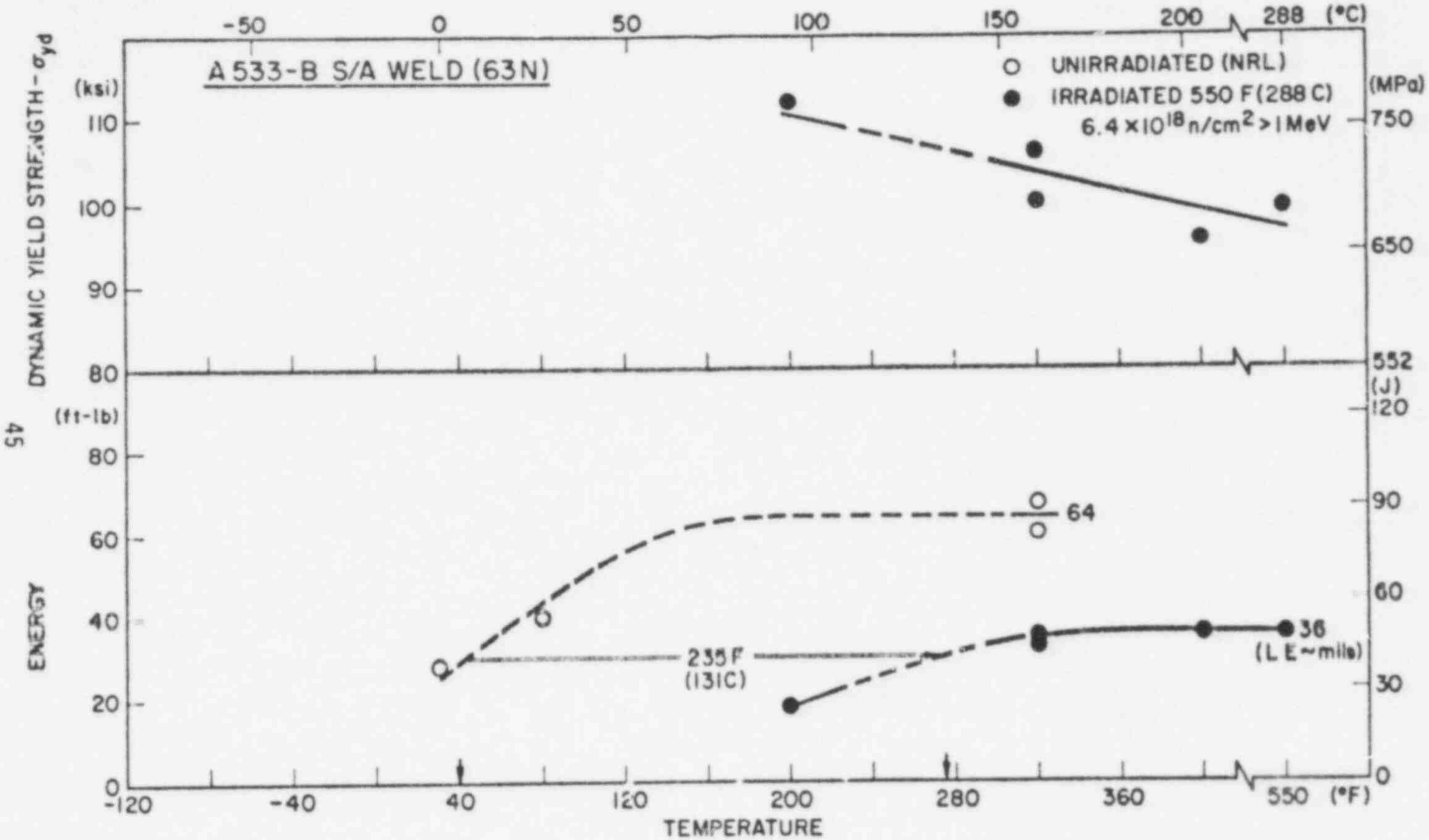

Fig. 14. Pre- and postirradiation Charpy-V notch ducti[illegible]y of weld 63N of NRC 4TCT program. Postirradiation dynamic yield strength deter[illegible]inations are also shown.

815 051

Preliminary findings include the observation of comparable radiation resistance in strong versus weak test orientations for the case of low copper content (radiation resistant) steel plate. (A companion test of high copper content plate with highly directional properties is planned.) In a companion test, a simulated weld heat affected zone showed a higher apparent radiation sensitivity than the base plate in the weak test orientation. Preliminary results from the second investigation suggest an effect of sulfur content on upper-shelf behavior (Fig. 15); however, alternate explanations for the experimental observations are under study.

Task D - Thermal Shock-Related Investigations

I. Investigation of Warm Prestress for the Case of Small ΔT During a LOCA
F. J. Loss, R. A. Gray, Jr., and J. R. Hawthorne

During a loss of coolant accident (LOCA) and operation of the emergency core cooling system, the inside wall of a nuclear pressure vessel is subjected to high thermal stresses (i.e., thermal shock) that may cause extension of a preexisting flaw. During this event, the applied K_I can achieve a maximum early in the transient as illustrated in Fig. 16. However, the maximum K_I may not exceed the critical (K_{Ic}) level for crack initiation until a later time at which the loading has decreased from its peak. The fact that the material was loaded, at elevated temperature, to a value that exceeds K_{Ic} at some lower temperature is termed warm prestress (WPS). It is believed that this phenomenon can preclude crack extension when K_I equals K_{Ic} during a thermal shock accident.

The potential benefit of WPS during a LOCA is that this phenomenon can result in a predicted crack extension that is much less than the value computed from an elastic analysis that does not consider WPS. In order to establish a technical basis for the use of WPS, an experimental program was undertaken in which notched three-point bend specimens were mechanically loaded to simulate the load vs temperature path in the region of a longitudinal flaw during a LOCA as in Fig. 16 (5).

This study verified the hypothesis that failure does not occur during the period when K_I decreases with time following WPS even though the K_I level exceeds the K_{Ic} of the virgin material. Furthermore, it was demonstrated that WPS produces an effective elevation in K_{Ic} whose magnitude depends on (a) the level of WPS,

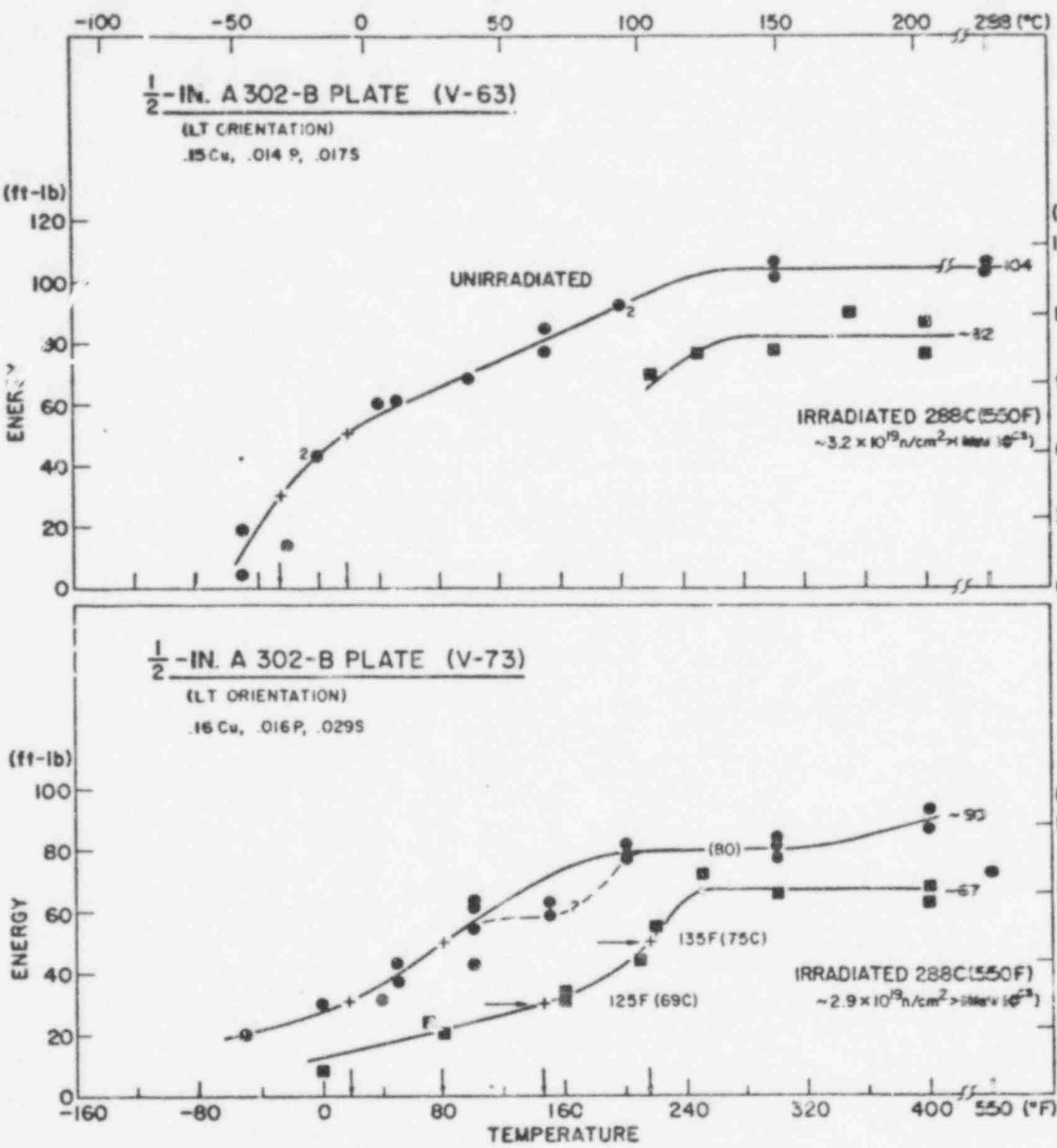

Fig. 15. Postirradiation Charpy-V upper shelf retention observed for two A302-B steel pl tes (laboratory melts) which differ in sulfur content.

815 053

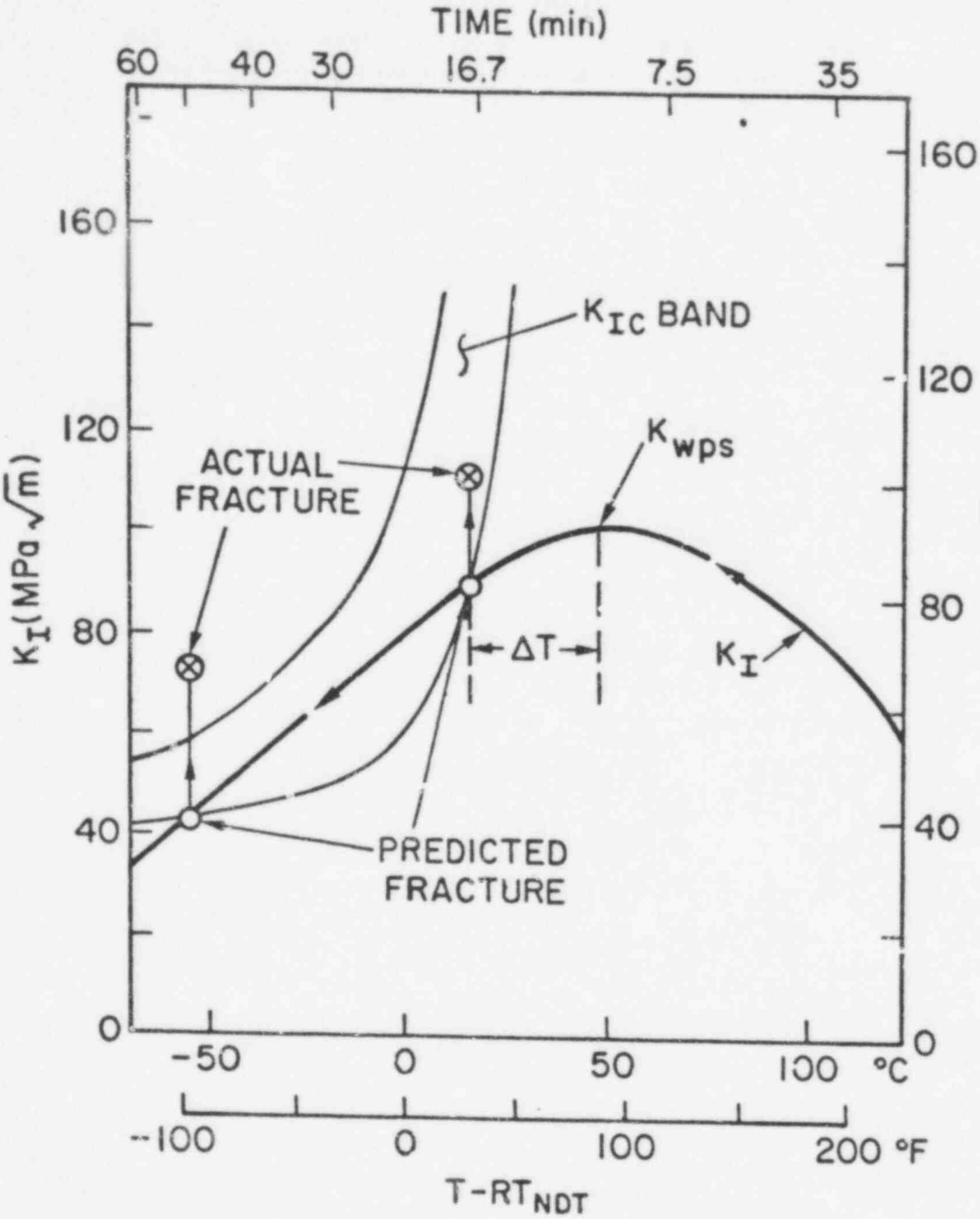

Fig. 16. Representation of the K_I levels at the tip of a longitudinal flaw in a nuclear pressure vessel during a LOCA-ECCS. The time scale originates with the LOCA: RT_{NDT} is the reference temperature for the material defined in Section III, ASME Boiler and Pressure Vessel Code.

(b) the magnitude of the ΔT between the temperature of WPS (T_{WPS}) and the failure temperature (T_F) (Fig. 16), and (c) the amount of unloading of the crack-tip region from the warm prestress level. These observations were used to project the degree of crack extension during a LOCA in a reference calculational model (RCM) (6) of a commercial, pressurized water reactor vessel. The RCM was used to construct a "worse-case" condition in terms of a steel that is highly sensitive to irradiation coupled with a high fluence level such as encountered near the end of vessel life.

The preceding program investigated a wide range of parameters that, in some cases, imposed conditions that were more severe than those projected for the LOCA-ECCS. Also, because of limited material availability, it was not possible to address the case of a small ΔT. Since the latter is characteristic of the projected behavior during a LOCA, a follow-on study was undertaken to demonstrate the phenomenon of WPS in terms of a small ΔT and to develop a correspondence with the results of the preceding program.

Investigation of a small ΔT presents certain difficulties in data interpretation. Because of the finite width of the K_{Ic} scatterband, coupled with a K_{WPS} level that must be imposed at a temperature above the K_{Ic} lower boundary, the failure levels also must lie within the K_{Ic} scatterband. Consequently, an uncertainty exists as to whether the specimen fracture level is in fact a consequence of the WPS or whether it is simply the result of K_{Ic} scatter. To address this question the program included the testing of many specimens at a single temperature to permit a statistical analysis.

The results of the current study (Fig. 17) are consistent with the trends evolved previously and therefore permit an optimistic assessment concerning vessel integrity during a LOCA. The major observations concerning the specimen behavior are (a) failure did not occur during the simultaneous unloading and cooling following WPS even though the critical K_{Ic} of the virgin material was attained, and (b) without exception, the failure level exceeded the level of WPS.

A statistical analysis of the specimen fractures within the K_{Ic} scatterband has demonstrated that WPS produces an increased resistance to crack initiation. For the case of a small ΔT it is therefore concluded that while WPS may not

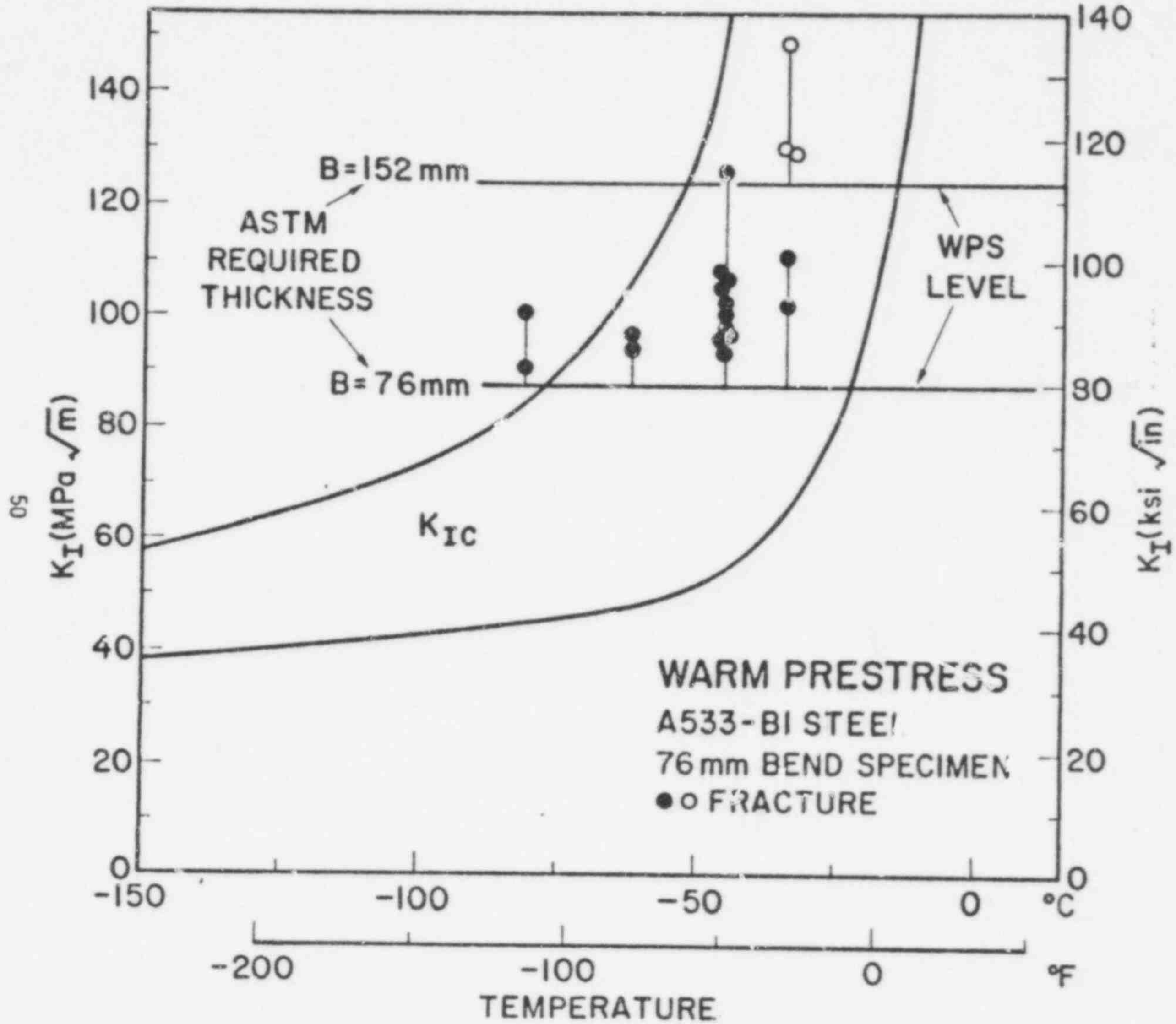

Fig. 17. Results of WPS experiments involving a small ΔT. Note that all failures are above the level of WPS that was imposed at a higher temperature.

elevate the toughness of a material whose K_{Ic} would be greater than K_{WPS}, it will produce an effective K_{Ic} elevation in material of lower toughness so that a value less than K_{WPS} will not be observed.

With respect to crack extension during a LOCA it was concluded that this event is precluded during the period of decreasing stress intensity with time following the WPS since this behavior removes a necessary condition for fracture initiation. However, minor temperature fluctuations in the ECCS water also will occur. This variation could result in a momentary reversal in the monotonic decrease in K_I at the crack tip. Fortunately, the present studies have demonstrated that minor perturbations in an overall decreasing K_I trend are not significant in that fracture is prevented unless the WPS level is exceeded.

Collectively, the two studies have provided a means for projecting vessel integrity during a LOCA-ECCS based upon the WPS phenomenon. While certain areas may require additional study to fully characterize vessel performance for all material conditions, it is concluded that WPS can provide a positive mechanism to limit crack extension during thermal shock. In terms of a reference calculational model of the vessel, under assumed worst case conditions, it was concluded that while WPS cannot prevent the initiation of shallow flaws, this phenomenon will limit crack penetration to a depth of one-third of the vessel wall. Thus WPS may form a key element upon which to base assurance of vessel integrity during a LOCA.

FUTURE RESEARCH PLANS

Task A - Fracture Toughness

In FY-78 we will continue to develop the unloading compliance technique and demonstrate its capability for testing in a hot cell. The method will be applied to characterize the upper shelf toughness of 1TCT specimens that have been irradiated as part of the IAR program. Size effects studies will also continue.

Task B - Fatigue Crack Propagation

Continue investigations of fatigue crack propagation as a function of environment (temperature, water chemistry, irradiation), loading variables (cyclic rate, waveform) and specimen size. Place new autoclave systems into operation. Develop a conservative data base to verify and improve ASME Code (Section XI) procedures relating to fatigue crack propagation

Task C - Radiation Sensitivity and Postirradiation Recovery

Complete exploratory investigation of steel irradiation - anneal - reirradiation properties behavior, including establishment of fracture toughness trends. Commence study of benefit of periodic annealing treatments to properties retention for other radiation exposure (fluence) conditions. Continue investigations of metallurgical factors influencing postirradiation upper shelf level and annealing response. Complete postirradiation studies on laboratory melt series having statistical variations in S, Cu, and P impurities. Commence radiation assessments on A508-2 steel forgings. Explore possible causes of inconsistency found between property changes produced by test reactor vs power reactor radiation exposures. Conduct investigations in support of NRC 4TCT program as required.

Task D - Thermal Shock Related Investigations

No further work is currently planned.

REFERENCES

1. Paris, P.C., Tada, H., Zahoor, A., Ernst, H., "A Treatment of the Subject of Tearing Instability," NUREG Report 0311, Aug 1977, U. S. Nuclear Regulatory Commission, Washington, D.C.

2. Bamford, W.H., Moon, D.M., and Ceschini, L.J., "Crack Growth Rate Testing in Reactor Pressure Vessel Steels," Fifth Water Reactor Safety Information Meeting, Gaithersburg, MD, 7-8 Nov 1977.

3. "Effects of Residual Elements on Predicted Radiation Damage to Reactor Vessel Materials," Regulatory Guide 1.99, U. S. Nuclear Regulatory Commission, Office of Standards Development, Washington, D.C., April 1977.

4. Private communication, P. N. Randall to J. R. Hawthorne, 19 Oct 1977.

5. Loss, F.J., Gray, R.A., Jr., and Hawthorne, J.R., "Significance of Warm Prestress to Crack Initiation During Thermal Shock," NRL Report 8165, Naval Research Laboratory, Washington, D.C., Sep 1977; also Proceedings, Fourth Intn. Conf. on Structural Mechanics in Reactor Technology, San Francisco, Ca., 15-19 Aug 1977.

6. Cheverton, R.D., Bolt, S.E., and Iskander, S.K., "Thermal Shock Studies Associated with Injection of Emergency Core Coolant in Pressurized Water Reactors," Proceedings, Fourth Intn. Conf. on Structural Mechanics in Reactor Technology, San Francisco, Ca., 15-19 Aug 1977.

CRITICAL EXPERIMENTS, MEASUREMENTS AND ANALYSES TO ESTABLISH A CRACK ARREST METHODOLOGY FOR NUCLEAR PRESSURE VESSEL STEELS

Contractor and Location

BATTELLE
Columbus Laboratories
505 King Avenue
Columbus, Ohio 43201

Principal Investigator

G. T. Hahn

The objective of this program is to provide a complete characterization of crack arrest as related to the primary system of LWR's and especially to the RPV's. This includes critical experiments to validate arrest theory and to verify dynamic analyses; development of a standard testing procedure, including specimen design; acquisition of an arrest toughness data base on RPV steels; and analyses using these data to assure safe operation of LWR's.

FY77 SCOPE

In 1977 the program was divided into a management task and the following 6 technical tasks.

(i) Dynamic Fracture Mechanics Analysis. A two-dimensional, dynamic analysis of an axial crack propagating radially in a cylinder subjected to thermal stress was assembled. A preliminary analysis of the ORNL Thermal Shock Experiment TSE-4 was compared with the results of the experiment. In addition, two-dimensional dynamic analyses of SEN and compact tension-type crack arrest test specimens were carried out.

815 059

(ii) Standard Test Practice. A test practice for measuring the crack arrest toughness, K_{Im} of unirradiated and irradiated nuclear steels and weldments was developed and proposed to ASTM.

(iii) Development of a Crack Arrest Toughness Data. Systematic measurements of the crack arrest toughness of pressure vessel steel and submerged arc weldment including several heats of both A533B and A508 were begun. Preparations for irradiating test specimens of a high copper weldment and the testing of samples in the irradiated conditions were also initiated.

(iv) Cooperative Test Program for Crack Arrest Toughness. A cooperative test program was organized to familiarize industrial laboratories with two test practices for measuring crack arrest toughness.

(v) Cooperative Program with the University of Illinois. Theoretical studies of a rapidly running crack in a DCB, CT and ring geometry were carried out under the direction of Professor H. Corten at the University of Illinois.

PROGRAM SUMMARY

The Battelle crack arrest program involves analysis and experimental work. Part of the research is being devoted to the development of two-dimensional, dynamic fracture mechanics analyses of crack arrest, initially of the events studied in the laboratory and those of structural interest. The analytical work is being carried out by P. C. Gehlen, C. Popelar, and M. R. Kanninen. Additional analysis is being carried out at the University of Illinois under the supervision of H. T. Corten. The experimental work is aimed at the validation of the analyses, the development of a crack arrest testing practice, and the establishment of a crack arrest data base for nuclear grades of steels. This phase of the work is being led by R. G. Hoagland, together with A. R. Rosenfield, C. W. Marschall, and G. T. Hahn. Overall responsibility for the program rests with G. T. Hahn.

The major accomplishments of FY 77 were the development of test procedures and the associated numerical analysis to the point that a reliable K_{Im} data base can be generated and the methodology validated by a cooperative test program. Initial inputs into the data bank were made. Substantial progress was made toward extending dynamic analysis to cracks propagating in cylinders under thermal stress.

Dynamic Fracture Mechanics Analysis

Two-dimensional, dynamic LEFM analyses of run arrest events in the compact tension specimen have been carried out using a finite difference procedure. The calculations treat stiff wedge loading and both ordinary and duplex specimens. The results obtained show that run-arrest events in the compact tension specimen (see Figure 1) have the same features as in the DCB (double cantilever beam) test piece. Cracks propagate at essentially constant velocity in the range 300 ms^{-1} to 800 ms^{-1}. Sinosoidal variations in the crack speed, shown in Figures 1a and 1b, appear to be an artifact of the model arising from the way crack blunting is simulated. Figure 1c illustrates that kinetic energy is returned to the crack tip and invalidates the static analyses of crack arrest for crack jumps $\Delta a/w > 0.25$.

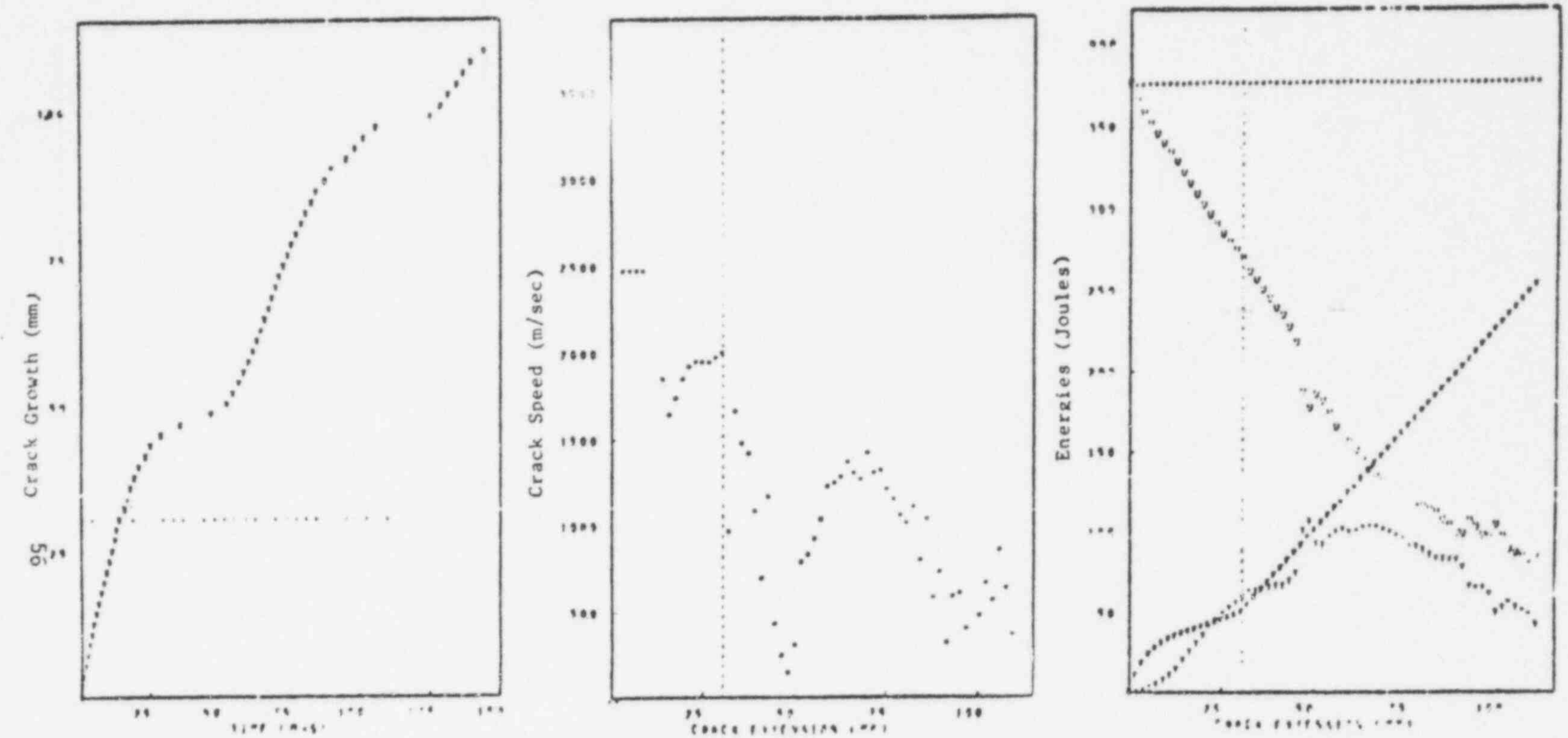

(a) (b) (c)

FIGURE 1. RUN-ARREST EVENT IN A COMPACT TENSION SPECIMEN CALCULATED WITH THE 2-D, DYNAMIC FINITE DIFFERENCE DIFFERENCE MODEL FOR $K_Q/K_{Im} = 1.5$.

(a) Crack growth versus time,
(b) Crack speed versus crack extension, and
(c) Energy components versus crack extension.
The broken line indicates the position of the weld line in the duplex specimen.

For smaller jumps the statically calculated value of stress intensity at arrest, K_{Ia} provides a good approximation of K_{Im} the crack arrest toughness of the material*. For larger jumps, K_{Ia} increasingly underestimates the arrest toughness (see Figure 2).

The calculations provide a set of reference curves defining the relations among the crack jump, Δa, the stress intensity ratio $\frac{K_Q}{K_{ID}}$ (or $\frac{K_Q}{K_{Im}}$) and the crack velocity, v. Reference curves for the compact tension of specimen are reproduced in Figures 3 and 4. The reference curves are similar to those previously obtained for DCB specimens and make it possible to infer K_{ID} (or K_{Im}) and crack velocity from measurements of K_Q and Δa.

The finite difference procedure has also been translated into polar coordinates to treat the problem of a long axial crack in a cylinder that propagates radially under the action of thermal stress. The aim of this work is to provide dynamic analyses of the ORNL TSE's (Thermal Shock Experiments) and of hypothetical thermal shock events in full scale vessels. Results have been obtained for the model of TSE-4 shown in Figure 5. The static stress intensity calculated at the onset of crack extension is very close to the value derived by ORNL from a finite element analysis. A preliminary dynamic analysis of this experiment, $\Delta a/w \approx 0.1$, indicates that the crack propagates with essentially constant velocity (Figure 6) and that no kinetic energy is returned in this case (Figure 7).

---

*The quantity K_{ID} is the material toughness encountered by the propagating crack which can be a function of crack velocity. The quantity K_{Im} is the minimum value of K_{ID} with respect to crack velocity. The quantity K_{Im} is is regarded as the crack arrest toughness of the material because stress intensity values smaller than this minimum cannot sustain continued propagation. The quantity K_{Ia}, also called the crack arrest toughness is an estimate of K_{Im} obtained from a static analysis of a run arrest event.

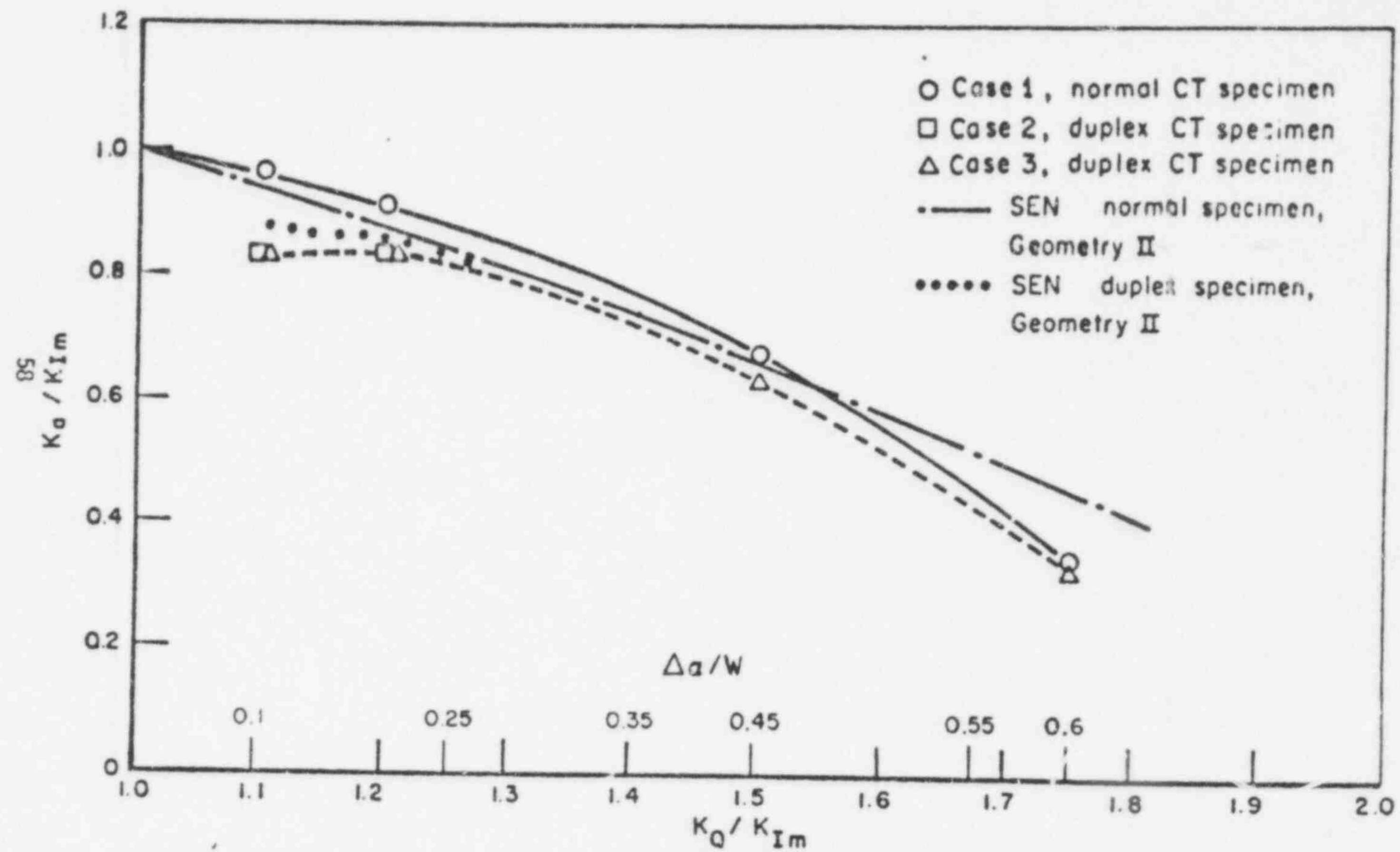

FIGURE 2. INFLUENCE OF THE RELATIVE INITIATION STRESS INTENSITY LEVEL AND $\Delta a/W$ ON THE K_{Ia}/K_{Im} RATIO

The SEN data are taken from Figure 2.23 of BMI-NUREG-1966, 1977.

815 064

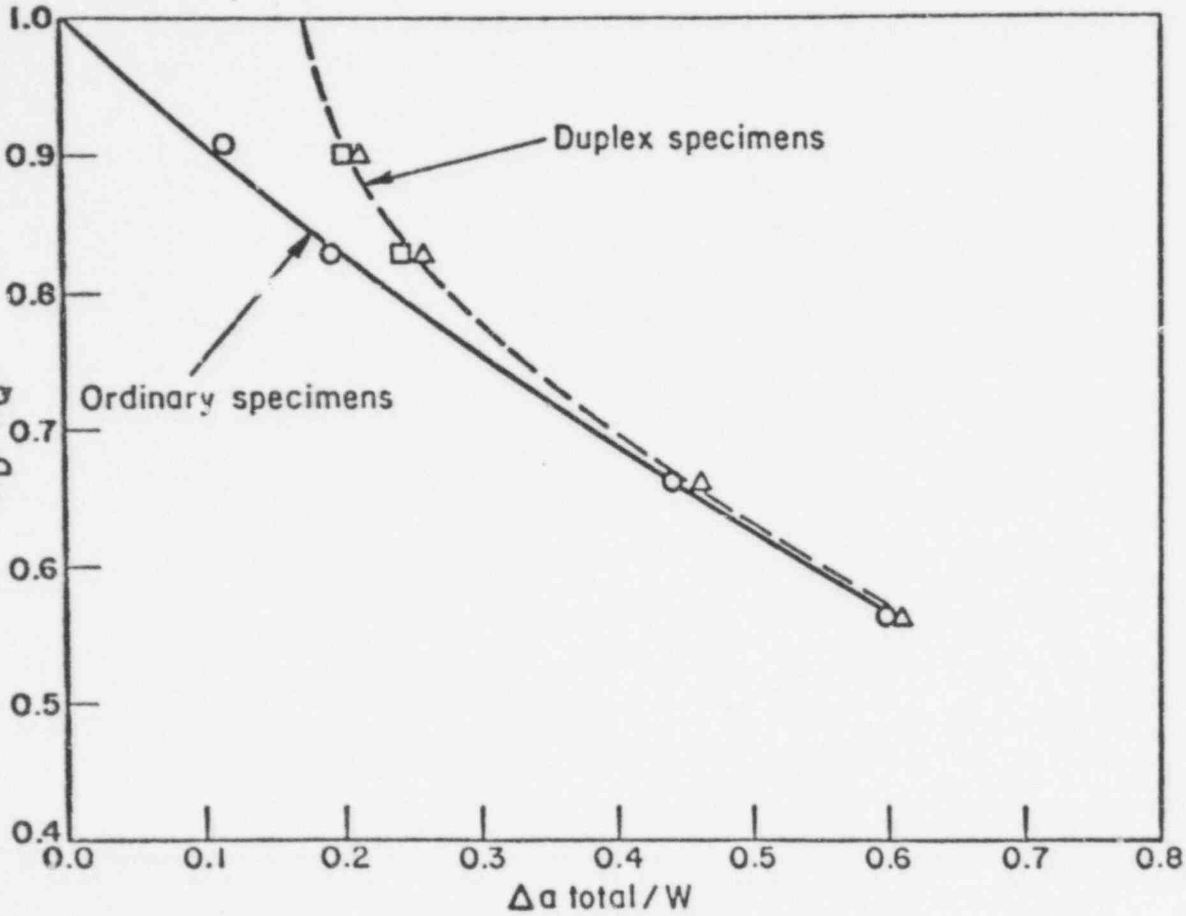

FIGURE 3. REFERENCE CURVES FOR ORDINARY AND DUPLEX COMPACT TENSION TEST SPECIMENS SHOWING THE RELATION BETWEEN $\Delta\bar{a}/W$ and K_{ID}/K_Q and K_{IDm}/K_Q

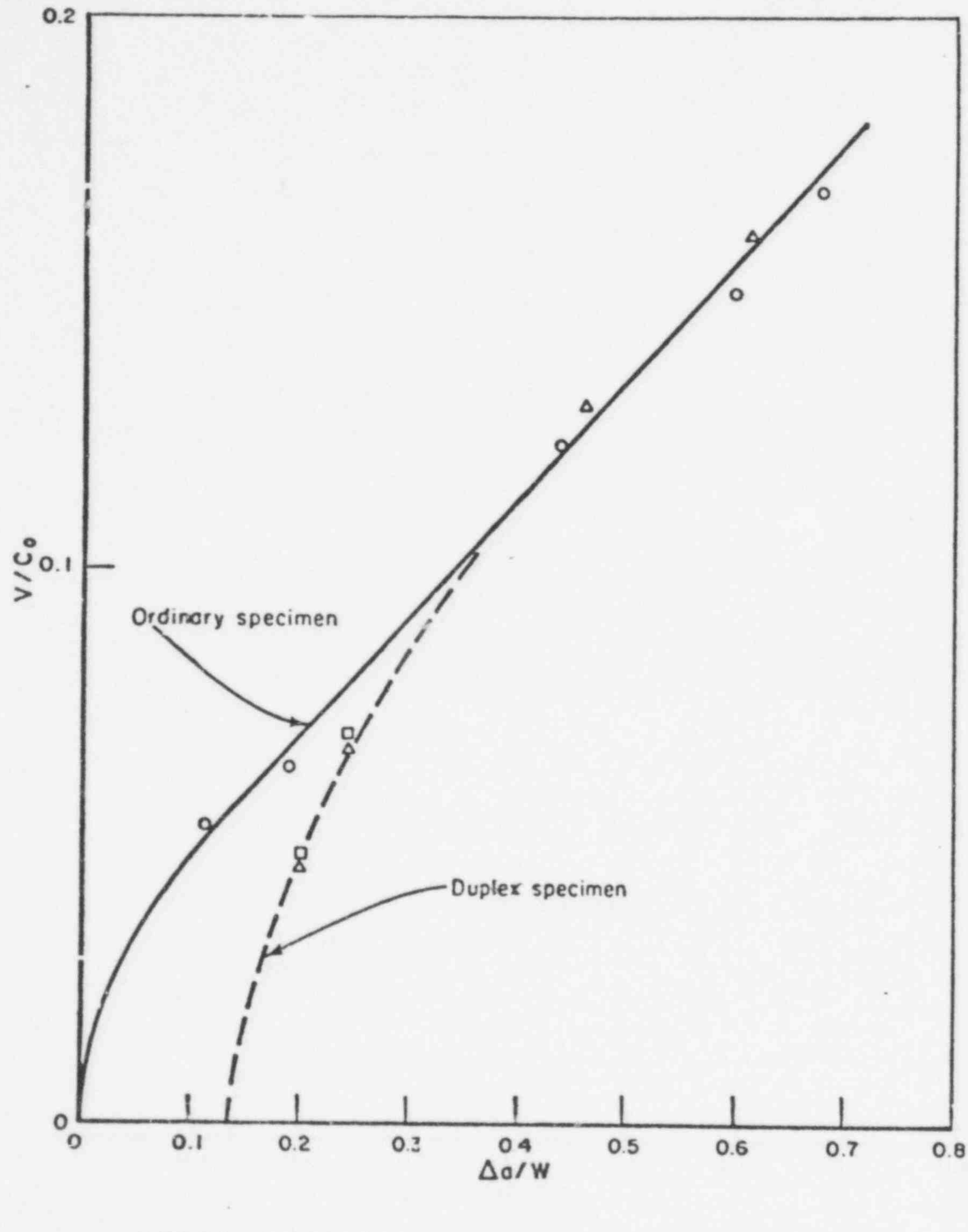

FIGURE 4. REFERENCE CURVES FOR ORDINARY AND DUPLEX COMPACT TENSION (CT) SPECIMEN SHOWING THE RELATIONSHIP BETWEEN $\Delta a/W$ and V/C_o

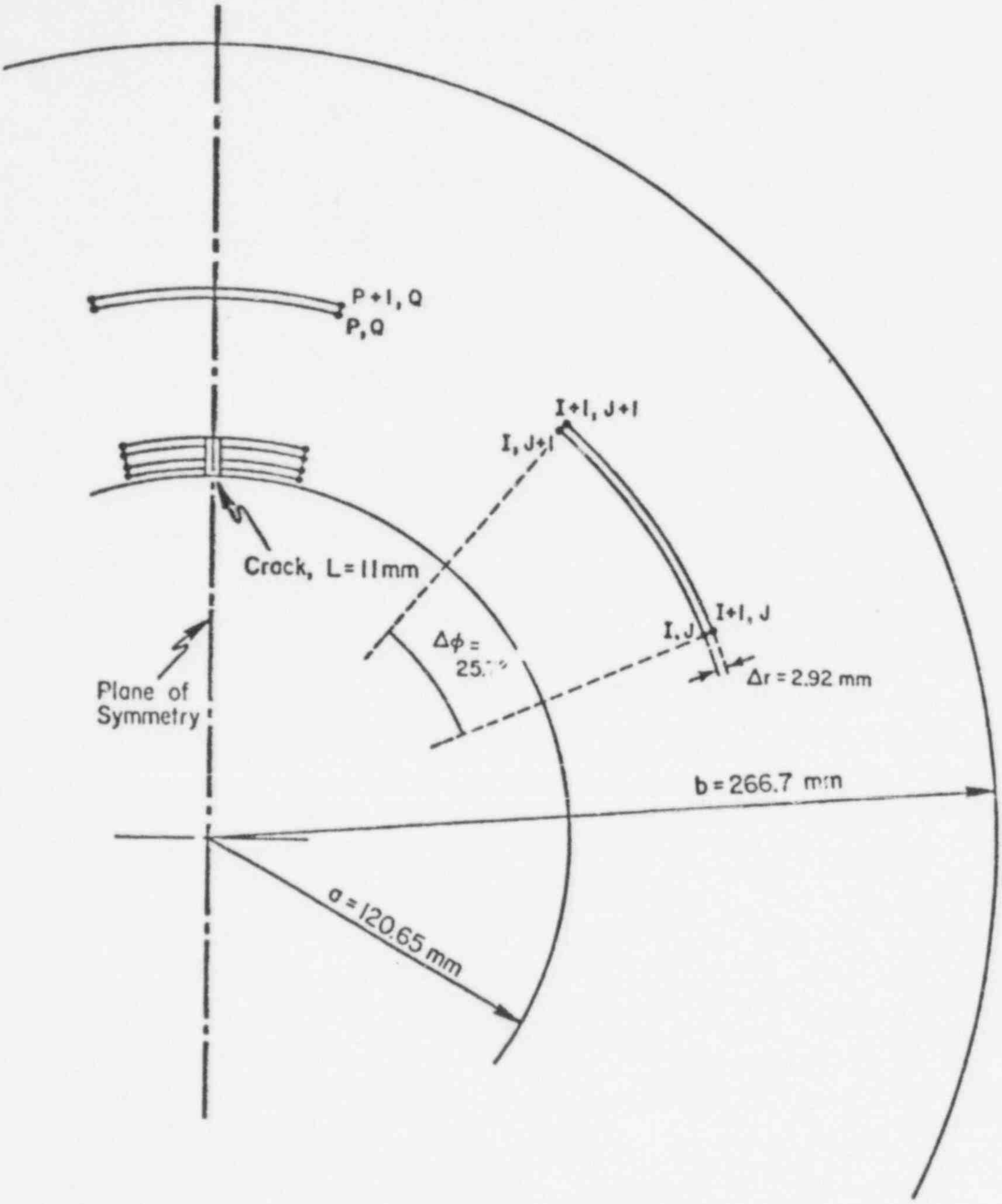

FIGURE 5. POLAR COORDINATE FINITE DIFFERENCE MESH FOR CYLINDER WITH LONG AXIAL CRACK PROPAGATING RADIALLY

815 067

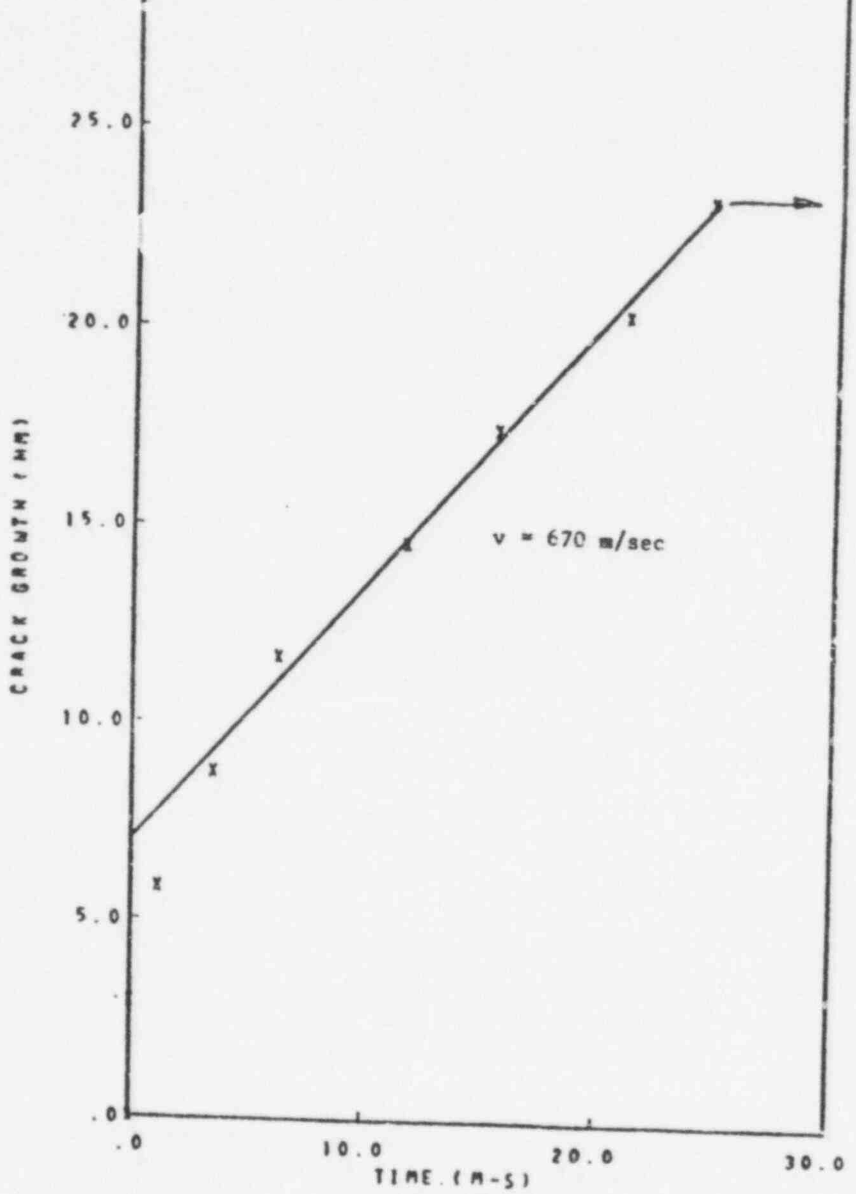

FIGURE 6. CALCULATED VARIATION OF CRACK LENGTH WITH TIME FOR TSE-4 FOR $K_Q/K_{Im} = 1.3$

815 068

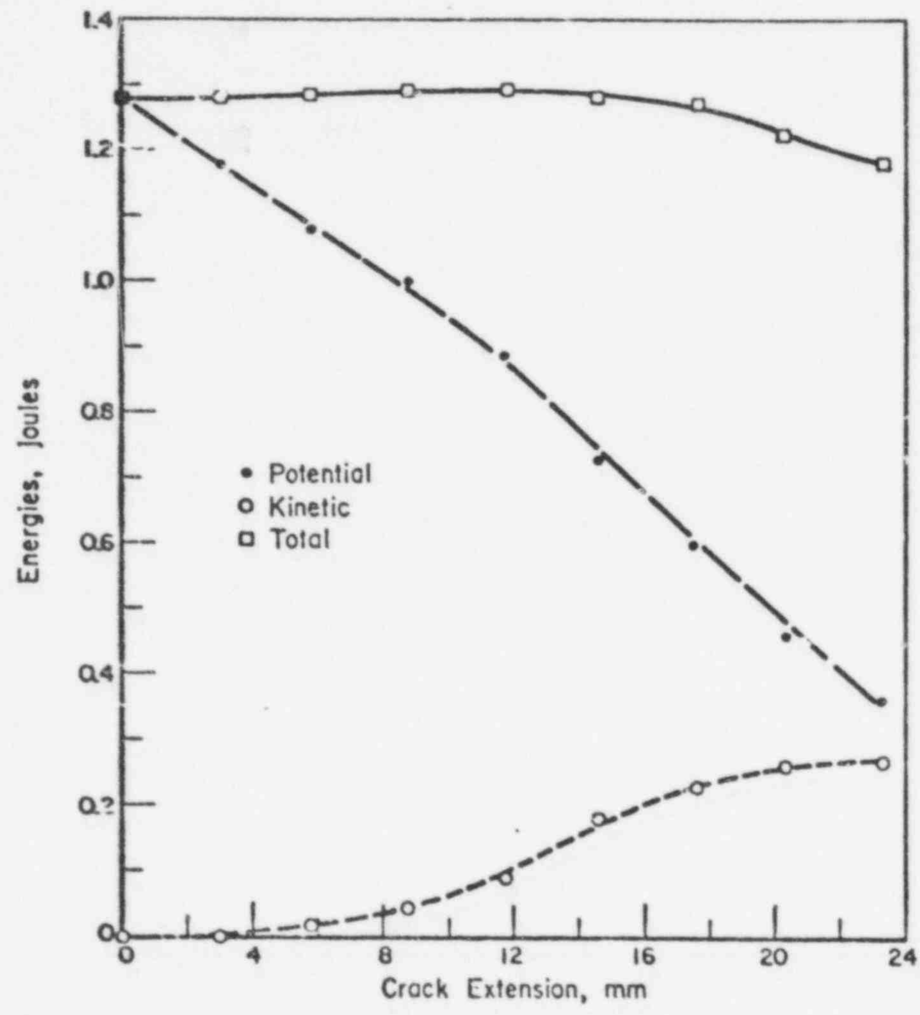

FIGURE 7. CALCULATED VARIATION OF ENERGY COMPONENTS WITH CRACK EXTENSION IN TSE FOR K_Q/K_{Im} = 1.3

Standard Test Practice

A relatively simple test method for measuring K_{ID} and K_{Im}-values with ordinary and duplex DCB and compact tension specimens has been developed. The method employs the reference curves obtained with the dynamic analyses which are valid provided the loading system is stiff and relatively little energy is exchanged between the loading system and the test piece while the crack is propagating. In this case K_{ID}- and K_{Im}-values can be inferred from 2 simple static measurements: (i) the load point displacement at the onset of propagation (which defines K_Q) and (ii) the crack jump length Δa (obtained by heat tinting after the jump). A practical procedure that embodies these features with a measuring capacity for $K_{Im} \lesssim 200$ MPam$^{1/2}$: "Proposed Tentative Method of Test for Fast Fracture Toughness and Crack Arrest Toughness" has been submitted to ASTM E24.03.04.

Fully instrumented crack arrest experiments were carried out on compact tension specimens to verify the proposed test procedure. Initial studies employed the pin-loaded, longitudinal wedge-loading arrangement previously developed for DCB specimens (see Figure 8). The experiments revealed surprisingly large arm movements during the run arrest event as illustrated by the results for Specimen DA-59 in Figure 9. In addition, crack jumps were substantially larger than those predicted for the measured crack velocities as shown in Figure 10. These effects were traced to inadequate load system stiffness, which result in the transfer of additional strain energy (the excess energy in Figure 10) to the test piece while the crack is running.

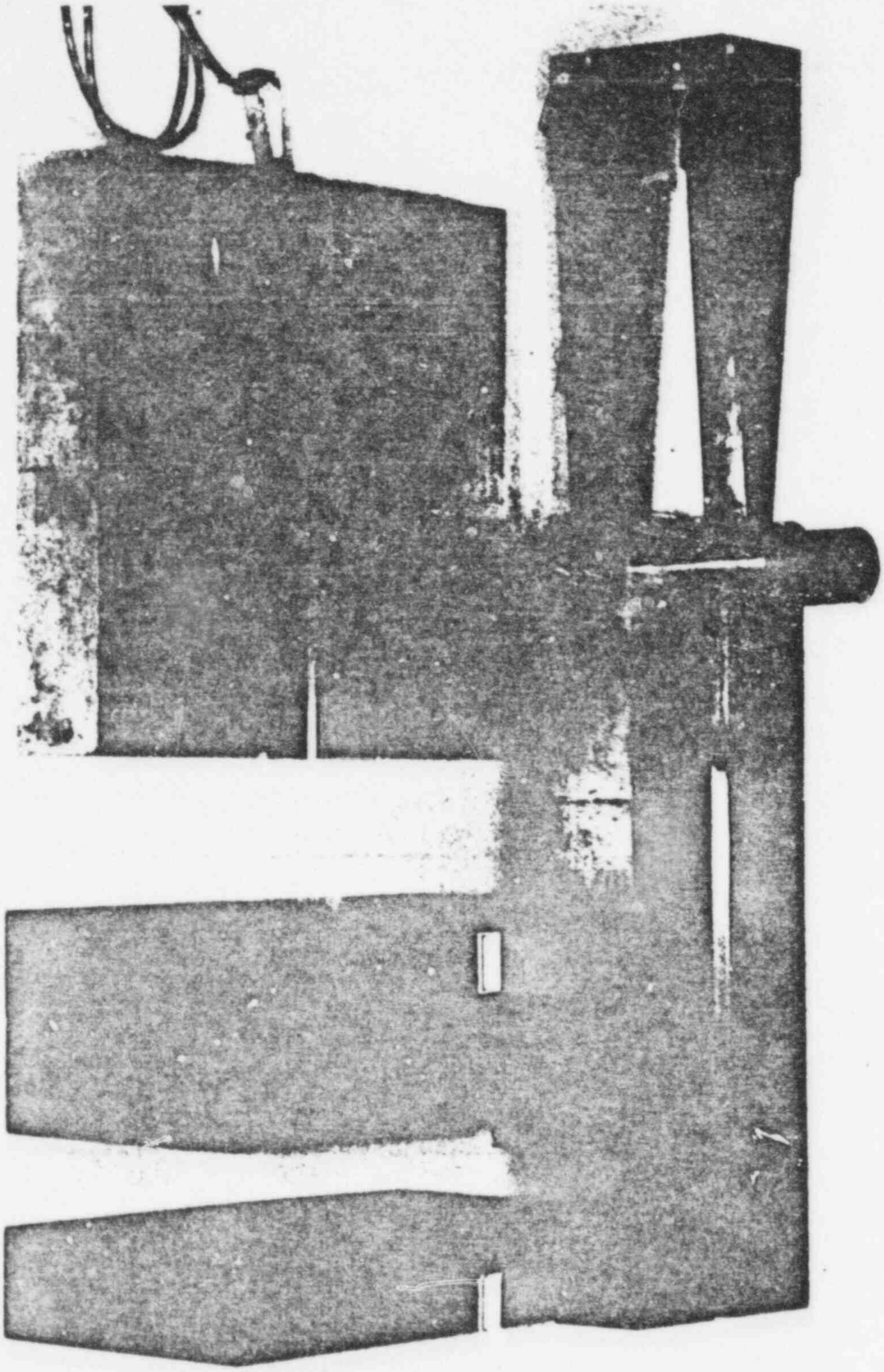

FIGURE 8. COMPACT TENSION AND DCB TEST SPECIMEN DESIGN SHOWING LONGITUDINAL WEDGE, PIN LOADING ARRANGEMENT, AND DISPLACEMENT GAGE

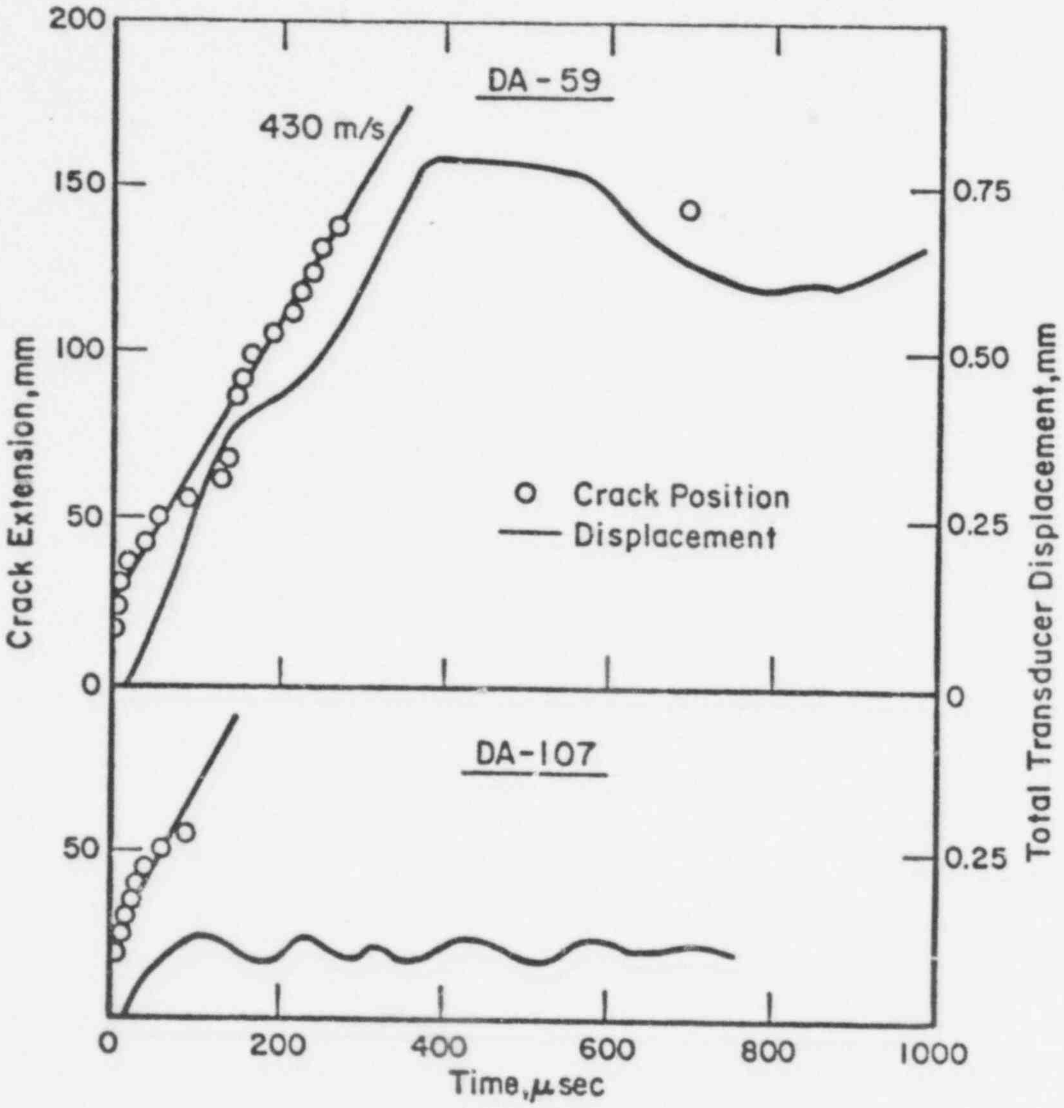

FIGURE 9. DISPLACEMENT OF THE ARM OF THE COMPACT TENSION SPECIMEN DURING A RUN-ARREST EVENT. Top: longitudinal wedge; bottom: transverse wedge

815 072

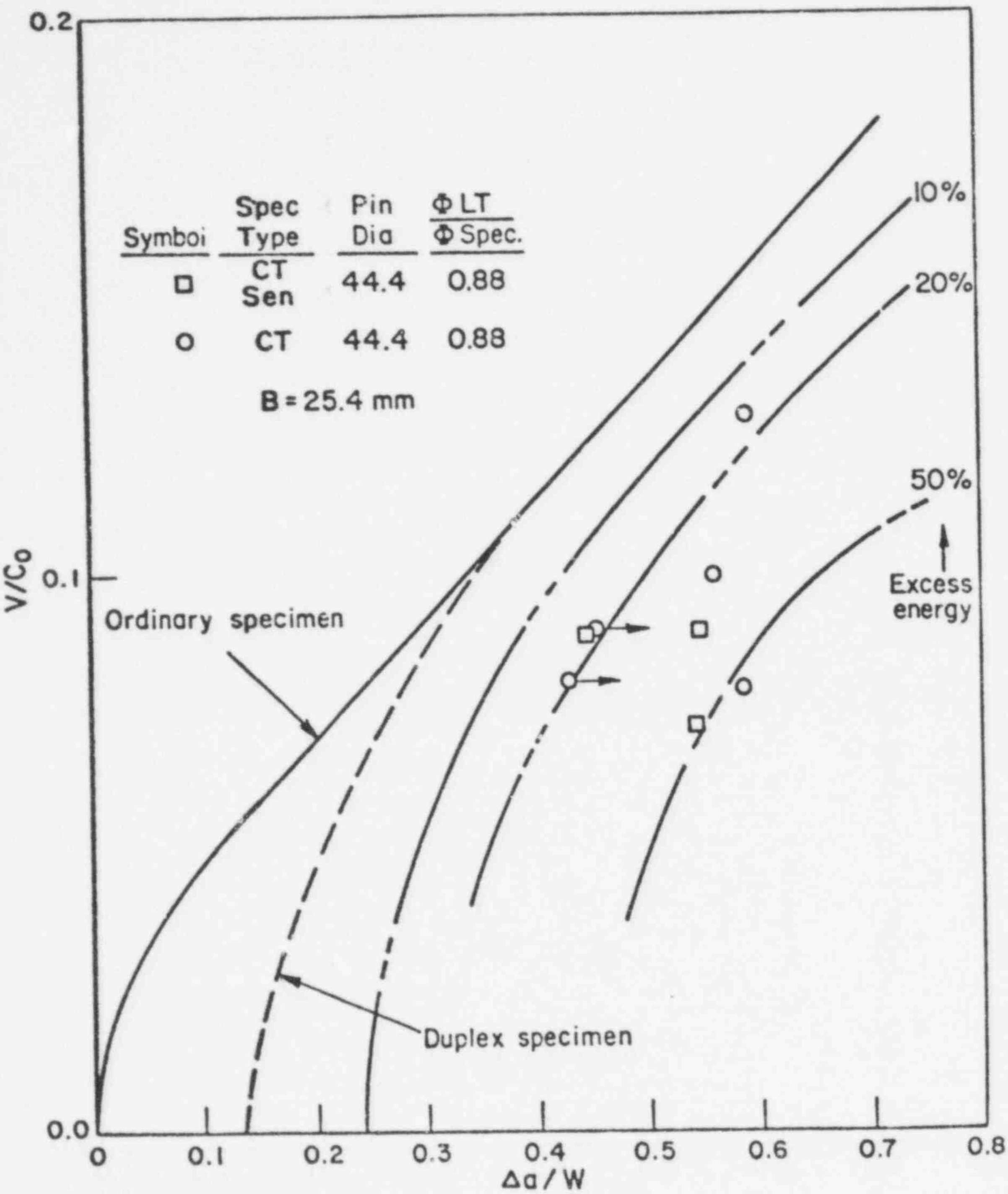

FIGURE 10. COMPARISON OF THE MEASURED AND CALCULATED RELATION BETWEEN CRACK VELOCITY AND CRACK JUMP DISTANCE IN THE CT SPECIMEN

An alternative loading system, involving transverse wedging through a single hole in the test piece was found to be ~10x stiffer. The configuration of the specimens and wedge are shown in Figure 11. The substantial reduction in load system compliance can be seen in Table 1. Results of instrumented tests of compact tension specimens with transverse wedging were found to agree with the dynamic analysis (see Figure 12) and provide verification for the reference curves.

Data Base

Systematic measurements of the crack arrest toughness, K_{Im}, of nuclear grades of steel are underway. The measurements employ the proposed test method, 2 in-thick compact tension and DCB specimens, and are being carried out in the range RTNDT to RTNDT + 100 C. The program includes A533B (2 heats), A508, a weldment (Type MIL-B-4 high manganese-molybdenum filler wire with Linde 0091 flux), samples from the "quenched-only" A508 Thermal Shock Experiment, and irradiated A533B and weldment. Preliminary results in Figure 13 indicate that K_{Im}-values are close to K_{Ic}, well above both the K_{IR}-curve and the trend for K_{Id}-values.* The K_{Im}-values are believed to be larger than K_{Id} because of the many ductile ligaments generated by the cleavage fracture process. Examples of these ligaments can be seen on the broken and heat tinted fracture surface as illustrated in Figure 14.

---

*The quantity K_{Id} is the material toughness experienced by a rapidly loaded stationary crack.

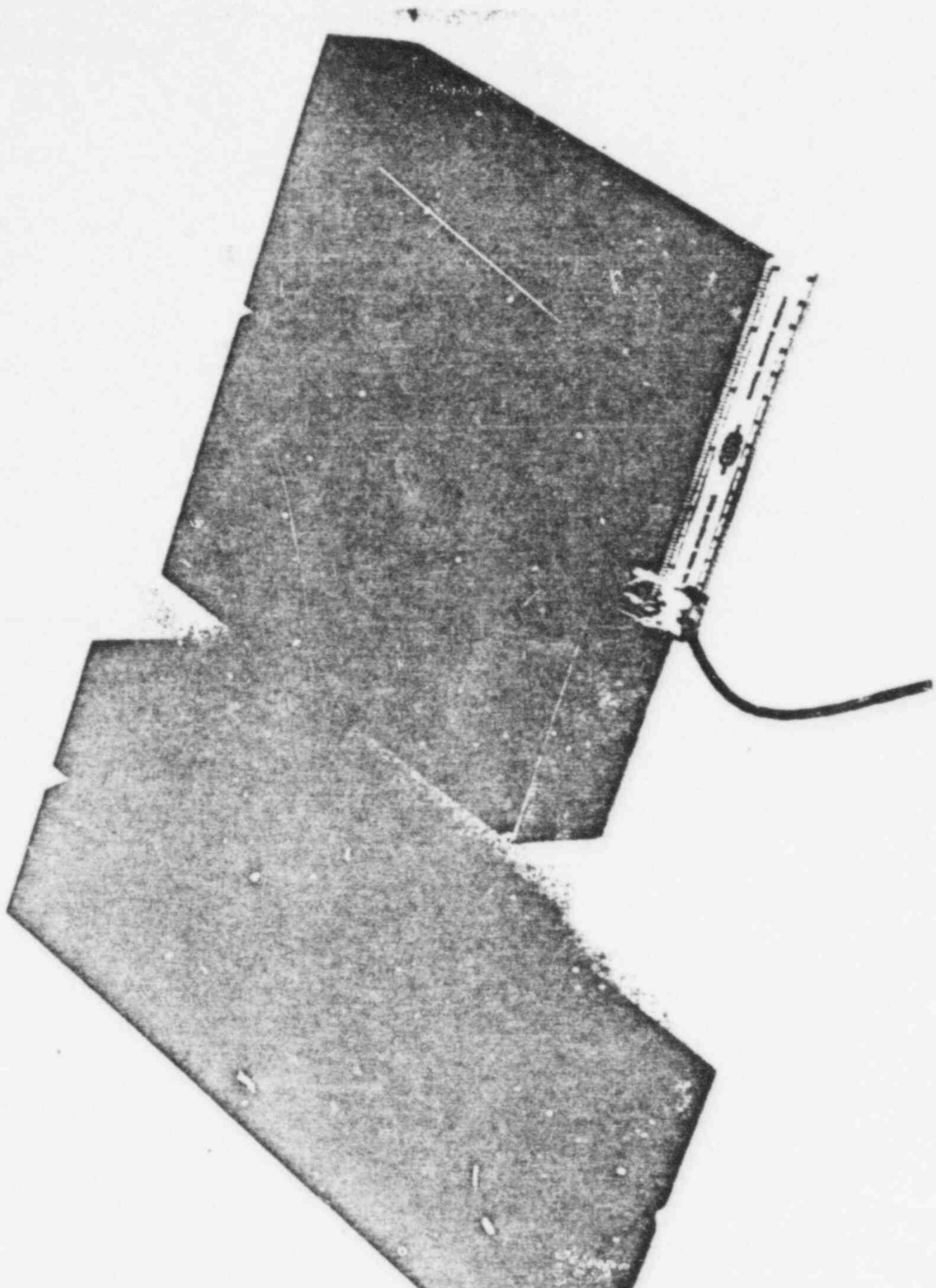

FIGURE 11. NEW COMPACT TENSION AND DECB SPECIMEN DESIGN SHOWING TRANSVERSE WEDGING ARRANGEMENT AND DISPLACEMENT GAGE

TABLE 1.

COMPARISON OF THE RATIO OF LOAD TRAIN-TO-SPECIMEN COMPLIANCE FOR SEVERAL LOADING CONFIGURATIONS

Loading Method	$\frac{\phi_{LT}}{\phi_{spec}}$
Longitudinal Wedging	
25 mm thick CT; 44 mm dia. round pins	0.88
25 mm thick CT; 44 mm dia. pins with 19 mm wide flats	0.52
25 mm thick CT; 58.7 mm dia. pins with 19 mm wide flats	0.42
Transverse Wedging	
50 mm thick CT; 52 mm dia. split pin	0.053

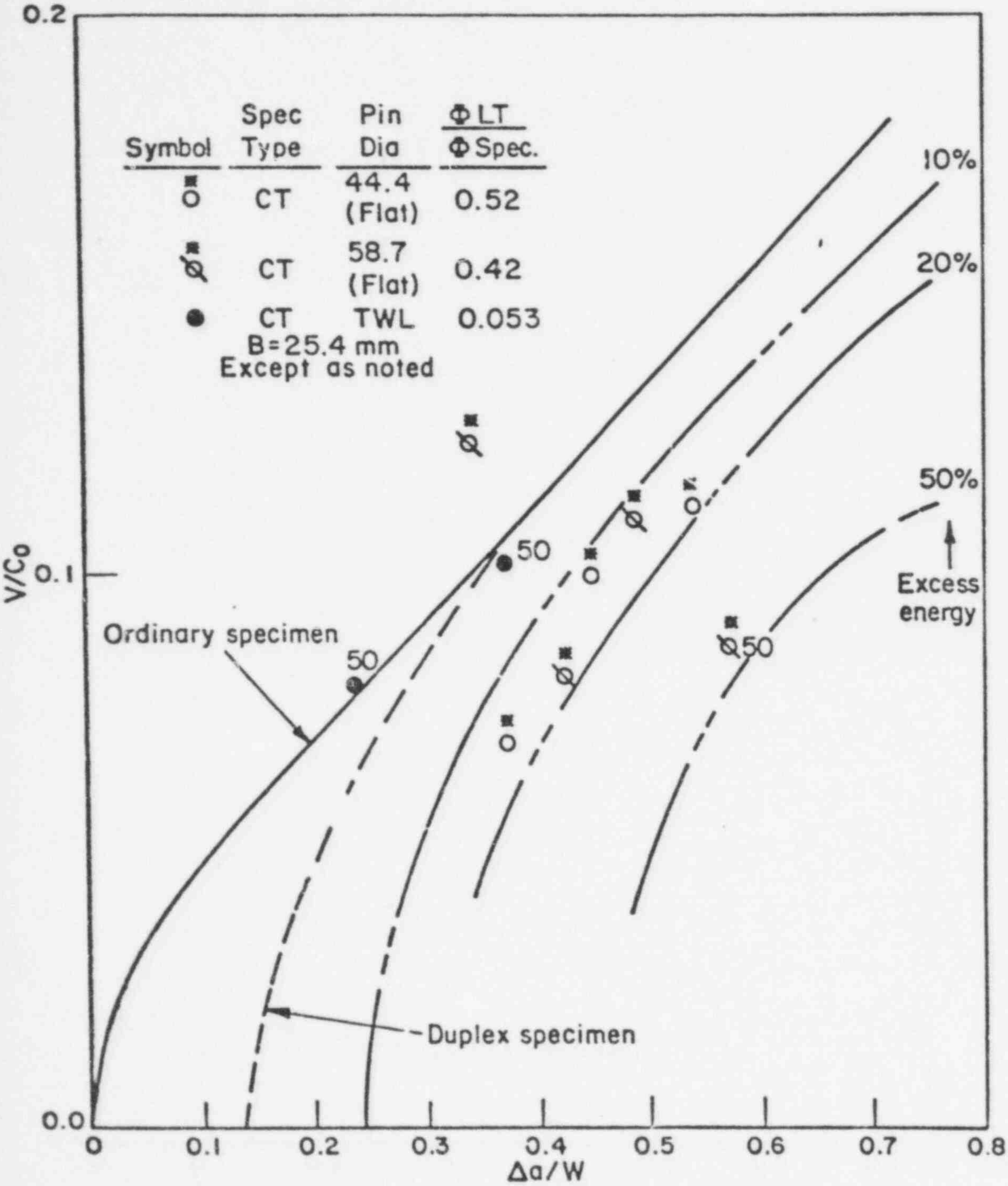

FIGURE 12. COMPARISON OF THE MEASURED AND CALCULATED RELATION BETWEEN CRACK VELOCITY AND CRACK JUMP DISTANCE IN THE CT SPECIMEN

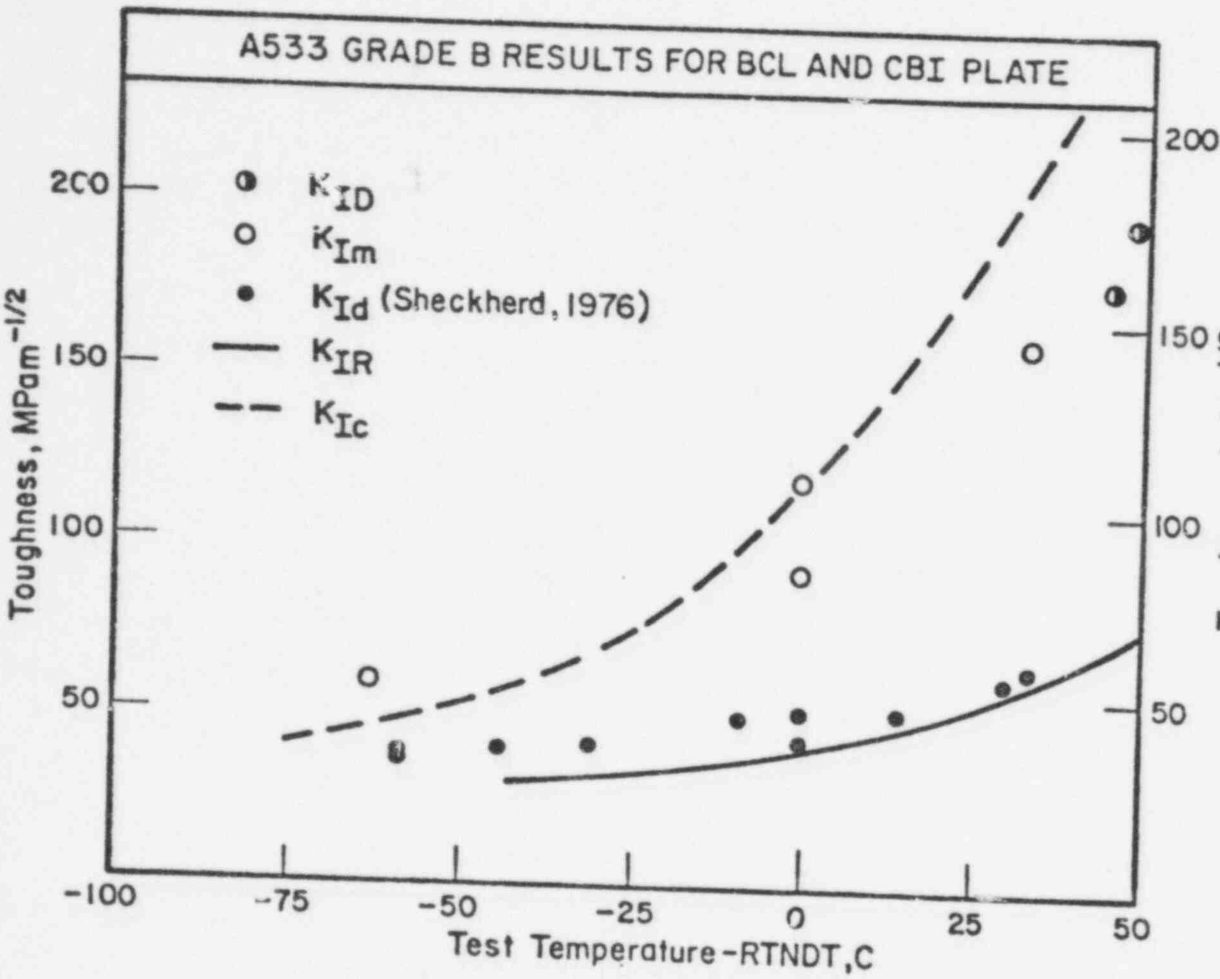

FIGURE 13. SUMMARY OF K_{ID}, K_{Im}, K_{Id}, K_{Ic} and K_{IR} VALUES FOR A533B STEEL

815 078

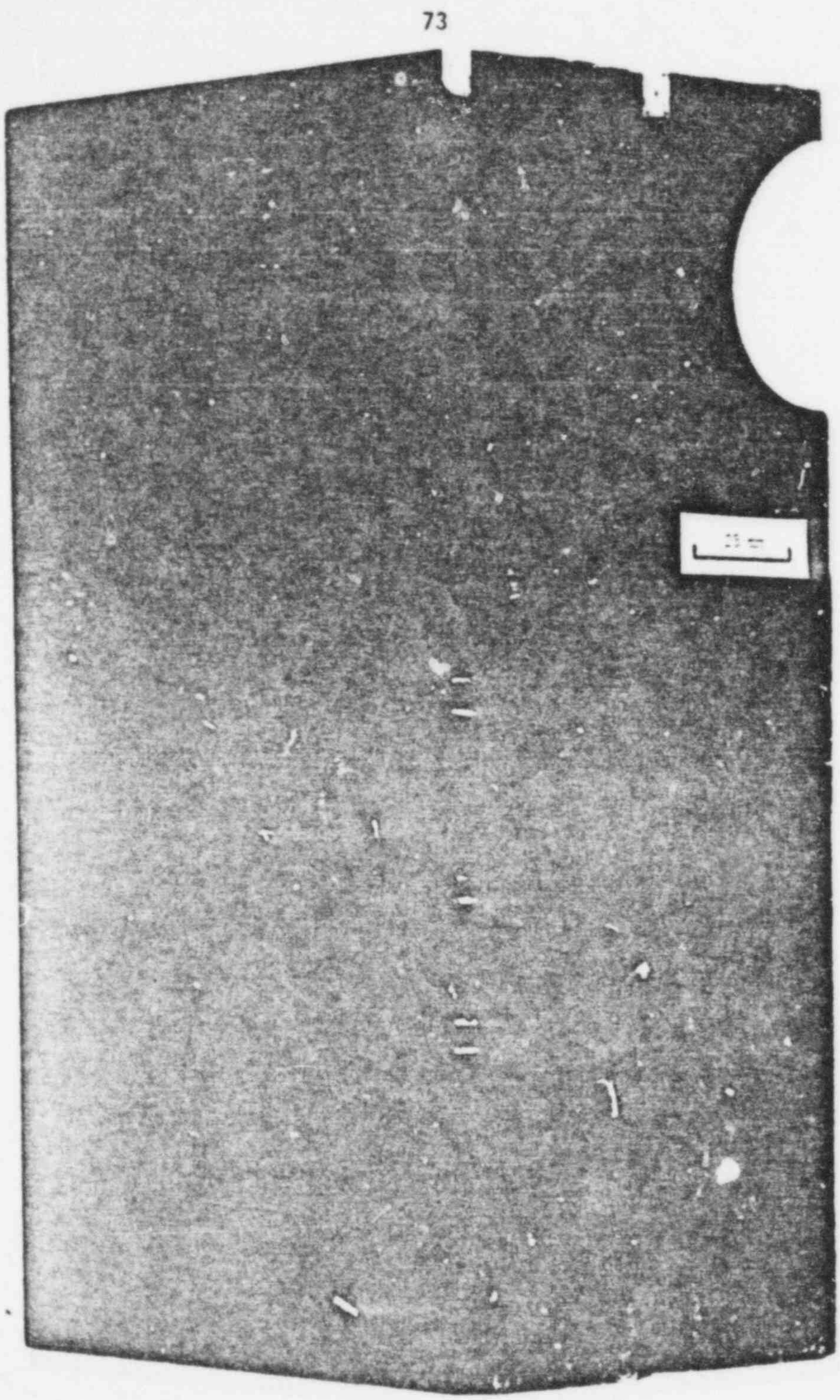

FIGURE 14. BROKEN COMPACT SPECIMEN AFTER HEAT TINTING TO REVEAL ARRESTED CRACK FRONT

Cooperative Test Program

A cooperative test program on crack arrest toughness measurements, was organized and will be carried out in 1978, under the auspices of ASTM Subcommittee E24.03.04 on dynamic testing and its Dynamic Initiation and Crack Arrest Task Group. The program is designed to familiarize potential test users with two candidate crack arrest toughness measurement procedures. Each participant will receive 10 test pieces made of a common plate of A533B steel and will examine the test procedures, described above and a similar procedure proposed by Materials Research Laboratory, Inc. At this writing over 25 institutions and companies, including 10 in the United States and 15 in Europe and Japan have made commitments to participate. Results of the program will be reported at an ASTM Symposium Scheduled for November 9, 1978.

Cooperative Program with the University of Illinois

A method has been developed to obtain the transient dynamic stress intensity factors for a class of plane-strain finite crack problems in which a crack may propagate at nonuniform rate under the action of an arbitrary time-dependent normal tranaction on the crack face. As example problems diffraction of a uniformly incident dilatational wave by:

1. A stationary crack,
2. A propagating crack with constant speed, and
3. A suddenly stopping crack propagating with constant speed was considered.

Dynamic stress intensity factors were computed for a wide range of time in each problem.

FUTURE PLANS

The major thrust early in FY 78 is completion of the data base on plates, forgings, weldments, and TSE material. (Noted: this task is essentially complete at the time of this writing. While the expanded data base shows more heat-to-heat scatter than indicated on Figure 3, the essential conclusions are unchanged). Test pieces from a high Cu weldment will be irradiated and K_{Im} measured in the hot cell. The cooperative test program will also be carried out and presented at a planned ASTM crack arrest symposium.

The analysis of radial crack propagation will be applied to the ORNL-TSE experiments and to a number of hypothetical situations modeling full-scale behavior.

ANNUAL SUMMARY

of

ANALYTICAL MODELS FOR RESIDUAL STRESSES AT
GIRTH-BUTT WELDS IN PIPES AND PRESSURE VESSELS

Contract No. AT(49-24)-0293

to

U.S. NUCLEAR REGULATORY COMMISSION

from

BATTELLE
Columbus Laboratories

November 22, 1977

Principal Investigators

E. F. Rybicki, R. B. Stonesifer, and J. J. Groom

OBJECTIVE

The objective of this research is to develop and verify an analytical method which will provide an adequate tool for calculating the magnitude and distribution of residual stresses in girth-butt welds. The model is to include the pipe and weld geometries, the material properties of the weld and pipe, and important weld parameters. Verification of the model is to be done by comparing computed values of residual stresses with laboratory measurements. Comparisons are to be made for various pipe diameters, thicknesses, and numbers of weld passes. In addition to pipes, the model is to be applied to pressure vessels.

FY77 SCOPE

The scope of the program consists of three tasks: (1) review of literature for available data and analytical methods pertinent to residual stresses in girth-butt welds, (2) experimental determination of residual stresses in a set of girth-butt welds having carefully selected parameters so as to provide maximum guidance for development of analytical methods, and (3) development of an analytical method or methods for calculation of residual stresses.

Test welds of girth-butt welds will be prepared using typical consumable insert and GTA plus SMA processes to duplicate field welding practices. Different heat inputs will be used on different pipe models. The material will be 304 stainless steel. Diameter measurements will be made before and after welding. Biaxial strain gages will be placed along the axial length of the pipe samples before welding, and will be read before and after making the welds.

Gages will also be placed on and adjacent to the weld after welding, and will then be trepanned off to measure residual stresses. These data and other residual stress data obtained from the literature and reports will be used to evaluate the capability of the analytical method to predict residual stresses for a range of parameters. A range of wall thicknesses from 0.18 to 1.30 inches and outside pipe diameters of 4.5 to 30.0 inches will be used to verify the model. Pipes will have either equal or unequal wall thicknesses on opposite sides of the weld.

The analytical prediction of residual stresses due to girth-butt welds requires a temperature analysis and a thermal stress analysis. The temperature analysis will be performed by one or more of the following three ways: analytical closed form equations, numerical solution techniques, and laboratory measurements. The temperatures will then be used with various thermal stress analysis techniques to calculate regions of plastic flow and the subsequent residual stresses. The finite element stress analysis model will consist of an axisymmetric presentation, and will evolve from three tasks: evaluate numerical and laboratory methods for obtaining temperature distributions; examine the influence of temperature dependent material properties and nonlinear stress/strain relations on the residual deformation, stresses, and strains; and evaluate the capability of the model to predict residual deformations, stresses, and strains with laboratory measurements available in the literature, and values obtained from the experimental phase of the research. Each configuration of pipe specimen will be analyzed by the analytical model. In addition to the finite element method above, the technique of Vaidyanathan, et al. (Trans. ASME J. Engr. Mats and Tech., Oct. 1973, p 233-237) will be used to develop a more economical analytical procedure.

SUMMARY OF RESEARCH ACTIVITIES AND RESULTS

A finite element model for predicting residual stresses due to girth-butt welds in pressure vessels and pipes was developed at Battelle's Columbus Laboratories. The residual stress model for girth-butt welds was verified for welds in pipes ranging from 2 to 30 passes. The model also accurately predicts residual deformations. Comparisons of results from the model with data indicate that the model can be extended to accurately represent weld repairs in pressure vessels. A summary of the accomplishments directed at developing and evaluating the model is given in the following:

- A critical review of the literature was made to evaluate analytical techniques for developing the model and identify residual stress data to be used in verifying the models.
- Experimental studies of two girth-butt welded pipes were conducted to provide temperature data and residual stress data for verifying the models. Data obtained from these experiments include residual stresses, temperatures during welding, strains during welding, and residual deflections of the welded pipe.
- Two experiments on girth-butt welded pipes were identified from the literature as test cases for the model.
- A description of the pipes for which data were obtained from the experimental study and through the literature is given in the following. All pipes are 304 stainless steel.

Pipe Identification	Outside Pipe Diameter (in.)	Pipe Wall Thickness (in.)	Number of Weld Passes
BCL Model No. 2	12.75	.180	2
BCL Model No. 3	12.75	.375	6
Argonne Pipe	4.50	.337	7
General Electric Pipe	28.00	1.300	30

- A model for predicting residual stresses in girth-butt welds of pressure vessels and pipes was developed. The model consists of two parts: a temperature model and a stress analysis model.
- The temperature model was developed through modification of a model described in the literature review. Good comparisons between temperature data and computations by the model were obtained for each pass of the two-pass and six-pass welds. The temperature model includes heat input, pipe thickness, location of weld pass, thermal properties of the pipe, torch speed, efficiency of the weld process, and time dependent effects.
- A finite element model for girth-butt welds was developed. The model is axisymmetric and includes temperature dependent material properties, elastic-plastic stress strain effects, the effects of changing geometry of the pipe as it is welded, and linear elastic unloading from an elastic-plastic state of stress. The weld geometry and number of weld passes are also represented by the model.
- Results of the residual stress model showed good agreement with residual stress data in the hoop and axial directions on the insides and outsides of the four pipes described above.
- A simplified model for residual stress predictions was developed and evaluated for a two-pass weld. While the generalization of this model to many passes has not been completed, good comparisons between predicted values and measured residual stresses and deformations were obtained for a two-pass weld.
- Preliminary results were obtained using the residual stress model to represent a weld repair of the HSST Intermediate Vessel V-8. While the model needs further development before it can adequately represent the weld repair geometry, qualitative agreement between residual stress data and results of the model were obtained.
- Thus, an analytical model for predicting residual stresses in girth-butt welds has been developed and verified by comparison with experimentally obtained data for four pipes. It was demonstrated that with further development, the model can be applicable to other weld configurations such as weld repair of pressure vessels.

The following sections describe the girth-butt welds used for the validation study and comparisons of predicted residual stress distributions with values obtained from the welds.

Analytical Method for Residual Stresses

Figure 1 shows an illustration of a girth-butt weld. The residual stress model is comprised of two parts: a heat flow model and a stress analysis model. The heat flow model provides transient temperature distributions which are the input for the finite element stress analysis model. The stress analysis model gives the magnitudes and distributions of the residual stresses including variations through the pipe thickness.

The model for pipe welds is limited to axisymmetric representations and hence does not contain variations in stresses around the circumference of the pipe. This is however not a serious limitation because circumferential variations in residual stresses can be explained with results of the model. Furthermore, the weld repair model does contain circumferential variations in the residual stress distribution.

In addition to the axisymmetric simplification of the girth-butt weld program, several additional simplifications were examined. One which was included primarily because of the reduction in computer costs, was treating the girth-butt weld procedure as being symmetric about the plane, which is perpendicular to the axis of the pipe and passes through the center of the weld bead. This resulted in a computer cost savings of approximately 50 percent. Closely related to this simplification and in part resulting from it, was the modeling of a sequence of weld passes as a layer rather than as individual weld passes. The savings resulting from this simplification is dependent on the pipe size and number of passes, with the savings being greater for pipes with more passes. The method of modeling a general multipass girth-butt weld under these two assumptions is shown in Figure 2.

Development and Evaluation of Temperature Model

The approach taken here was to develop a temperature analysis procedure and verify the capability of the model to predict temperature distributions by comparing results with the data. The temperature model is based on a concentrated heat source moving on a plate.

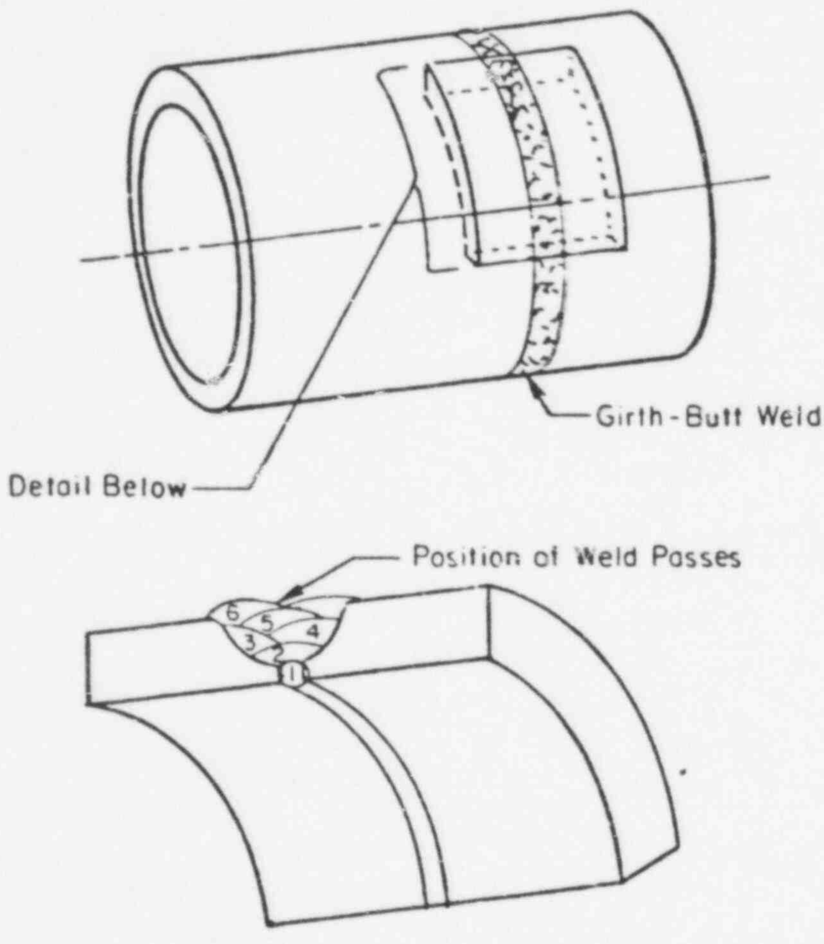

FIGURE 1. ILLUSTRATION OF GIRTH-BUTT WELD

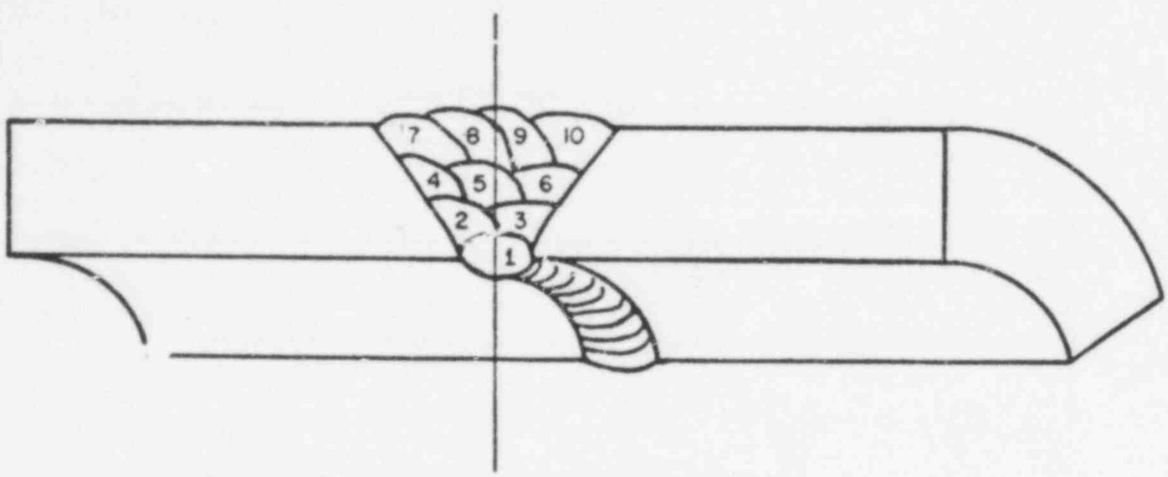

a. Weld Cross Section Geometry with Ten Passes

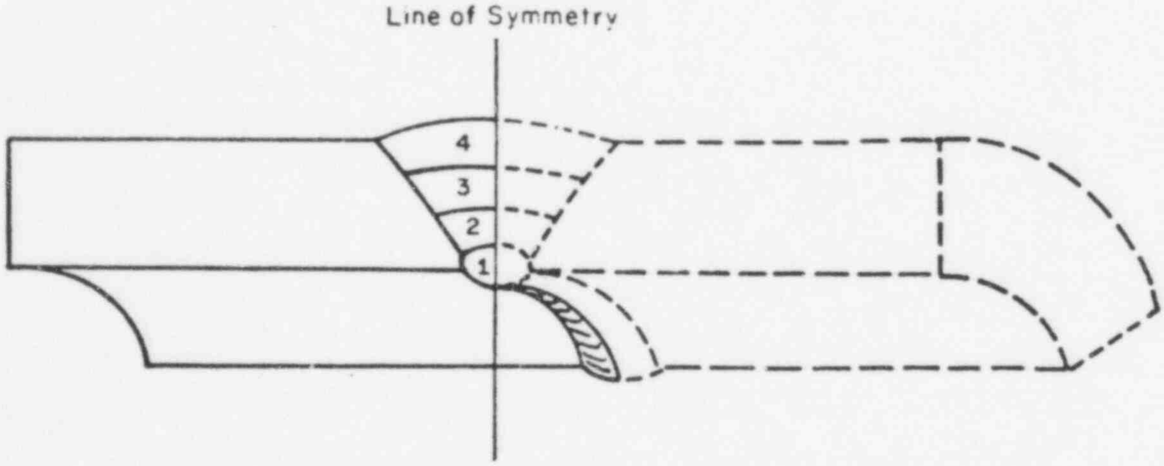

b. Model of Weld Cross Section Geometry Using Four Layers

FIGURE 2. COMPARISON OF ACTUAL AND MODEL WELD CROSS SECTIONS

The temperature model was used to generate temperature-time profiles for comparison with the thermocouple data. These comparisons are shown in Figures 3 and 4. Figure 3 displays comparisons for the gas tungsten arc root pass and Figure 4 shows comparisons for the second or gas-metal arc pass. The smallest time value in each figure corresponds to the time at which the thermocouple nearest the weld centerline reached its maximum temperature. The difference between the results of the temperature model and the experimental data was less than 9 percent for the first pass and less than 17 percent for the second pass.

Development and Evaluation of a Finite Element Model for Residual Stresses

Figure 5 shows an axisymmetric, finite element representation for a portion of a 12.75 inch diameter pipe welded by two passes. The cross section of the pipe and the weld groove are represented by finite elements. Each element is assigned to one of three zones. One zone is the weld material that is being deposited. The second is a zone to be filled by subsequent passes. The third zone consists of a portion of the pipe and the previously deposited weld material that experience a transient temperature increase as a result of the welding.

During each weld pass, thermal deformations are calculated from temperature distributions determined by the thermal model. These residual deformations at the end of each pass are added to determine an updated configuration of the model before analyzing the next pass. Therefore, a large deformation, elastic-plastic problem is broken into a series of incrementally linear problems. The analysis procedure also includes temperature-dependent material properties which are varied for each pass. Material properties of 304 stainless steel used in this study are shown in Figure 6 as a function of temperature.

The analysis procedure is also based on several assumptions given as follows. Melting or dilution of the pipe material is not included in the analysis. The mass of the weld and base materials are also neglected. The shape of each weld pass is obtained from photographs of the experimental weld-pass cross sections.

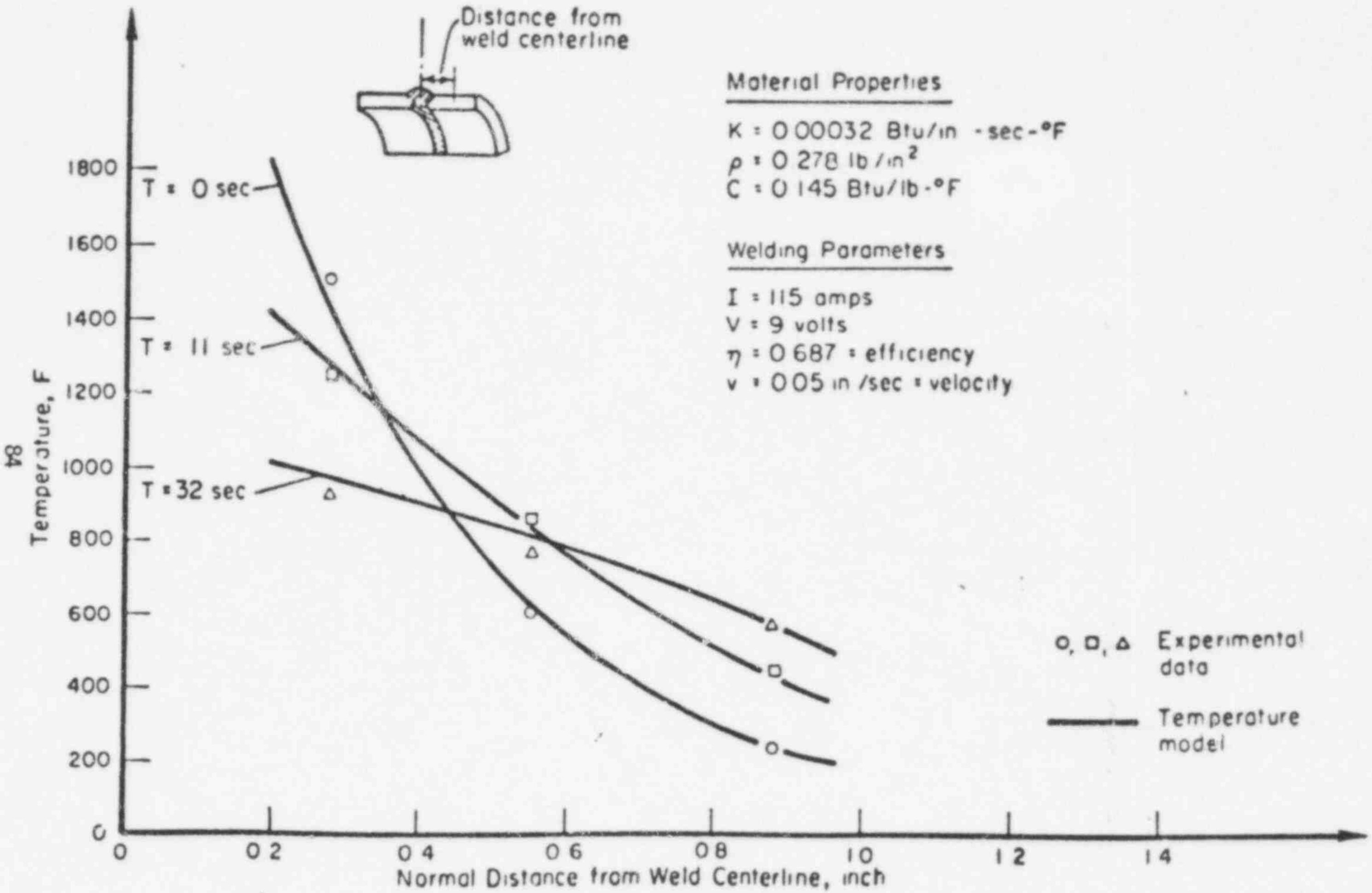

FIGURE 3. CALCULATED TEMPERATURE CURVES AND EXPERIMENTAL DATA FOR THE ROOT PASS

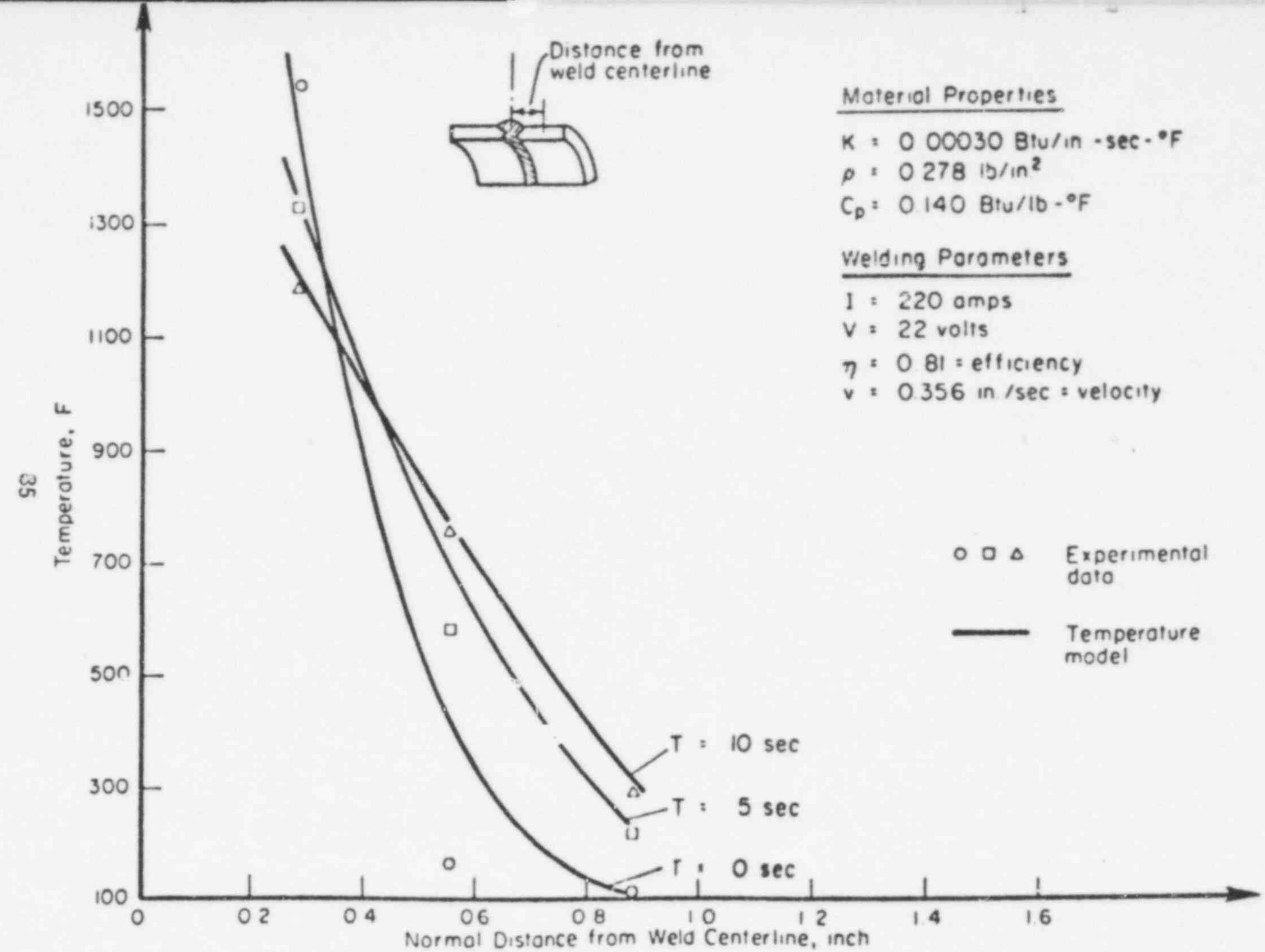

FIGURE 4. CALCULATED TEMPERATURE CURVES AND EXPERIMENTAL DATA FOR PASS 2

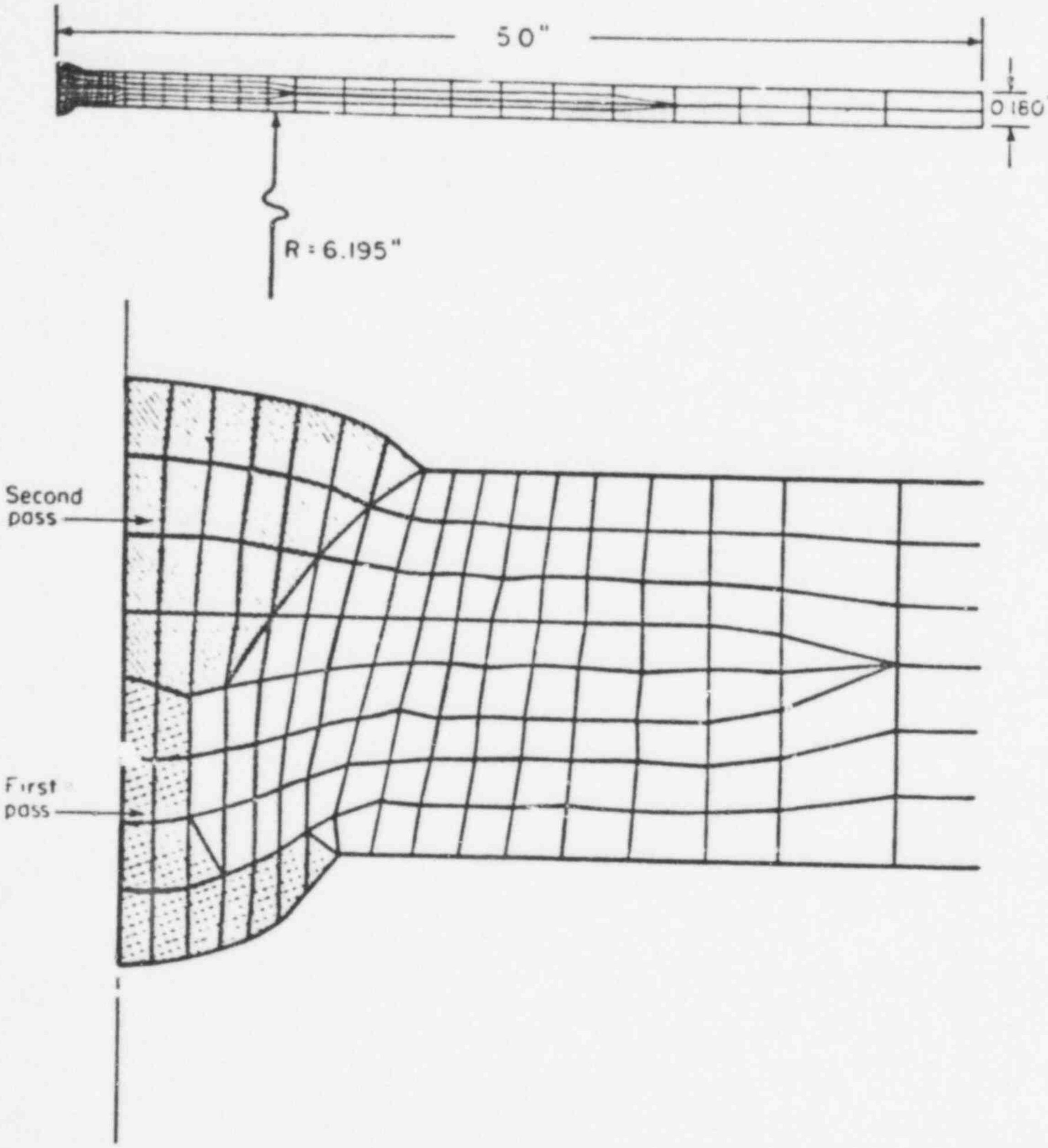

FIGURE 5. FINITE ELEMENT MODEL FOR TWO-PASS WELD

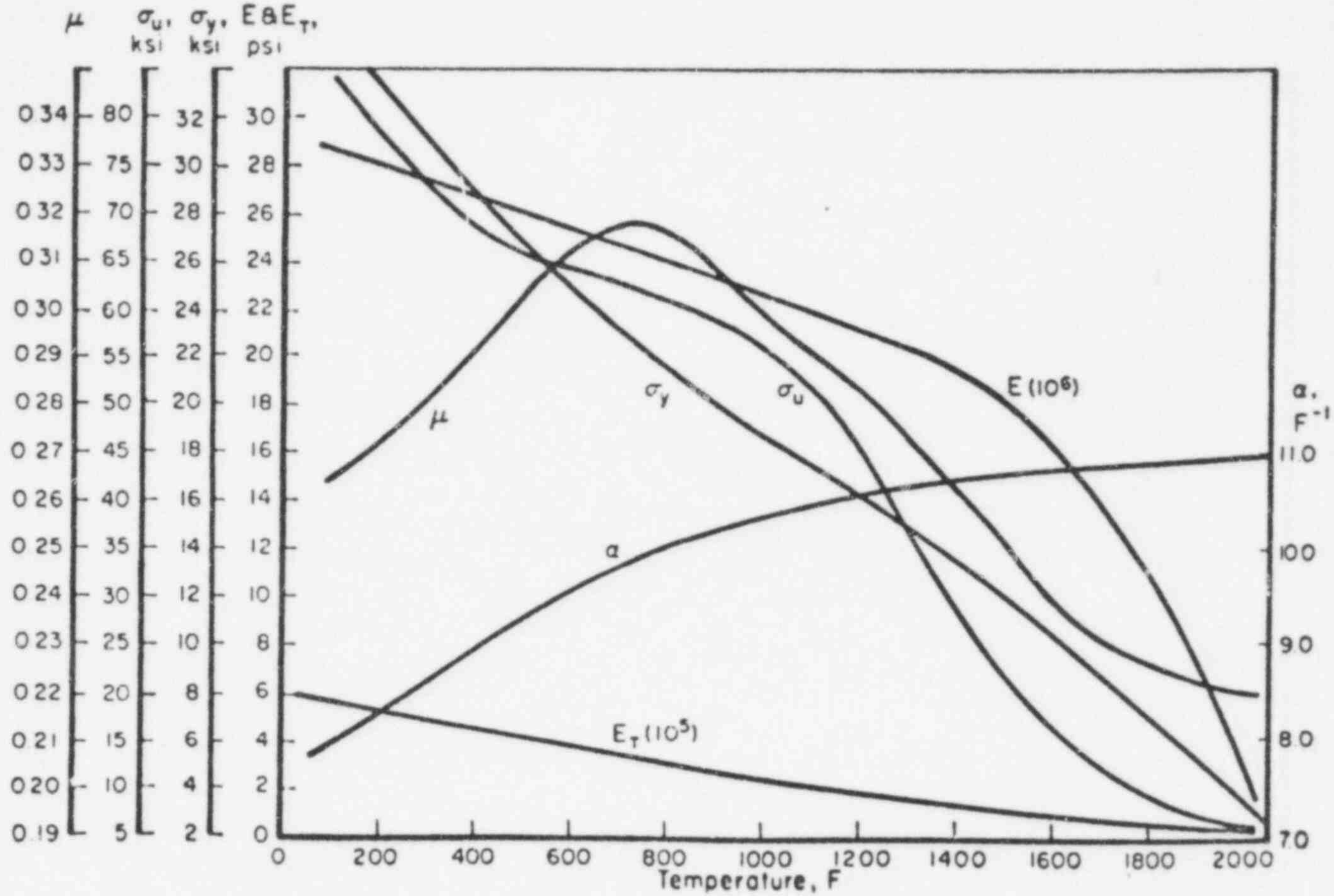

FIGURE 6. 304 STAINLESS STEEL TEMPERATURE DEPENDENT PROPERTIES USED FOR FINITE ELEMENT STRESS ANALYSIS

Battelle Two-Pass Weld

Computed values for the residual stress at the inner and outer surfaces of the two-pass welded pipe are compared to the experimentally obtained values in Figures 7 and 8, respectively. Qualitatively, the experimental points and the analytical curves agree well. As can be seen from these figures, the quantitative agreement at the inner surface is better than that for the outer surface, and the hoop stresses generally show better agreement than the axial stresses at both surfaces. The figures show that some oscillation in the calculated hoop stresses occurs in the hoop stresses at the outer surface. This is due to the discontinuity of modulus which results at the interface between the weld material and pipe material. This behavior is more noticeable at the outer surface because during the placement of the outer pass, the root pass and the pipe material act as one material, and oscillations in the stresses due to the prior application of the inner pass are reduced by the plasticity resulting from the outer pass.

Deformations of the welded pipes were also compared with measured values as a means of verifying the model. A comparison of predicted values and measurements for the two-pass weld are shown in Figure 9. This figure shows good agreement between the predictions on the model and the data. The figure also shows that the results are not overly sensitive to logical variations in representing the temperature distributions. This is a desirable trait for the model.

Modeling Argonne National Laboratory (ANL) Experiment, Seven-Pass Weld

The data for this girth-butt welded pipe was obtained from measurements taken by ANL based on References [24] and [25]. The weldment is denoted by W 27A and was selected because of the relatively small pipe diameter. This pipe is Type 304 stainless steel with an outer diameter of 4.5 inches and a thickness of 0.337 inch. The cross section is shown in Figure 10.

The finite element grid generated for the seven-pass pipe is shown in Figure 11. The model has 314 elements and 350 nodes. The material was 304 stainless steel with the assumed temperature dependent properties shown in Figure 6. Figure 13 shows a comparison of the calculated and experimentally measured maximum temperature profiles.

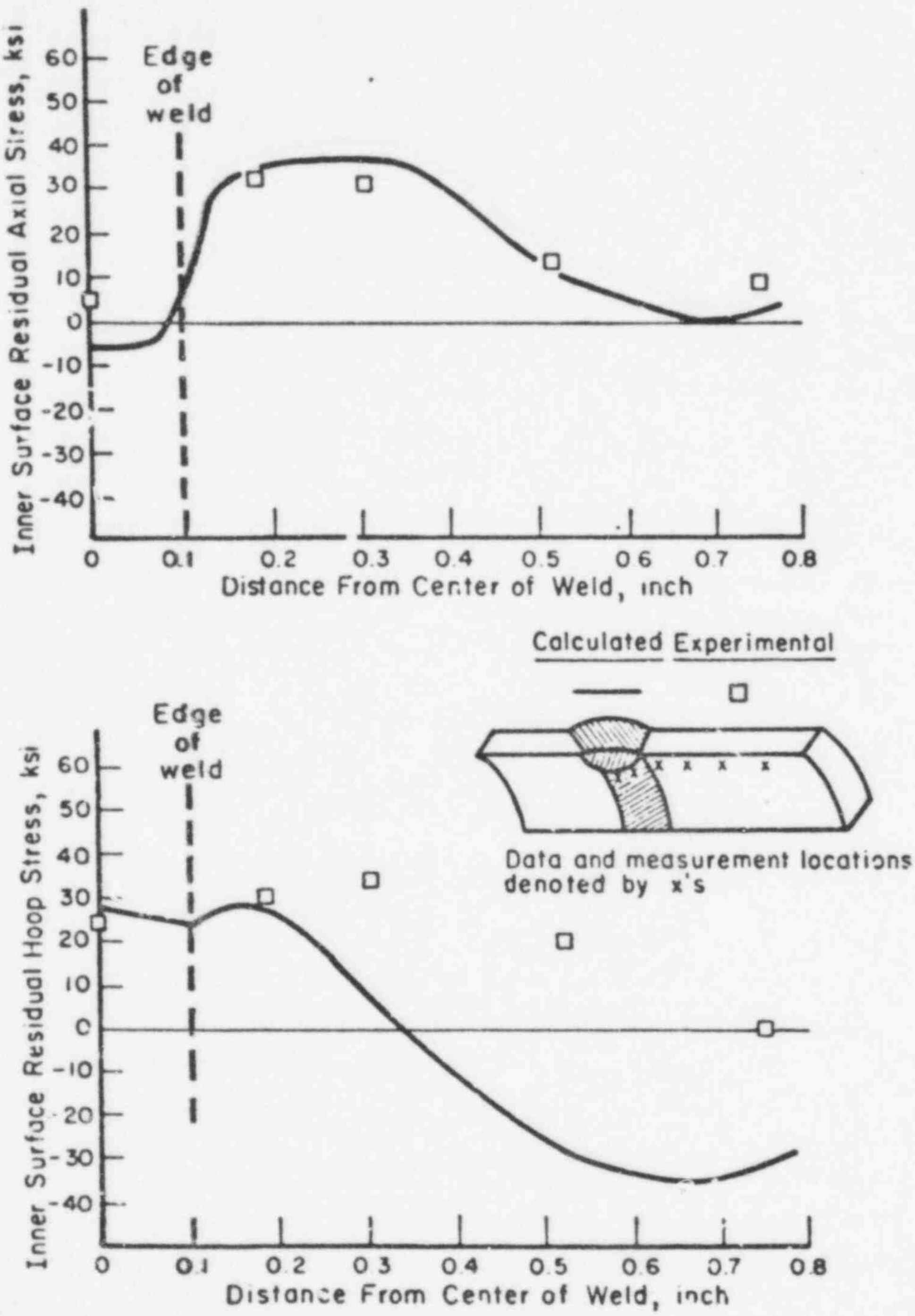

FIGURE 7. COMPARISON OF CALCULATED AND EXPERIMENTALLY OBTAINED RESIDUAL STRESSES AT THE INNER SURFACE FOR TWO-PASS WELD

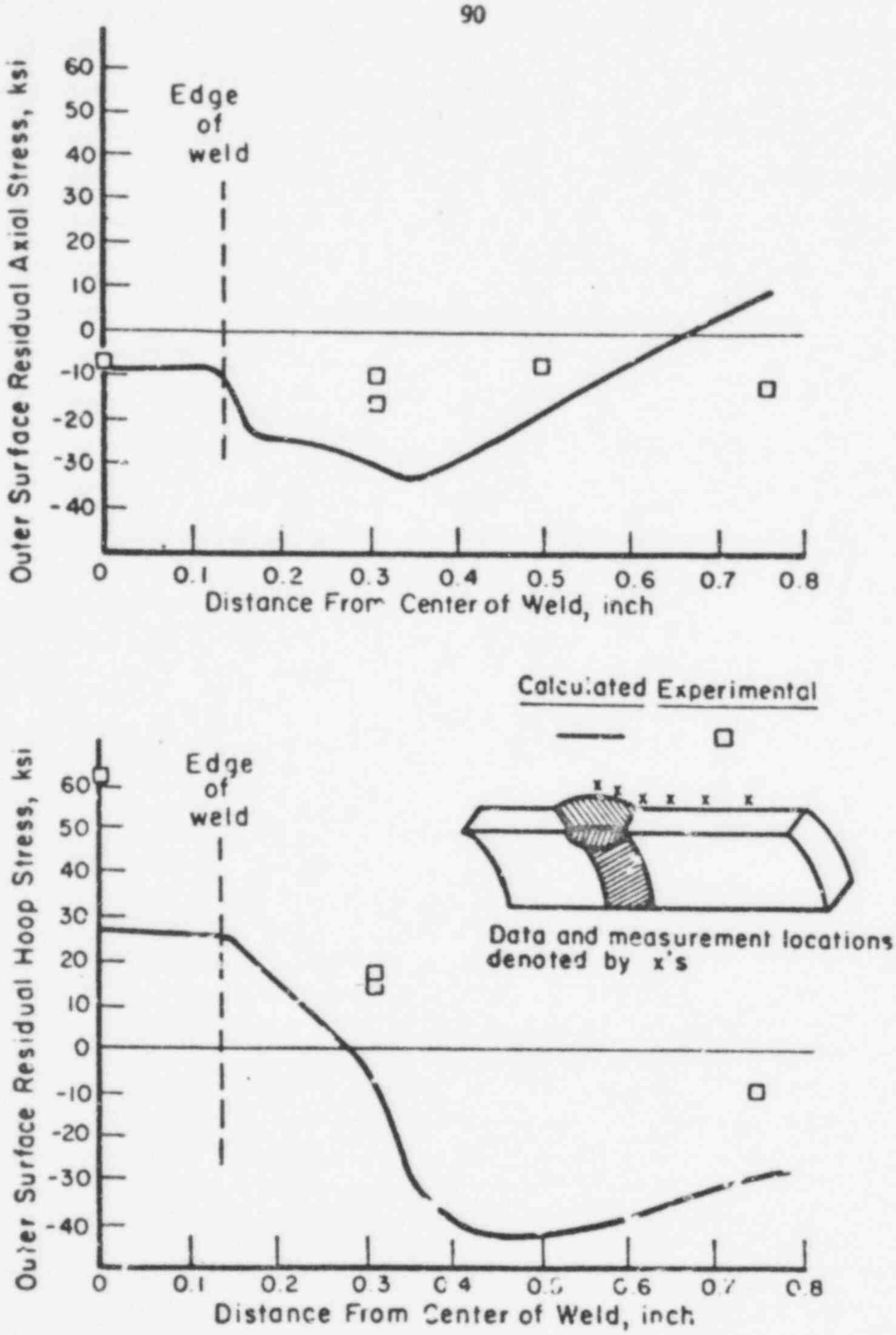

FIGURE 8. COMPARISON OF CALCULATED AND EXPERIMENTALLY OBTAINED RESIDUAL STRESSES AT THE OUTER SURFACE FOR TWO-PASS WELD

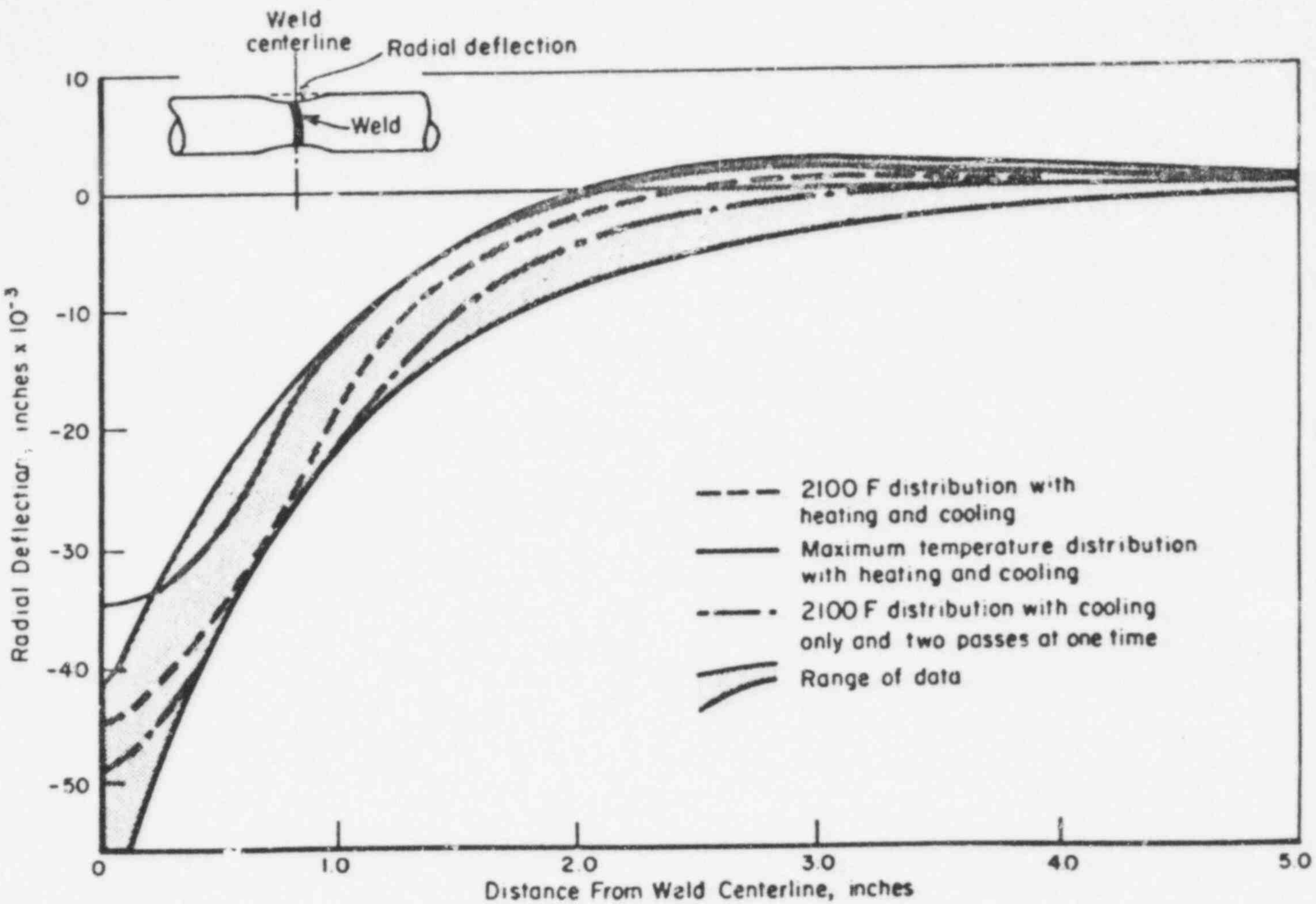

FIGURE 5 COMPARISON OF RESIDUAL DEFLECTION FOR THREE ALTERNATIVE METHODS OF REPRESENTING THE THERMAL LOADING FOR A TWO-PASS WELD

FIGURE 10. CROSS SECTION OF SEVEN-PASS ANL EXPERIMENTAL GIRTH-BUTT WELD W 27A

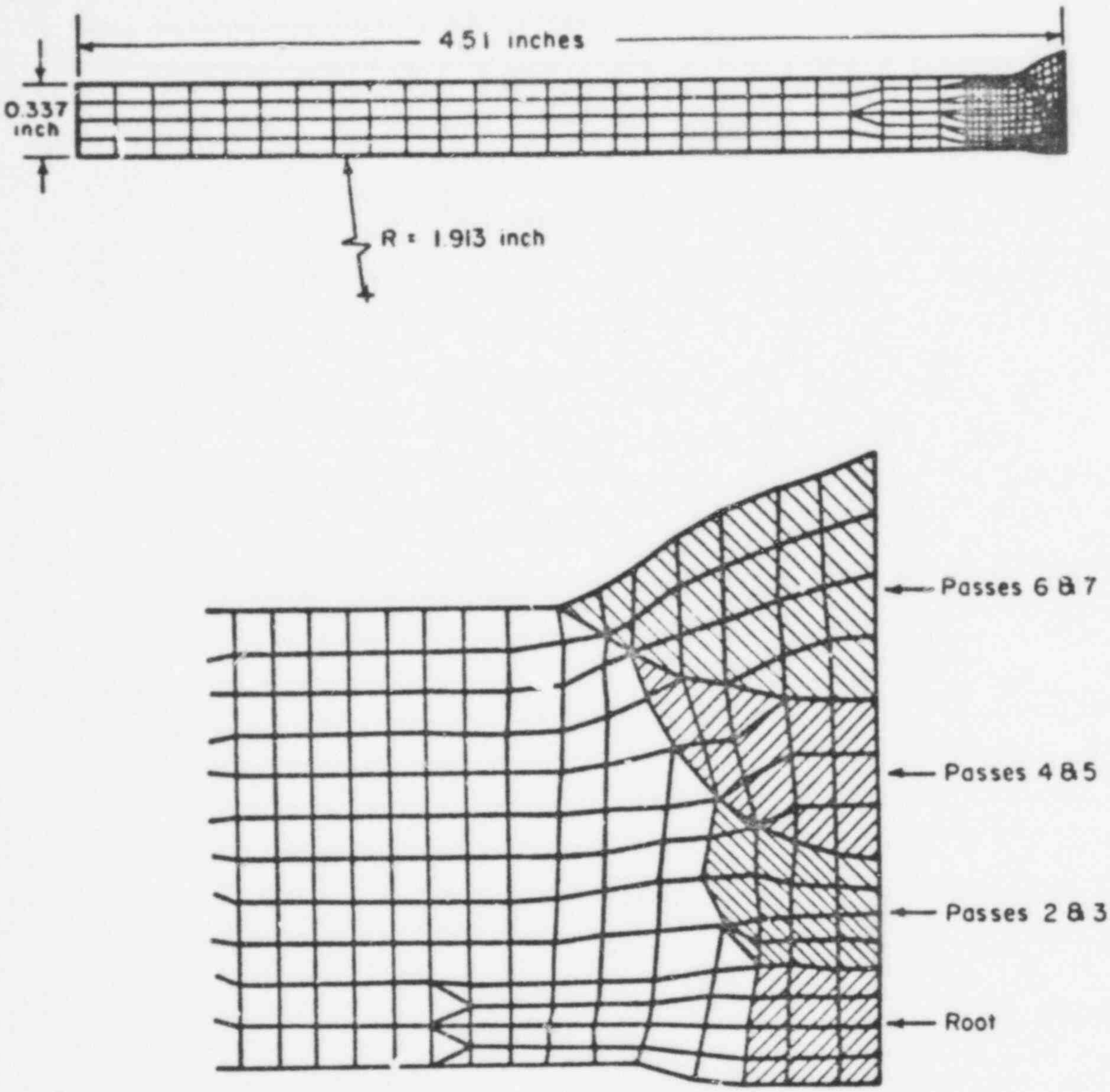

FIGURE 11. SEVEN-PASS FINITE ELEMENT MODEL FOR ANL EXPERIMENT W 27A

815 099

POOR ORIGINAL

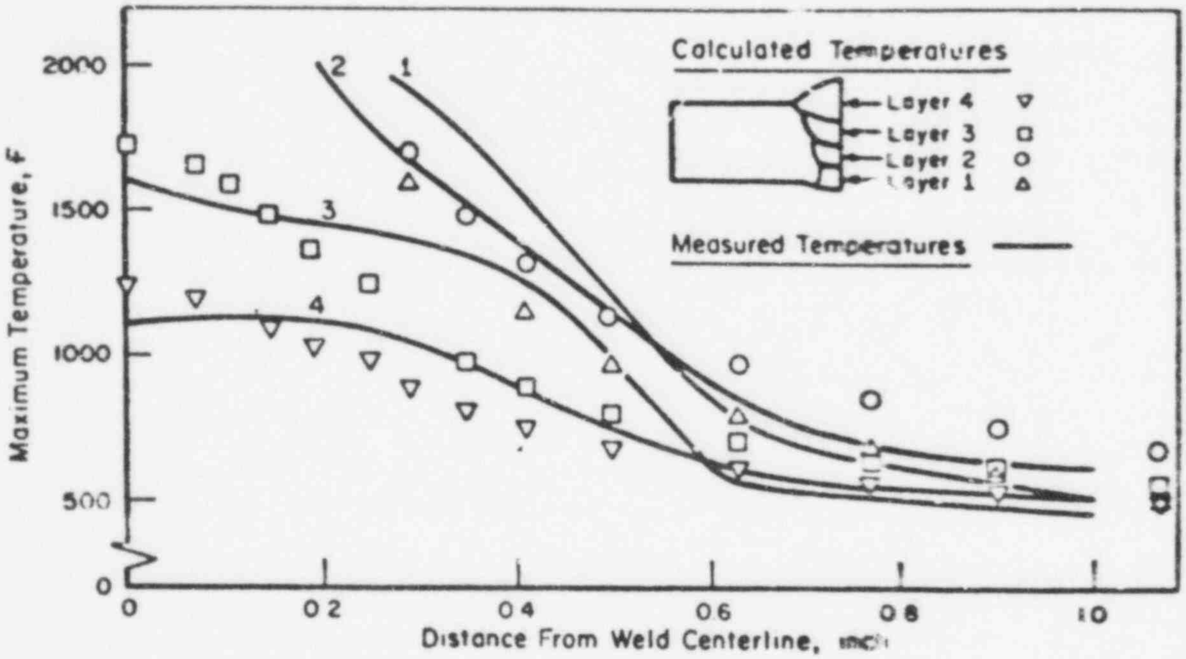

FIGURE 12. COMPARISON OF MEASURED AND CALCULATED MAXIMUM TEMPERATURE PROFILES ALONG INSIDE SURFACE FOR SEVEN-PASS ANL WELD W 27A

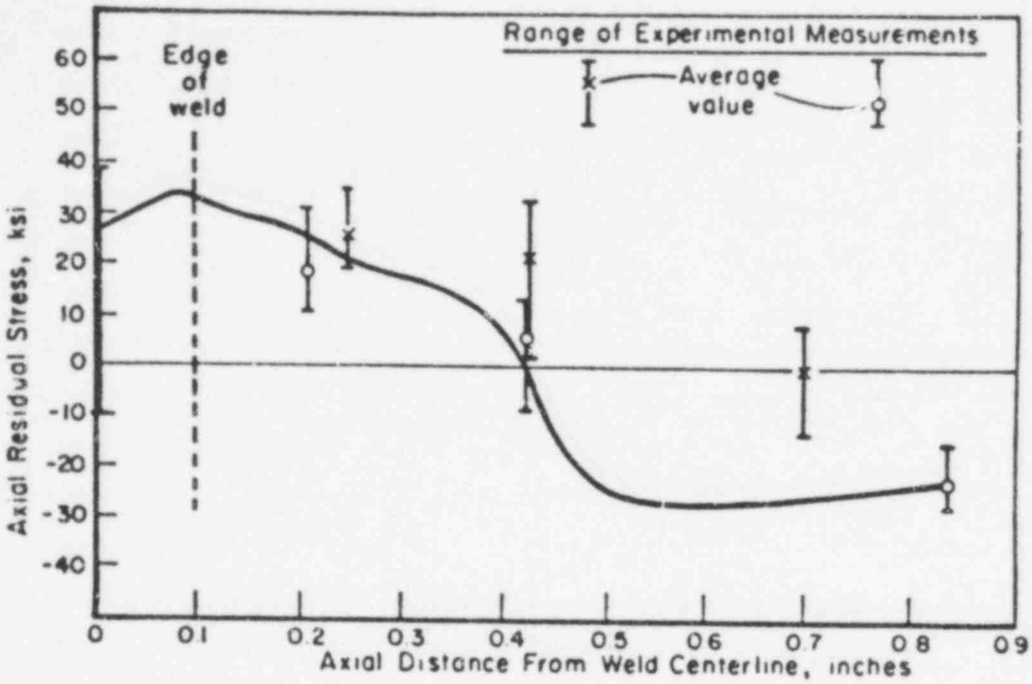

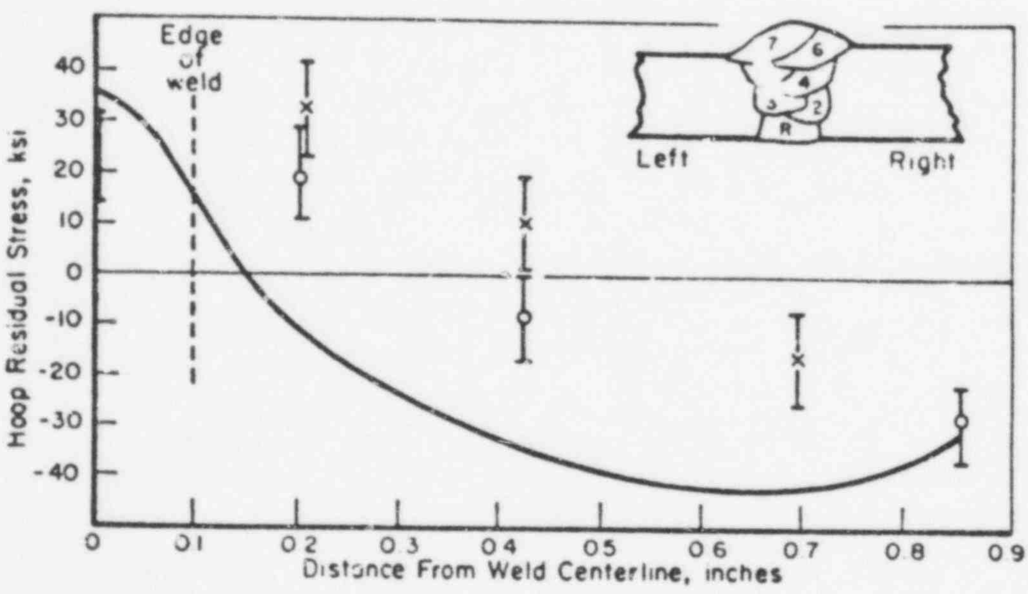

FIGURE 13. COMPARISON OF CALCULATED AND EXPERIMENTAL DETERMINED RESIDUAL STRESSES FOR THE INNER SURFACE OF SEVEN-PASS AND EXPERIMENT W 27A

Figure 13 shows a comparison of experimentally determined stresses and values computed from the model for the inside surface of the ANL seven-pass welded pipe. The bars on this figure indicate the effect of taking data at different angular positions about the pipe circumference. The effect of non-symmetric behavior about the weld centerline is indicated by the right and left symbols. The side of the pipe on which the last pass was applied showed the largest experimentally measured stresses.

Modeling General Electric Company Experiment, Thirty-Pass Weld

This girth-butt welded pipe was fabricated by GE and selected because of the relatively large number of weld passes. The pipe material is Type 304 stainless steel with an outer diameter of 28 inches and a thickness of 1.3 inch. The cross-sectional geometry of the thirty-pass weld was obtained from Figure 14 which was obtained from the GE report describing the experiment, Reference [26].

The finite element grid for the thirty-pass pipe is shown in Figure 15. The model has 214 elements and 248 nodes. The material properties used with this model are shown in Figure 6.

The computed residual stresses for the inside surface of the thirty-pass model are compared with experimental measurements in Figure 16. The bars on this figure indicate the effect of taking measurements at different angular locations around the pipe circumference. Though experimental measurements were made on both sides of the weld centerline, data points from both sides generally fell within the same range.

The calculated stresses in both the axial and hoop directions agree quite well with the data. The axial stress sign reversal agrees with the experimental values better than for the seven-pass pipe.

One aspect of the modeling of pipes with large numbers of passes, that was briefly addressed during the study of the thirty-pass pipe, is the possibility of grouping layers of passes in the analysis procedure. At this time, not enough studies have been done to fully answer the question of how many passes can be represented by one layer in the model. However, results indicate there is merit to the concept of modeling each row of weld passes as a separate layer.

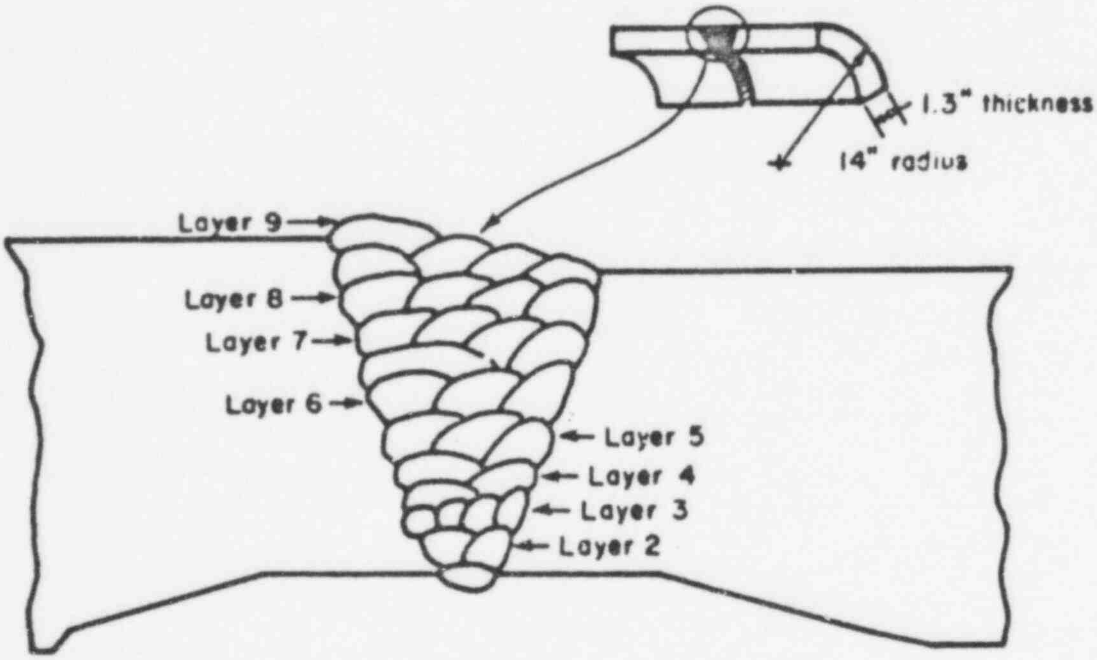

FIGURE 14. CROSS SECTION OF THIRTY-PASS GE EXPERIMENTAL GIRTH-BUTT WELD

Simplified Model for Residual Stresses

In addition to the finite element analysis, the applicability of a simplified residual stress analysis procedure was evaluated for the Battelle two-pass weld. The basis of the model is described in Reference [13]. Several assumptions simplify the computational procedure for this model. The material has an elastic-perfectly plastic stress-strain behavior. The transient temperature distribution is represented by a single cooling temperature drop based on the distribution of maximum temperatures that the material experiences. Figure 17 shows the comparison of the residual stress data for the Battelle two-pass weld and the computed values from the simplified model. This model also predicts residual deformations. Figure 18 shows a comparison of measured and calculated residual deformations for the Battelle two-pass weld.

Preliminary Application of the Residual Stress Model to a Weld Repair of a Pressure Vessel

The residual stress model described here has many potential applications to welds of pressure vessels and pipes. One such application is to understanding the residual stresses resulting from a weld repair of a pressure vessel. It is emphasized that the model, in its present form, would require some extensions before accurately representing several aspects of the problem. Nonetheless, it is of value to apply the model to this problem with the intent of obtaining qualitative results.

The weld repair of interest was done on the HSST intermediate vessel V-8. The same weld repair procedure was applied to a two foot long prolongation cylinder with comparable dimensions to the cylindrical section of the vessel. The dimension of the weld cavity and the cylindrical section of the pipe are shown in Figure 19. The vessel material is ASTM A533, Grade B Class 1 carbon steel. The size of each weld bead is about .1 inch by .1 inch. Thus, it is estimated that close to 1000 weld passes were required to fill the weld cavity.

The residual stress data for this weld repair was available along a line around the circumference of the cylindrical section of the vessel. The model is not three-dimensional and cannot represent the three-dimensional aspects of the weld cavity geometry. The model represented a section of the vessel in

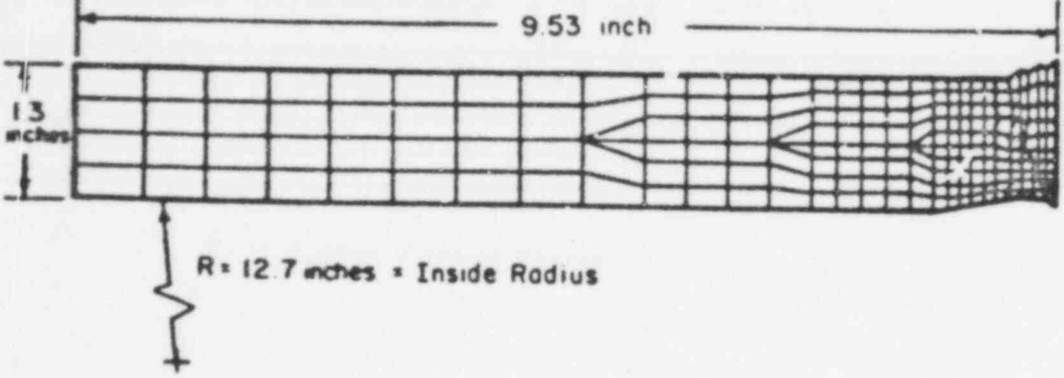

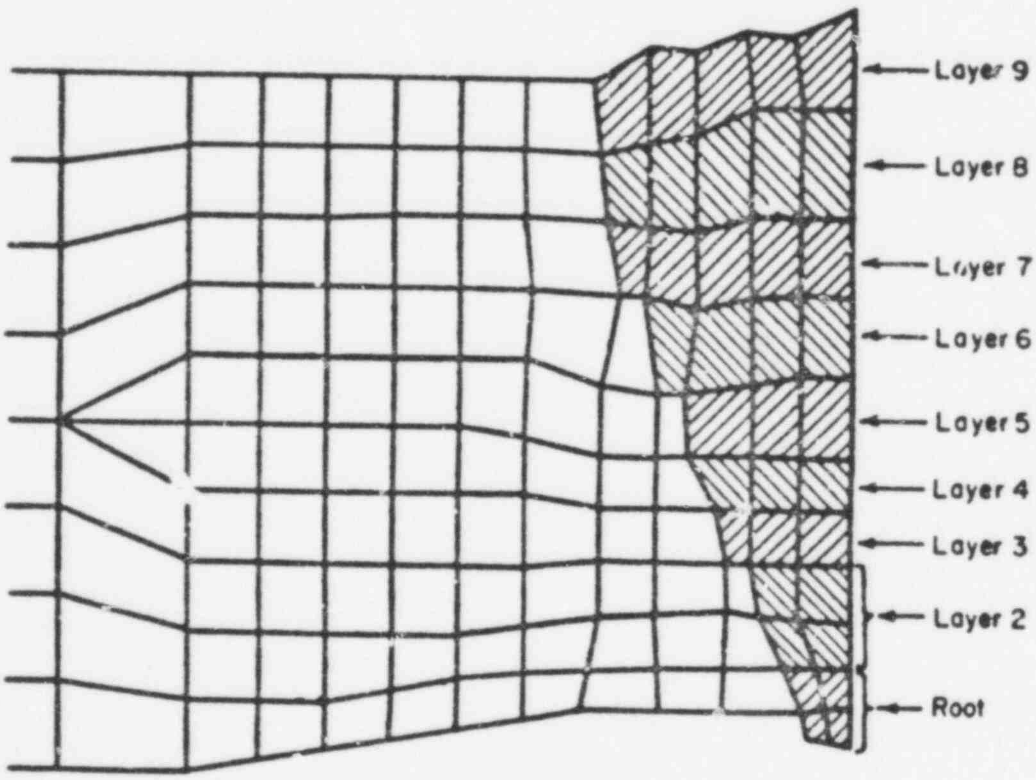

FIGURE 15. FINITE ELEMENT MODEL FOR THIRTY-PASS GE EXPERIMENTAL GIRTH-BUTT WELD

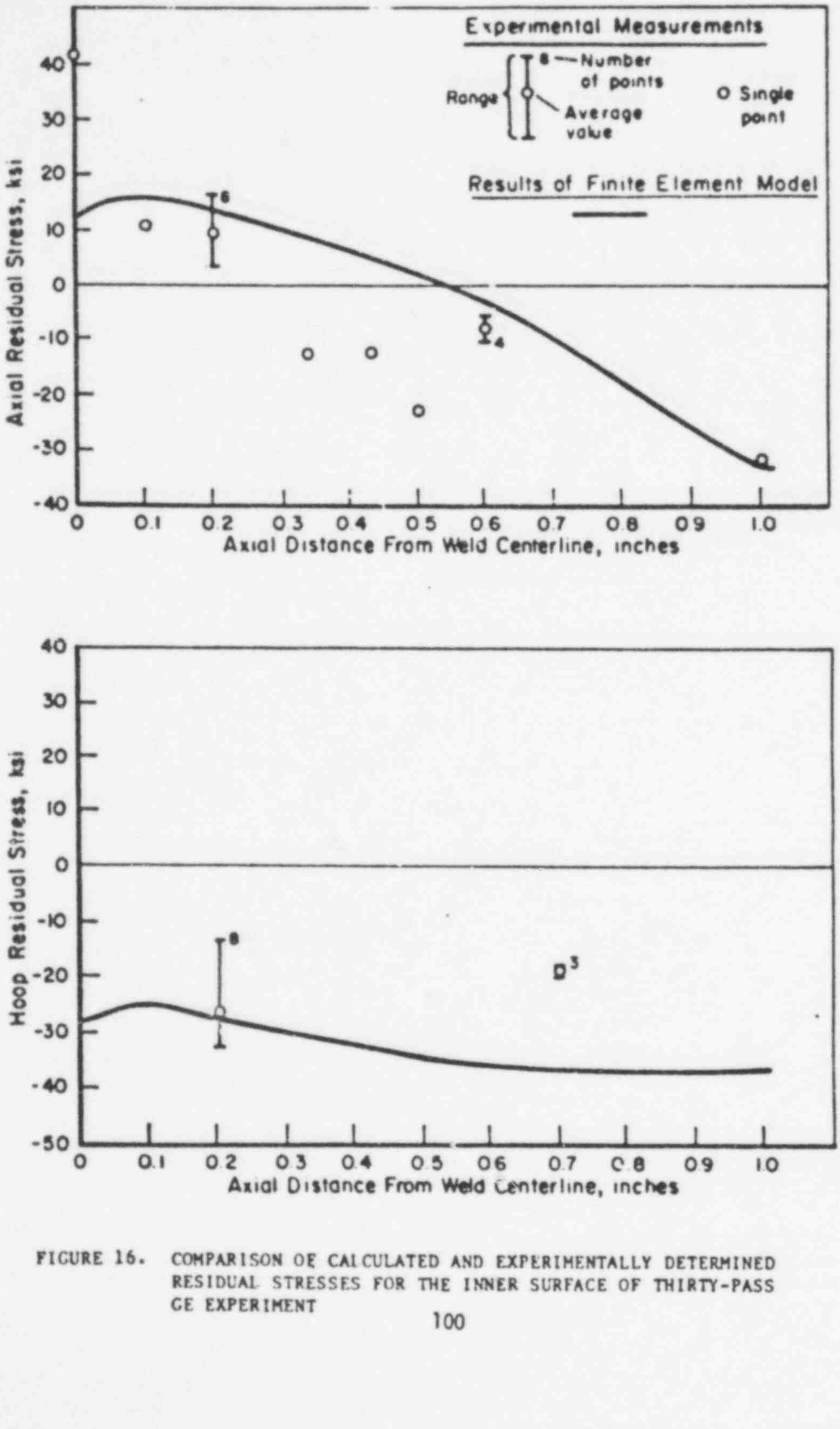

FIGURE 16. COMPARISON OF CALCULATED AND EXPERIMENTALLY DETERMINED RESIDUAL STRESSES FOR THE INNER SURFACE OF THIRTY-PASS GE EXPERIMENT

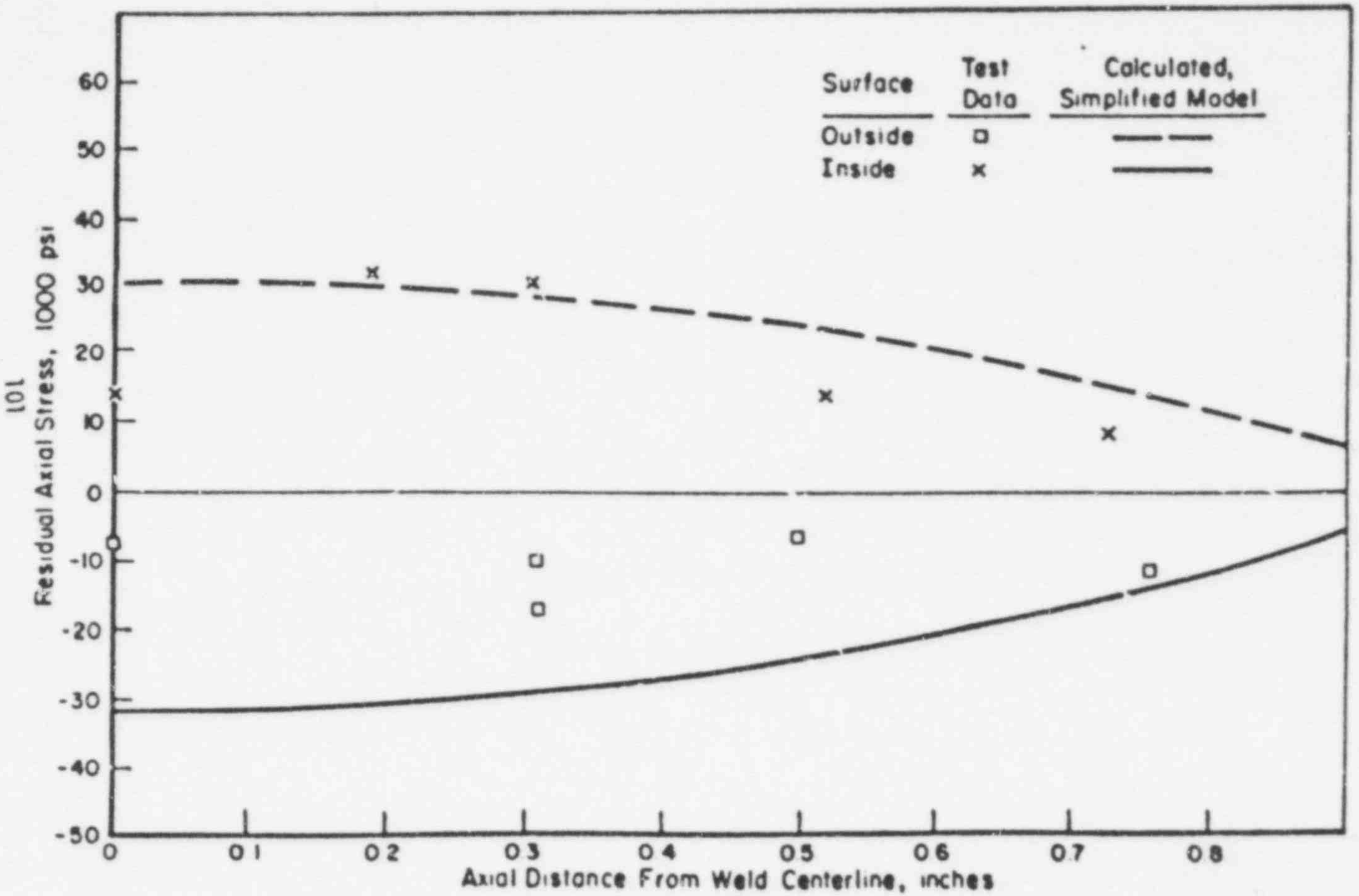

FIGURE 17. COMPARISON OF AXIAL RESIDUAL STRESSES

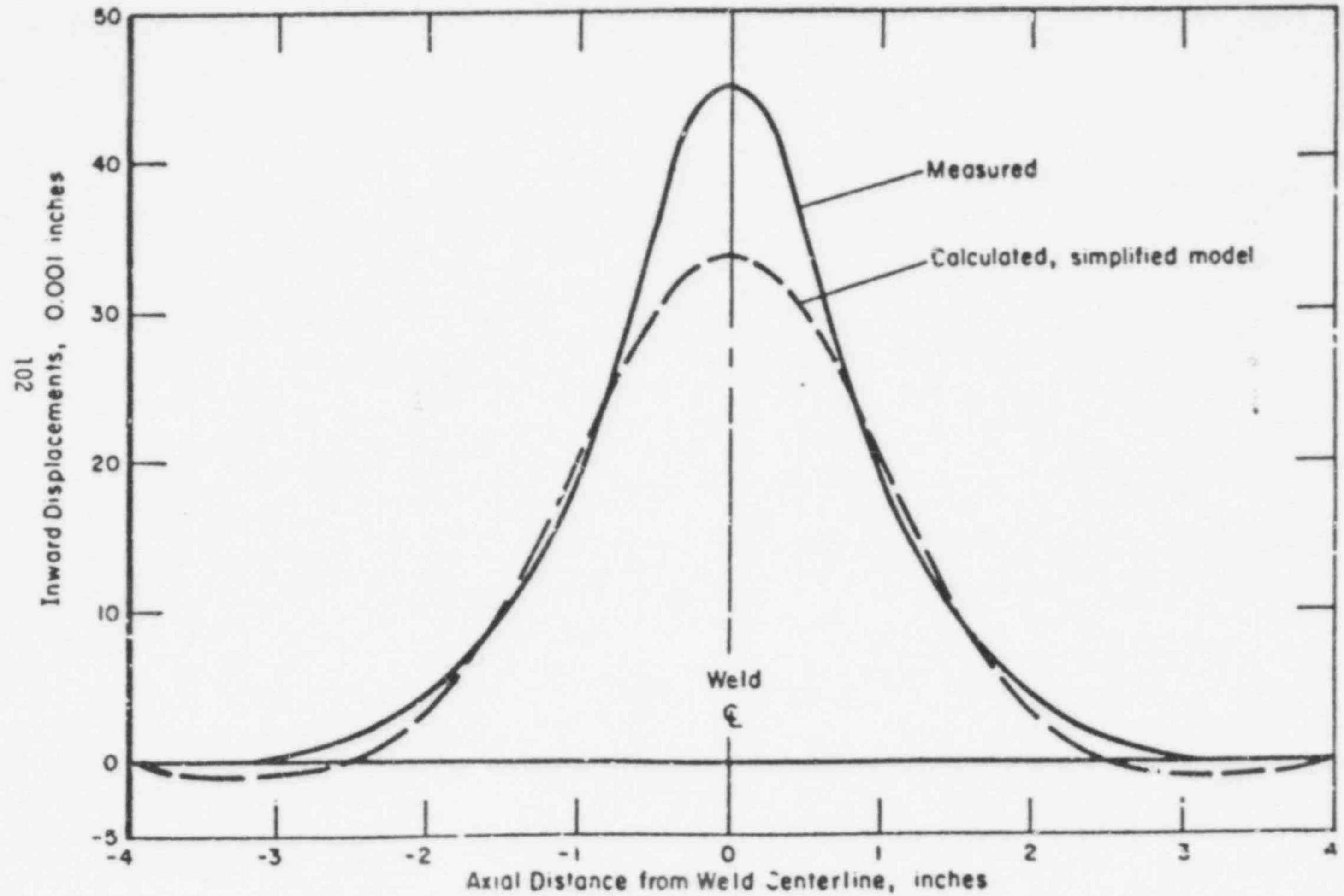

FIGURE 18. COMPARISON OF MEASURED AND CALCULATED RADIAL DISPLACEMENTS

815 108

the hoop direction through the center of the weld cavity. Another approximation in the model concerns modeling the large number of weld passes. The total number of filler passes were modeled as a single deposit of material. Because of these approximations in the model, quantitatively accurate results were not expected. However, qualitative comparisons with the data should be attainable because the model does include some aspects of the geometry and the material properties. Figure 20 shows the comparison of results obtained by computations with the model and residual stress data obtained at Oak Ridge National Laboratory. The model exhibits good agreement with the hoop stress data as shown by comparing the solid and dotted lines. Hoop and axial stress distributions from the model are on the outer surface of the vessel. The Oak Ridge data were obtained on the outer surface and from points just below the outer surface. Axial stress data are shown at one location and are also in agreement with the results of the analysis. These comparisons are very encouraging and suggest that the model can be a useful tool for residual stresses in weld repair.

Conclusions

Good comparisons between experimentally obtained residual stress data and computed values from the finite element model were obtained for the two pipes welded during the program and for two pipes reported in the literature. The number of weld passes in these pipes ranged from two to thirty. A comparison of residual stress data and preliminary results obtained for a weld repair of the HSST-Intermediate Pressure Vessel (ITV-8) indicate the model can, with modifications, be applied to studying weld repairs.

The residual stress data were not all obtained in the same manner. The Battelle data were obtained by a chip removal procedure. The Argonne and General Electric data were obtained by removing sections of the weldment, and the Oak Ridge data were obtained by a hole drilling technique. Thus, the model results compared well with various types of residual stress measuring techniques.

Based on the results of this study, it is concluded that

- A mathematical model was developed to predict the magnitude and direction of residual stresses in girth-butt welds.
- The model has been evaluated for pipe welds varying from 2 to 30 passes. A total of four pipes were used in the verification. Preliminary results for a thick section weld

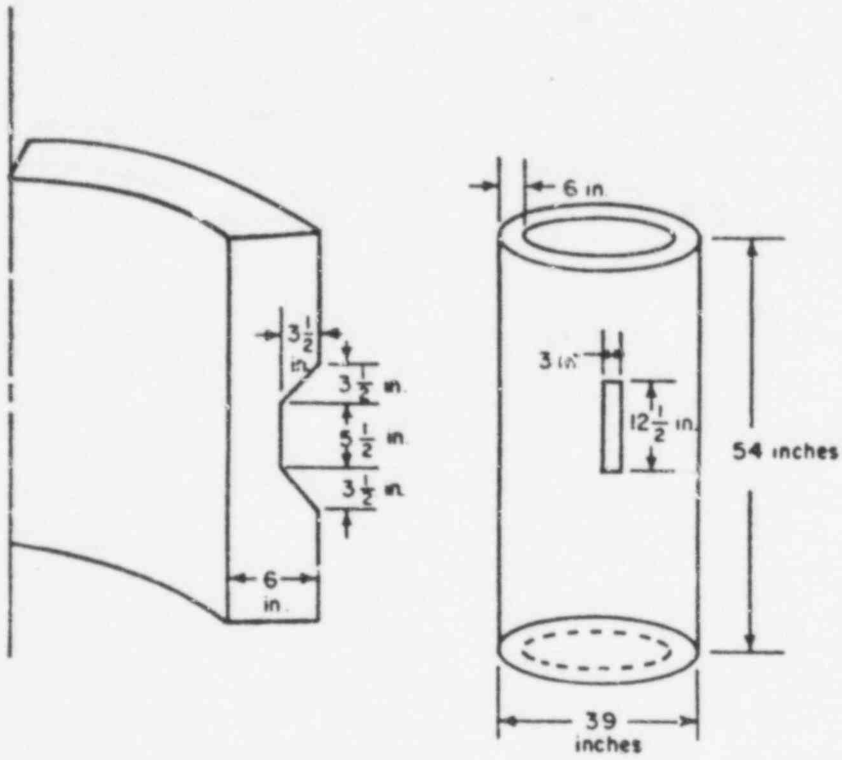

FIGURE 19. ILLUSTRATION OF WELD REPAIR CAVITY IN CYLINDRICAL SECTION OF HSST INTERMEDIATE VESSEL V-8

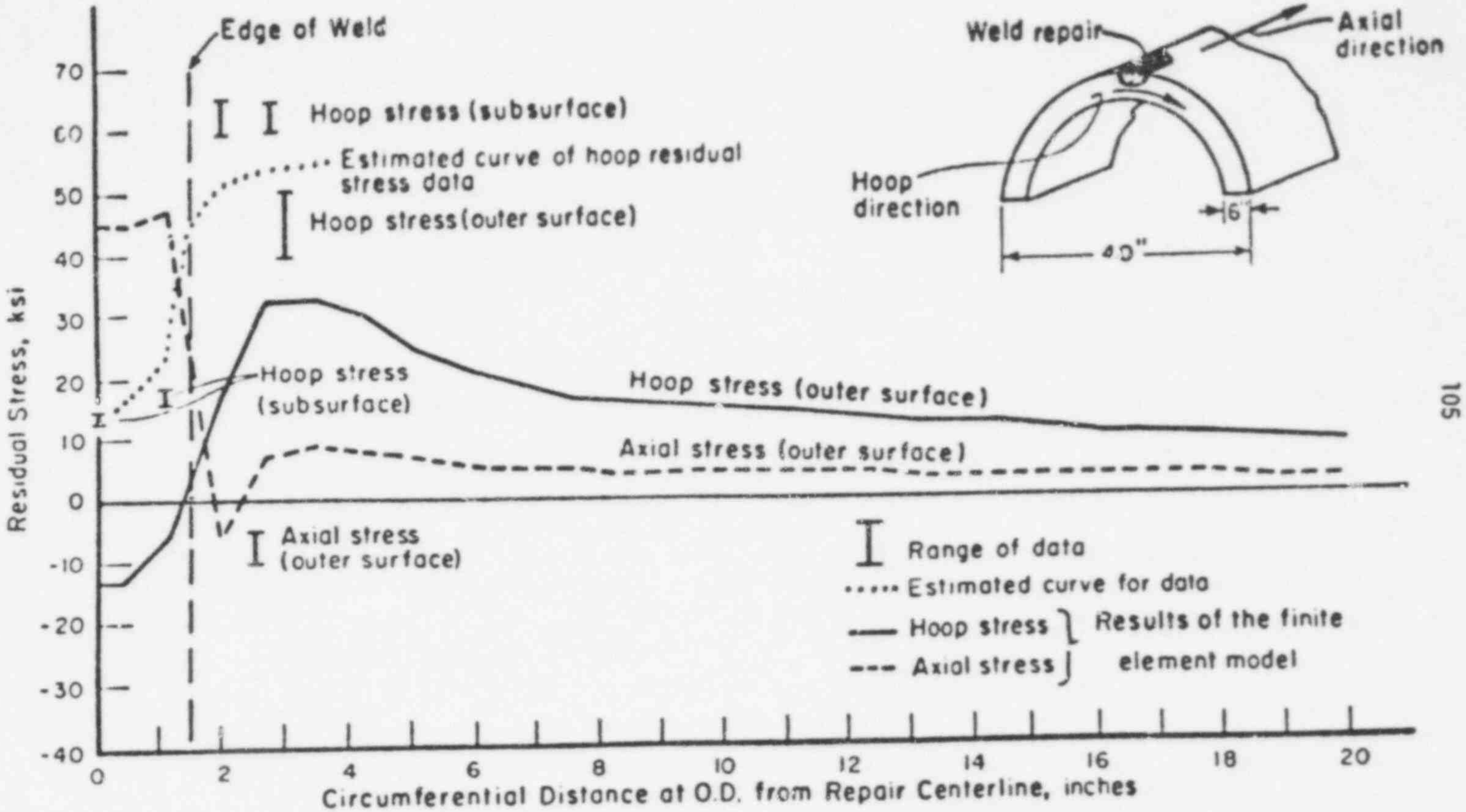

FIGURE 20. COMPARISON OF RESIDUAL STRESS DATA FOR WELD REPAIR OF HSST INTERMEDIATE VESSEL V-8 AND PRELIMINARY COMPUTATIONS BASED ON RESIDUAL STRESS MODEL

815 111

re,air of the intermediate HSST ITV-8 pressure vessel showed good qualitative agreement with residual stress data.

- The model predicted residual deformations that were in excellent agreement with data taken from a welded pipe.
- The model for the pipes is axisymmetric and does not contain circumferential variations of residual stress. However, the model for the weld repair does contain circumferential variations in the residual stresses.
- The accuracy of the model is due to the representation of the complex nature of the welding process. Hence, the program is of equal complexity and sophistication.
- A simplified model was developed and evaluated. Residual stresses and deformations were in good agreement with data obtained from a two-pass weld.
- The model has been verified for the welds described here. Further studies are needed before it can be verified for other geometries or weld types.

Publications of this Research

The results of this study in which an analytical model was developed and verified are described in the final report "Residual Stresses in Girth-Butt Welds in Pipes and Pressure Vessels", prepared for the U.S. Nuclear Regulatory Commission Office of Nuclear Regulatory Research under Contract No. AT(49-24)-0293, Task 1, August, 1977. A paper describing the model and comparisons with laboratory measurements for residual stresses has been accepted for presentation at the American Society of Mechanical Engineers Winter Annual Meeting to be held November 27 to December 2, 1977, in Atlanta, Georgia. The paper is entitled "A Finite Element Model for Residual Stresses in Girth-Butt Welded Pipes", by E. F. Rybicki, D. W. Schmueser, R. B. Stonesifer, J. J. Groom, and H. W. Mishler.

RESEARCH PLAN FOR FY78

The overall scope involves development, verification, and utilization of an analytical model or models for calculating residual stresses due to weld repair and specific welding applications. The program consists of three tasks. Task I deals with residual stresses due to weld repair of pressure vessels. Task II is concerned with the residual stress distribution resulting from an electron beam weld of a compact tension specimen. In Task III, the focus is on the residual stresses induced by cladding. A brief description of each task follows.

In Task I, an analytical method or methods will be developed to provide an adequate tool for calculating the magnitude, direction and distribution of residual stresses in weld repairs of pressure vessels and pipes. The model will consist of two parts, a temperature analysis model and a finite element stress analysis model. Parameters of the weld repair process that will be included in the analysis are heat input, size and number of the weld passes and the geometry of the cutout section for the weld repair.

Verification of the models will be carried out by comparing computations made with the models with residual stress data including the data obtained by Oak Ridge National Laboratory on the HSST V-8 vessel. A sensitivity study to evaluate the effects of the weld repair parameters on the residual stresses will be conducted. Based on the results of the sensitivity study, guidelines for reducing residual stresses due to weld repair will be stated.

In Task II, the residual stress analysis for welding will be applied to obtain an estimate of the residual stress distribution due to an electron beam weld. The weld configuration is a compact tension specimen selected to represent a particular test specimen. The focus will be on obtaining the magnitude, direction and distribution of the residual stresses.

In Task III, the residual stresses in the vicinity of the vessel beltline and nozzle regions will be investigated using the residual stress analysis for welding. Of particular interest is the residual stress state due to cladding. Both the beltline region and the nozzle region will be considered. The effects of nonlinear stress-strain behavior and temperature dependent properties of the cladding and the vessel materials will be included. The magnitude and direction of the residual stress distribution near the cladding-vessel interface of each region will be obtained from results of the analysis.

POOR ORIGINAL

BIBLIOGRAPHY AND REFERENCES

1 Myers, P. S., Uyehara, D. A., and Borman, G. L., "Fundamentals of Heat Flow in Welding", Welding Research Council Bulletin No. 123, July 1967.

2 Masubuchi, K., "Control of Distortion and Shrinkage in Welding", Welding Research Council Bulletin No. 149, April 1970.

3 Adams, C. M., "Cooling Rates and Peak Temperatures in Fusion Welding, Welding Journal Research Supplement, May 1958, pp 210-215.

4 Jhaveri, P., Moffatt, W. G., Adams, C. M., "The Effect of Plate Thickness and Radiation on Heat Flow in Welding and Cutting", Welding Journal Research Supplement, January 1962, pp 12-16.

5 Paley, Z., Lynch, L., Adams, C., "Heat Flow in Welding Heavy Steel Plate", Welding Journal Research Supplement, February 1964, pp 71-79.

6 Paley, Z. and Hibbert, P., "Computation of Temperatures in Actual Weld Designs", Welding Journal Research Supplement, November 1975, pp 385-392.

7 Tall, L., "Residual Stresses in Welded Plates - A Theoretical Study", Welding Journal Research Supplement, January 1964, pp 10-23.

8 Rodgers, D. E. and Fletcher, P. R., "The Determination of Internal Stresses from the Temperature History of a Butt Welded Pipe", Welding Journal Research Supplement, 1938, pp 4-7.

9 Masubuchi, K., Simmons, F. B., and Monroe, R. E., "Analysis of Thermal Stresses and Metal Movement During Welding", Battelle Memorial Institute, RSIC-820, Redstone Scientific Information Center, NASA-TM-X-61300, N68-37857, July 1968.

10 Gatovskii, K., "Determination of Welding Stresses and Strains with Allowance for Structural Transformations of the Metal", Svar. Proiz., No. 11, 1923, pp 3-6.

11 Makhnenko, V., Shekera, V., and Izbenko, L., "Special Features of the Distribution of Stresses and Strains Caused by Making Circumferential Welds in Cylindrical Shells", Avt. Svarka., No. 12, 1970, pp 43-47.

12 Tall, L., "Residual Stresses in Welded Plates - A Theoretical Study", Welding Journal Research Supplement, January 1964, pp 10-23.

13 Vaidyanathan, S., Todaro, A. F., and Finne, I., "Residual Stresses Due to Circumferential Welds", Trans. ASME, Journal of Engineering Materials and Technology, October 1973, pp 233-237.

14 Paley, Z., Lynch, L., and Adams, C., "Heat Flow in Welding Heavy Steel Plate", Welding Journal Research Supplement, February 1964, pp 71-79.

815 114

15 Wilson, E., Nickell, R., "Application of the Finite Element Analysis to Heat Condition Problems", Nuclear Engineering and Design, No. 4, 1966, pp 276-284.

16 Sagalevich, V. and Mežentseva, S., "Calculation of Strains and Stresses in Circular Welds", Svar. Proiz., No. 9, 1974, pp 7-10.

17 Kamichika, R., Yada, T., and Okamoto, A., "International Stresses in Thick Plates Weld-Overlaid with Austenitic Stainless Steel (Report 2)", Transactions of the Japan Welding Society, Vol. 5, No. 1, April 1974.

18 Hibbitt, H. and Marcal, P., "A Numerical Thermo-Mechanical Model for the Welding and Subsequent Loading of a Fabricated Structure", Contract No. N00014-67-A-D191-0006, Brown University, 1972.

19 Nickel, R. and Hibbitt, H., "Thermal and Mechanical Analysis of Welded Structures", Nuclear Engineering and Design, No. 32, 1975, pp 110-120.

20 Friedman, E., "Thermomechanical Analysis of the Welding Process Using the Finite Element Method", Journal of Pressure Vessel Technology, August 1975, pp 206-213.

21 Iwamura, Y. and Rybicki, E. F., "A Transient Elastic-Plastic Thermal Stress Analysis of Flame Forming", ASME Trans. Journal of Engineering for Industry, February 1973.

22 Rybicki, E. F., Ghadiali, N. D., and Schmueser, D. W., "An Analytical Technique for Evaluating Deformations due to Welding", Paper Submitted to ASME WAM, November 27, December 2, 1977, held in Atlanta, Ga.

23 Rosenthal, D., "Mathematical Theory of Heat Distribution During Welding and Cutting", Welding Journal Research Supplement, May 1941, pp 220-234.

24 Cheng, C. F., Ellingson, W. L., Kupperman, D. S., Park, J. Y., Poeppel, R. B., and Reiman, K. J., "Corrosion Studies of Nuclear Piping in BWR Environments", Quarterly Report, Argonne National Laboratories, June, 1976.

25 "Studies on AISI Types -304, -304L, and -347 Stainless Steels for BWR Applications", NEDO-20985-1, September, 1975.

26 Klepzer, H., et al., "Investigation of Cause of Cracking in Austenitic Stainless Steel Piping", General Electric Report No. NEDO-21000-1, July, 1975.

Contract Title: A Dynamic Photoelastic Investigation of Crack Arrest

Contractor: University of Maryland

Location: Mechanical Engineering Department
College Park, Maryland 20742

Principal Investigators: Dr. George R. Irwin
Dr. James W. Dally
Dr. Takao Kobayashi
Dr. William L. Fourney

Objective: The overall objective of the research program is to determine appropriate characterization methods for crack arrest in terms of a measurable physical property of the material, development of test methods and specimens for standardized crack arrest toughness measurements, and adoption by ASME Code and Regulatory authorities for design and operation of pressurized water primary system components.

FY-77 Scope: 1. Determination of Crack Velocity $\dot{a}$ vs Stress Intensity Factor K Relationship with SEN, R-DCB, C-DCB and M-CT Specimens.

2. Interaction with Battelle-Columbus Laboratory (BCL), and Materials Research Laboratory (MRL) - Photoelastic Verification of BCL and MRL crack arrest toughness measurement procedures.

3. Development of a Ring Specimen - Development of a ring specimen and a loading system to produce a high stress gradient at the inside boundary simulating thermal stress. Dynamic photoelastic study of crack propagation and arrest in the ring specimen.

4. Influence of Damping - Measurement of damping coefficients for three polymeric materials and correlation with previously measured fracture characteristics.

5. Birefringent Coatings on Metallic Specimens - Initiation of the development of a method to measure instantaneous K values in metallic specimens.

6. Consultation to NRC - Dr. G. R. Irwin will provide consulting services to NRC.

Summary of Research Activities and Results

A. Introduction

The research program at the University of Maryland is directed toward achieving understanding and characterization of dynamic crack behavior, particularly crack arrest phenomenon. The program has several objectives which are listed below:

1. The determination of crack velocity $\dot{a}$ - stress intensity factor K relationship for Homalite 100 with different types of fracture specimens.
2. Verification of testing and analytical procedures developed by Materials Research Laboratory (MRL) and Battelle Columbus Laboratory (BCL) for determining K_{Ia} and K_{IDm}.
3. Characterization of the dynamic aspects of fracture in duplex specimens.
4. Investigation of crack propagation in thermally stressed ring specimens.
5. Development of a numerical code to describe straight line crack propagation in two-dimensional rectangular fracture specimens.
6. Providing consulting services for NRC.

This research program is one part of a much larger co-ordinated effort involving BCL (Hahn, Kanninen and Hoagland), MRL (Ripling and Crosley), and the University of Illinois (Corten). The progress made in characterizing the dynamic aspects of fracture is due to the combined efforts of the four laboratories and the free exchange of ideas, data, codes and experience.

815 118

B. K vs $\dot{a}$ relationships from the M-CT Specimen and the Machine-Loaded C-DCB Specimen

As part of the effort to show that the K vs $\dot{a}$ relationship is a material property independent of the specimen geometry and method of loading, the K vs $\dot{a}$ relationships were determined from a modified compact tension specimen and a machine-loaded C-DCB specimen and these relationships were compared with those obtained from SEN, wedge-loaded R-DCB and wedge-loaded C-DCB specimens in Fig 1. The agreement of the K vs $\dot{a}$ curves for the different specimens is excellent. This fact is further evidence that the K vs $\dot{a}$ relationship is a material property independent of specimen geometry. These curves also suggest that there exists a minimum stress intensity factor, K_{Im}, which is necessary to maintain crack propagation. When the stress intensity factor goes below K_{Im}, a crack arrest occurs.

One phenomenon which the K vs $\dot{a}$ relationship does not reveal is the oscillation of K during the crack propagation event and after the crack arrest. These oscillations are demonstrated in Figs 2 and 3. In order to understand the behavior of the crack it is necessary to understand the nature of oscillation. The Cranz-Schardin camera, which photographs the crack propagation event, is not adequate to observe oscillation since its number of frames is limited and the observation interval is not sufficiently long. The investigation of the oscillation of K in different specimens in the post-arrest period will be accomplished in the coming year by employing a Beckmann-Whitley drum camera which produces 224 frames over a 5 to 10 ms recording time.

C. Verification of the BCL One-Dimensional Code

Experimental results from a wedge-loaded R-DCB specimen of Homalite 100 were used to check the crack behavior predicted from the one-dimensional finite program developed at Battelle Columbus Laboratory. The experimentally established K vs $\dot{a}$ relationship, along with the specimen geometry and other properties of Homalite 100 were utilized as input for the computer code. The comparison of the experimentally observed crack behavior -- crack position as a function of time -- with the computer predicted behavior is shown in Figs 4 and 5. Fig 4 shows that a close agreement exists between experimental and predicted crack behavior in the early stage ($t < 200$ μs). For $t > 200$ μs the results tend to deviate. The first arrest predicted by the BCL code at $t = 230$ μs and $x = 158$ mm did not occur. The second arrest position predicted by the code at $x = 188$ mm was in reasonably close correspondence with the first experimentally observed arrest at $x = 197$ mm.

Fig 5 compares crack reinitiation behavior. The predicted reinitiation time of $t = 1205$ μs compares well with the experimental result of $t = 1070$ μs. However, the experimentally observed crack reinitiation velocity of 71 m/s was significantly lower than the predicted velocity of 218 m/s. The code predicted a region of slow growth or arrest at $x = 203.5$ mm which agreed closely with experimentally observed arrest at $x = 219$ mm.

From these observations it was determined that the BCL one-dimentional code closely predicted the initial crack velocity, crack arrest and crack reinitiation.

D. Verification of the MRL Procedure for K_{Ia} Measurements with Homalite 100 Machine-Loaded C-DCB Specimen

The MRL Procedure which utilizes a static analysis of the machine-loaded C-DCB specimen for determining K_{Ia} was checked. The calculation of K_{Ia} was made from the dimensionless equation shown in the MRL procedure (1):

$$\frac{K_{Ia} B h^{1/2}}{P_a} \left(\frac{B_N}{B}\right)^{1/2} = 5.44$$

for $0.394 \leq a/h \leq 1.1181$

where a is the crack length, h is the specimen height at the end of the contour, B is the thickness of the specimen, B_N is the net section thickness in the crack plane, and P_a is the load measured on the pins shortly after arrest.

The results are shown in Table 1 which indicates that the values of K_{Ia} determined with the MRL procedure were quite consistent irrespective of crack jump distance and were about 6 percent higher than K_{Im} established from photoelastic determinations shown in Fig 1. ($K_{Im} = 0.385$ MPa$\cdot\sqrt{\text{m}}$ for a machine-loaded C-DCB). These findings deviate from the predictions of dynamic analysis of fracture, and further investigation is needed.

E. Fracture Behavior in Duplex Specimens

A significant effort was devoted to an experimental study of crack propagation in duplex specimens of both the M-CT and R-DCB types. The fabrication of a duplex specimen with a joint material which has a toughness that is significantly different than the starter or arrest sections causes marked changes in the fracture behavior. Indeed, the duplex specimen should really be considered as a triplex specimen consisting of a starter section, the joining section and the arrest section.

The influence of the joining section on fracture behavior is profound. The joining section can produce crack arrest, crack branching, crack blunting, and splitting. The factors which control the fracture behavior include K_{Ic}, K_{Im}, and K_{Ib} for all three materials and the thickness of the joint.

The number of parameters which can be varied in an experimental program to study fracture behavior in duplex specimens are so large as to prohibit a complete investigation. Instead it was necessary to limit the variation of the parameters and to conduct small numbers of tests in an effort to observe general effects.

In the first series of tests with the M-CT Duplex (H-100/KTF_2) with a very tough Hysol EA 9410 adhesive joint, it was observed that the joint served to arrest the cracks. The cracks arrested abruptly upon penetrating about 0.01 to 0.02 mm into the adhesive (see Fig 6). The deceleration of the crack is of the order of 4×10^7 g's. After arrest the K value increases rapidly with respect to time as kinetic energy in the duplex specimen is converted to strain energy. If K is sufficiently high, the crack will reinitiate in the adhesive and extend into the arrest section of the duplex specimen (see Fig 7). If K is not sufficient for reinitiation the crack remains at arrest and the K field at the crack tip oscillates at a frequency of approximately 1800 Hz (see Fig 8).

In the second series of tests the effect of the adhesvie joint (Hysol EA 9410) was isolated by fabricating both the starter and arrest section from Homalite 100. It was observed that stable arrest could be achieved with joint thicknesses as low as 0.102 mm where K exceeded $3K_{Ic}$ for Homalite 100. It appeared that increasing the joint thickness increased the arrest capabilities of the joint.

In the third series, the effect of toughness of the adhesive joint was examined by using a EPON/DETA epoxy to join two sections of Homalite 100. This adhesive is relatively brittle and there is no tendency for arrest when the crack enters the joint (See Fig 9). However, for relatively thick joints the crack will branch and divide the energy available producing arrest at the second interface (See Fig 10). For relatively thin joints, surface roughening will tend to blunt the crack which can also cause arrest at the second interface for low energy tests.

The fourth series of tests utilized a tough KTE_2 arrest section with the brittle EPON/DETA adhesive joint. Again surface roughening and/or branching acts to arrest the crack at the second interface. For very thick joints branching occurs which results in a mixed mode K at the second interface. If K_{II} is sufficiently high relative to K_I/K_{Ic} for the arrest section then the crack will re-initiate and propagate with a low velocity along the adhesive joint (See Fig 11).

This experimental survey shows that at least three different mechanisms exist for crack arrest in the joining section (tough arrest, branching with energy division and mixed mode, and crack blunting). Often the arrest is stable and the crack cannot penetrate into the arrest section of the duplex specimen. In all cases the arrest affects the dynamic behavior of the specimen with very large oscillations in K occurring.

Fabricating metallic duplex specimens by welding may introduce similar fracture behavior as the toughness of the weld and the weld heat affected regions of the starter and arrest sections may deviate so as to produce either stable crack arrest, crack branching, weld splitting or violent K oscillation.

F. Crack Propagation in a Thermally Stressed Ring Specimen

The thermal stress distribution in a ring specimen has been simulated with a mechanical deformeter shown in Fig 12. The dynamic stress intensity factor was found to decrease with slight oscillations both with time and crack length in the ring type fracture specimen as shown in Figs 13 and 14. This behavior was quite different from the static stress intensity factor which was found to increase until $\frac{a}{w} = .4$ and then decrease monotonically (2). The small oscillations in the dynamic stress intensity factor were produced because of the dynamics of the specimen loading system.

Stress intensity factor K versus $\dot{a}$ relation was established for the ring specimen as shown in Fig 15. This gave $K_{Im} = 0.38$ $MNm^{-3/2}$. This value was found to compare well with similar values for R-DCB, C-DCB and SEN specimens (see Fig 1).

It was determined that the crack would arrest in the compression zone for $1 < K_Q/K_{Ic} \lessapprox 2$ and would pass through the specimen for $K_Q/K_{Ic} > 2$ for an initial crack length of .08 w.

The experimental results from this study provide a guide to understand the crack propagation in a thermally stressed cylindrical vessel. However, it should be recognized that the actual transient temperature distribution has not been simulated. Also, the toughness variation across the section is not modelled. In a continuation of this work, duplex and triplex rings will be examined to study the effect of changes in fracture toughness across the ring specimen.

G. Development of a Two-Dimensional Code

A two-dimensional dynamic finite difference analysis is under development. This code will be employed to predict fracture behavior in rectangular components such as M-CT or R-DCB fracture specimens and to study the influence of the form of the $\dot{a}$ - K relation on fracture behavior.

H. References

1. Crosley, P. B. and Ripling, E. J., "Guidelines for Measurement of K_{Ia} with Tapered DCB Specimens", prepared for ASTM committee E24, T. G. E24-03.04 March 1977.
2. Cheverton, R. D., "Pressure Vessel Fracture Studies Pertaining to a PWR LOCA-ECC Thermal Shock, Experiments TSE1 and TSE2", ORNL Sept. 1976.

I. Plan of Research for Future Years

The research program in the coming years will involve work on 6 different tasks.

Task 1. Verification of BCL and MRL test and analytical procedures leading to a standardized test for crack arrest toughness.

Task 2. Development of a method utilizing birefringent coatings to determine instantaneous K values associated with cracks propagating in steel specimens.

Task 3. Continued development of a ring specimen and a mechanical method to simulate thermal stresses in a ring.

Task 4. Continued studies of duplex specimens where the adhesive line may closely model the weld line in a structure.

Task 5. Continued development of a two-dimensional computer code for crack propagation along a straight line in a rectangular fracture specimen.

Task 6. Provide consultation services - Dr. George R. Irwin will consult for the NRC approximately three days per month.

TABLE 1

SUMMARY OF K_{Ia} TEST RESULTS

Model No.	Specimen Thickness B (mm)	P_Q (N)	P_a (N)	a_o (mm)	Δa (mm)	$\Delta a/a_o$	K_Q ($MPa\sqrt{m}$)	K_{Ia} ($MPa\sqrt{m}$)	K_{Ia}/K_Q
169A	12.95	381	317	43.2	12.4	0.288	0.502	0.418	0.833
169B	12.95	336	301	60.6	8.1	0.134	0.443	0.397	0.896
170	13.03	406	338	40.3	10.8	0.267	0.532	0.443	0.832
172	13.67	423	316	39.4	52.2	0.323	0.528	0.395	0.748
174	13.51	449	311	58.1	28.9	0.498	0.567	0.393	0.693
224	12.90	445	309	54.8	25.8	0.471	0.589	0.409	0.694
225-	12.45	449	298	55.3	31.8	0.596	0.616	0.409	0.662
								Av. 0.409	

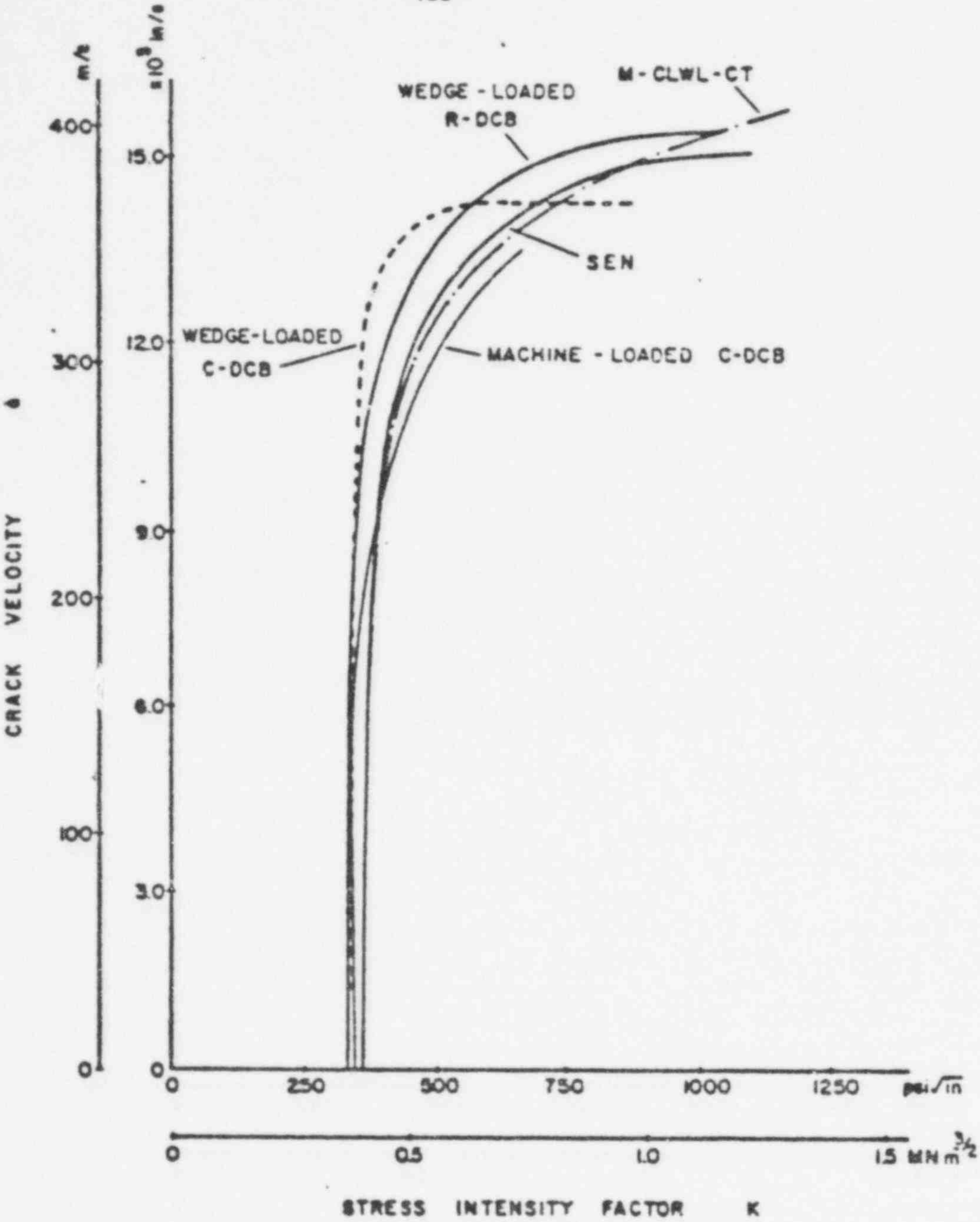

Fig 1 Comparison of K - ȧ Curves from Five Different Specimens (Homalite 100)

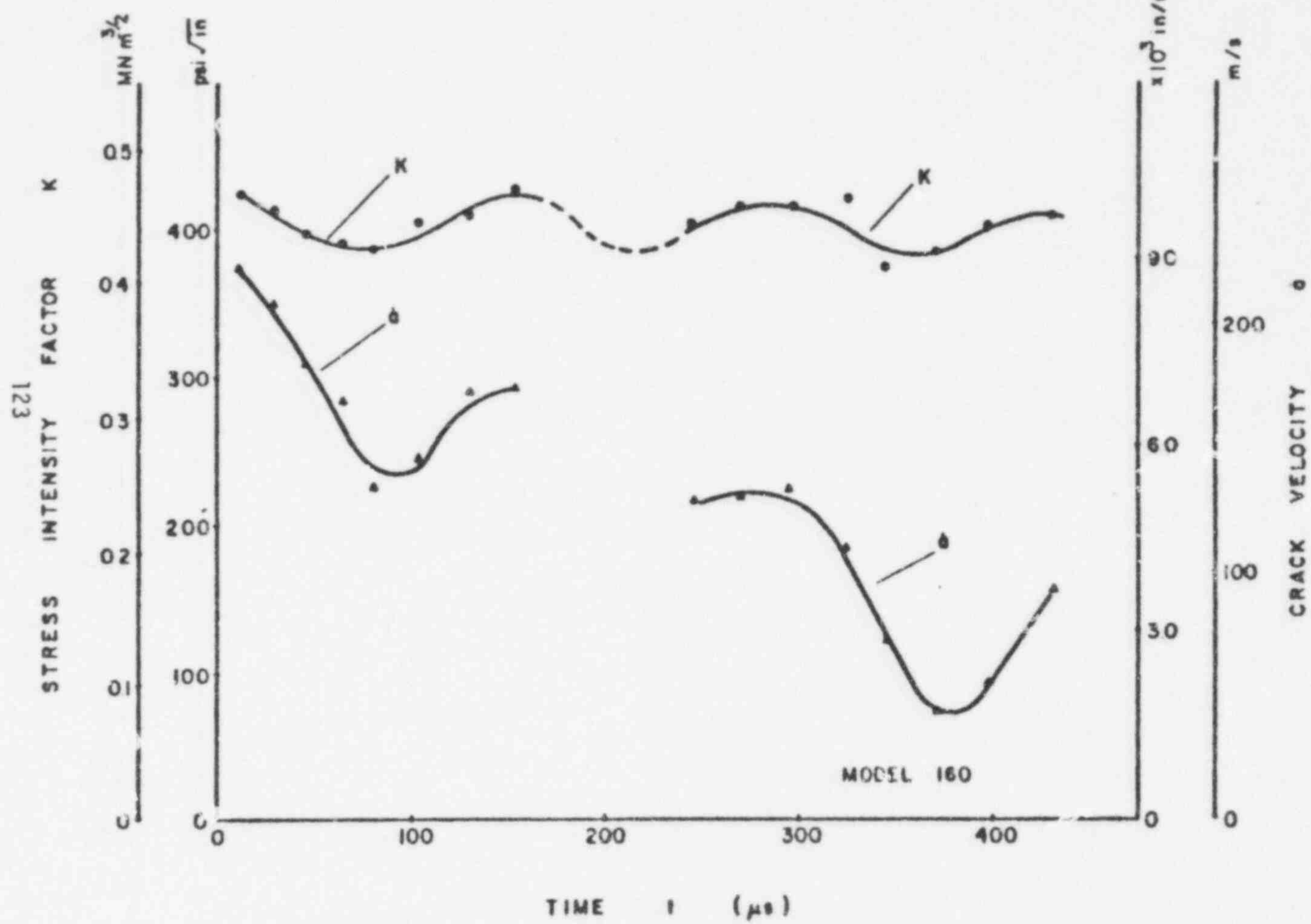

Fig 2 Stress Intensity Factor K and Crack Velocity $\dot{a}$ as a Function of Time for M-CT No. 160

815 129

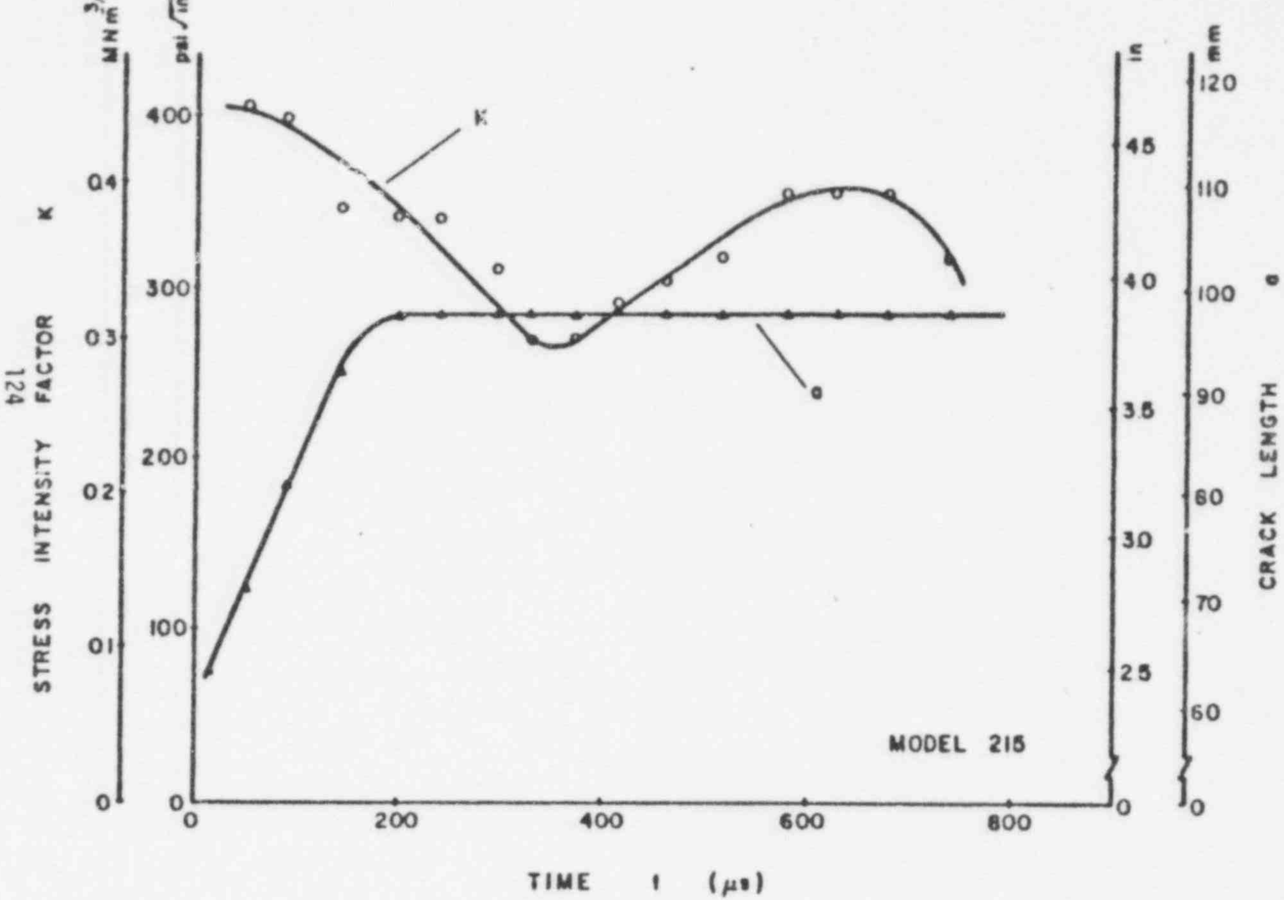

Fig 3 Stress Intensity Factor K and Crack Length a as a Function of Time. C-DCB Model 215

815 130

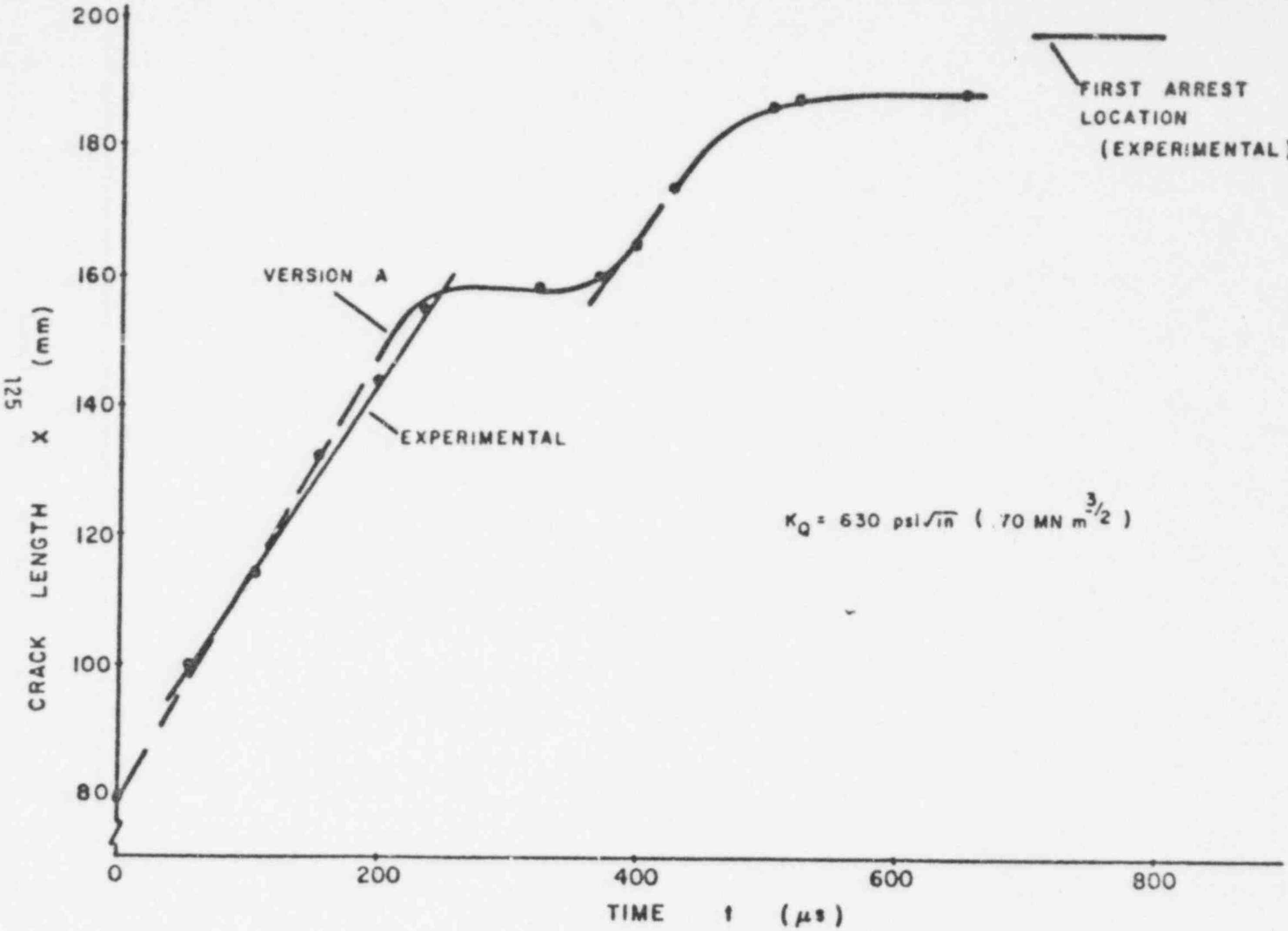

Fig 4 Crack Length as a Function of Time from BCL Program

815 131

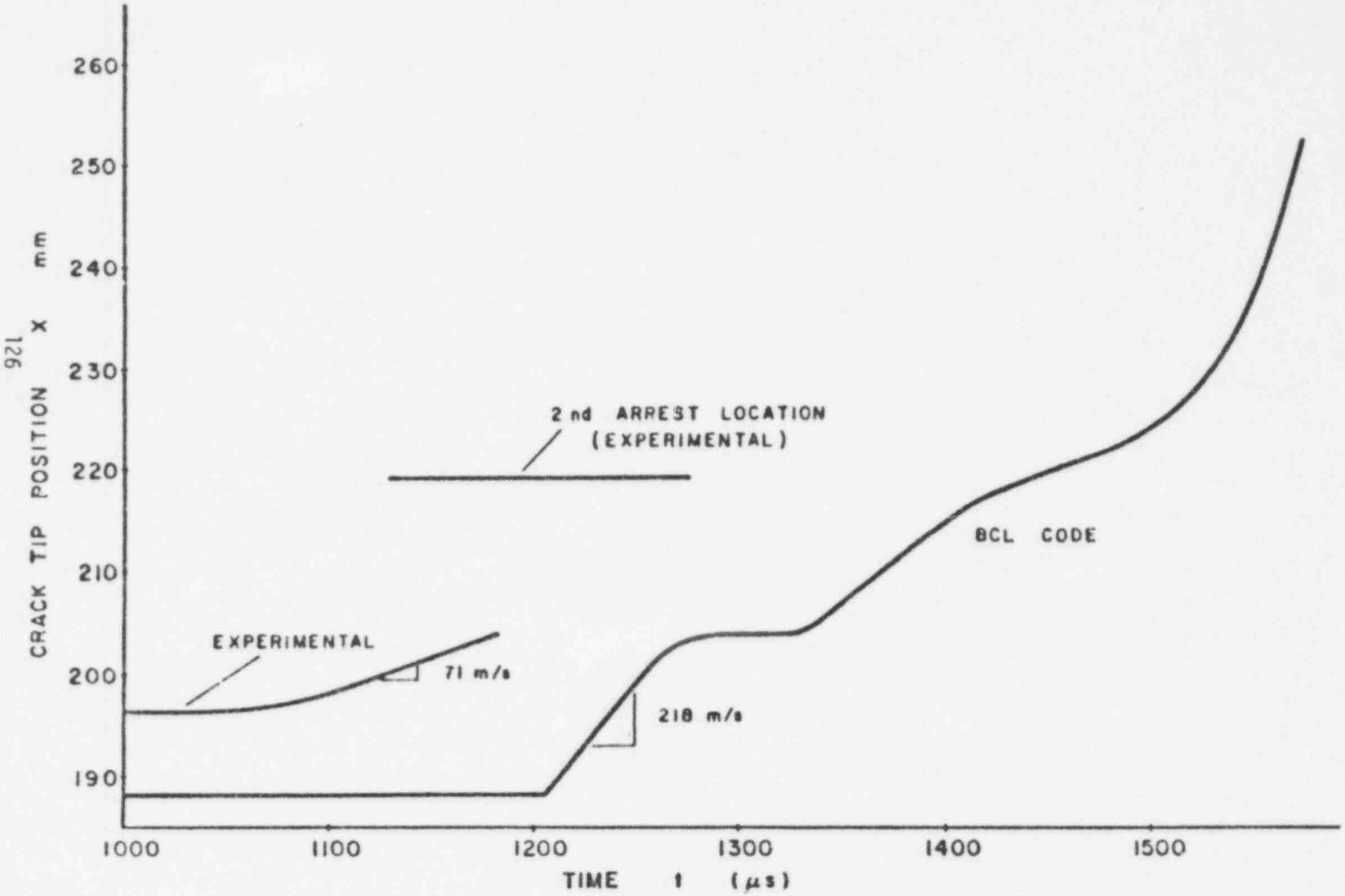

Fig 5 Crack Length as a Function of Time - Late Event - Version A

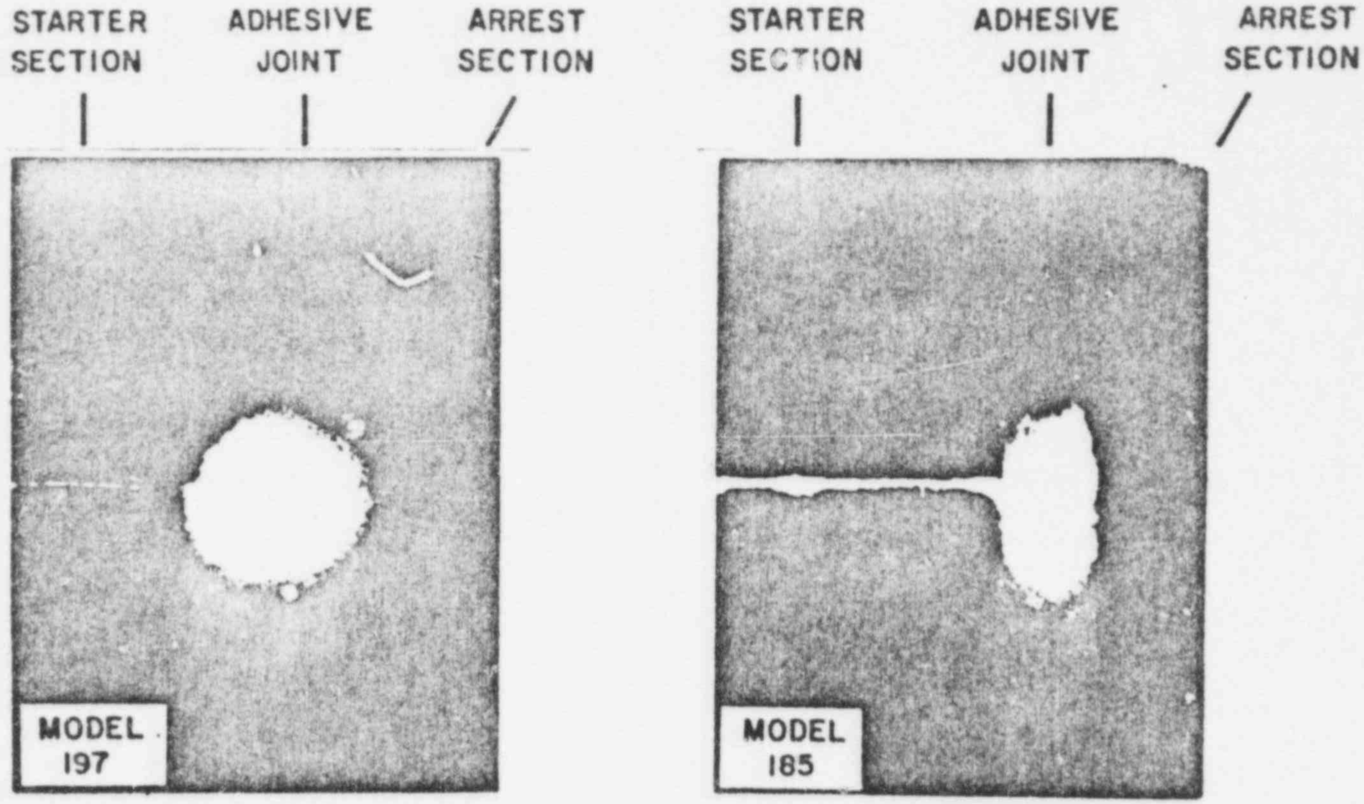

(a) $S = 0.36$ mm

$\Delta a = 0.02$ mm

(b) $S = 0.15$ mm

$\Delta a = 0.01$ mm

Fig 6A Photomicrographs of the Arrested Crack in the Adhesive Joint

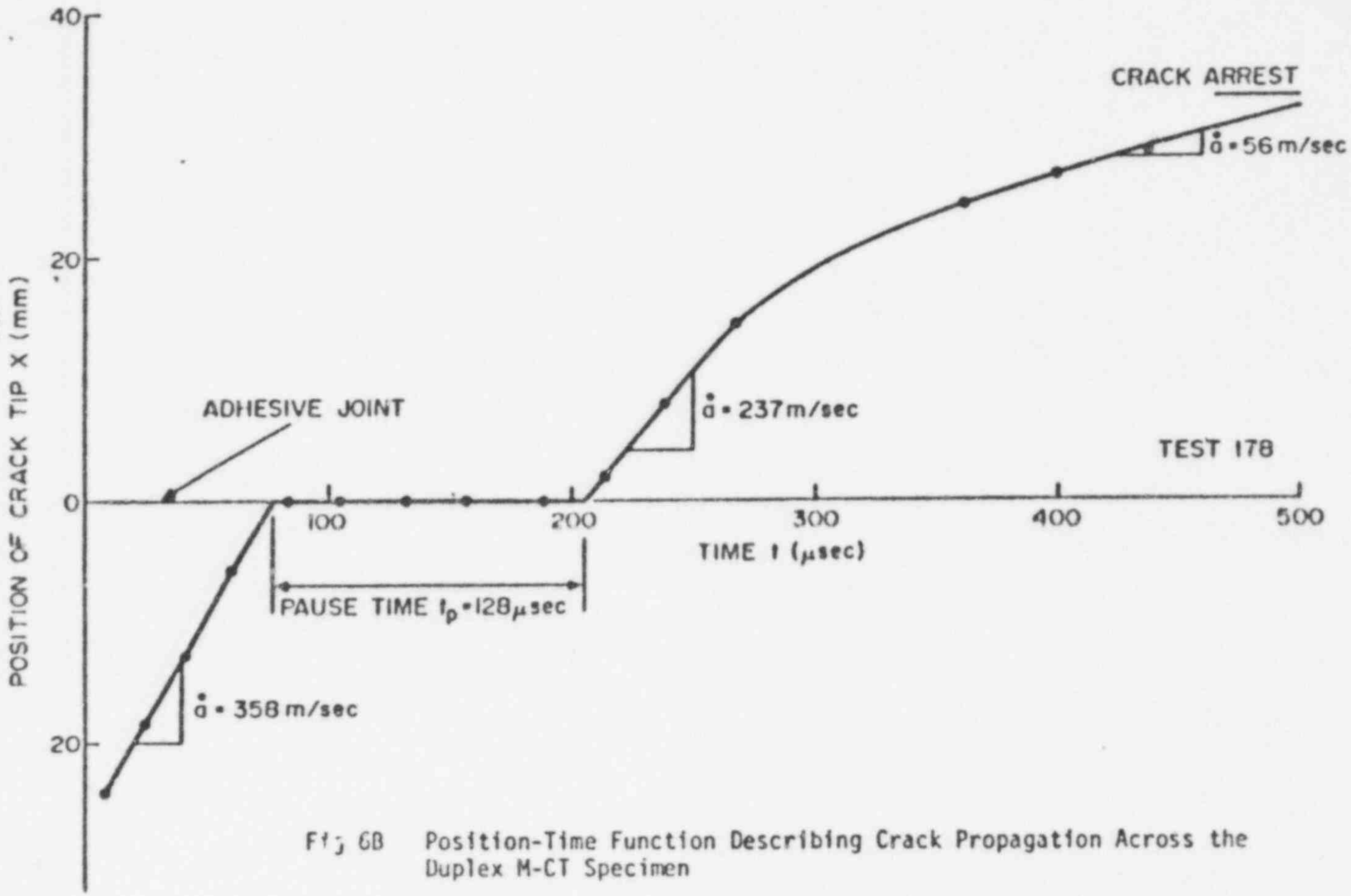

Fig 6B Position-Time Function Describing Crack Propagation Across the Duplex M-CT Specimen

128

815 134

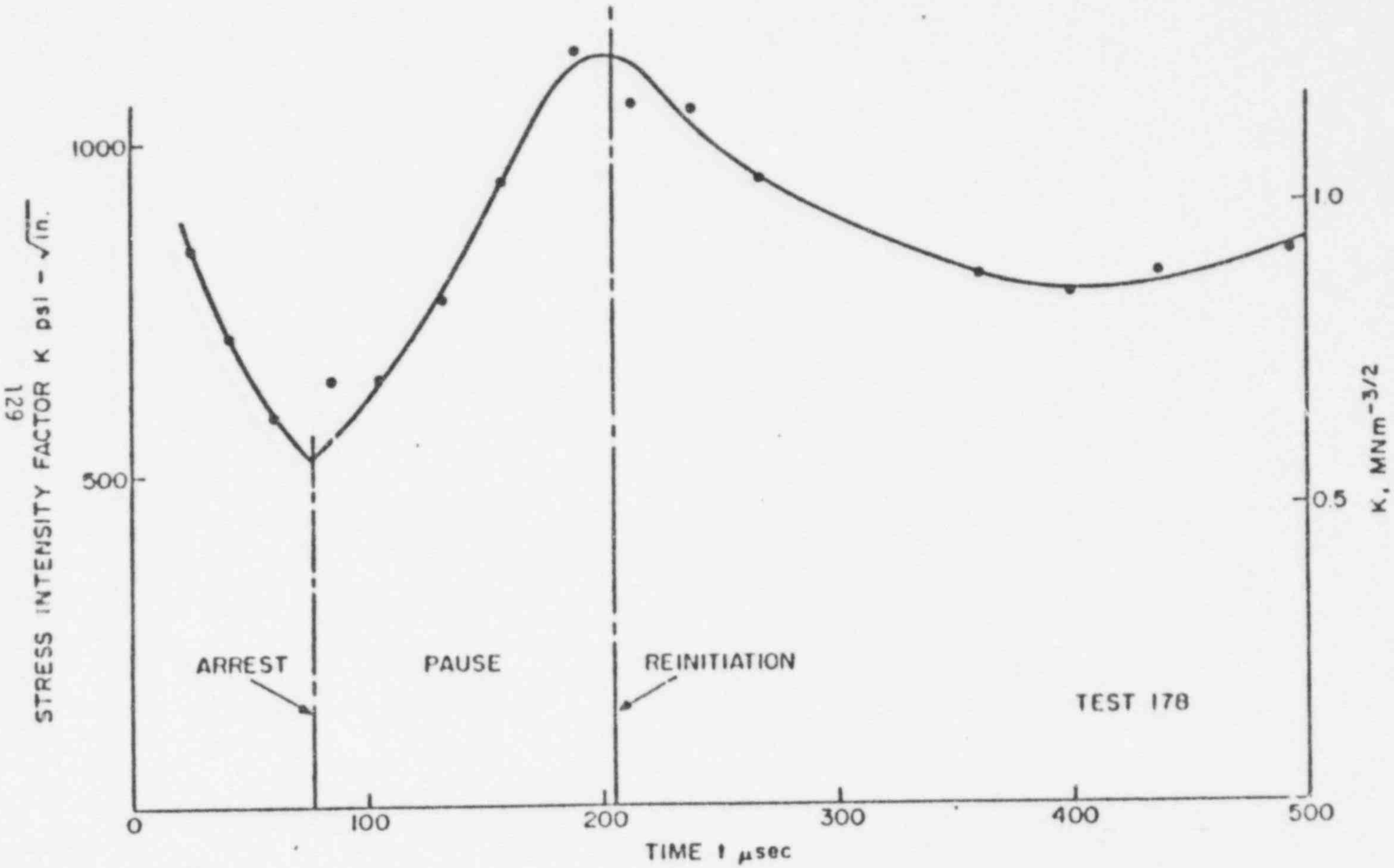

Fig 7 Stress Intensity Factor as a Function of Time in a Duplex M-CT Specimen with Crack Reinitiation

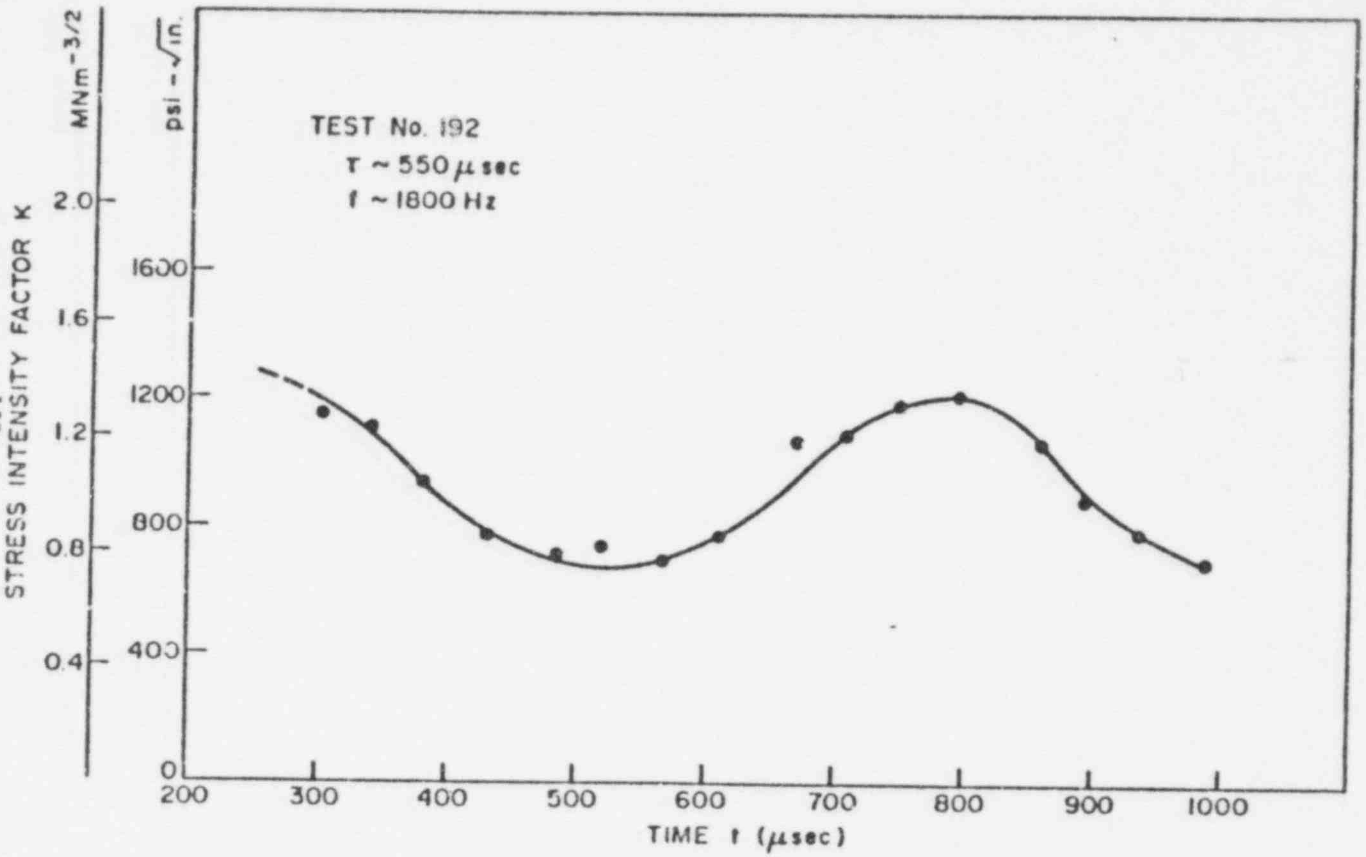

Fig 8 Oscillation of K with Time for a Duplex M-CT Specimen with Stable Arrest

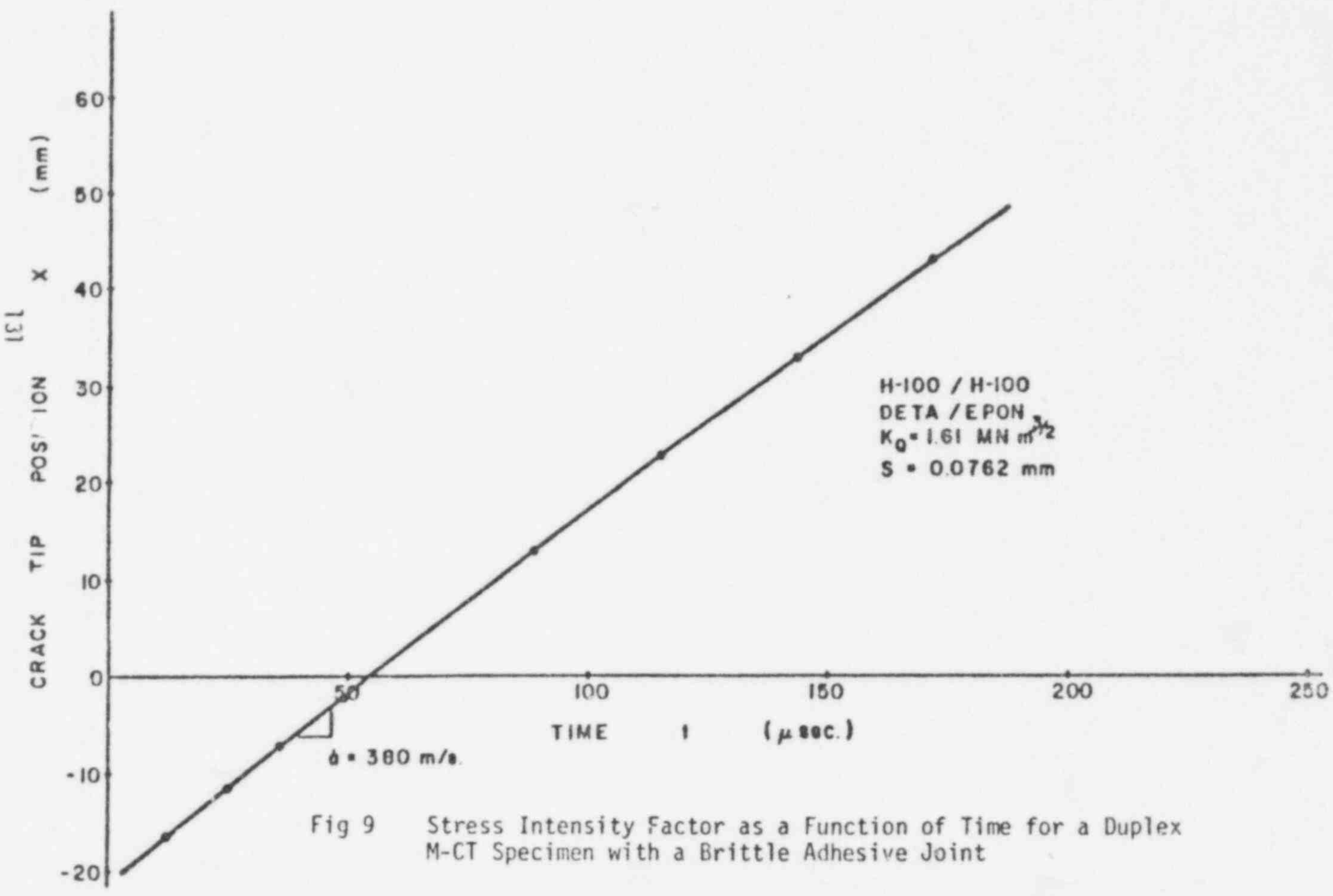

Fig 9 Stress Intensity Factor as a Function of Time for a Duplex M-CT Specimen with a Brittle Adhesive Joint

815 137

MODEL 236

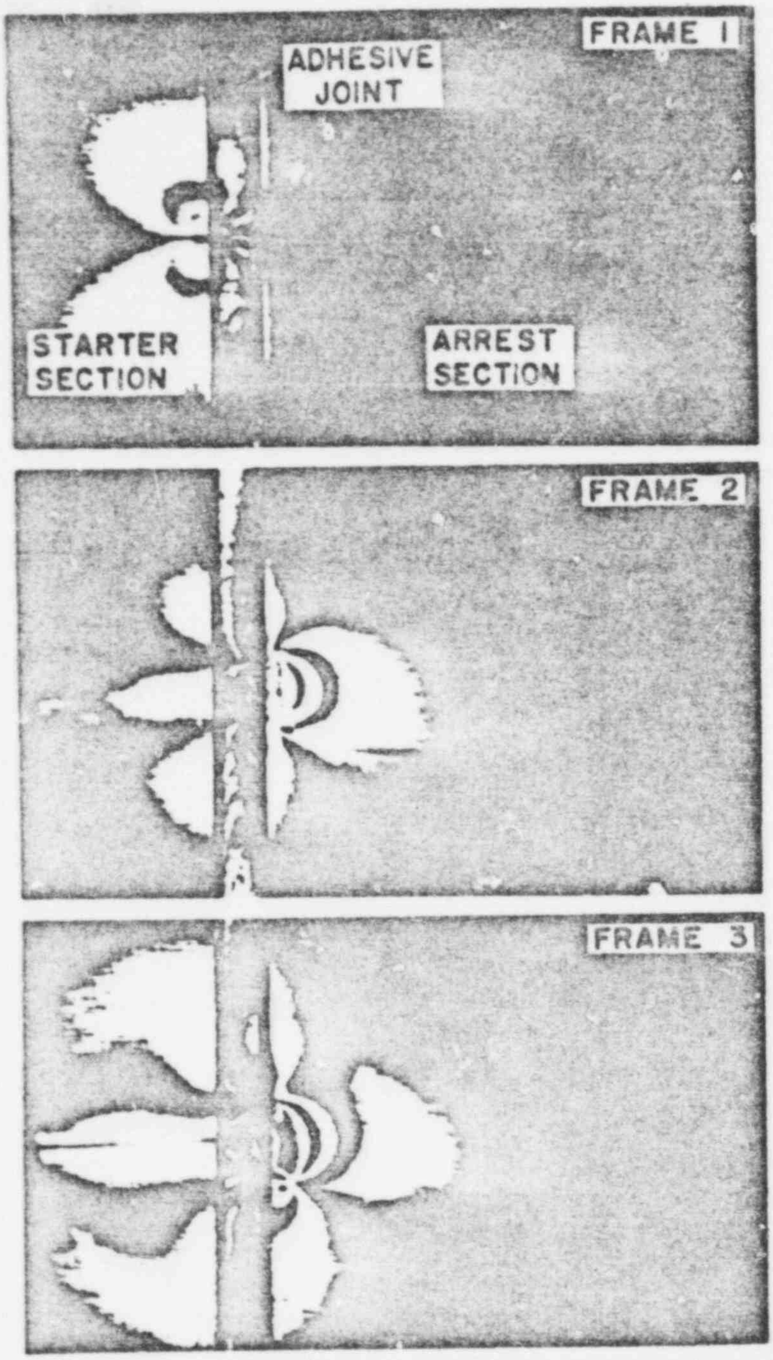

Fig 10 Crack Branching and Crack Arrest in a Duplex M-CT Specimen with a Thick (3.175 mm) DETA/EPON Adhesive Joint

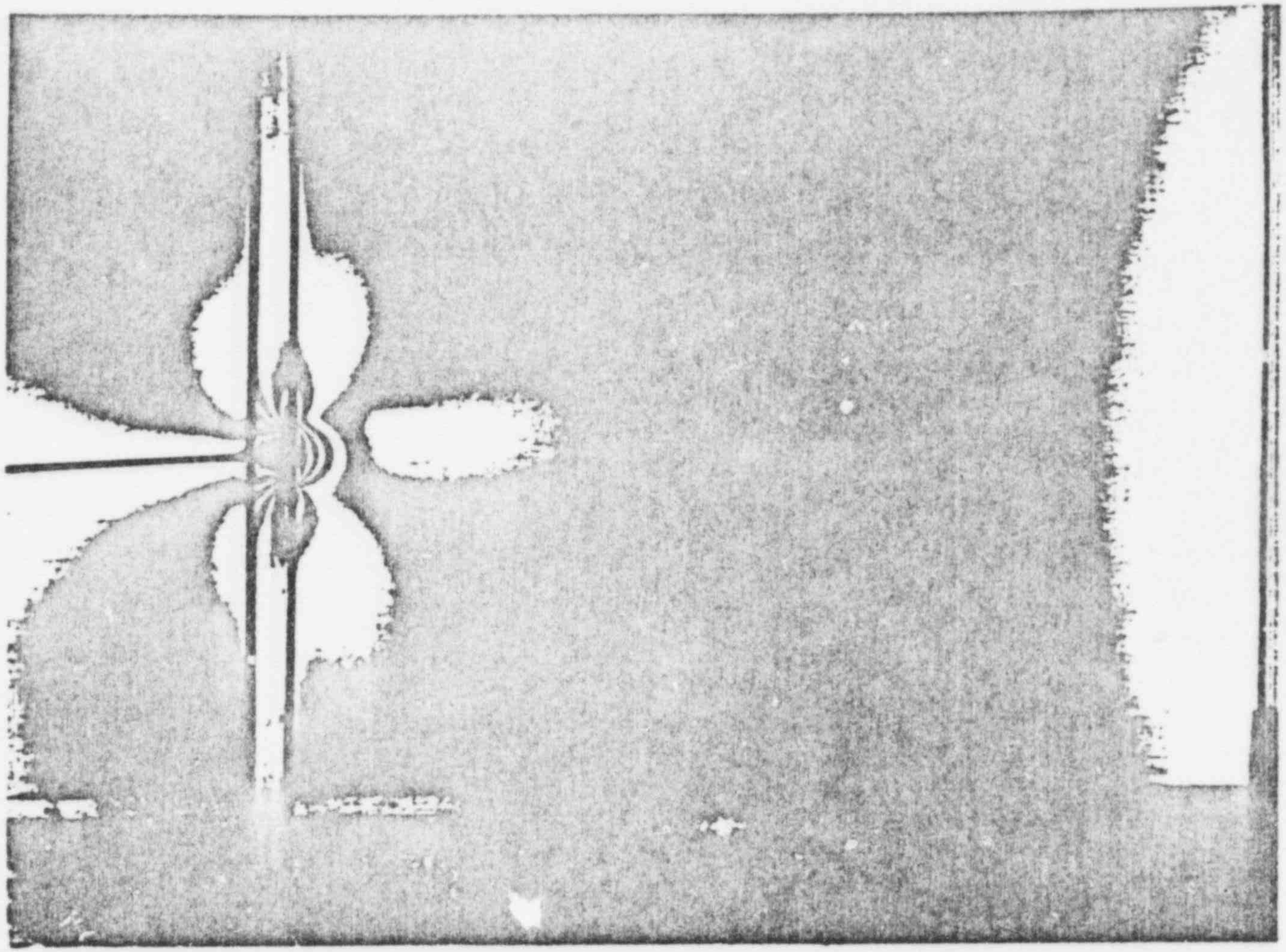

Fig 11 Crack Branching, Arrest and Reinitiation in a Duplex M-CT Specimen with a Thick (3.175 mm) DETA/EPON Adhesive Joint

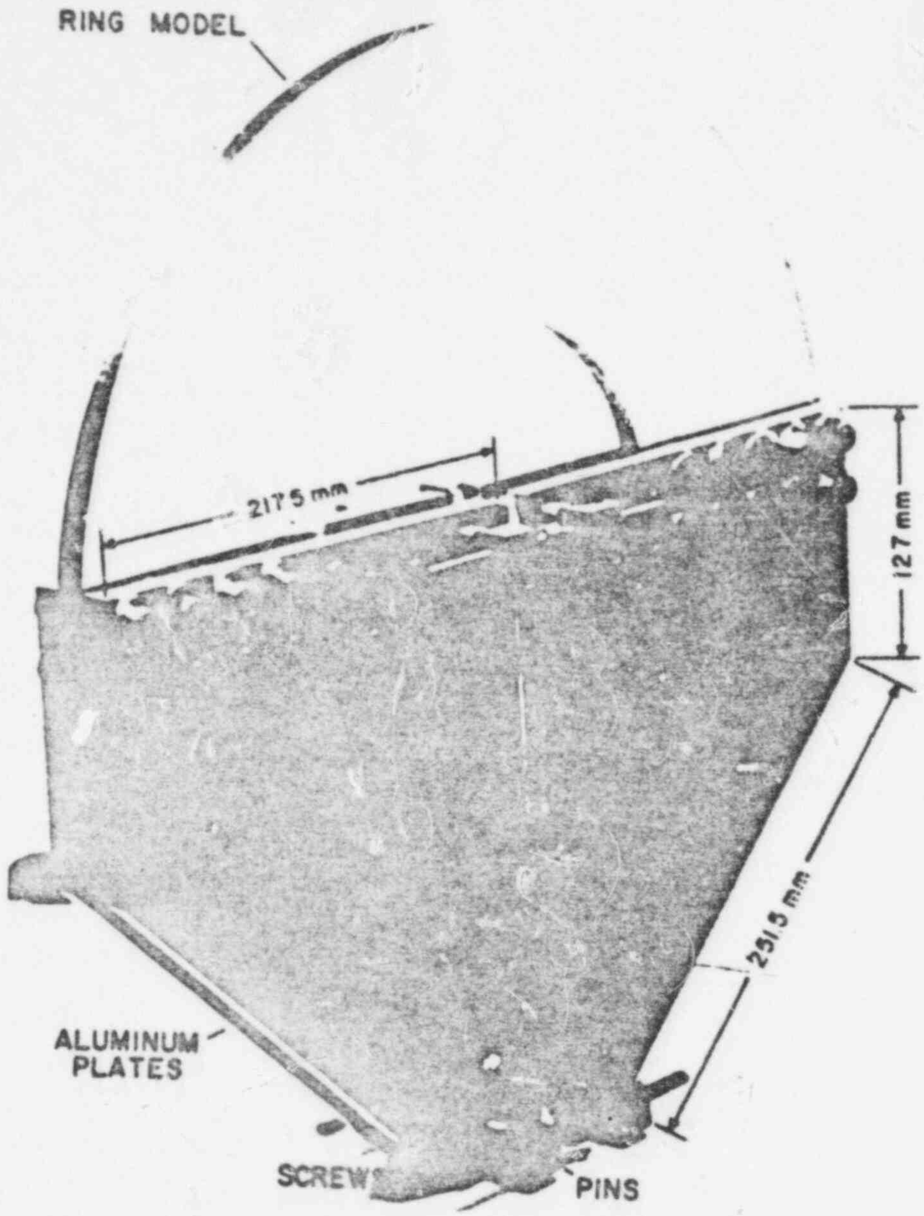

Fig 12 Loading Fixture Together with the Ring Specimen

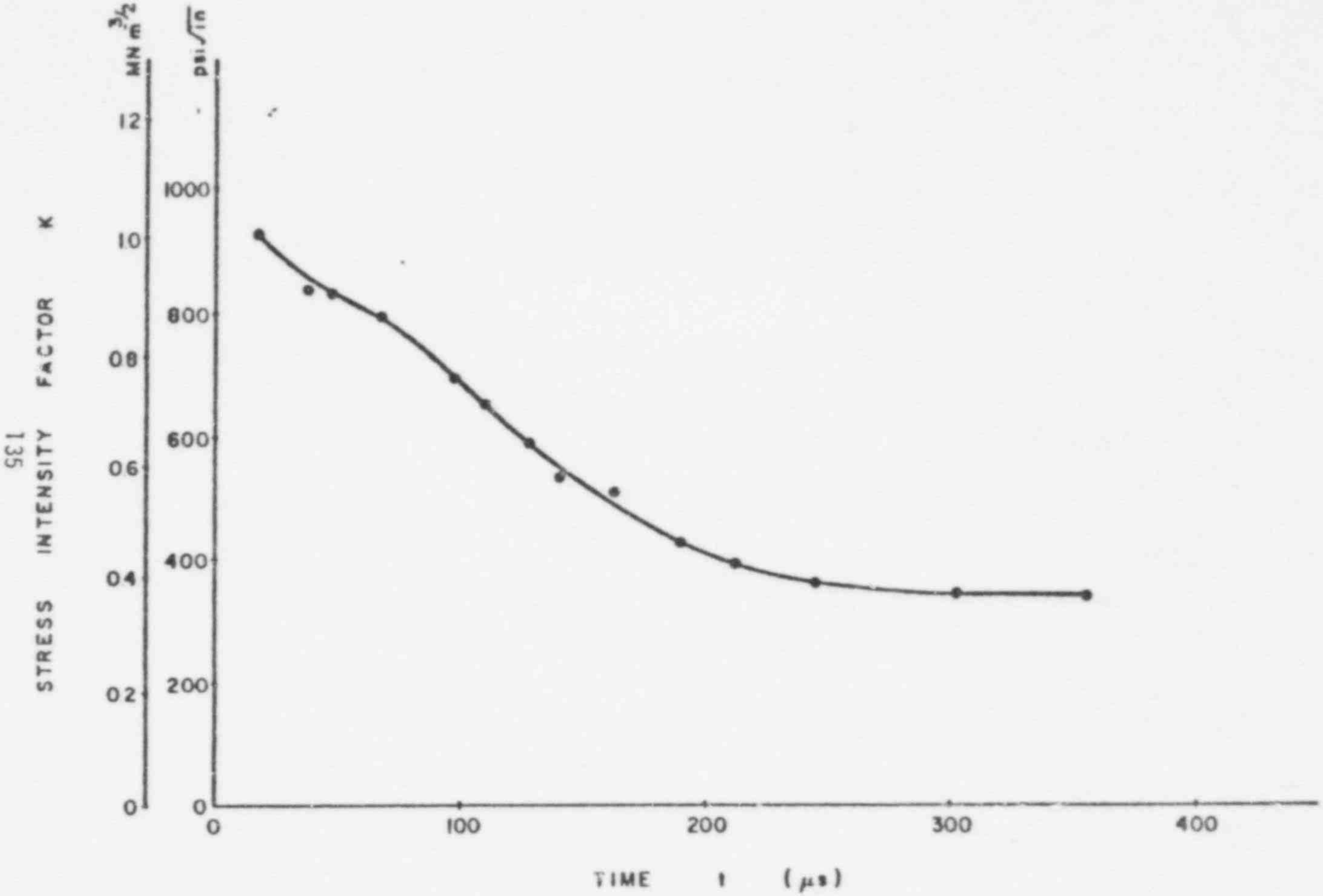

Fig 13 Stress Intensity Factor as a Function of Time for Model R-1

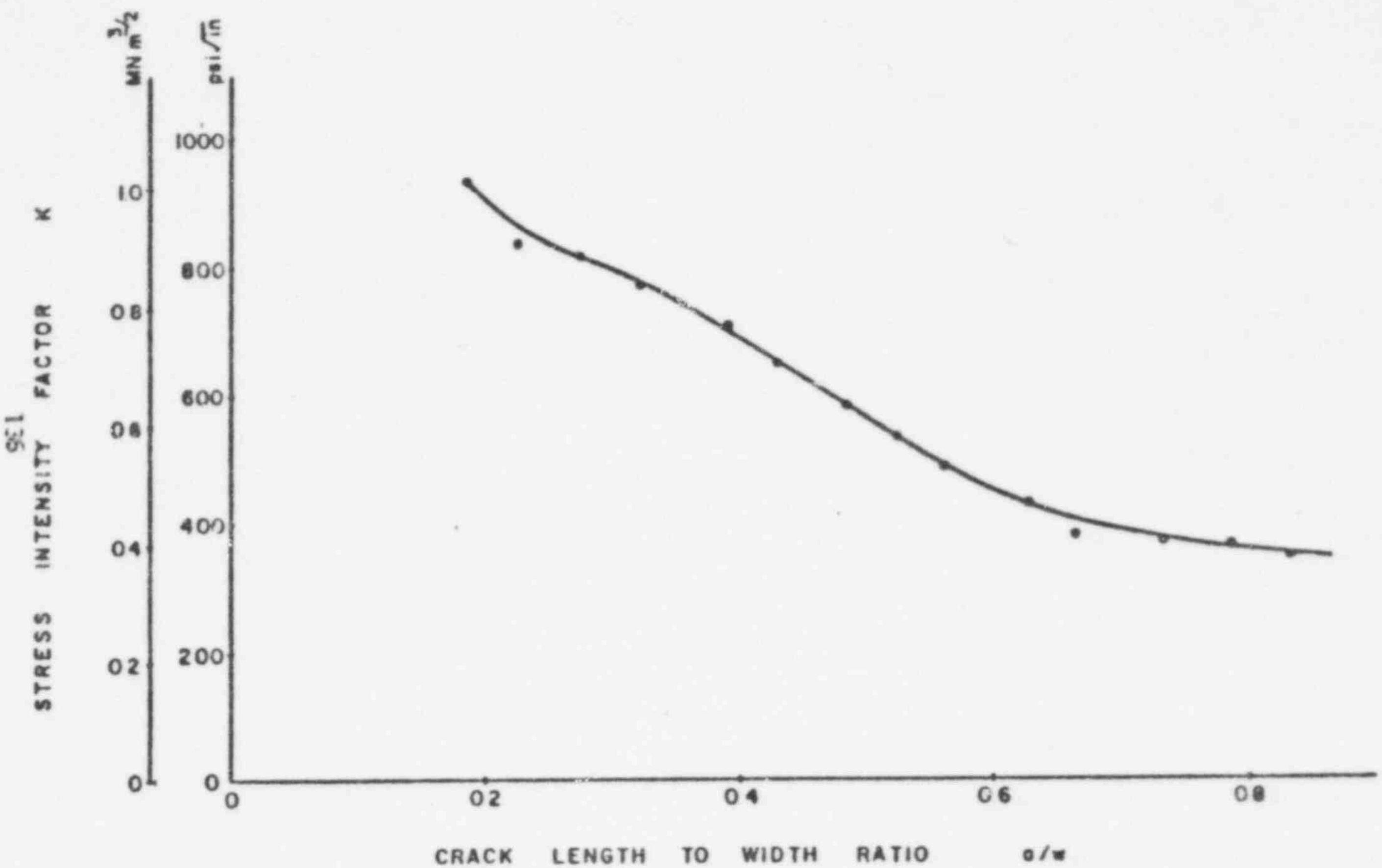

Fig 14 Stress Intensity Factor as a Function of Crack Length to Width Ratio for Model R-1

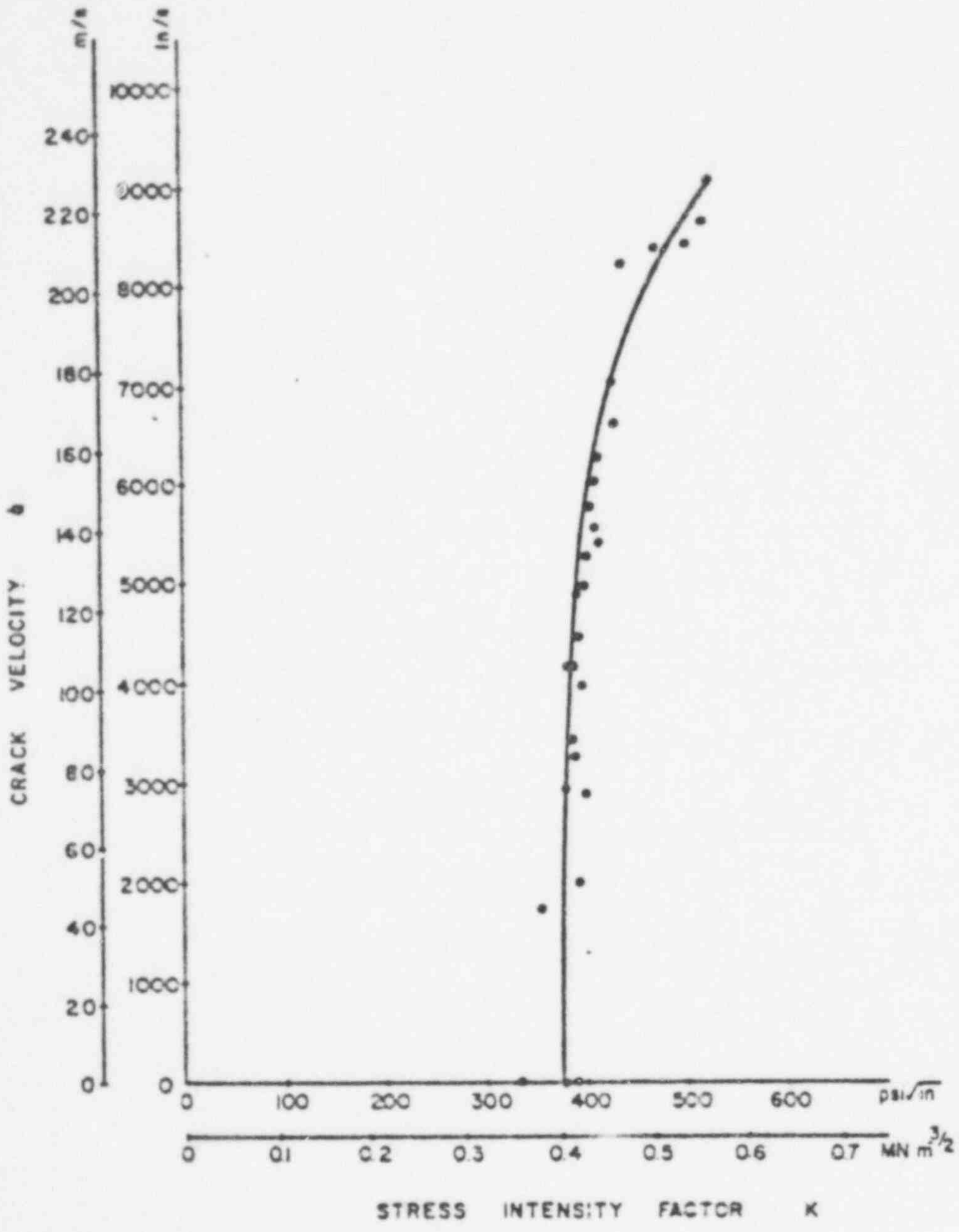

Fig 15 Stress Intensity Factor as a Function of Crack Velocity for Ring Specimen - Homalite 100 - 3rd Shipment

<u>Contract</u>: Primary Coolant Pipe Rupture Study AT (49-24)-0202

<u>Contractor</u>: General Electric Co.
Nuclear Energy Division
Boiling Water Reactor Systems Dept.
San Jose, CA

<u>Principal Investigators</u>: D. A. Hale/J. Yuen

<u>Objectives</u>:

<u>Task K - Environmental Fatigue Behavior of Piping Steels</u>

Develop environmental fatigue data to determine whether the existing ASME design rules for fatigue adequately account for the effects of the BWR primary water environment. Fatigue data to include both crack initiation and crack growth data developed in an operating plant water environment and in a simulated BWR water environment at several loading frequencies and mean stress levels. Analyze these data to develop appropriate design rule changes which properly account for frequency, mean stress and environment.

<u>FY 76 Scope</u>:

<u>Task K_D - Environmental Fatigue</u>

1) Complete a topical report summarizing results of environmental low cycle fatigue crack initiation work done during the previous contract year in a BWR primary water environment (Dresden I) and a reference 500°F lab air einvironment.

2) Complete fatigue crack growth rate testing of LWR primary piping and pressure vessel materials in a simulated BWR primary water environment to determine effects of frequency and mean load. Prepare a topical report summarizing results of this work.

TASK K - ENVIRONMENTAL FATIGUE BEHAVIOR OF LWR PRIMARY PIPING AND PRESSURE VESSEL STEELS

Introduction

In recent years, the question of material/environment interaction has received increased attention due to problems being experienced by operating LWR power plants involving cracking in both piping and reactor pressure vessels. Attempts to understand and analyze these problems have pointed to a need for increased understanding of the processes involved in initiating and propagating cracks in the presence of an operating plant environment and, more importantly, for data representative of service conditions.

Work has been done by GE during the last year, under the auspices of the Pipe Rupture Study, to generate needed engineering data. This data includes results from both crack initiation and crack growth tests conducted in either an operating BWR or simulated BWR water environment. These results are compared with applicable sections of the ASME code.

Test Program

Fatigue Crack Initiation (Task K_a, K_b) - In the area of fatigue crack initiation, work was concluded this past year on a topical report summarizing an experimental program begun in 1970. This program was designed to produce fatigue crack initiation data in an actual operating BWR primary water environment.

With the cooperation of Commonwealth Edison, a special test loop was installed at their Dresden-I nuclear power plant. With this loop, a number of test specimens were mechanically loaded while exposed to Dresden-I primary water (500°F, 1050 psig). A schematic of the loop is shown in Figure 1.

A special test specimen was developed for this program - See Figure 2. This specimen is a cantilever beam which is loaded through a fixed cyclic deflection range to develop the desired cyclic strains in the reduced thickness test section.

A small capillary hole was drilled on the neutral axis of each specimen beginning at the fixed end of the specimen and terminating in the middle of the reduced thickness test section. This capillary hole formed a drywell within each individual specimen which was connected to an individual external pressure via capillary tubing. This hole served both to automatically define and signal specimen failure, i.e. a macro crack which initiates on the surface of the specimen and grows to a depth sufficient to intersect the "drywell" thereby allowing full vessel pressure to be applied to the external switch is defined as failure.

A total of 150 of these specimens were tested in the Dresden-I facility. These 150 represented four piping materials (T-304 and 304L SS, Inconel 600 and A-516 CS) in a variety of metallurgical conditions including weldments. In order to provide baseline data to properly interpret this BWR data, a total of 36 of these same type specimens were tested in a 500°F air environment.

A topical report summarizing work done on this task was completed during this past year.* Significant results are hi-lited below:

1) The effects of the BWR environment on the Low Cycle Fatigue (LCF) life of T-304 and 304L stainless steels tested in the as received condition is negligible. Therefore, the existing ASME B&PV Code Section III fatigue design rules are adequate for these particular material/environment combinations.

2) A significant decrease in LCF life was observed for both the T-304 and 304L stainless steels in the fully furnace sensitized condition. The fracture surface of these specimens displays a mixed mode transgranular and intergranular character suggestive of Intergranular Stress Corrosion Cracking (IGSCC). Therefore, these same ASME III fatigue design rules do not yield conservative results when used in a material/environment combination where IGSCC is involved.

---

*GEAP-20244, "Low Cycle Fatigue Evaluation of Primary Piping Materials in a BWR Environment," D. A. Hale, S. A. Wilson, E. Kiss and A. J. Giannuzzi, September, 1977.

3) A reduction in LCF life is observed for the A-516 carbon steel tested in the BWR data. This reduction is strongly linked to surface pitting which occurs in this material. In spite of this reduction in LCF life, the ASME III fatigue rules yield conservative results.

Fatigue Crack Growth

The major effort on this contract during this past year dealt with environmental fatigue crack growth in piping and pressure vessel steels.

Environmental fatigue crack growth tests were conducted in a GE high pressure/temperature test loop which circulates a nominal 10 gpm of 550°F, 1150 psig demineralized water through two autoclaves. The dissolved oxygen level and conductivity of this circulating water was constantly monitored and controlled within limits which are typical of operating BWR primary water system. A schematic of this "simulated BWR water" test loop is shown in Figure 3.

Two autoclaves were committed for use with this loop. Both were used to load a series chain of 1T-WOL test specimens (See Figure 4), eight in one vessel, three in the other. This WOL specimen is a standard fracture mechanics specimen widely used by many other investigators for these type studies.

Both autoclaves were equipped with closed-loop, servo controlled loading systems which constantly monitor the load being applied to the specimen chain. Both systems were capable of applying any desired time/load waveshape over a wide range of frequencies.

Crack growth data for the individual specimens were obtained using two independent schemes. In the first approach, a line of capillary holes on 0.100" centers were drilled from either side of the specimen normal to and intersecting the plane of fatigue crack growth (See Figure 5). These holes were connected to external pressure switches via capillary tubing. Therefore, as the fatigue pre-crack propagates and intersects each succeeding hole, an individual external pressure pulse was received so that the progress of the crack could be monitored.

Although most of the fatigue crack growth data obtained in this past year were obtained via this technique, limited data were obtained using displacement transducers mounted on the face of the test specimen to monitor specimen compliance. The use of specimen compliance to measure crack progress is a standard approach used by many experimentors. However, its success is directly dependent upon the availability of suitable transducers. Several prototype units, capable of operating in this 550°F, 1220 psig water environment, were evaluated during this past year. The limited data which were obtained from these transducers were used to augment the capillary hole data.

The focus of these tests were the effect of cyclic test frequency and mean stress. Test frequencies of 5 cpm, 1.25 cpm and 0.3 cpm were used. R ratios of 0, 0.6 and 0.78 were employed. All tests were conducted with a saw tooth waveshape.

Results

Five environmental fatigue crack growth tests were completed as part of the Task K_D test matrix. Pertinent parameters for these tests are listed in Table A.

At the conclusion of each test, test specimens were sectioned so that the fracture surface(s) could be examined. Typical fracture surfaces for Inconel 600 and A508 alloy steel are shown in Figures 6 and 7, respectively. The artifacts which are visible on the fracture surfaces are due either to deliberate changes in loading conditions (i.e. stress change marking fronts) or unintentional test interruptions which occurred periodically.

Post-test fracture surface measurements were made to accurately determine the location of the capillary holes and any artifacts which might be present. These measurements were used to establish crack location as a function of test cycles.

This resultant crack length versus cycles data was used to calculate macroscopic crack growth rates where:

$$\text{Macroscopic Crack Growth Rate} = \frac{\Delta A}{\Delta N} = \frac{A_{i+1} - A_i}{N_{i+1} - N_i}$$

A value of stress intensity was calculated corresponding to the average crack length within the interval used for the macroscopic crack growth.

This macroscopic crack growth rate data is plotted as a function of calculated stress intensity range in Figures 8 and 10 for T-304 SS and carbon/alloy steel, respectively.

T-304/304L Stainless Steel

In Figure 8, are shown the T-304 and 304L stainless steel data from three high R* ratio tests covering a frequency range from 5 to 0.3 cycles/minute. Furnace sensitized (FS) T-304 specimens were included in the 5 cpm and 0.3 cpm tests. Interestingly, the FS data do not differ appreciably from the as received (AR) data. This is consistent with results of post-test metallographic examination of the fracture surfaces of these specimens. Both the FS and the AR specimens exhibit a transgranular fracture morphology.

The data from Figure 8 are replotted in Figure 10 in terms of an "effective stress intensity factor" which incorporates R ratio and maximum stress intensity value. This is an empirical technique used to normalize data taken at various R ratios. In this particular instance, a value of m = 0.5 was used to obtain the fit shown in Figure 10. The 5 cpm and 1.25 cpm data fit very well to a common line; however, the 0.3 cpm growth data appeared to be between two to three times greater than the common 5/1.25 cpm data line.

---

*R $\triangleq$ Minimum load ÷ Maximum Load

Carbon Alloy Steel

The carbon and alloy steel data from these tests are shown in Figure 10. Both piping and pressure vessel steels are included. The solid lines in Figure 9 are the recommended flow evaluation lines from the ASME B&PV Code. Section XI for an air and a water environment. The dotted lines represent the upper and lower bounds for work previously done by GE on A-508-2 alloy steel in this same simulated BWR water environment at an R ratio near zero. Also shown are data from a test run earlier in this same environment using the same heat of A-516 piping in a 2T-WOL specimen configuration. It is important to note that all these comparison data (the ASME Section XI lines, the GE A-508 "LEFT" lines and the A-516 2T-WOL points) were generated under zero-tension loading conditions (i.e. R = 0).

The significant feature of Figure 9 is the fact that most of the high R ratio data fall above the ASME XI recommended design line. Therefore, it is conceivable that a safety analysis which is made using this ASME XI "water" line could be non-conservative. One problem is that ASME XI does not take mean stress (i.e. high R ratio loadings) into account.

The high R ratio data from Figure 10 are replotted in Figure 11 using the previously mentioned concept of an effective stress intensity factor. Note, that since the other data in Figure 10 are R = 0 data, they are uneffected by this change from ΔK to $K_{effective}$. An exponent of m = 0.5 is used in Figure 11. The resulting agreement between the high and low R ratio data on this normalized basis is encouraging. These results suggest that the use of an effective stress intensity factor which accounts for mean stress effects is a possible solution to the present inability of ASME XI design rules to conservatively deal with high R ratio loading situations.

Future Work

While the final two tests in this program have been completed, the data from these tests are still being analyzed. As a result, not all data are shown in Figures 8 - 11. These are low R ratio data which should allow a more accurate assessment to be made of the validity of the "Keff" approach shown in Figures 9 and 11.

A summary topical report detailing all the work done on environmental fatigue crack growth on this program is also being prepared. This report should be available by January, 1978. No further work beyond issuance of this report is presently planned.

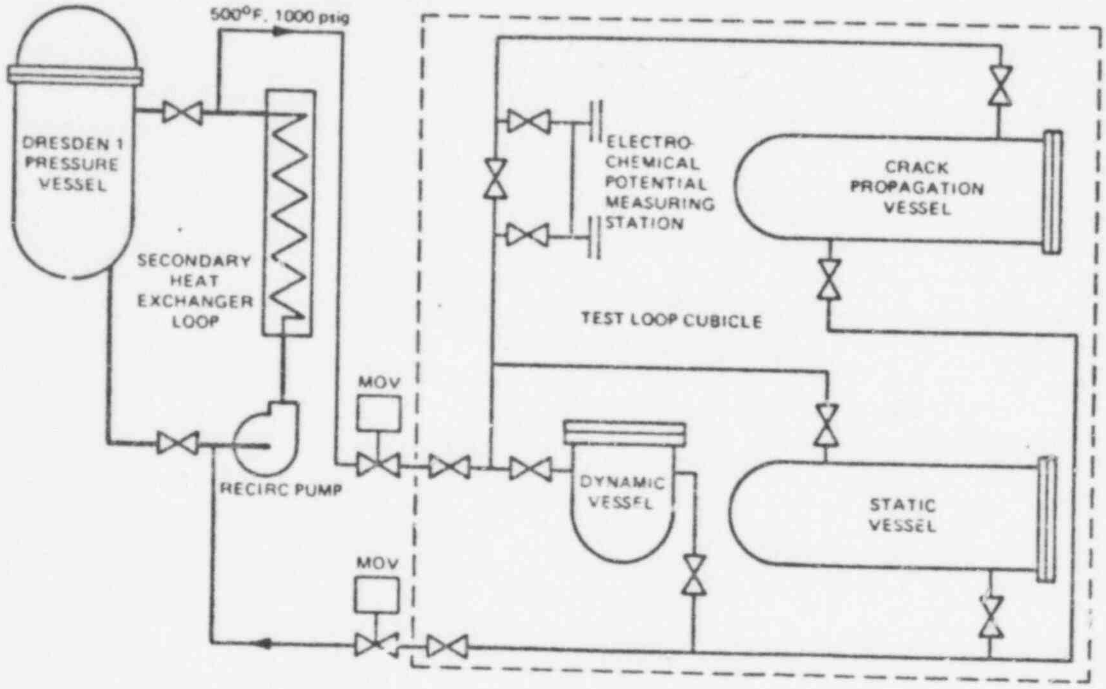

Figure ι   Dresden 1 Corrosion Fatigue Test Loop

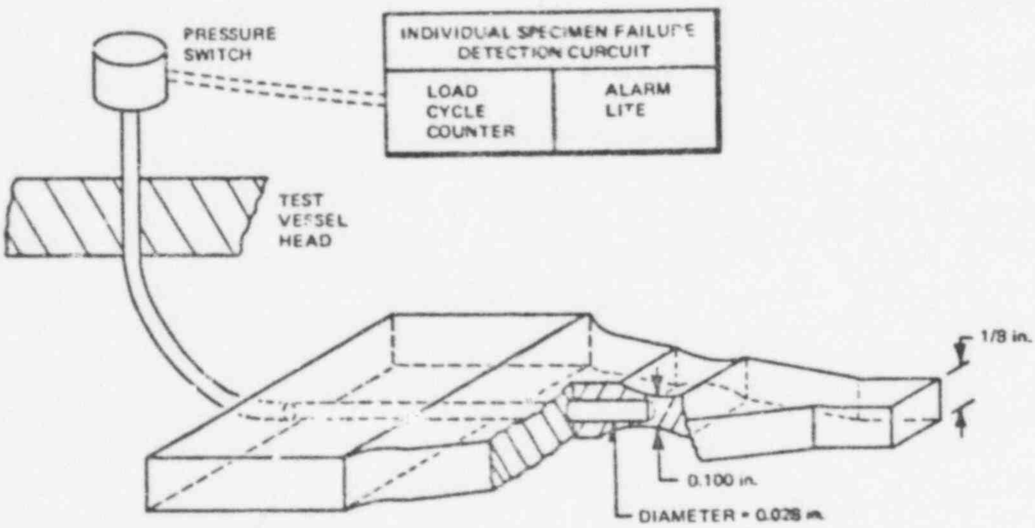

Figure 2. Axial Hole Specimen Concept

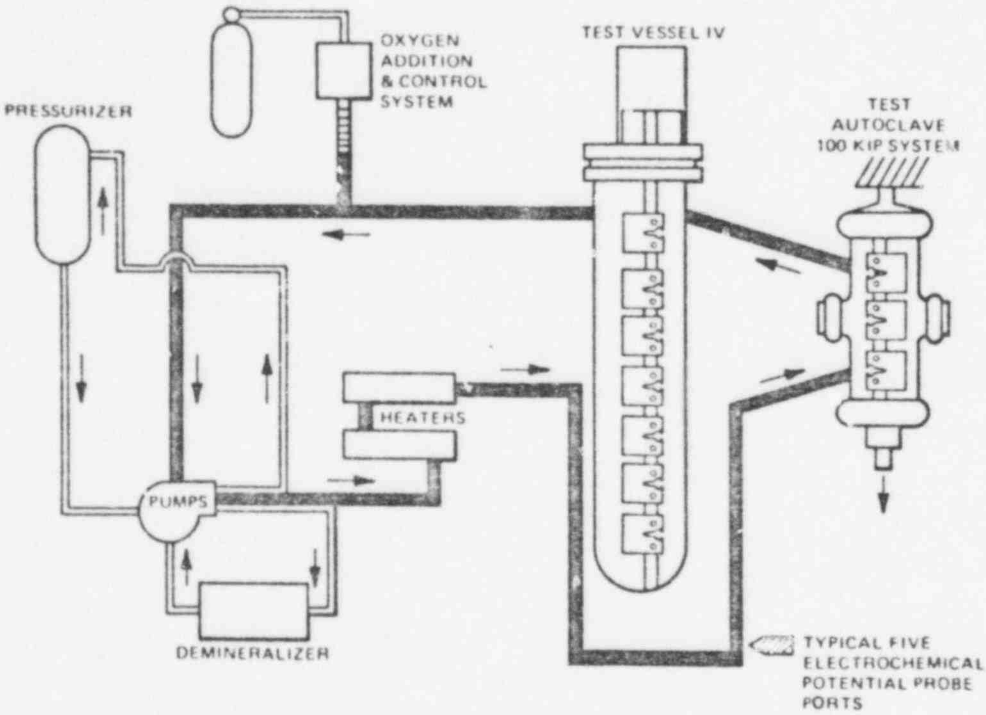

Figure 3. General Electric Simulated BWR Water Test Loop Schematic

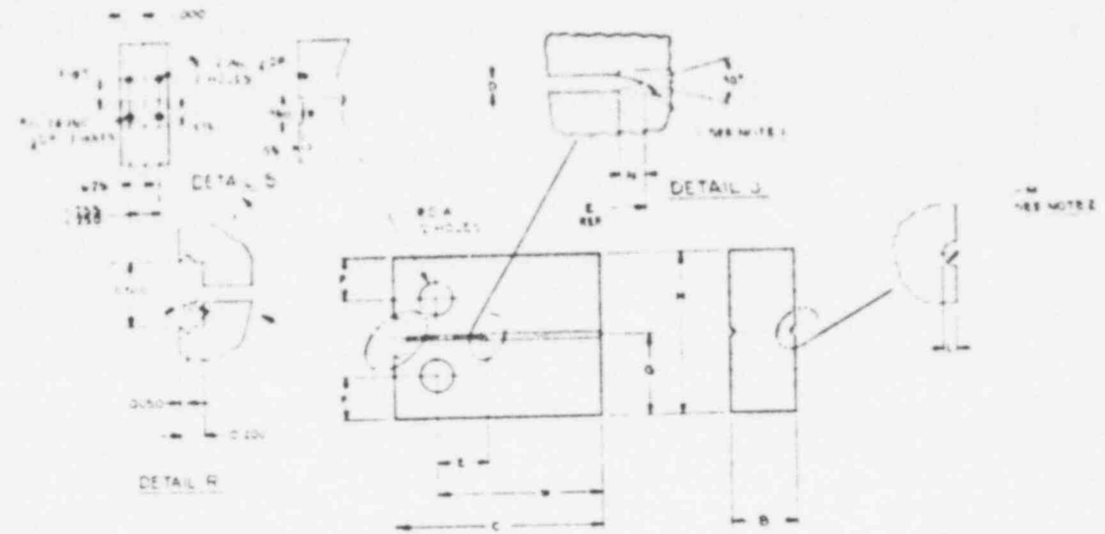

TYPE B

PART No.	SPEC No.	B	W	C	D	E	F	G	H	L	M	N	O	P	R	S
3	1T-B	$1.000^{+0.010}$	2.55	3.200	0.094	0.767	0.650	1.240	2.480	0.060	0.047	$0.175^{+0.020}$	$0.500^{+0.005}_{-0.000}$	–	YES	NO

NOTES

1. 0.007 in. MAX. RADIUS (EDM)
2. LAY MARKS TO FALL PARALLEL TO AXIS OF RADIUS SURFACE FINISH TO BE 32.

Figure 4. WOL Specimen for Crack Growth Rate Studies

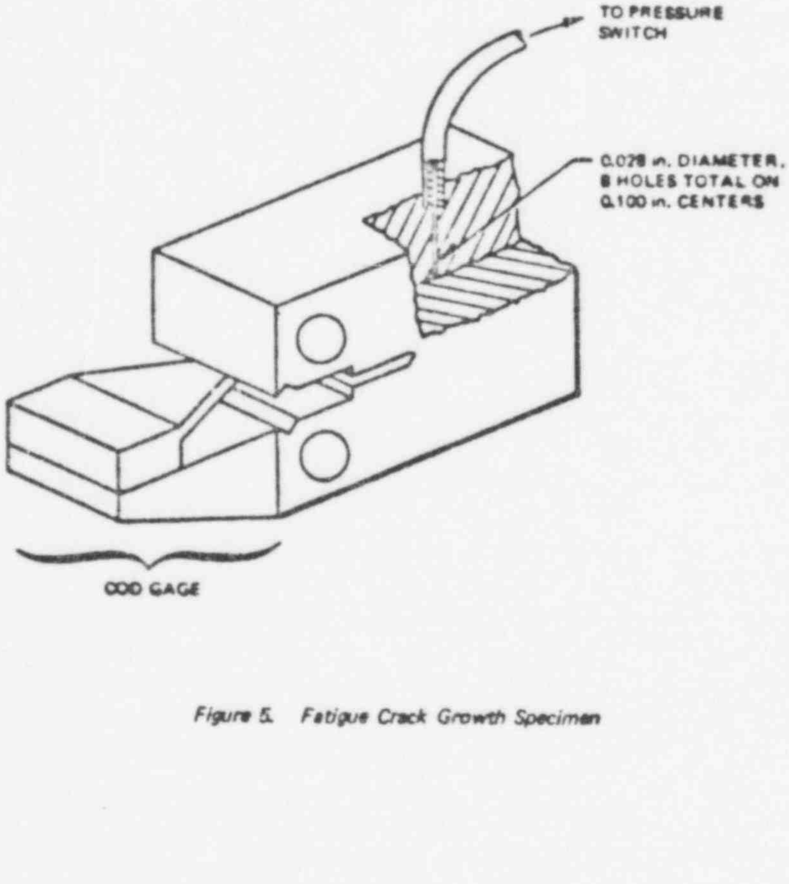

Figure 5. Fatigue Crack Growth Specimen

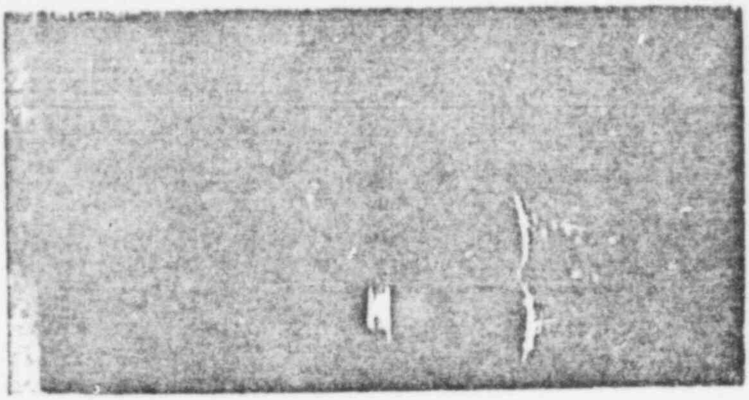

IN-3

Figure 6. Fracture Surface, Inconel 600 Specimen IN-3

C 11

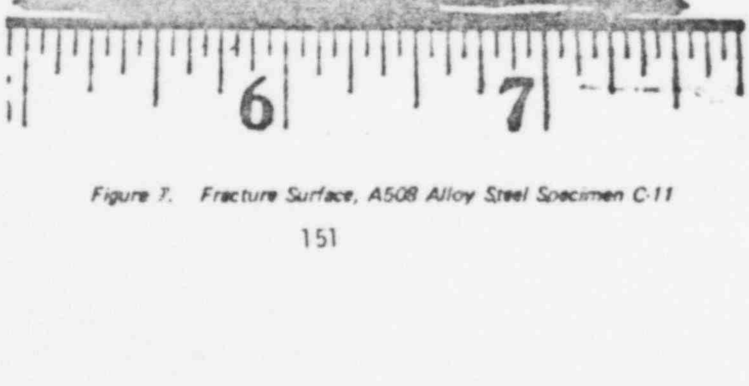

Figure 7. Fracture Surface, A508 Alloy Steel Specimen C-11

POOR ORIGINAL

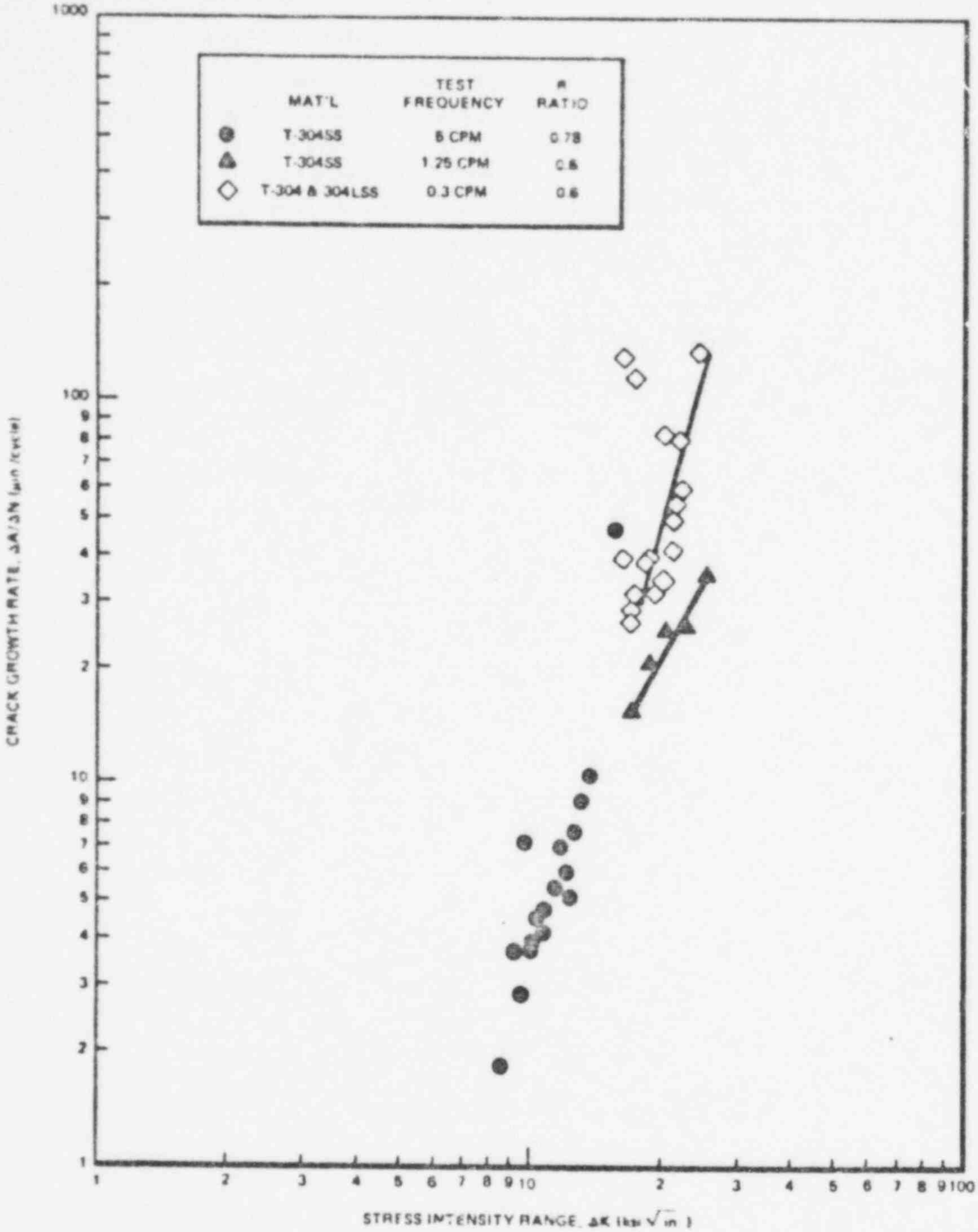

Figure 8. Fatigue Crack Growth Data, Type-304/304L Stainless Steel in Simulated BWR Water

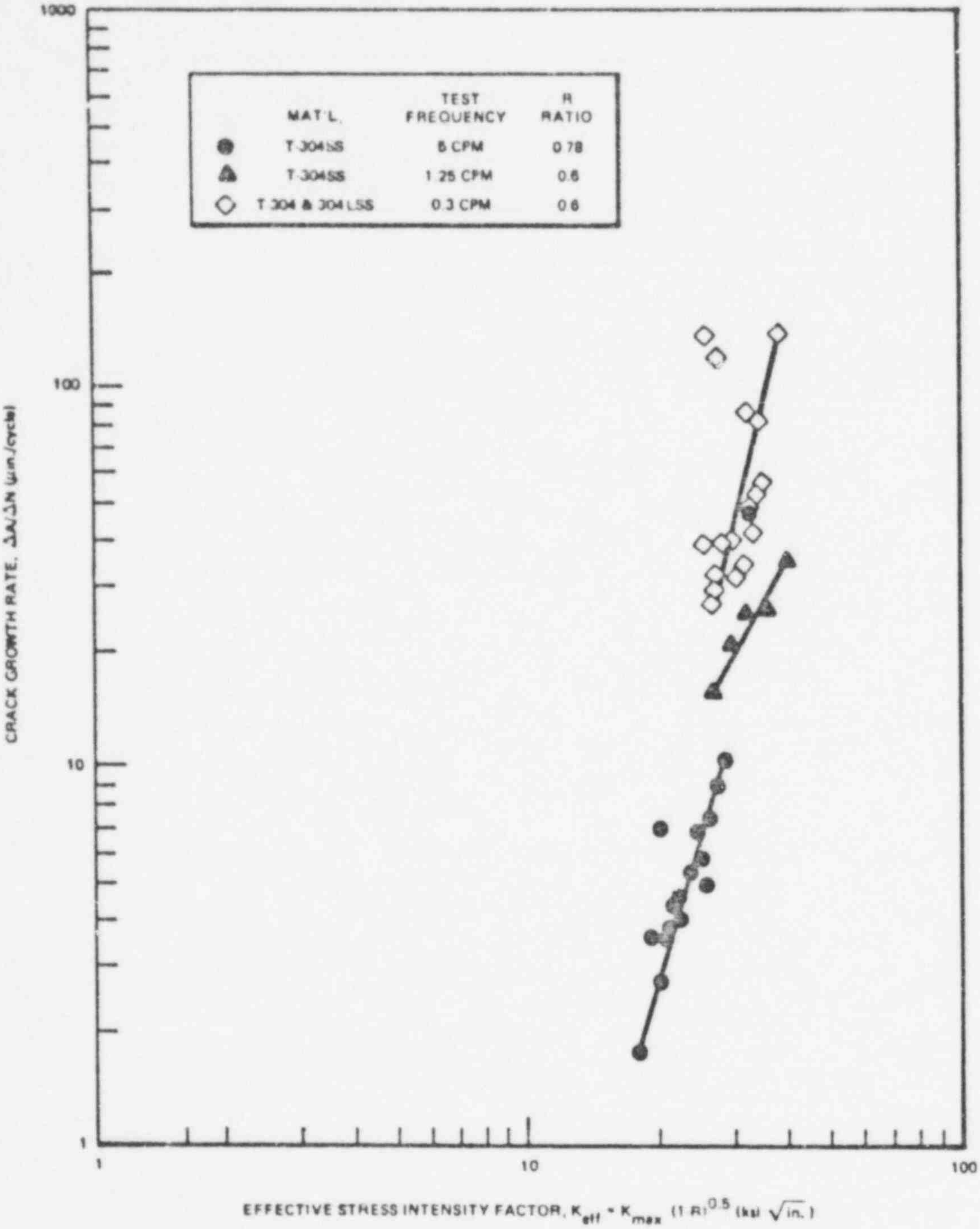

Figure 9. Fatigue Crack Growth Data, Type-304/304L Stainless Steel in Simulated BWR Water

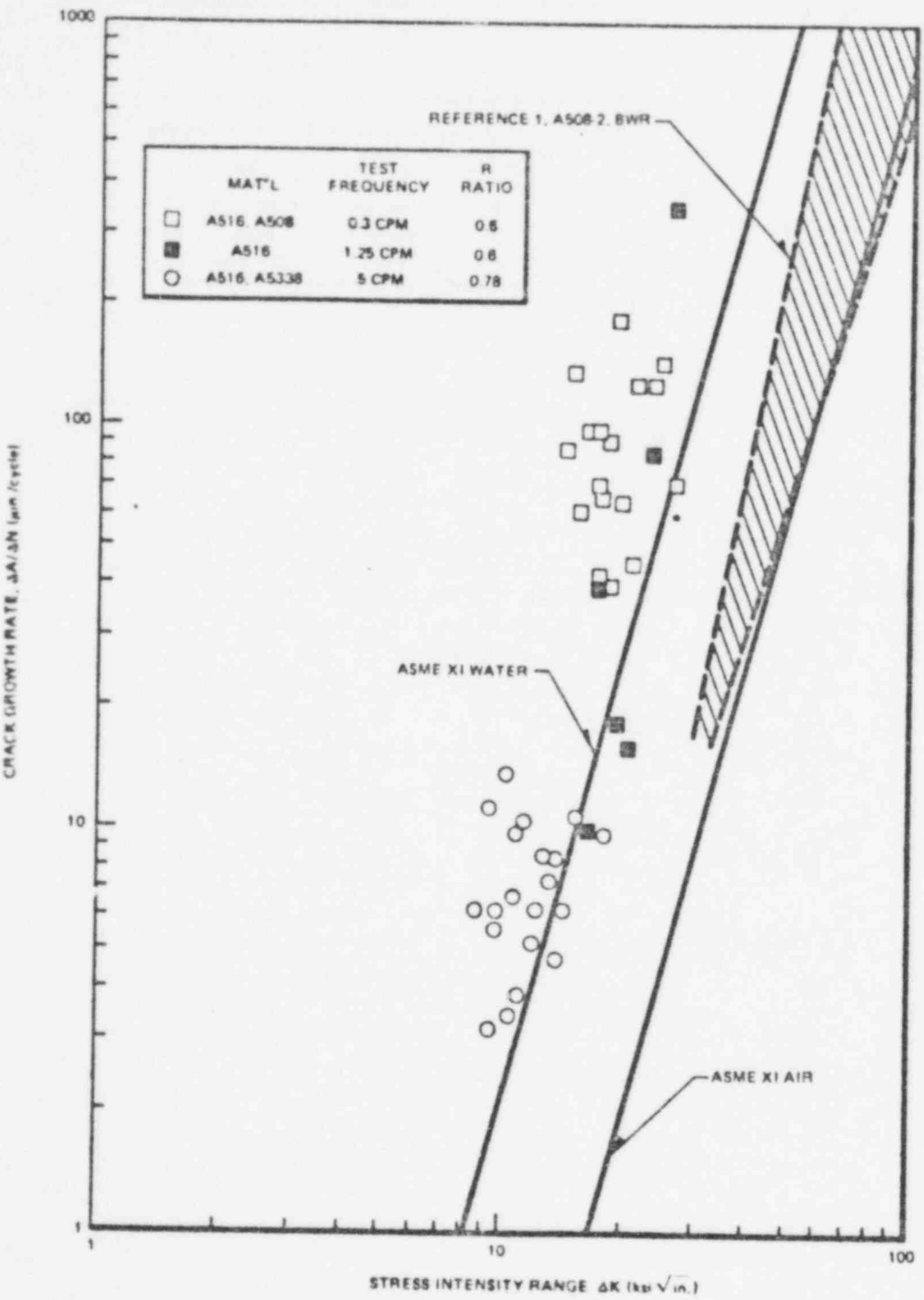

Figure 10. Fatigue Crack Growth Data, Carbon/Alloy Steel in Simulated BWR Water

POOR ORIGINAL

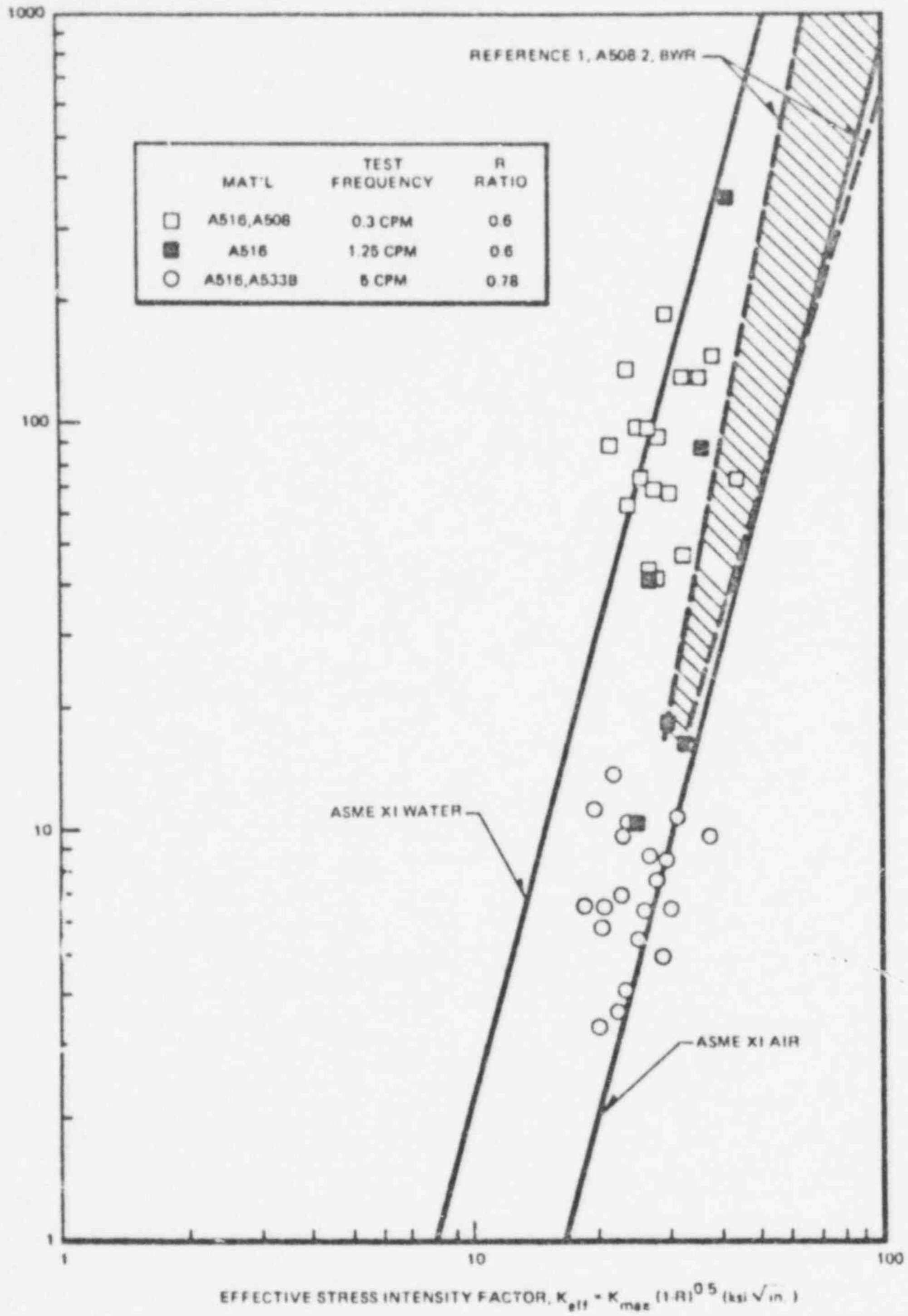

Figure 11. Fatigue Crack Growth Data, Carbon/Alloy Steel in Simulated BWR Water

Table A
TASK K, TEST MATRIX

Test Number	R* Ratio	Loading Frequency (cpm)	Wave Shape	Specimen Layout	Remarks
III	0.78	5	Symmetric Sawtooth	T-304 SS, As-Received T-304 SS, Furnace Sensitized A516 CS, As-Received A533B CS, As-Received	
A	0.6	0.3	Skewed** Sawtooth	T-304 SS, As-Received T-304 SS, Furnace Sensitized T-304 SS, Cast CF8 T-304L SS, As-Received Inconel 600, As-Received A516 CS, As-Received A508-2 CS, As-Received A508-2 CS, Weld (HAZ)	
B	0.6	1.25	Skewed** Sawtooth	T-304 SS, As-Received A516 CS, As-Received A508-2 CS, As Received	
C	0.05	0.3	Skewed** Sawtooth	T-304 SS, As-Received A516 CS, As-Received A508 CS, As-Received	Test complete, data being reduced.
D	0.05	5	Skewed** Sawtooth	T-304 SS, As-Received T-304 SS, Furnace Sensitized T-304L SS, As-Received Inconel 600, As-Received A516 CS, As-Received A508-2, As-Received	Test complete, data being reduced.

* R Ratio = Minimum Load ÷ Maximum Load
**Special waveform details

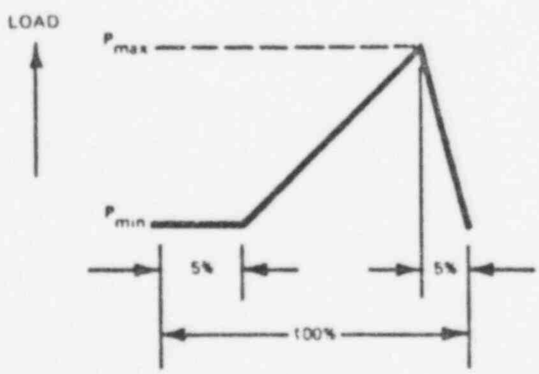

815 162

IMPROVED ULTRASONIC NON-DESTRUCTIVE
TESTING OF PRESSURE VESSELS

The University of Michigan
Mechanical Engineering Department
Ann Arbor, Michigan 48109

Project Director: Professor Julian Frederick

INTRODUCTION

A synthetic aperture focusing technique for ultrasonic testing (SAFT UT), which has been under development at the University of Michigan over the past three years, has the promise of overcoming many of the problems which currently face the NDE engineer. Notably the technique has the following attributes·

1) Simultaneous high lateral and longitudinal resolution ($\sim 1\lambda$)
2) High signal-to-noise ratio
3) Wide beamwidth insonification (multiangle)
4) Wide bandwidth insonification (multi-frequency)
5) Inherently quantitative and volumetric.

As a result of these attributes the technique has the following important advantages:

1) Discontinuity sizing is relatively insensitive to echo amplitude.
2) Heavy sections can be penetrated with wide beamwidths.
3) Discontinuities that are directional reflectors can be imaged in a single scan.
4) The results are in a form which is directly suitable for evaluation using the ASME Section XI Boiler and Pressure Vessel Code.

In addition the technique is:

5) relatively insensitive to false indications caused by multiple scattering in large grain size materials,

6) relatively insensitive to variations in beam profile in a given search unit or between similar search units,
7) adaptable to inspecting components with non-planar surfaces such as nozzles and piping,
8) and computer automated to a large extent, leaving little room for human error.

DATA COLLECTION, PROCESSING AND DISPLAY

A 32-bit minicomputer with 256k bytes of core-memory controls the entire SAFT UT system. Test specimens are submerged in a water tank as shown in Fig. 1, and transducer scanning is performed on the basis of coordinates entered by the operator. A conventional RF pulse-echo system is used with a modification to provide synchronous operation with the analog-to-digital converter which converts the RF A-scan signal to a series of digital values. The digital A-scan representations are stored in sequence on magnetic disc or tape.

Once a volume has been scanned, synthetic aperture processing is employed to produce a high-resolution processed image. Briefly, the processing technique is one of coherently summing all the echoes from a flaw as seen by the transducer in its various scanning positions, thereby synthesizing an accurate picture of the flaw location and shape. Since the data are inherently three-dimensional it is necessary to create a subset of the data for presentation on a two-dimensional display device as shown in Fig. 2. Since all the data and plot files are in digital form they may be stored indefinitely on magnetic tape with no loss in fidelity and can be retrieved automatically for comparison with subsequent inspections. Perspective, contour, and grey-scale displays have been developed at the University of Michigan and further optimization of the display systems for ease of operator interpretation is a current research activity.

EXPERIMENTAL RESULTS

The research this past year at the University of Michigan has emphasized both system improvements and verification of system imaging capability. A major improvement in the system was completed in the summer of 1977 with the installation of the presently-used 32-bit minicomputer which replaced the 16-bit machine used previously. The larger machine has greatly increased the data storage and handling capabilities. In addition, a transient recorder is being installed which will greatly increase the speed of data-taking.

Verification of the imaging capability has received the major effort. A simple example test specimen is depicted in Fig. 3. It consists of a 20mm thick aluminum block with four flat-bottom holes drilled to a depth of 9.5 mm. Each hole is 1.5 mm in diameter and the holes are separated diagonally by a distance of 6.5 mm. A 10 MHz transducer was scanned in a raster above the specimen. Fig. 4 shows perspective plots of the raw data and processed data sets. In this case the plots are similar to C-scan in that the maximum signal amplitude throughout the depth of the specimen is plotted as a function of the two lateral positions. The improvement in lateral resolution produced by SAFT UT processing is immediately evident. An alternate form of display known as a contour plot is used in Fig. 5 on the same test data. Whereas the perspective plot is a qualitative display which is useful for image interpretation, the contour display is quantitative in nature. Measurements are easily performed on the contour plot taking into account the known scaling factor introduced during plotting.

The inspection of GARD, Inc., weld samples was an important verification test carried out in 1977. Fig. 6 shows an orthographic projection of a typical inspection as generated by the SAFT UT plotting and display system. A perspective view of the inspection volume has been added to orient the reader. Each view corresponds to a projection of the internal discontinuities in one of the three othogonal directions. One can think of the volume as being transparent with opaque discontinuities. With a little effort it is possible to match up the corresponding projections of a particular indication and thus visualize the location and shape with the inspection volume. The flaws in this case have been verified by destructive examination to be slag inclusions introduced during the welding process. The test confirms the capability to image flaws within welded sections, which is necessary for nuclear reactor safety.

Other studies during 1977 have included the imaging of flaws within the Pressure Vessel Research Committee Test Block No. 202, development of techniques for front surface noise removal, development of algorithms for V-path inspection, and the development of deconvolution techniques to increase the longitudinal resolution.

SUMMARY

A synthetic aperture focusing technique for ultrasonic pulse-echo nondestructive testing has been developed and implemented in a laboratory environment. The technique promises to overcome several of the problems currently encountered in the inspection of nuclear pressure vessels and piping.

Future effort will be directed at further defining and improving the imaging capability of the system, improving the scanning mechanism to allow high resolution studies, and improving the display systems for ease of interpretation.

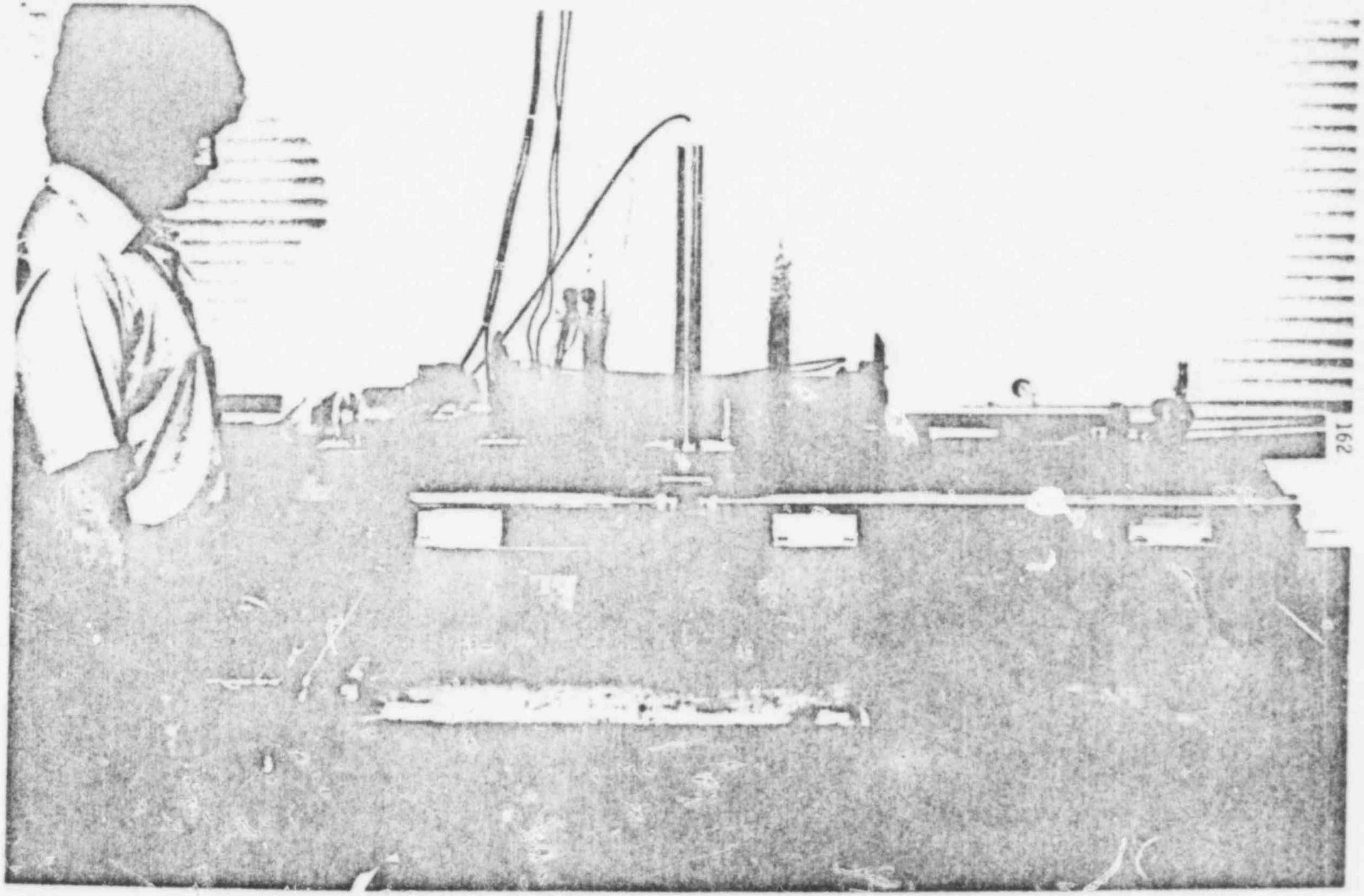

Fig. 1. SAFT UT laboratory scanning tank. Test specimens are placed in the tank which is filled with water during a test. The ultrasonic transducer (mounted on the vertical pole at the center) moves over the surface of the specimen by means of stepping motors.

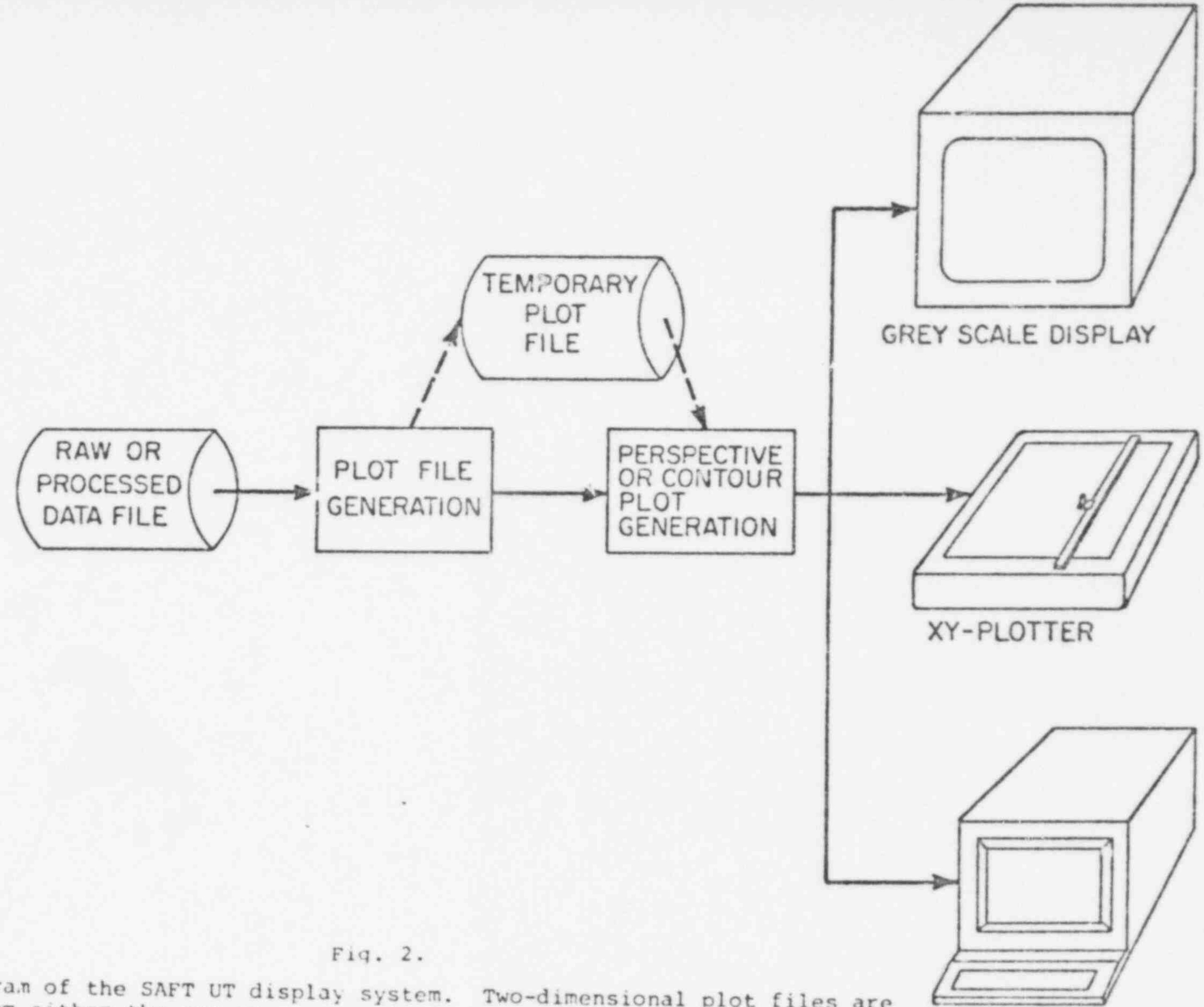

Fig. 2.

A block diagram of the SAFT UT display system. Two-dimensional plot files are generated from either the raw or processed ultrasonic data and the resulting pictures can be displayed on a variety of devices at the command of the operator.

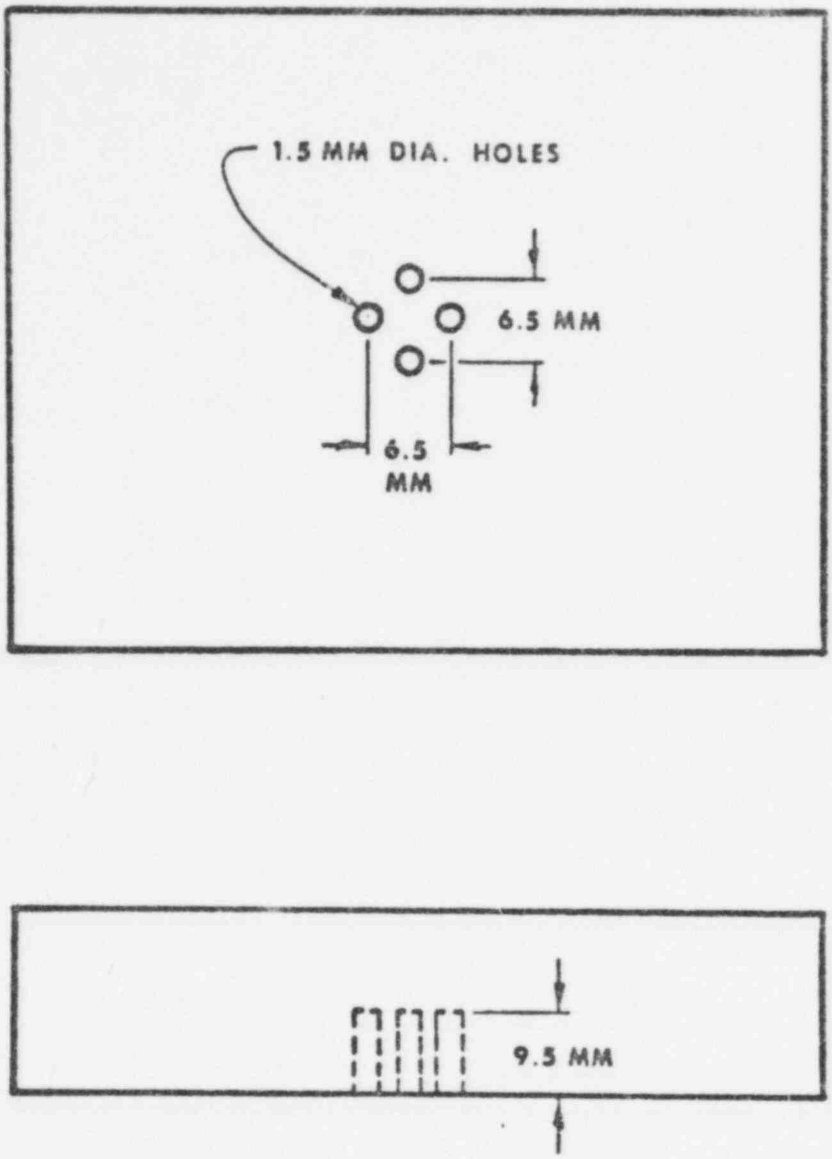

Fig. 3. Flat-bottom hole array specimen. This specimen consists of an aluminum block with four blind holes drilled in the bottom. During test the block is placed in the tank so that the holes are on the side opposite the transducer.

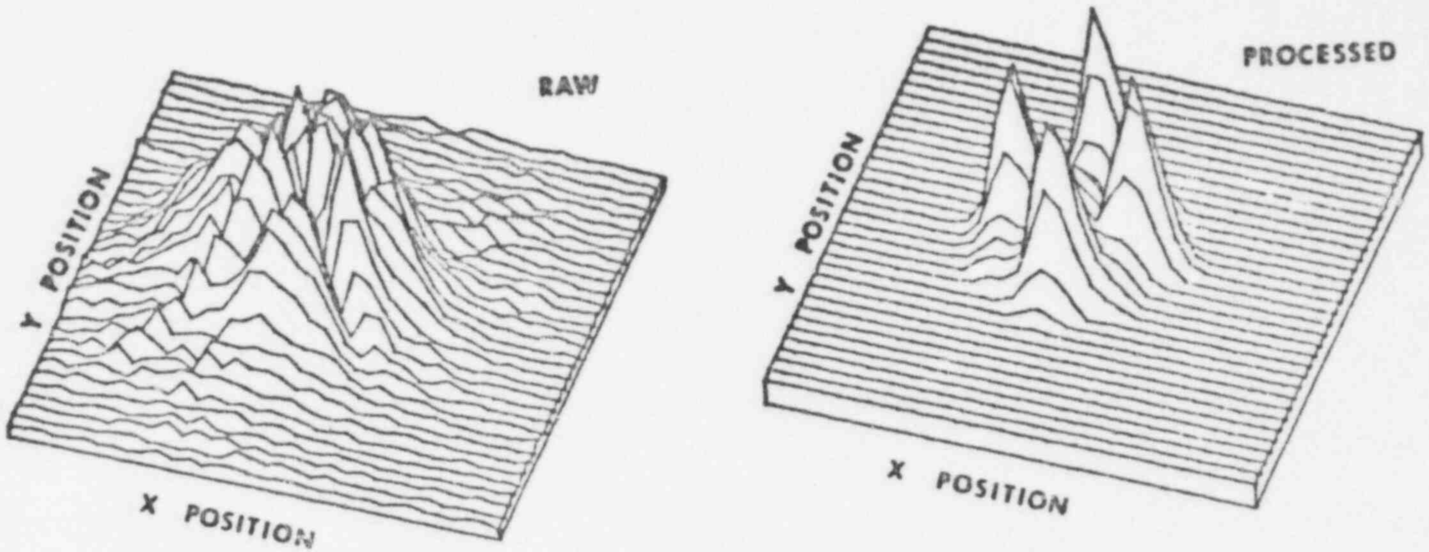

Fig. 4. Perspective display of a flat-bottom hole array. On the left is a display of the test data taken with the block in Fig. 3 before SAFT UT processing. The resolution is roughly equivalent to what one could obtain using conventional ultrasonic testing equipment. The figure on the right shows that the SAFT UT method of processing the data reveals separate echoes from each of the four holes.

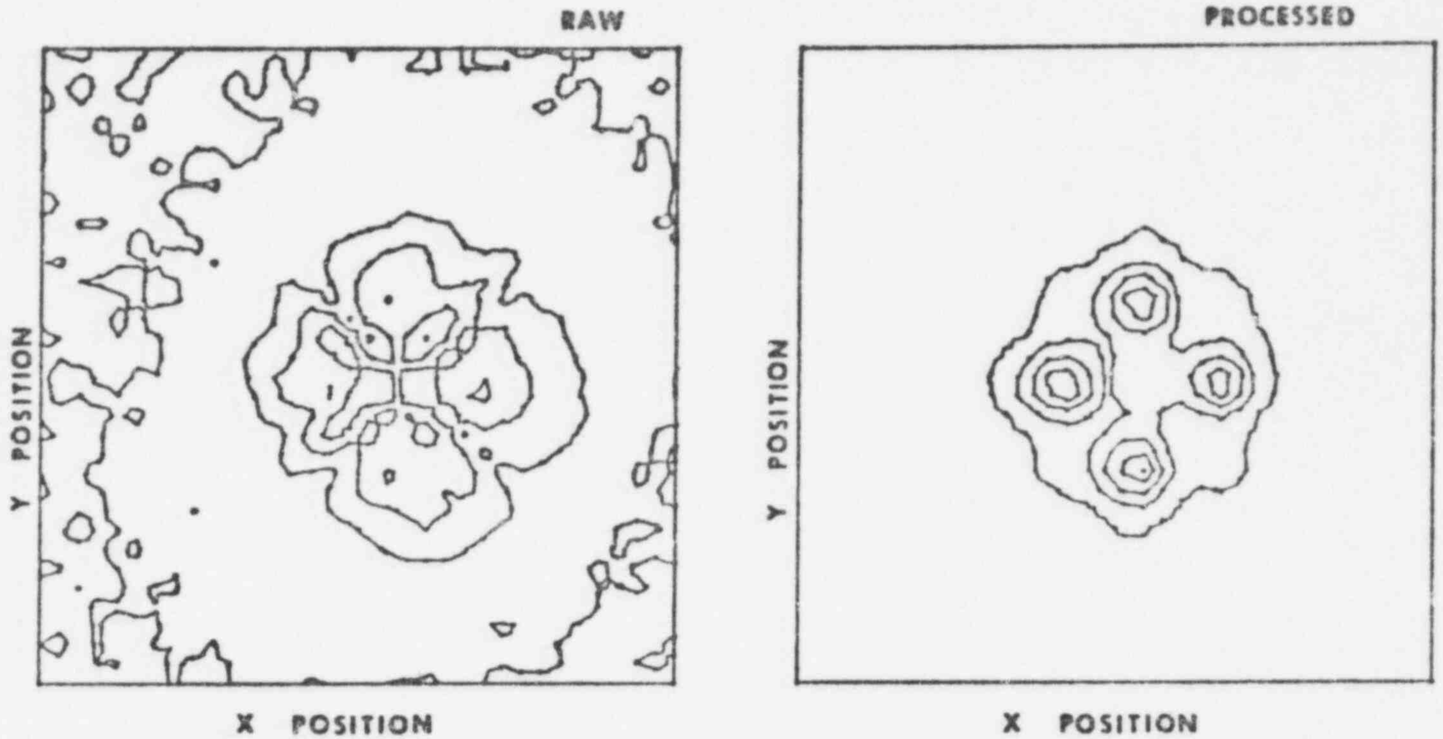

Fig. 5. Contour display of flat-bottom hole array. This display is derived from the perspective display by taking horizontal slices just as in making a geographical map . Again one easily sees the improvement in resolution provided by SAFT UT processing on the right.

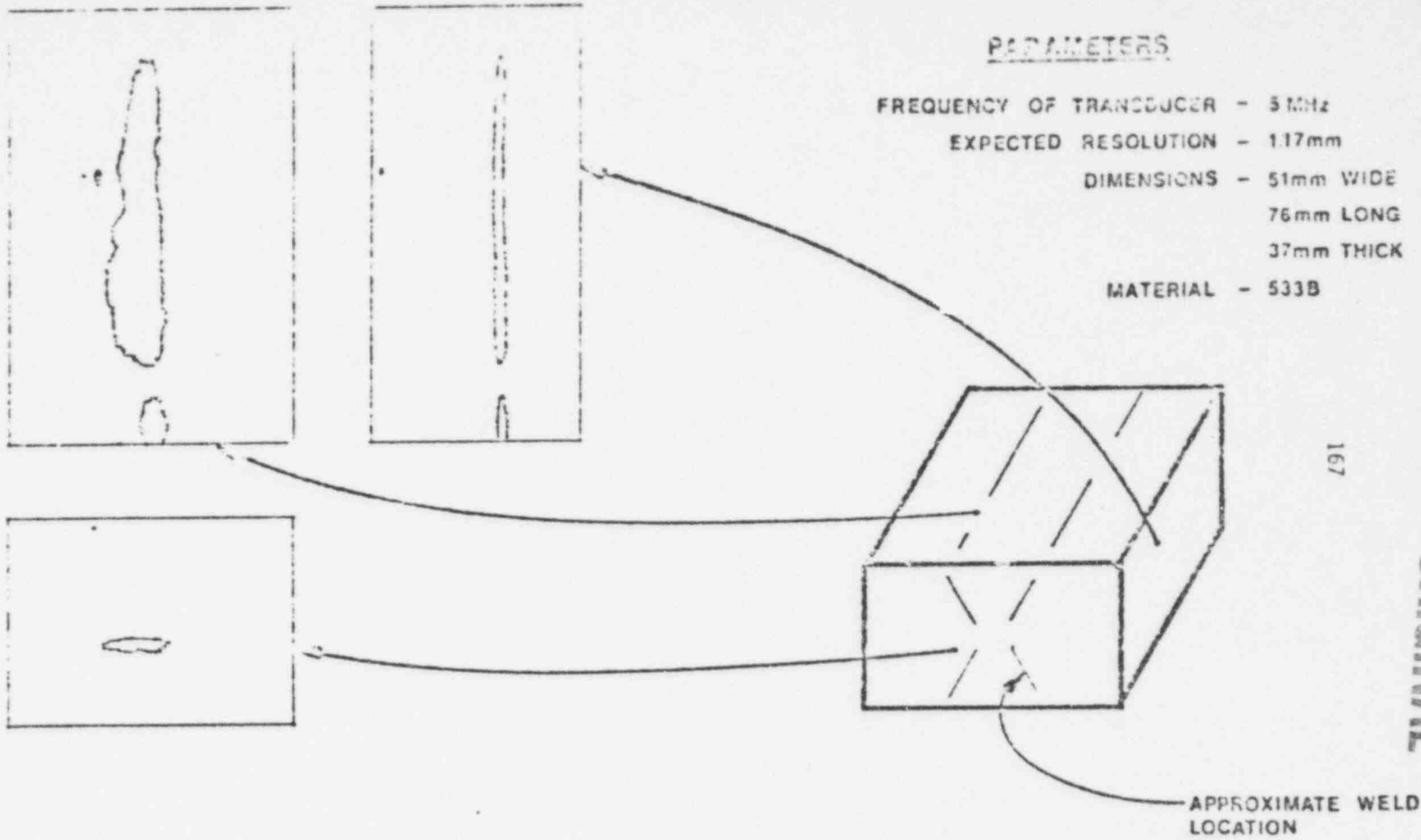

Fig. 6. Computer-generated orthographic projection of flaws in a specimen of pressure vessel steel containing a weld. The weld specimen is depicted on the right. The three different computer-generated views of the weld area are indicated by arrows. These views show the flaw outline just as though the inspection volume were transparent.

Contract Title: Development of High-Sensitivity Ultrasonic Techniques for In-Service Inspection of Nuclear Reactors

Contractor and Location: Institute for Materials Research
National Bureau of Standards
Washington, D. C. 20234

Principal Investigators: Dr. Melvin Linzer (Project Leader), Dr. Dennis Dietz and Dr. Stephen I. Parks

Objective: The principal objective of the program is to develop techniques to enhance the sensitivity of ultrasonic signals which are below the random noise of the system. A secondary objective is to develop instrumentation for improved discrimination of flaw signals from background "clutter". The improved techniques will be applied to detect flaws in nuclear reactor pressure vessel and piping materials.

FY 77 Scope: An ultrasensitive ultrasonic system, incorporating real-time signal averaging, pulse compression, dynamic focusing and transducer matching, has been developed. The system was shown to be capable of penetrating highly-attenuating material, such as austenitic steel, and of detecting reflections in the presence of strong background signals due to grain scattering.

Summary of Research Activities and Results

Techniques which improve the signal-to-random noise ratio of ultrasonic signals may be used to locate minute flaws, presently undetectable, which might grow to larger size during service: to remotely inspect regions which have limited access, either because of the physical constraints of the reactor design or because of radiation hazards, and to locate flaws which are embedded within or accessed through highly-attenuating material, such as coarse-grain austenitic steel.

An ultrasensitive ultrasound inspection system with orders of magnitude improvement in signal-to-random-noise ratio over conventional devices has been developed. Sensitivity enhancement is achieved by increasing the energy transferred to and from the material in the region of interest. Major features of the system include the use of repetitive pulses combined with signal averaging, the use of time-coded expanded pulses, and dynamic focusing. A real-time A-scan averager has been constructed which is capable of a S/N improvement of 1000:1 in about one minute of averaging. Pulse expansion and compression are accomplished by means of chirp radar techniques, with a compression ratio of 30:1 and compressed pulse width of 0.20 μs (~ 0.6 mm range resolution in the case of steel) demonstrated to date. For dynamic focusing, a unique signal processing scheme based on the use of a "constant f-number" annular-array transducer is employed. Other high-sensitivity techniques which have been investigated include high-power insonification and matching of the acoustic impedances of the transducer and material.

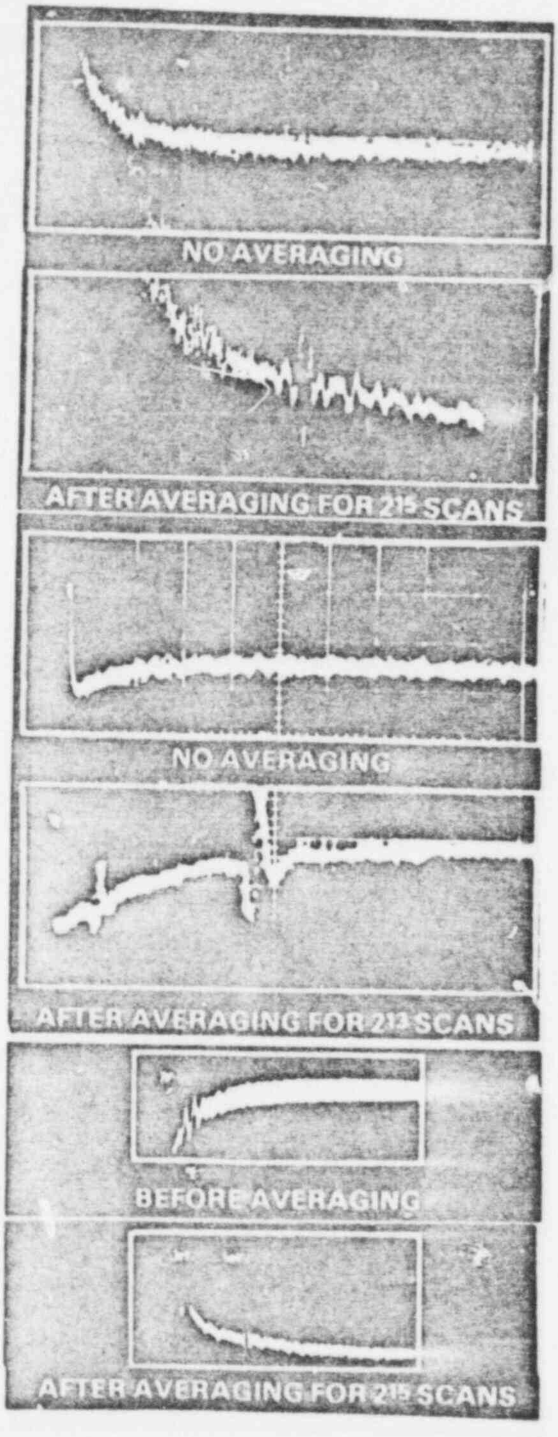

(a)

(b)

(c)

Figure 1. Demonstration of sensitivity-enhancement capability of signal averager: (a) Backwall reflection from 5 cm thick polymethylmethacrylate/stainless steel fiber composite, (b) Backwall reflection from 13 mm thick teflon, (c) Reflection from 4 mm hole, 6.5 cm deep, in austenitic stainless steel.

The system was used to penetrate highly-attenuating material, such as austenitic steel. Furthermore, the dynamic focusing system was shown to be capable of reducing coherent background noise arising from grain scattering.

1. Signal Averaging

A high-speed signal averaging system, supported by the NBS program in NDE, has been completed. The system is capable of real-time (unbuffered) averaging at 50 MHz rates. Major features include 4K 24 bit words, 12.5 KHz maximum repetition rate, computer interface, 6-digit cursor readout of signal amplitude, region of interest expand (up to a factor of 16), 3-digit settability of sample rate, internal/external trigger, internal delay, segmented memory capability (full, halves, quadrants, octants), plug-in ADC's (4 bit, 50 MHz; 8 bit, 20 MHz), display normalization and semi-real time display at high frequencies. The sensitivity-enhancement capability of the averager was demonstrated on a number of highly-attenuating materials, including centrifugally-cast stainless steel, a fiber composite (Figure 1a), teflon (Figure 1b) and austenitic steel (Figure 1c). Flaw detection in the case of austenitic steel was limited by the coherent background signals arising from grain scattering within the material.

2. Pulse Compression

The pulse compression ratio of our chirp radar system was increased to 30:1 with a compressed pulse width of 0.20 μs (Figure 2). This pulse width corresponds to a range resolution of ~ 0.6 mm (longitudinal waves)

(a)

(b)

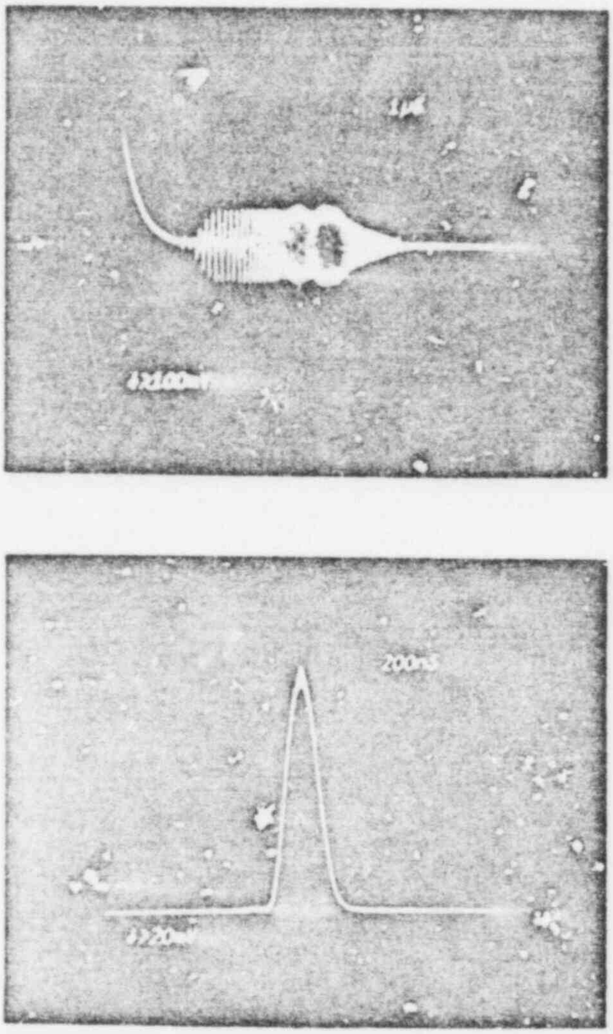

Figure 2. Demonstration of pulse compression capability of chirp radar system: (a) preamplified normal echo from rear of a 1" thick aluminum block, (b) the same signal following compression and detection. A 6 μs pulse is compressed to a halfwidth of 0.2 μs.

and 0.3 mm (shear waves) in steel. The 3:1 improvement over our previous system was achieved by operating our SAW filter in the third harmonic mode.

3. Dynamic Focusing

Dynamic focusing not only improves sensitivity but also improves lateral resolution, and, as is demonstrated below, discriminates against coherent background caused by grain scattering. A unique dynamically-focused annular array suitable for contact B-scanning has been constructed under this program. The array approximates a constant f-number lens by dynamically expanding the lens aperture as the focal length increases. This approach minimizes the total number of discrete delay elements as well as the rate at which they must be switched. The loss of the outer annuli at short focal lengths only slightly degrades theoretical resolution. An additional aspect of the constant f-number design is that the outer annuli are of constant width, permitting a large active area. Apodization is achieved by appropriately spacing the array elements and weighting the amplifier gains. The initial design (Figure 3) uses five annuli for the near focal length of 1.5 cm. As the focal length increases, the array expands to a total of 12 rings, 4 cm diameter, for foci at 10 cm and beyond. A single tapped delay line provides the required time delays. In the transmit mode, a continuously-variable point or line focus is provided.

Beam plot measurements of the array for a water medium are shown in Figure 4. The half-width at the focus ranges from 0.85 mm at 1.5 cm to 2.2 mm at 10 cm. These values are in close agreement with theoretical predictions. Switching noise and sidelobe levels are approximately 40 dB down.

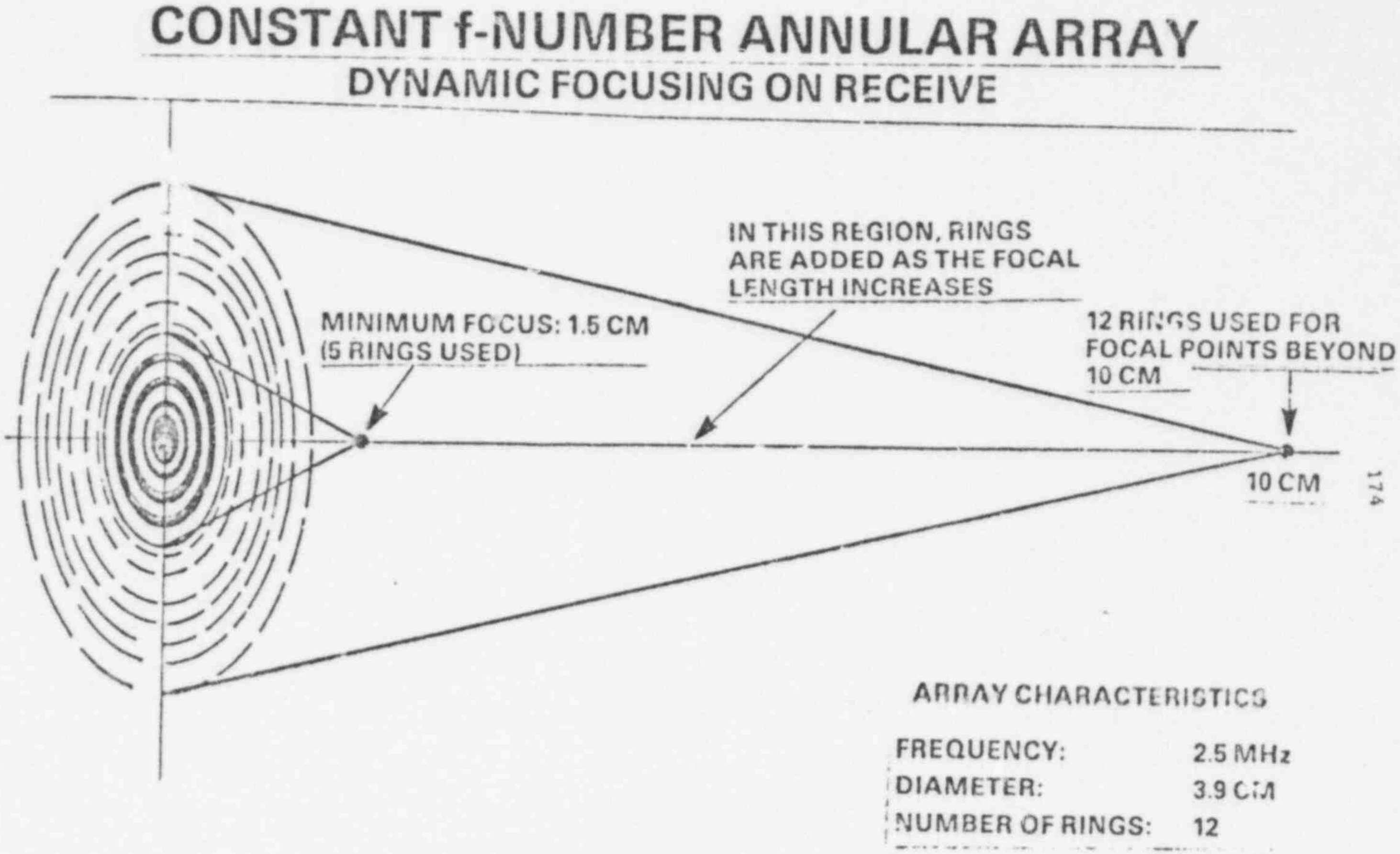

Figure 3. Operation of constant f-number annular array on receive.

815 180

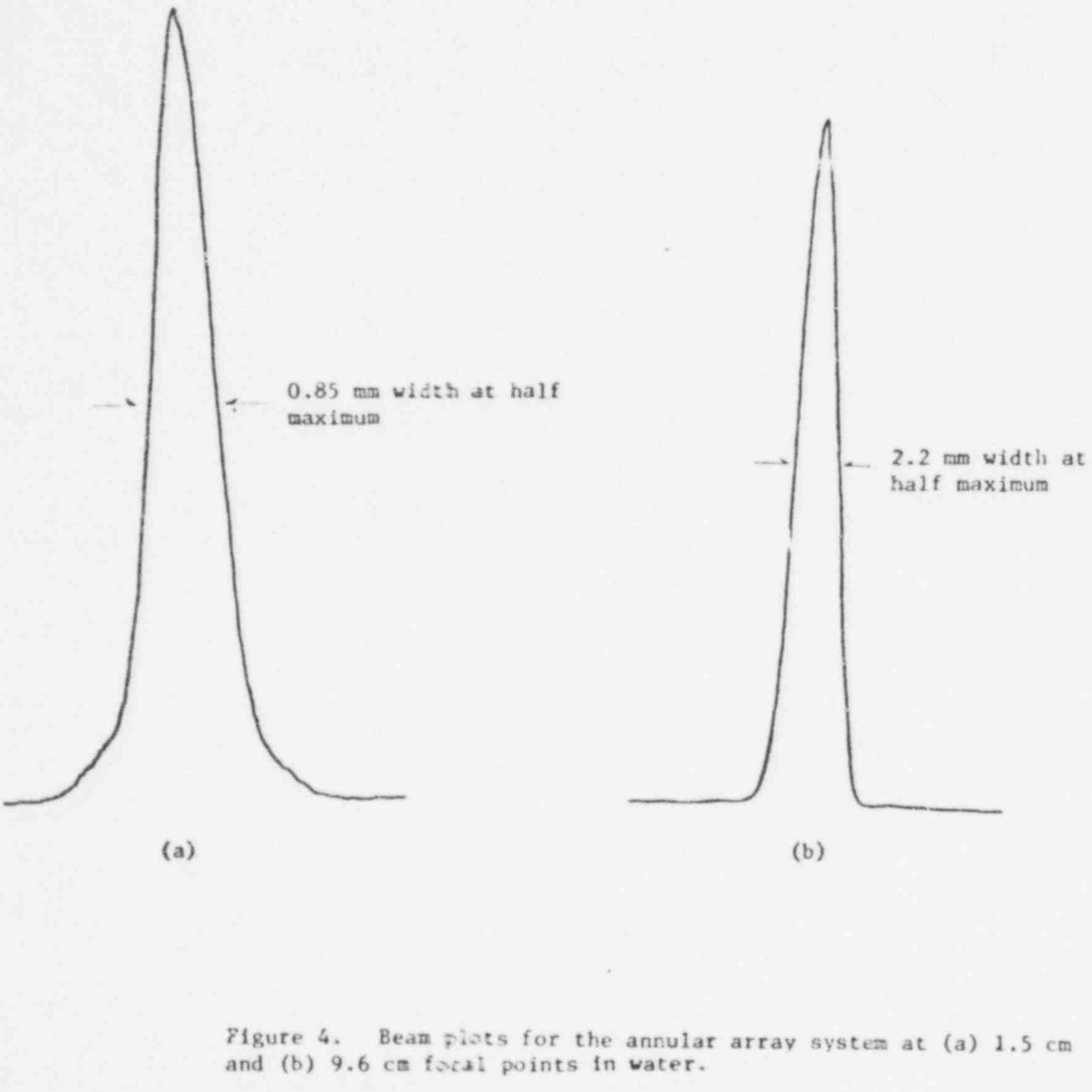

Figure 4. Beam plots for the annular array system at (a) 1.5 cm and (b) 9.6 cm focal points in water.

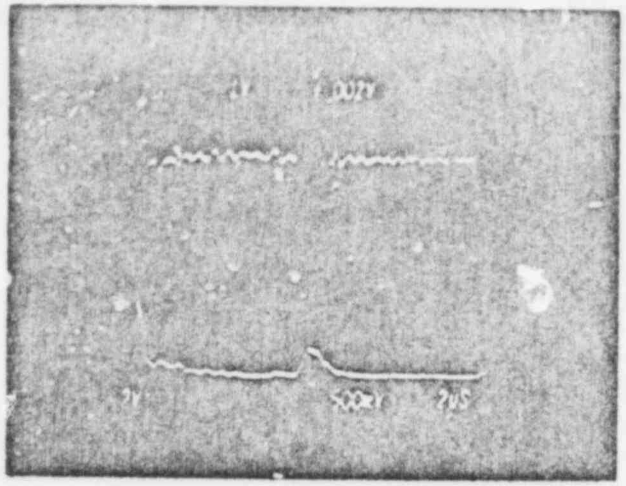

(a) 1 2 3

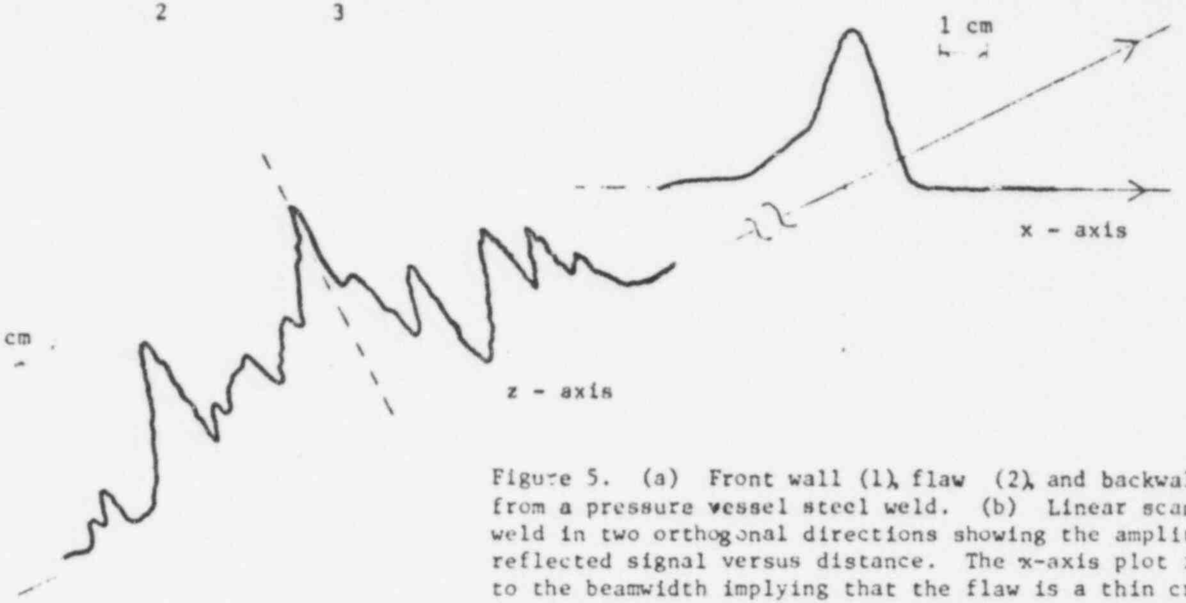

(b)

Figure 5. (a) Front wall (1), flaw (2), and backwall (3) reflections from a pressure vessel steel weld. (b) Linear scan of the same weld in two orthogonal directions showing the amplitude of the reflected signal versus distance. The x-axis plot is comparable to the beamwidth implying that the flaw is a thin crack. The z-axis plot shows the length of the crack.

(a)

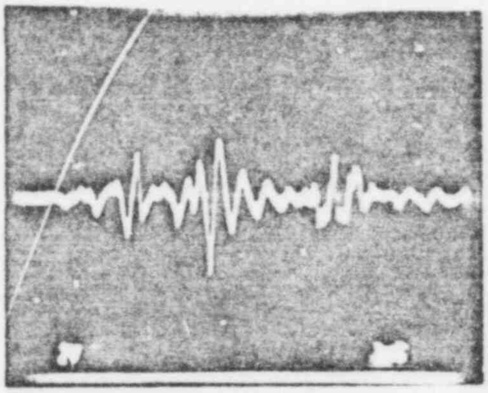

1 2 3

(b)

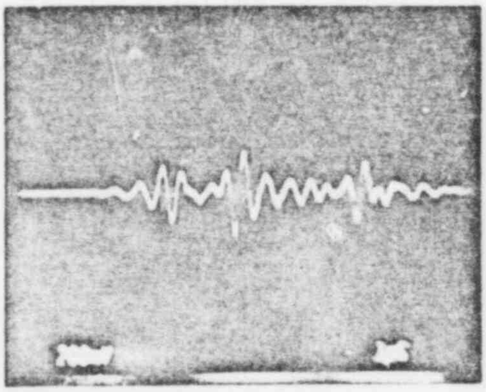

1 2 3

(c)

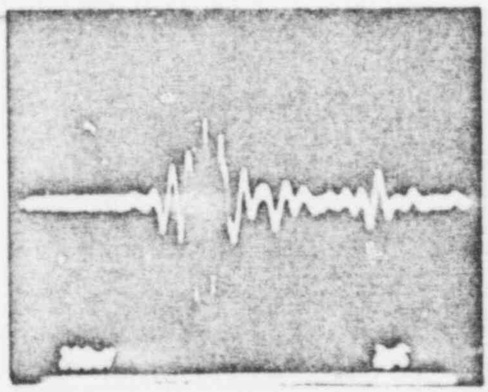

1 2 3

Figure 6. A scans from weld section in 14" diameter x 7/16" wall stainless steel pipe showing reflections from front wall (1), flaw (2), and backwall (3): a) Mode I focusing, b) Mode II focusing, c) Unfocused transducer.

One of the principal objectives of this program is to develop a very high quality focusing system which would be sufficiently inexpensive to be practical for in-service inspection of nuclear reactors. Our annular array design achieves this goal to a large extent. The constant f-number approach significantly reduces the hardware required for an annular array focusing system. An even simpler system, with trivial electronic hardware costs, can be obtained by using all the rings to focus to a point in the transmit mode but only a single annulus to receive the echoes. The delay line as well as the dynamic-focus electronics are eliminated in this case. The system exhibits focusing properties which results from a combination of a point transmit focus and a line (axicon) receive focus.

Annular array focusing using both all annuli (Mode I) and only the outer annulus (Mode II) during the receive phase of operation was demonstrated on several samples of interest to nuclear reactor monitoring. Figures 5 - 7 show results of these measurements, for natural weld flaws in a pressure vessel steel (Figure 5) and a steel pipe (Figure 6), and for a backwall reflection from a two-inch thick wall of centrifugally-cast stainless steel pipe. (Figure 7). Note the high-resolution achieved with the focused system, even with the Mode II approach, compared with the nonfocused system. The nonfocused transducer system cannot even detect the backwall reflection from the centrifugally-cast tubing. This is due primarily to the coherent background noise arising from grain scattering, with the increased attenuation due to the scattering playing a secondary role. The annular-array focusing system not only increases the signal-to-random noise

(a)

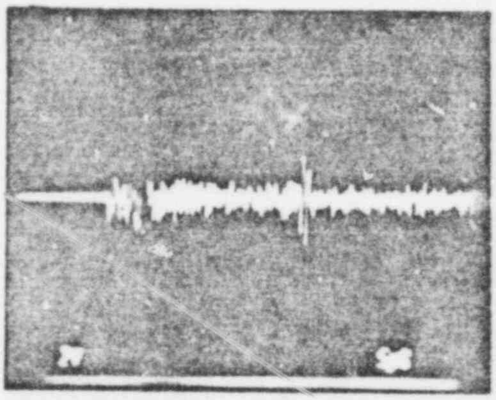

(b)

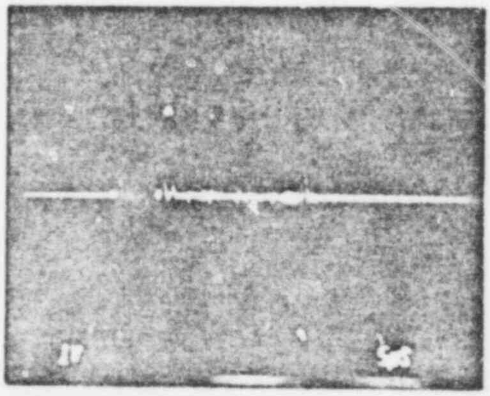

(c)

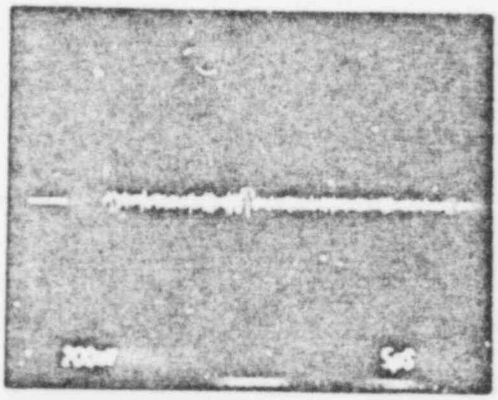

Figure 7. A-scans from section of 24" diameter x 2" wall centrifugally-cast stainless steel pipe. Backwall reflection is seen at location 1 in the case of (a) Mode I focusing and (b) Mode II focusing, but is absent when a nonfocused transducer (c) is used.

ratio and hence overcomes the attenuation due to scattering, but, more importantly, reduces the coherent noise since fewer grains are observed within the small focal region.

4. Transducer Matching and High-Power Insonification

Transducer matching increases the power transmitted to and received from the region of interest. Because of the commercial availability of matched transducers, we have decided to purchase our annular array transducer already matched rather than attempt to fabricate our own matching layers.

Sensitivity enhancement by high-power insonification is ultimately limited by the power handling capability of the transducer. As the power is increased, a dangerous feedback mechanism comes into play, where the increased power dissipated in the transducer raises its temperature, thereby increasing the loss tangent, which, in turn, raises the temperature further. Estimates from work reported in the literature (D. Berlincourt, B. Jaffe, H. Jaffe and H. H. Krueger, IRE Trans. Ultrasonics Eng., pp. 1-6, 1960) indicate a power limit of the order of 0.5 kilowatts (CW) for a PZT transducer. In our own laboratory, we have transmitted 60 watts CW (the maximum power available to us) to a transducer immersed in water without any noticeable rise in temperature or change in the lineerity of the output. CW rather than pulse insonification was employed in these tests because maximum power transmission in pulse echo devices can be obtained by use of expanded waveforms, such as in the chirp radar system which we have developed.

5. Integration of the Components of the Ultrasensitive Ultrasonic System

Signal averaging, transducer matching, pulse compression and high-power insonification can be cascaded very easily to form an ultrasonic system with an enormous increase in sensitivity over current devices. Incorporation of the annular array into this system, however, would require separate high power amplifiers for each ring, and separate pulse compression filters for each ring in Mode I operation (all annuli active in receive) and one filter for Mode II (only outer annulus active in receive).

Conclusions and Plans for Future Research

The highly-sensitive system which we have developed should be capable of overcoming almost all random noise problems which are encountered in ultrasonic inspection of reactors. Other major needs in this field are improved lateral resolution and improved discrimination against coherent background due to grain scattering. As this study has shown, electronic focusing will significantly increase not only the signal-to-random noise ratio, but also the resolution and background-suppression capability of the system. However, because of the rigidity of the materials of interest and the large differences between the ultrasonic velocities in these materials and in typical transducer coupling media (water, oil, grease), image distortions will be produced when inspecting through surfaces which are not flat. Our efforts in the next two years will therefore concentrate on developing focusing and beam deflection schemes which, at reasonable cost, will allow inspection of hard materials. The use of shear waves will also be investigated since it will provide a factor of two improvement over the use of longitudinal waves, due to its lower velocity. A theoretical analysis of array performance in the wideband case will be undertaken in order to optimize array design for the focusing techniques under consideration. A two-dimensional stepper-motor driven scanner, with computer interface, will also be developed and used to generate B-scan images of flaws in materials.

INSPECTION OF NUCLEAR REACTOR WELDING BY ACOUSTIC EMISSION

GATX/GARD, INC.
7449 No. Natchez
Niles, Ill. 60648

Principal Investigator David W. Prine

OBJECTIVE

The overall objective of this work is to provide improved detection and characterization of flaws by nondestructive testing during the fabrication of nuclear piping and pressure vessel weldments using acoustic emission monitoring during the welding process.

To accomplish this end, the following specific goals were set within a three year program:

1. Show feasibility of in-process acoustic emission monitoring on nuclear piping and pressure vessel welds.
2. Fabricate piping and pressure vessel monitoring equipment and evaluate under nuclear fabrication shop conditions.
3. Provide data to be used as a basis for development of a case for NRC acceptance of in-process acoustic emission monitoring of welds in nuclear components.

FY77 SCOPE

1. Additional laboratory testing to aid in determination of AE flaw detectability and flaw type discrimination.
2. Development of correlation between AE and flaw size by analyzing AE data and cross validating of flaws with other NDE techniques as well as quantitive metallography.

3. Construction of a prototype vessel weld monitor and testing under shop conditions.
4. Completion of the shop evaluation of both the piping and pressure vessel AE monitors.
5. Analysis of all the data and experience generated during the program and establishment of a case for NRC and code acceptance of AE in-process weld monitoring of nuclear components.

SUMMARY OF RESEARCH ACTIVITIES FOR FY77

The major accomplishments during FY77 were:

1. Completion of Piping Laboratory tests, including 49 welds and 540 feet of weld pass on A312T304 and A106 material. Over 60 planned flaws were generated.
2. Construction of a prototype pressure vessel weld monitor.
3. Production shop evaluation of the piping AE weld monitor at G & W Plant # 1, Cicero, Illinois; consisting of 80 welds and 5800 feet of weld pass on A106 material.
4. Completion of pressure vessel laboratory tests consisting of 15 welds and 900 feet of weld pass containing over 70 planned flaws in A533 material.
5. Production shop evaluation of the pressure vessel AE weld monitor at B & W, Mt. Vernon, Indiana and Westinghouse, Tampa, Florida; consisting of 5 welds and 4,480 feet of weld pass on A508 and A533 material.
6. Analysis of AE data for correlation of AE activity and flaw detectability and flaw type discrimination.

PIPING AND PRESSURE VESSEL LABORATORY TESTS

A total of six laboratory tests have been run during this [illegible] year program. The first three (one on piping type welds and two on pressure vessel welds) were used for initial calibration and proof of feasibility purposes. A limited number of flaws were generated in three categories; cracks; slag inclusions and porosity.

The latter three tests conducted during the past fiscal year (FY77) consisted of very large bank of flaws (approximately 130) in both piping and pressure vessel welds. Analysis of this data has so far shown that probabilities of AE detection for cracks and slag inclusions are 100%. Incomplete penetration was detected 100% in submerged arc welds and about 75% in gas shielded welds. Porosity has shown an 80% detection probability, with detected porosity strongly associated with slag entrapment. Lack of fusion was not detected, nor were tungsten inclusions although both show some low level AE activity. The AE signals from cracks, incomplete penetration and slag inclusions show general correlation with size. In addition, analysis has so far has shown the feasibility of AE discrimination between cracks and slag inclusions or the basis of differing delay times for the onset of AE activity.

PIPING AND PRESSURE VESSEL PRODUCTION SHOP EVALUATION TESTS

Production shop evaluation of a single channel piping monitor was conducted during FY77. The 5800 feet of weld passes were in nuclear grade carbon steel piping, and produced the following results. AE detected 61% of X-ray indications with a 3.9% over-call. On a type basis, AE detected 100% of cracks, 59% of porosity and 63% of slag inclusions. Production radiography was the means of flaw confirmation for the piping tests.

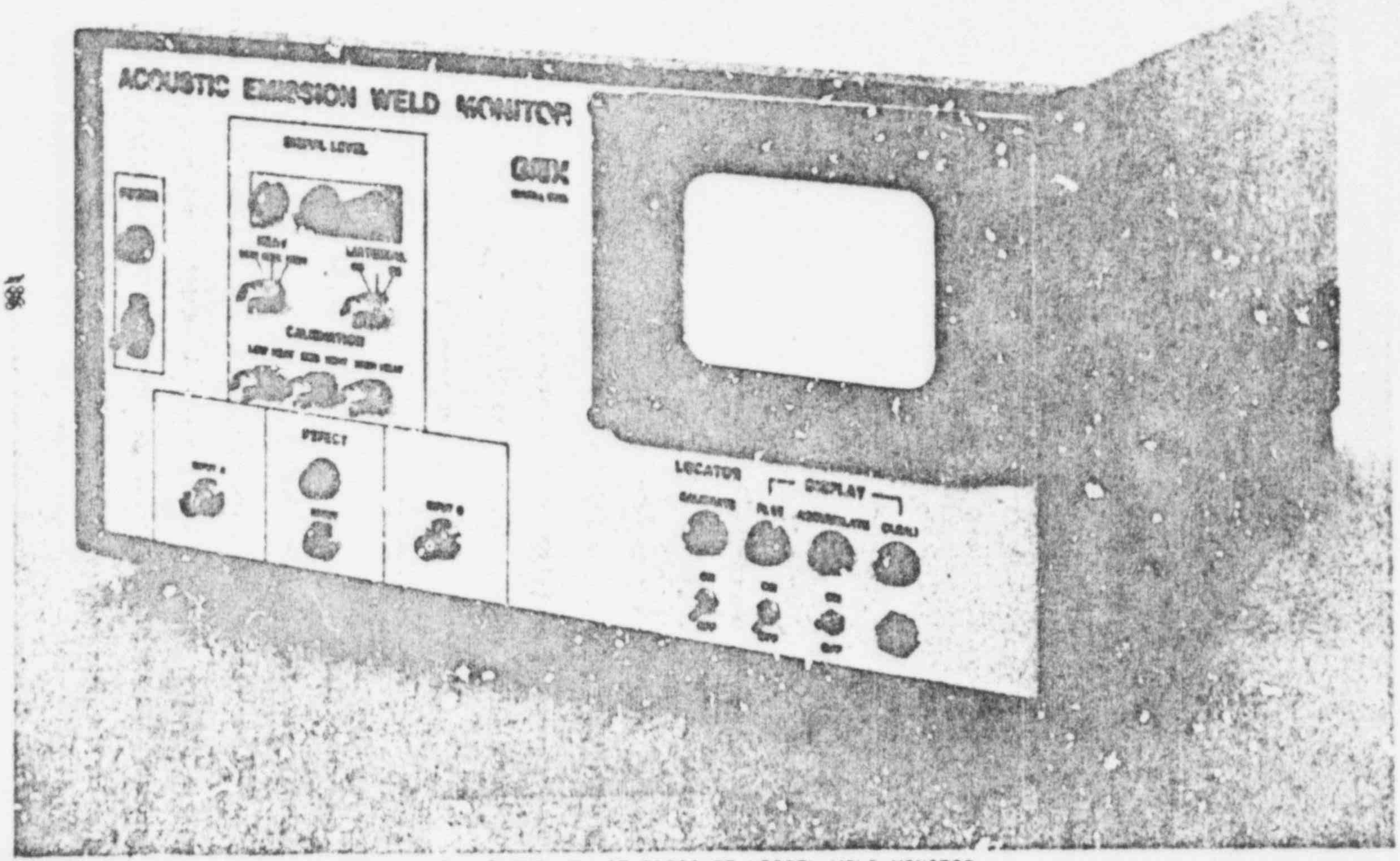

186

Figure 1 2 CHANNEL AE PRESSURE VESSEL WELD MONITOR

ANALYSIS OF AE DATA

The AE data from both laboratory piping and pressure vessel tests welds was used to determine correlation of AE activity with flaw detectability and flaw types. These tests included both planned and natural flaws.

The AE data was stored in raw analog form on magnetic tape and in pre-processed digital form on computer data storage diskettes. The data was then recovered and analyzed as to ring-down count (energy) levels and distributions, and spectral content. The computer aided analysis system generates a variety of plots and histograms of the various AE signal parameters, performs some statistical analysis on the data, and generates print-outs for each weld. The analysis so far has yielded considerable information as to:

- o AE flaw detection probabilities for the various flaw types.
- o AE signal correlation with flaw size.
- o AE signal characteristics which may allow flaw type to be determined.
- o Basic AE flaw detection mechanisms.

Future work in this program will include:

1. More detailed analysis of the existing AE data bank to provide better understanding of the flaw size and type discrimination characteristics and to provide additional evidence of the effectiveness of in-process AE weld monitoring.
2. Development of an AE monitor that not only detects flaws during welding but provides information on size and type of flaw.

Production pressure vessel shop evaluation of in-process AE monitoring consisted of 3 tests, two with the laboratory system, and one with the two channel AE pressure vessel production weld monitor (Figure 1). The first test consisted of monitoring the O.D. weld on a vessel inlet nozzle. The weld was approximately 12 inches thick A508 pressure vessel steel, and produced only one AE indication. The indication correlated visually with a slag entrapment on a cap pass later to be removed by machining. Radiograpy has not been completed as of this writing.

The second pressure vessel test was a half bead temper repair on a HSST test vessel. The weld was accomplished with manual stick welding. The weld was very quiet acoustically and produced only a few scattered AE indications. The more severe of these led to the grinding away of a portion of the weld to reveal scattered porosity. Radiography and ultrasonic testing confirmed further areas of porosity, but these were judged code-acceptable.

The third pressure vessel test was a series of longitudinal seams in three nuclear steam generator shells. Approximately 1500 feet of weld pass showed 6 indications which were visually confirmed. The indications were in run-off pads and lower root passes which were later ground out. Production radiography has confirmed AE findings. No rejectable flaws were found with radiography. The production shop tests have shown that:

1. Utilization of Acoustic Emission monitoring is feasible in a shop environment to detect and locate flaws in nuclear component fabrication welds.
2. Acoustic Emission results correlate well with current NDE methods (i.e., radiography and ultrasonic).
3. Acoustic emission monitoring of welds can be applied without interfering with normal production processes.

CONTRACT TITLE

Acoustic Emission-Flaw Relationships for
In-Service Monitoring of Nuclear Pressure Vessels

CONTRACTOR AND LOCATION

Battelle
Pacific Northwest Laboratories
Battelle Boulevard
Richland, WA 99352

PRINCIPAL INVESTIGATORS

P.H. Hutton

E.B. Schwenk

OBJECTIVE

The purpose of this program is to develop an experimental/analytical evaluation of the feasibility of detecting and analyzing flaw growth in reactor pressure boundaries by continuously monitoring for acoustic emission (AE). Major specific program objectives are:

- Develop criteria to distinguish flaw growth AE from other non-significant acoustic signals.
- Develop an AE-flaw growth model as a basis for relating inservice AE to flaw significance.

FY-77 SCOPE

The program scope for FY-77 included:

1. Procure A533 Grade B, Class 1 plate and fabricate test specimens
2. Establish a calibrated mechanical-electronic test system
3. Start developing AE signatures for fracture, fatigue crack growth and innocuous noise sources.
4. Investigate effect of prior plastic deformation on generation of AE by crack growth.

815 195

5. Start developing AE-fracture mechanics model as a basis for evaluating defect significance by AE.

6. Evaluate availability of high temperature sensor suitable for reactor service.

7. Collect and analyze AE data from HSST tests.

8. Develop a library of relevant work published by others and evaluate for useful findings.

9. Prepare a year end report including preliminary conclusions on the feasibility of inservice AE monitoring for detection and evaluation of flaws.

SUMMARY

Since this program was initiated in late FY-76, this report actually covers the period July 1, 1976 to October 1, 1977. A brief review of major accomplishments includes:

- Forty-two specimens, including skin-base and skin-weld material from an 8 in. thick plate of A533 Grade B, Class 1 steel, have been fabricated.
- A multiparameter AE detection and analysis system has been assembled and calibrated.
- A method of rating AE system detection capability has been devised to facilitate relating AE results to other tests and other AE systems.
- Fourteen tensile specimens, two fracture specimens, three fatigue crack growth specimens - base metal, weld metal, and 3% plastic prestrain base metal - have been tested.
- Measured AE from the HSST V-7B intermediate pressure vessel test.

815 196

Results will be discussed under the following topics:

1. AE instrumentation and techniques
2. Tensile and fracture tests
3. HSST V-7B vessel test
4. Fatigue crack growth
5. AE characteristics
6. Fracture mechanics relationships and application.

AE Instrumentation and Techniques

The multiparameter AE detection and analysis system shown in Figure 1 is the primary measurement system being used on this program. It measures seven parameters (five AE parameters and two mechanical test parameters) simultaneously and records these on solid state digital memories. The digital memory recording method greatly facilitates subsequent analysis by providing a direct tabulated printer readout with all parameters coordinated.

A source isolation feature limits accepted AE data to that originating in the predetermined area of interest. The source isolation also controls a transient wave analyzer so that displayed signals for wave form and frequency spectrum analysis are limited to those originating in the area of interest.

A method for rating the sensitivity of the entire AE monitor system has been devised to make the results of this program relatable to othe AE monitor systems and tests. We call it "Effective Sensitivity". To illustrate, assume a monitor system operating with a total gain of 90 dB, a detection threshold of 1.5 volts peak, and a sensor with an absolute sensitivity calibration of -65 dB re 1 volt/μbar in the frequency range being monitored. The minimum input voltage to the system from the sensor that the system would respond to is $\frac{1.5 \text{ volts}}{90 \text{ dB gain}}$ of 47 μ volts. Considering

815 197

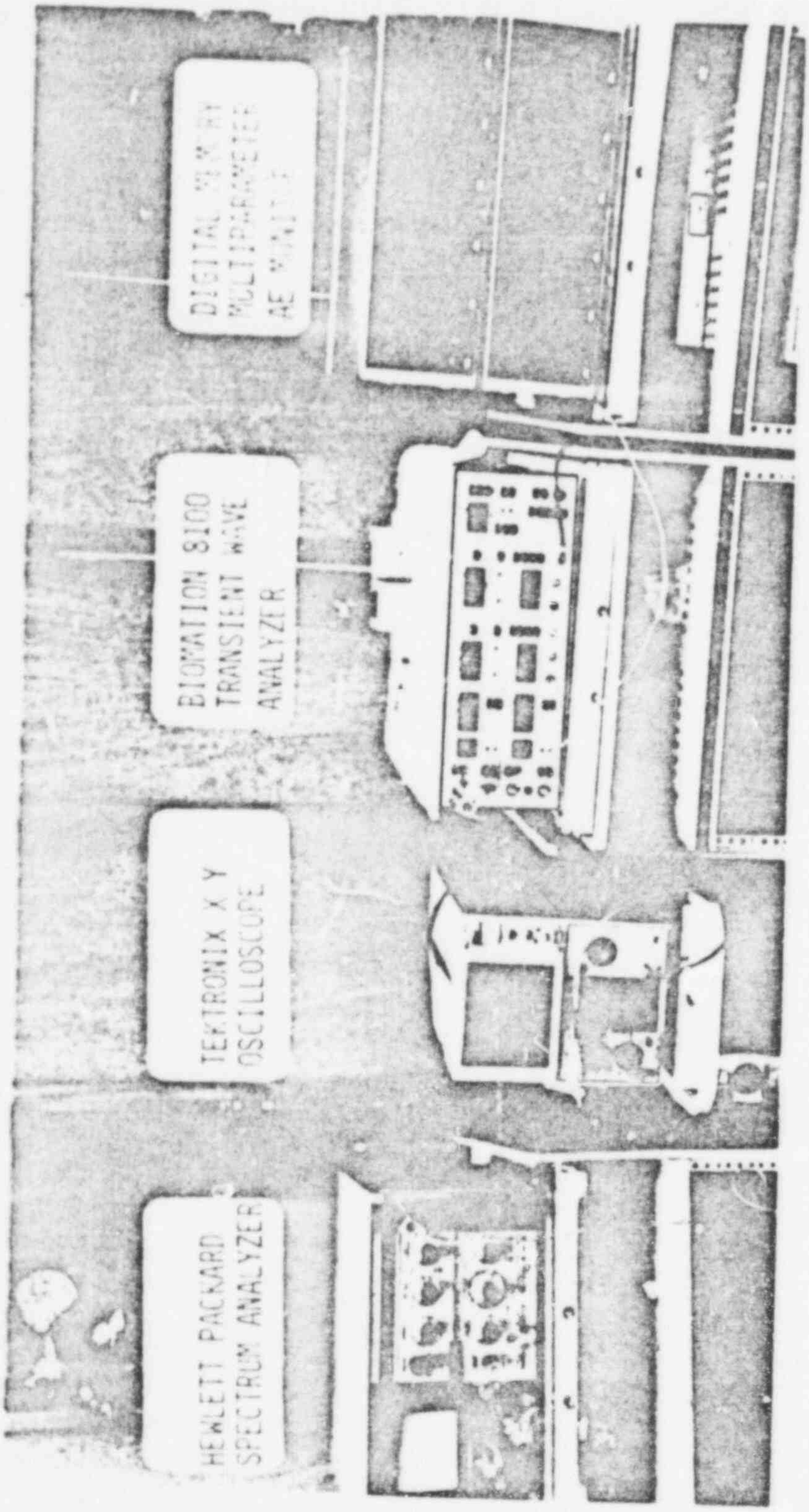

FIGURE 1. Acoustic Emission Analysis System

the sensor, it should produce $\frac{1 \text{ volt}/\mu\text{bar}}{65\text{dB}}$ or 562 μ volts/μbar of front face pressure. If we now compare these two values, the total system should respond to $\frac{47}{562}$ or 0.08 μ bar pressure on the front face of the sensor. Thus 0.08 μ bar is called the effective sensitivity of the measurement system.

Tensile and Fracture Tests

Smooth tensile specimens of both base metal and weld metal tested at room temperature and at 550°F produced essentially no detected AE (Figure 2). This suggests that elastic/plastic deformation in a vessel in the absence of stress concentrations (K_t) may produce little or no detectable AE.

Total acoustic signals detected without source isolation restriction is plotted in Figure 2 as acoustic noise. This plot uses the AE event count scale. Where the total valid AE count was 10, the total acoustic noise count was 1550. This illustrates the effectiveness of the source isolation in screening out misleading test system noise.

On the other hand, notched tensile specimens and fracture toughness specimens both produced readily detectable AE (Figures 3 and 4). This implies a K_t level threshold below which AE is not readily detectable. This could be a very useful phenomenon if the K_t threshold is similar to that for the upper limit of acceptable defects in a vessel.

The fracture toughness specimens indicated that AE is detectable not only for grossly elastic loading with a stress concentration, but also for discontinuous crack growth through highly strained materials.

HSST V-7B Vessel Test

The HSST V-7B vessel test produced AE data which followed flaw development and correlates with crack growth. Figure 5-9 illustrate how the AE source location pattern shifts with development of the flaw machined into the vessel wall. Up to about 18,000 psig, most of the AE sources are clustered around the center of the flaw (Figures 5, 6, 7). As the

AE-SMOOTH TENSILE SPECIMEN A1-4

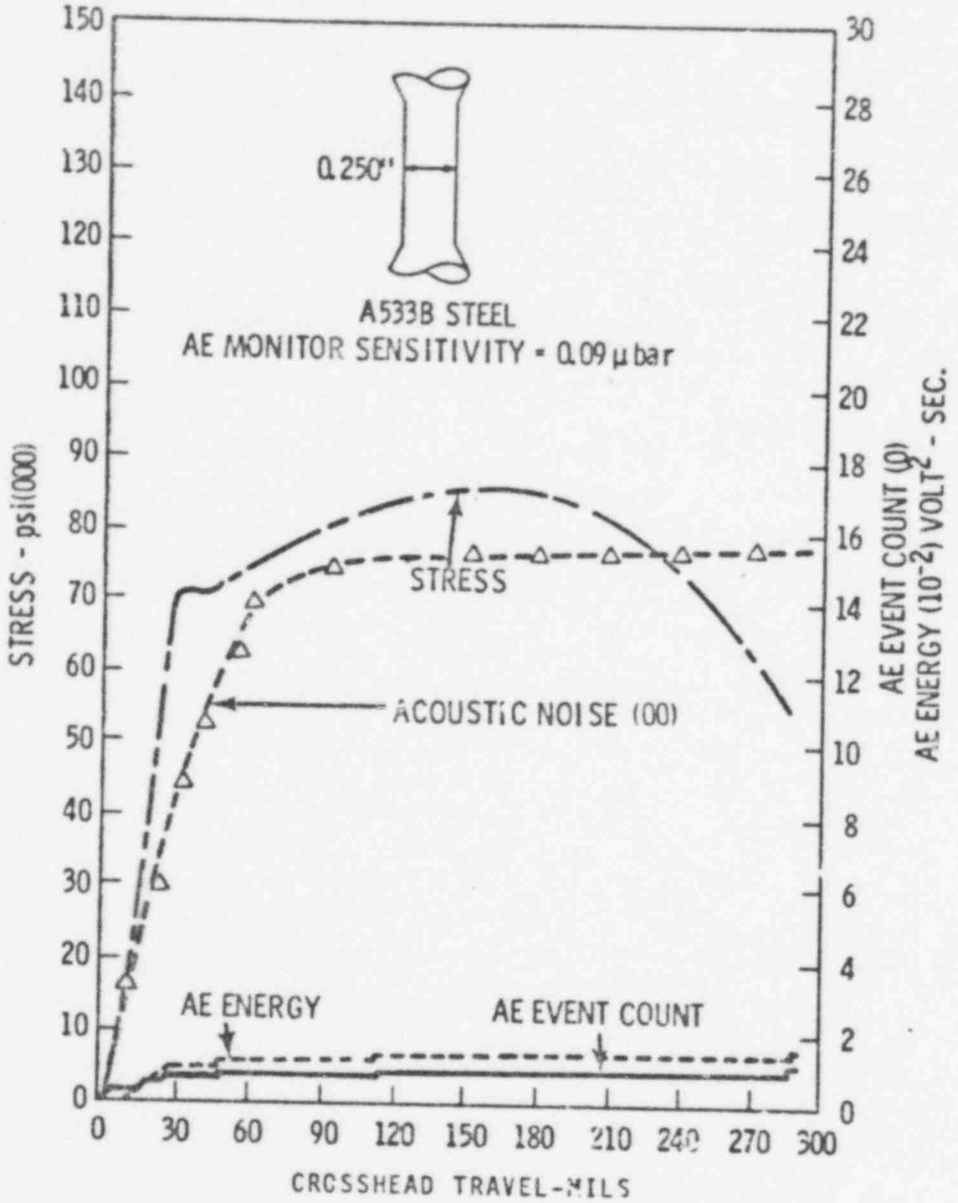

FIGURE 2. AE from Tensile Test A1-4, Skin Weld Material, A533B, Room Temperature

815 200

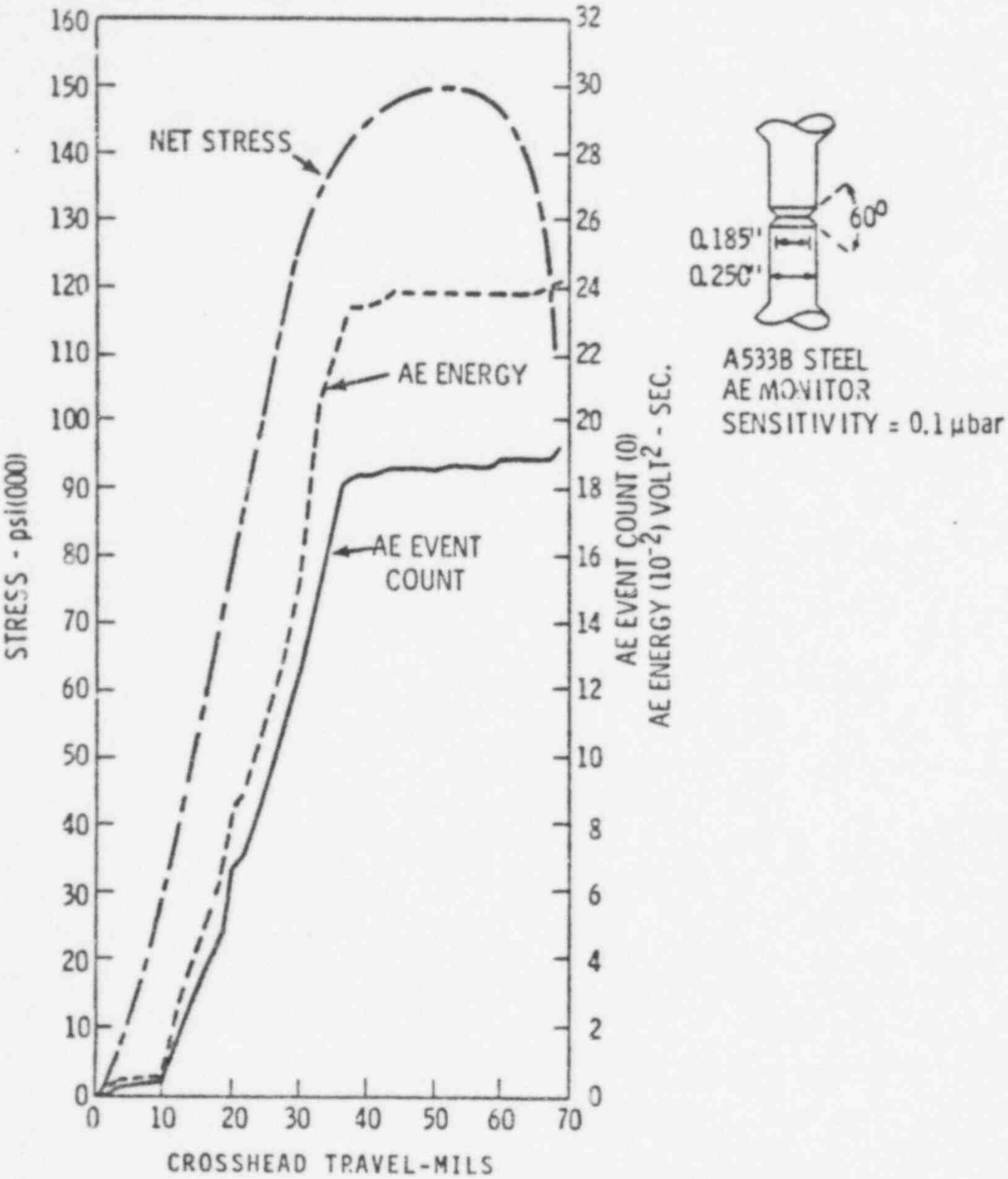

FIGURE 3. AE from Notched Tensile Test AET-25, A533B Material, Room Temperature

TEST SPECIMEN - 2T COMPACT TENSION - B2-3B
AE SYSTEM EFFECTIVE SENSITIVITY = 0.19 μbar
CROSSHEAD TRAVEL - 0.067 IN./MIN.
FREQUENCY RANGE - 0.2-0.8 MHz

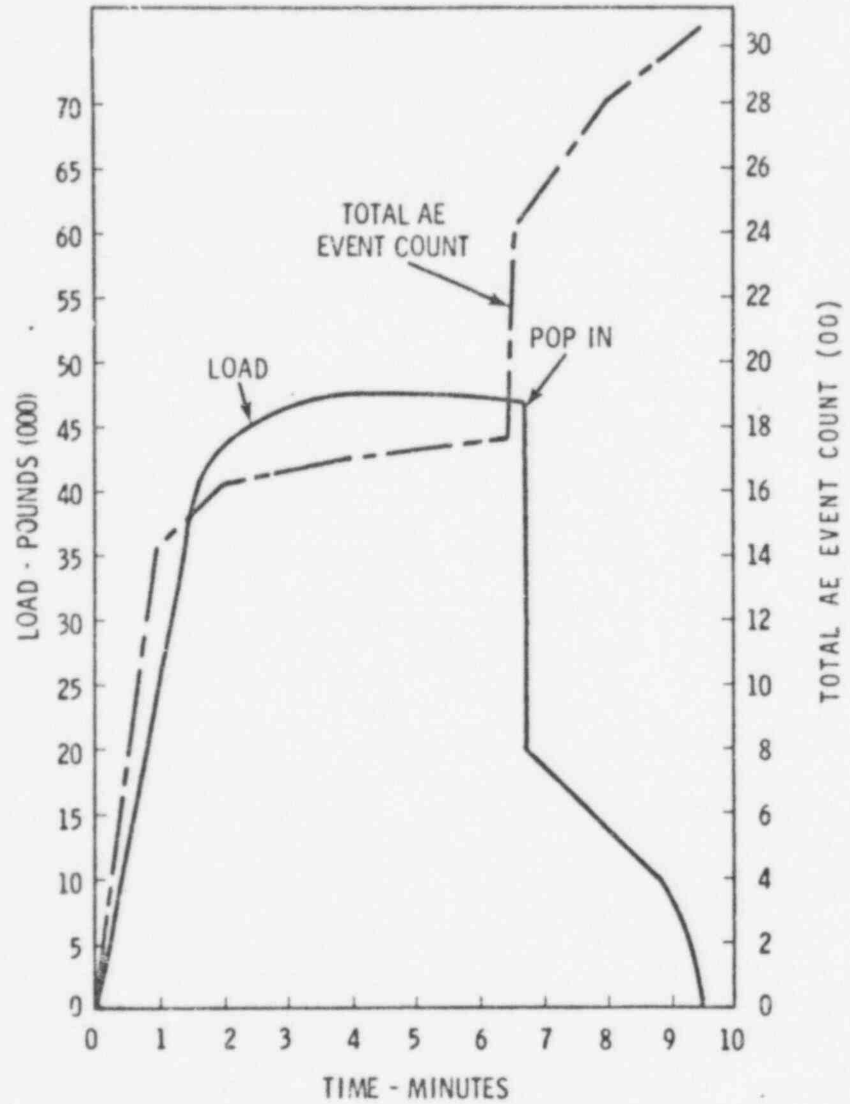

FIGURE 4. AE from Fracture Test B2-3B, Skin Weld Material, A533B Steel, Room Temperature

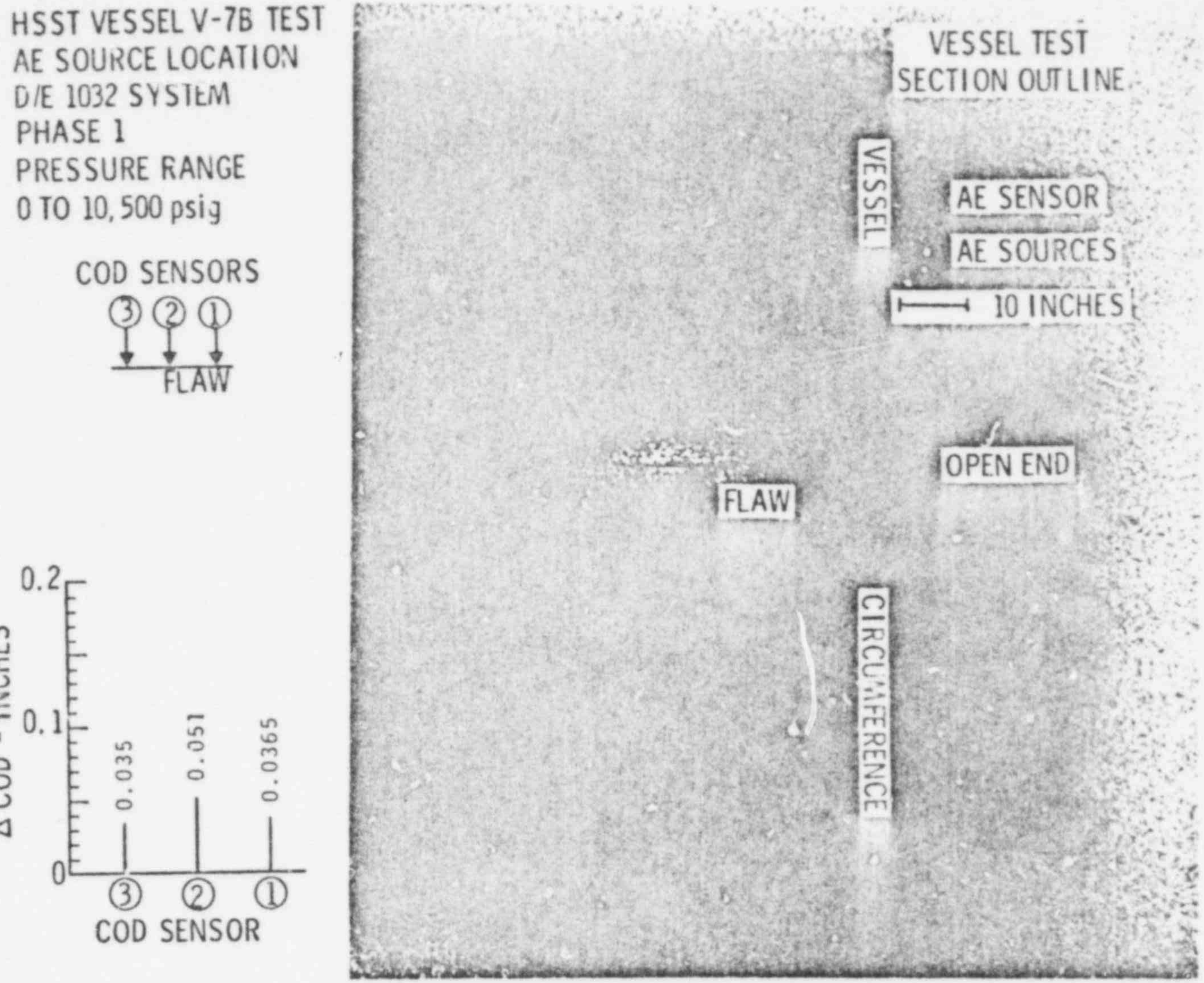

FIGURE 5. HSST V-7B Test AE, Phase 1, 0-10,500 psig

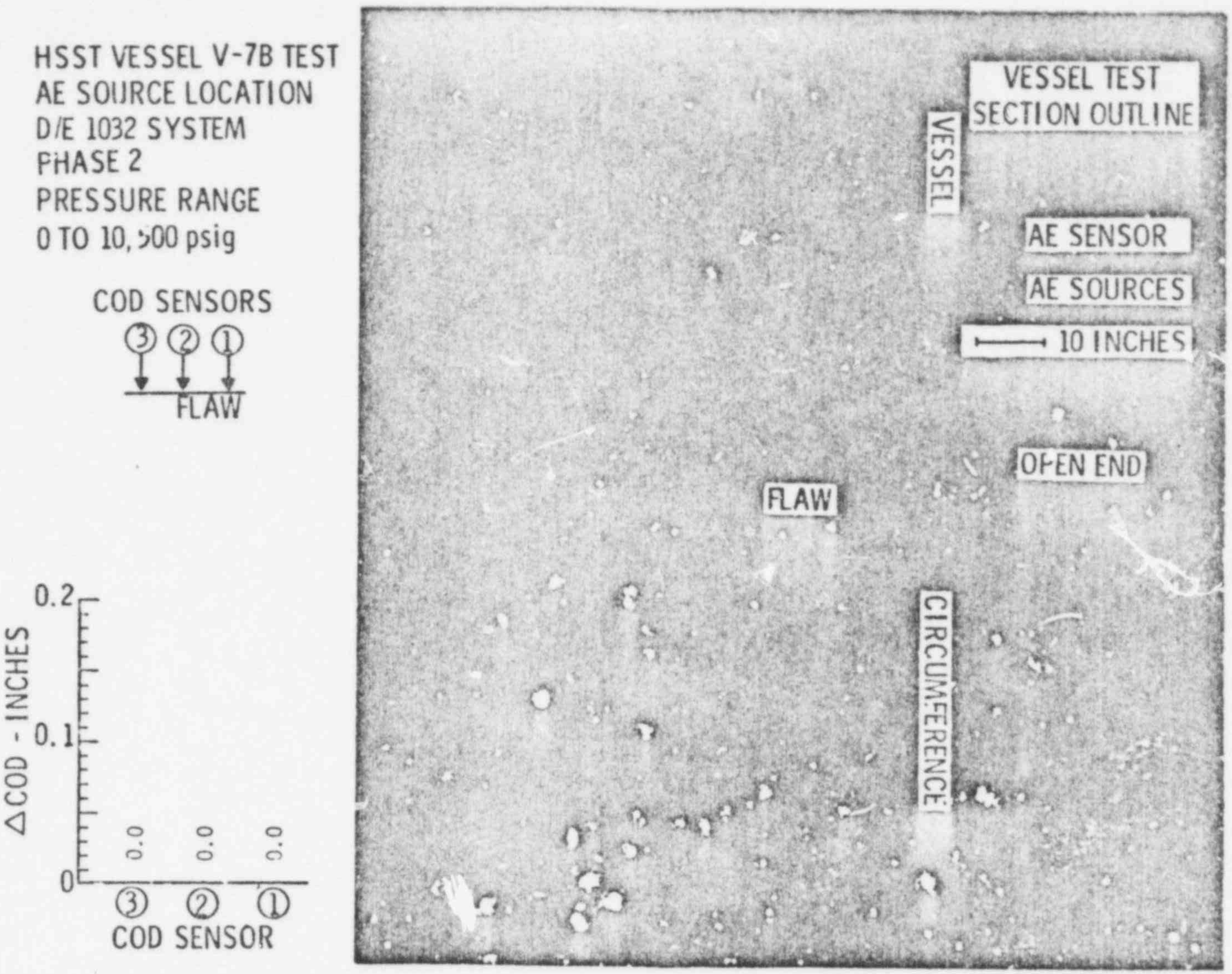

FIGURE 6. HSST V-7B Test AE Phase 2, 0-10,500 psig

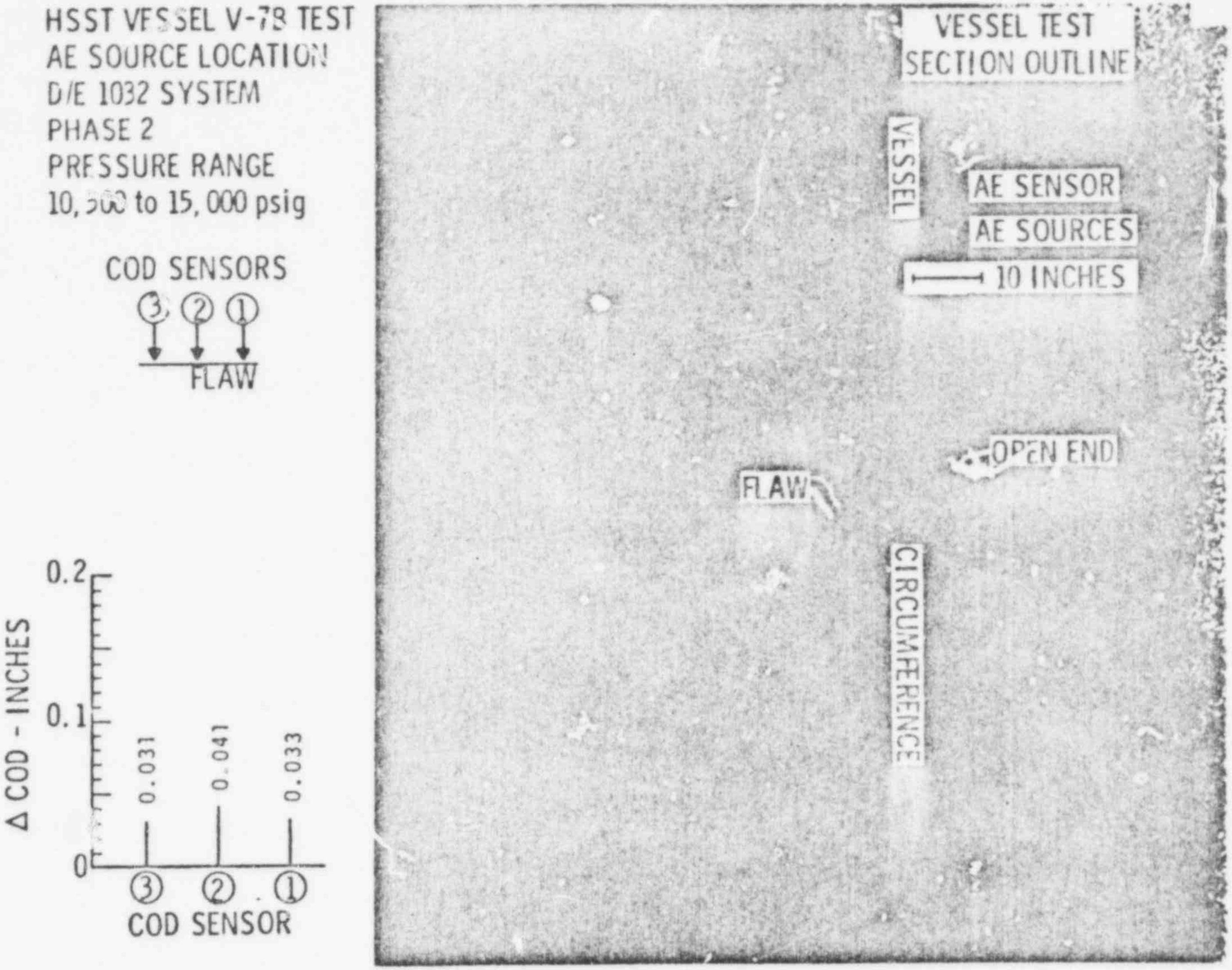

FIGURE 7. HSST V-7B Test AE Phase 2, 10,500-15,000 psig

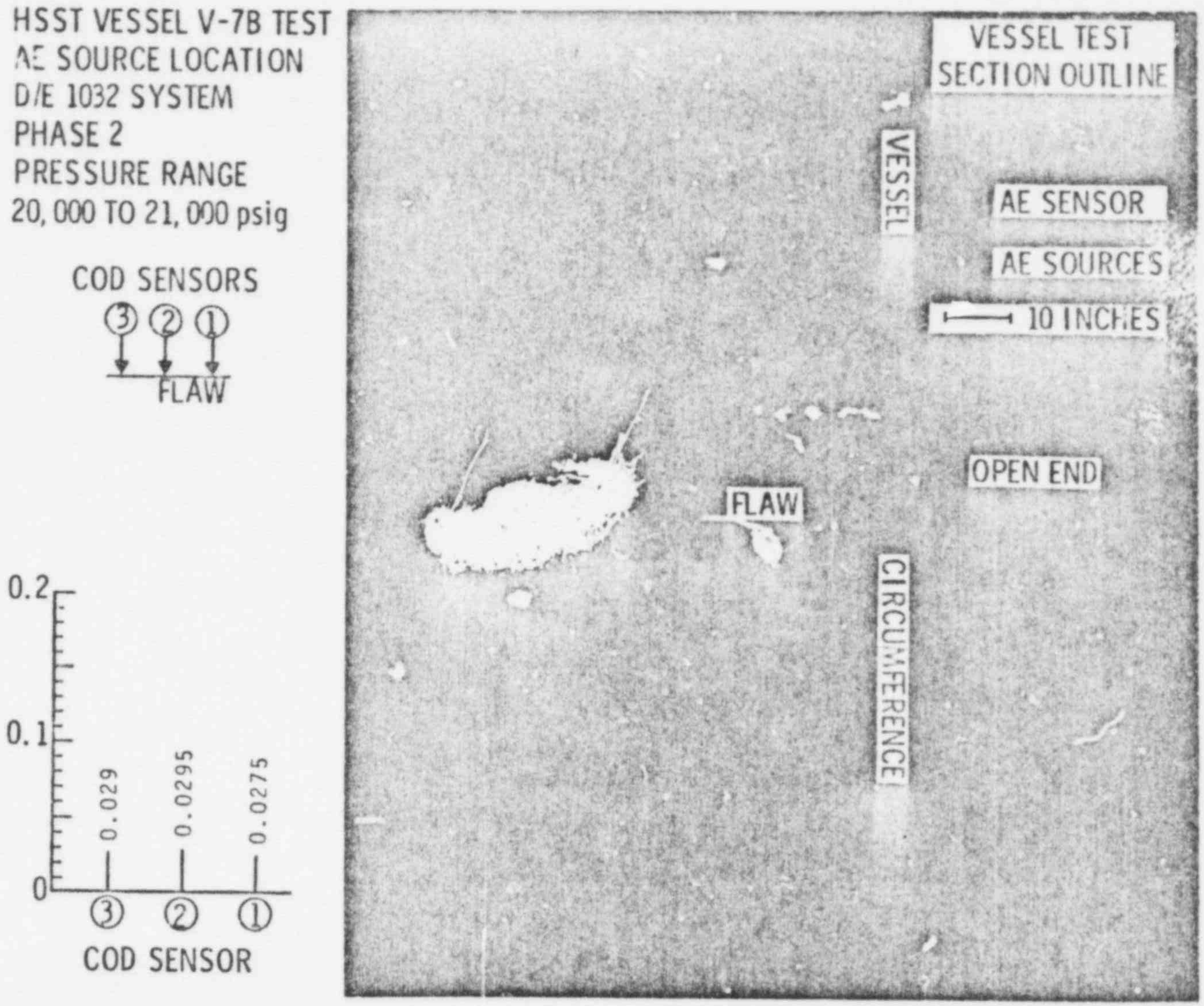

FIGURE 8. HSST V-7B Test AE Phase 2, 20,000-21,000 psig

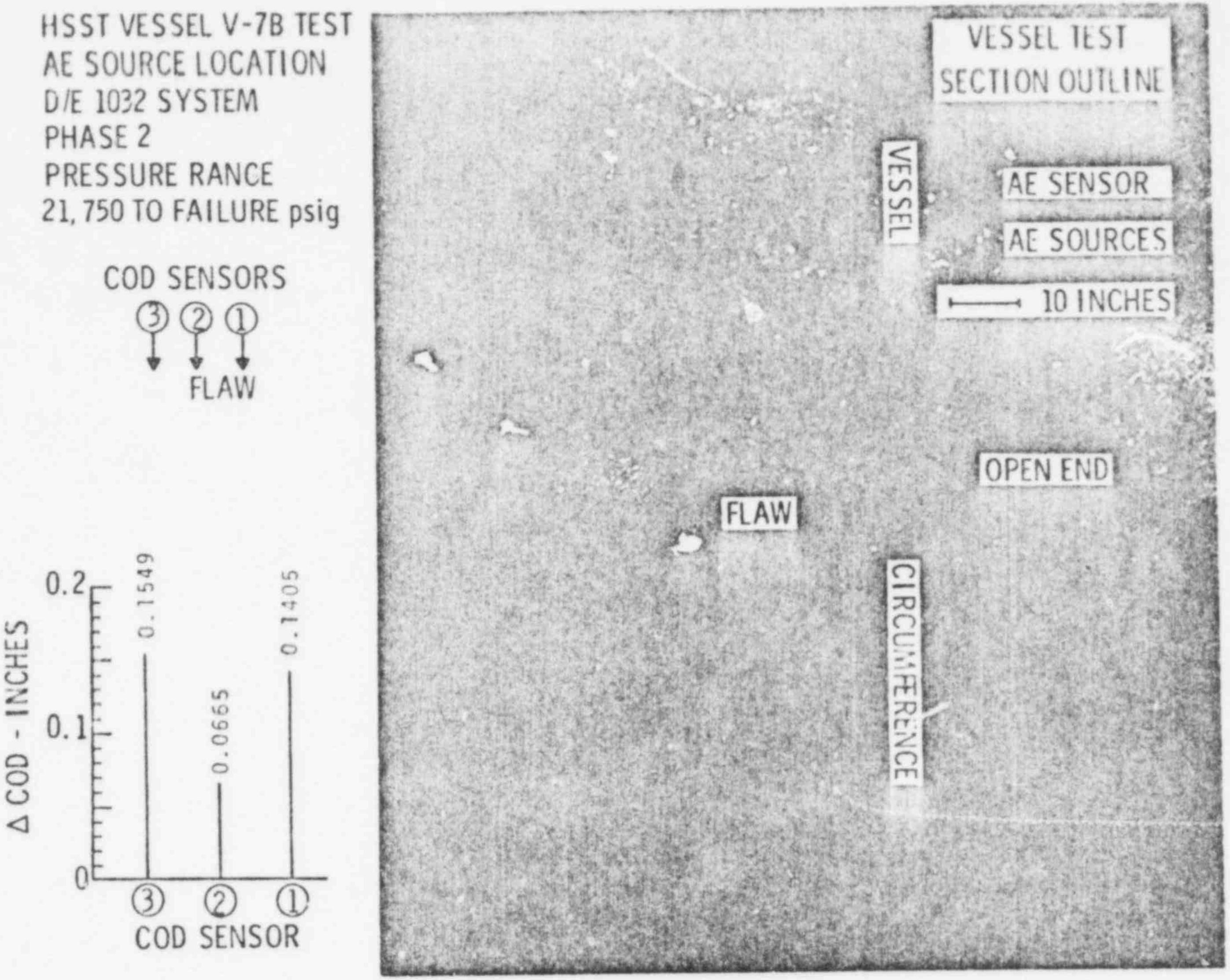

FIGURE 9. HSST V-7B Test AE Phase 2, 21,750-Failure psig

pressure continues to increase to vessel failure at the flaw, the AE source indications move to the outer ends of the flaw (Figure 8) and indicate the crack extending out from the ends of the machined flaw (Figure 9). Figures 5 and 6 illustrate the Kaiser Effect where in the first pressurization to 10,500 psig, many AE signals were detected, but in the second pressurization through the same range a short time later, very few AE signals were detected. This phenomenon has been shown to be reversible with appropriate time and temperature exposure.

AE data and crack opening displacement (COD) data plotted against test pressure are presented in Figure 10 - 13. AE event count and energy (Figure 11) appear to relate well to the COD curves (Figure 10). The apparent magnitude of event count from the D/E system in Figure 11 is misleading. This system was operated at about half the sensitivity of the BNW system to provide one system that was less subject to being overwhelmed by unexpected noise. Comparing AE signal amplitude and rise time (Figures 12 and 13) with COD (Figure 10), the low amplitude and fast rise time signals show the best relationship to COD. This is consistent with results evolving from laboratory specimen tests to date. Further analysis is in progress to relate the AE data to fracture mechanics parameters.

Fatigue Crack Growth

The primary emphasis has been to identify AE-fracture mechanics relationships which hold a potential for defining flaw significance from AE data. To this point, such analysis has been focused on fatigue crack growth. The overall concept being applied in analysis is illustrated in Figure 14. The concept considers that a flaw growing in a pressure vessel will produce AE and that advanced instrument systems are available for developmental detection and analysis of AE signals. Present effort is on determining which AE parameter(s) most effectively correlates with flaw growth to provide a basis for flaw evaluation relationships.

A statistical approach has been used to screen the various parameter combinations for the most promising relations in the following manner. Rate data are developed from the basic crack length (a) and AE event count

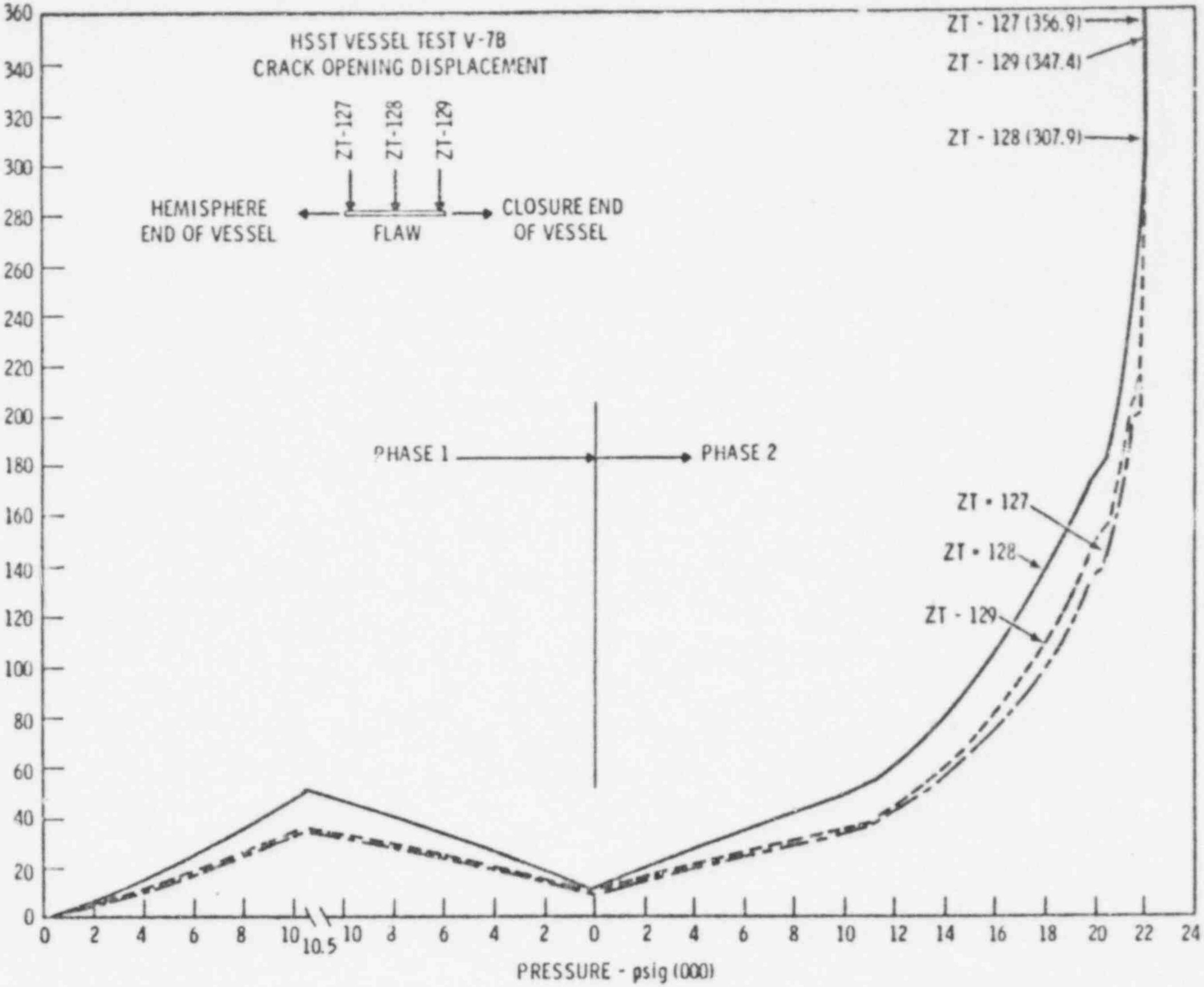

FIGURE 10. HSST V-7B Test, Crack Opening Displacement

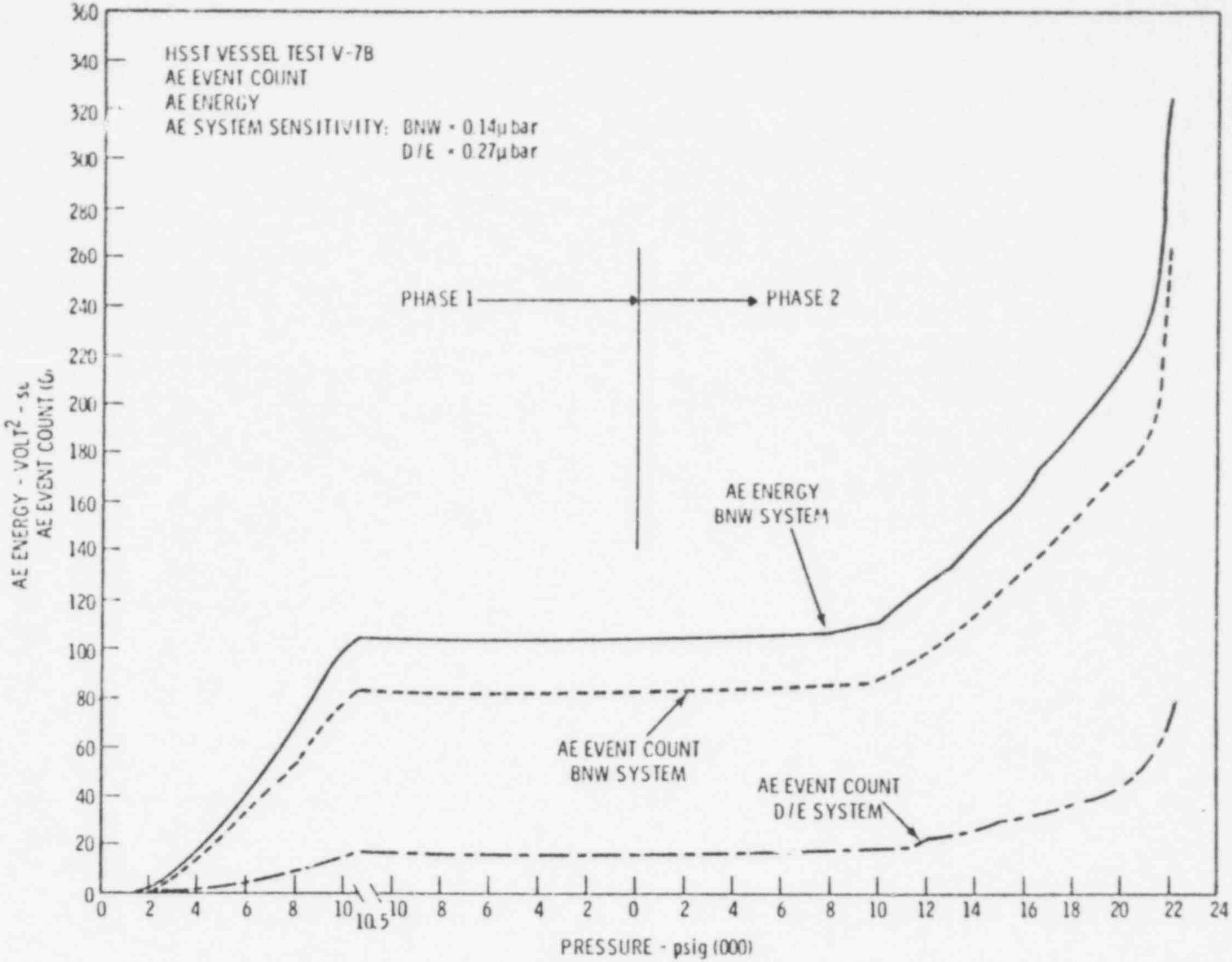

FIGURE 11. HSST V-7B Test, AE Event Count & Energy vs. Pressure

815 210

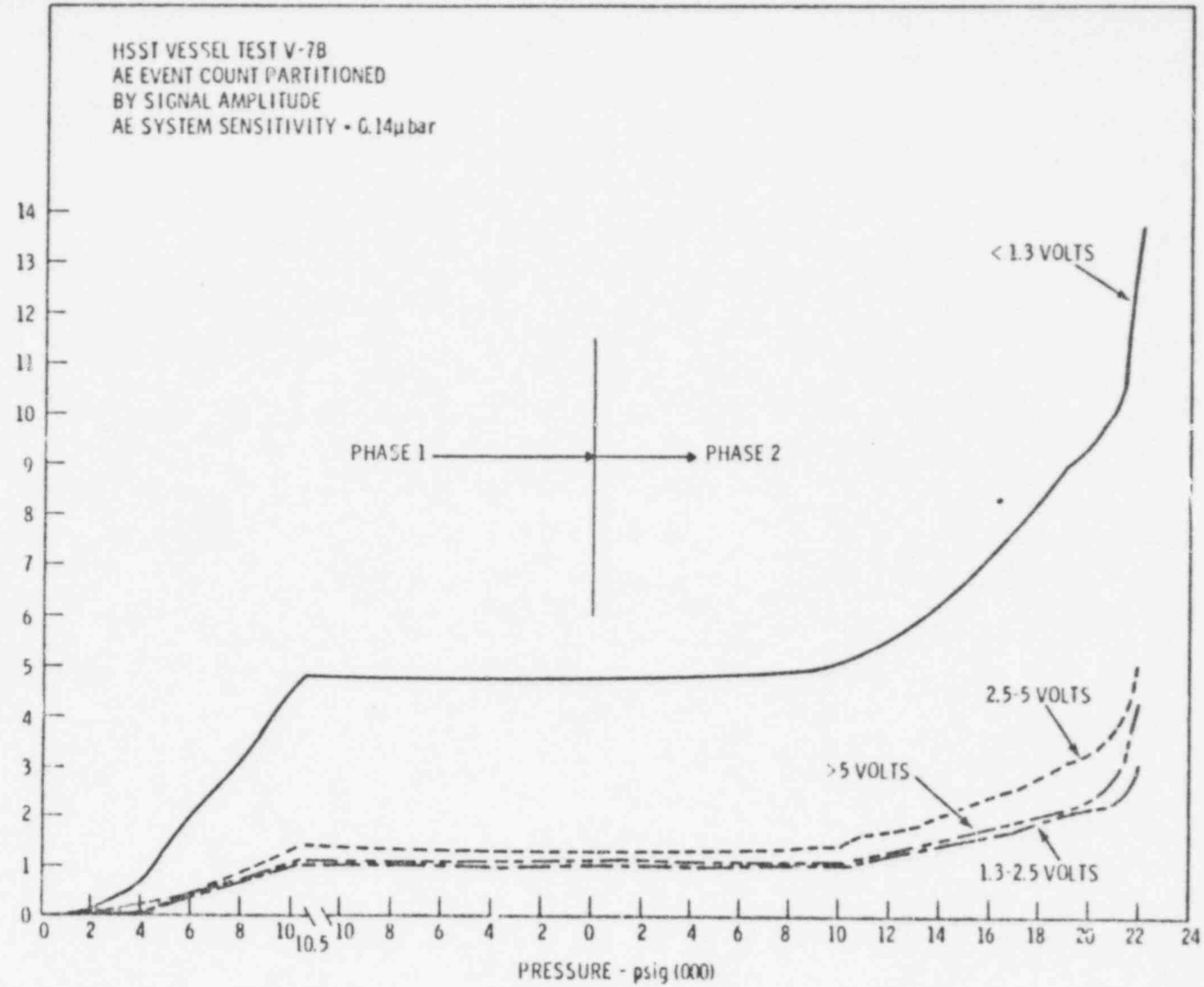

FIGURE 12. HSST V-7B Test, AE Event Count Partitioned by Amplitude vs. Pressure

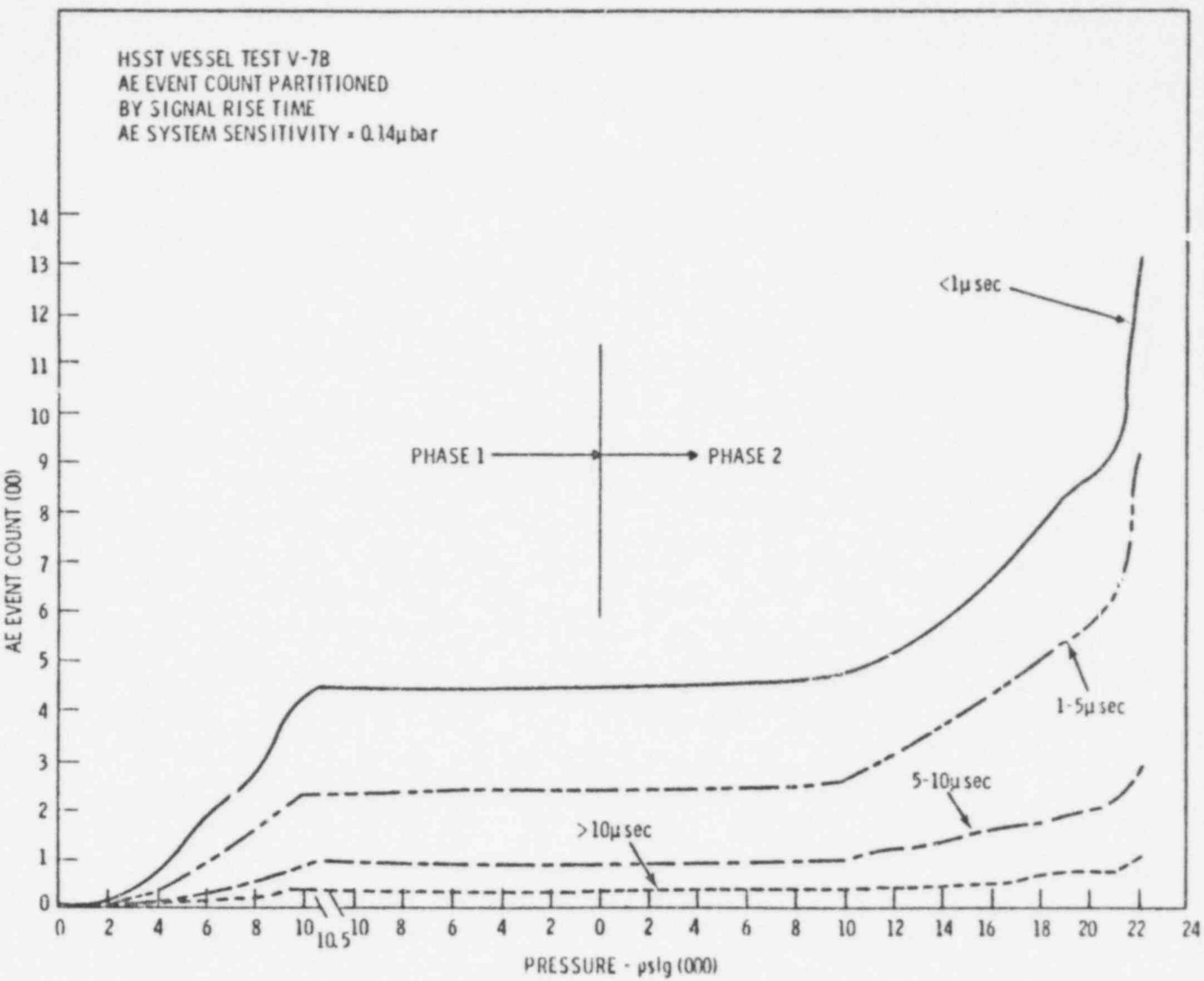

FIGURE 13. HSST V-7B Test, AE Event Count Partitioned by Rise Time vs. Pressure

207

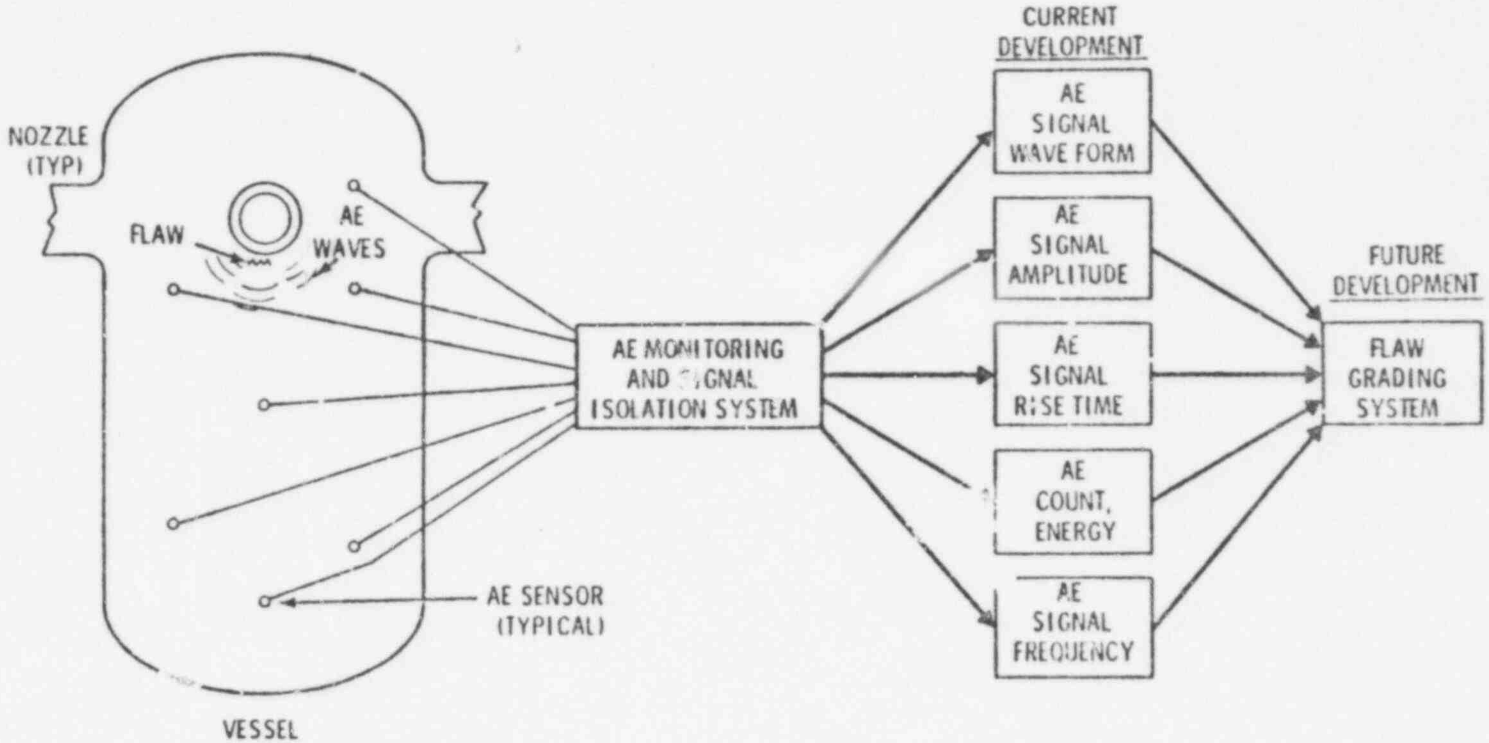

FIGURE 14. AE-Flaw Relationship Development Concept

(C3) and energy (E) data versus load cycles (N) curves of Figures 15, 16 and 17 by determining the slope of the various curves (e.g., da/dN, dC3/dN and dE/dN) between each value of N.

Fatigue crack growth rate (da/dN) is characterized by using the stress intensity factor range (ΔK), Figure 18.

Figures 19 and 20 compare AE rate data with da/dN. A power law relationship was derived where

$$dC3/dN = 4.942 \times 10^5 \, (da/dN)^{1.233} \text{ for a 99.9\% correlation}$$

dC3/dN could also be compared with ΔK, in the same manner. The correlation however, would be about the same because da/dN also correlates very well with ΔK (Figure 18).

Comparison of the change in event count (dC3) with change in calculated plastic zone volume (dV_p) also correlates well with da/dN where,

$$dC3/dV_p = 0.6495 \, (da/dN)^{-1.2354} \text{ for 99.9\% (Figure 20).}$$

Figures 19 and 20 indicate that the rate of change of AE event count is a measure of da/dN (and ΔK) and that the rate of change of C3 is controlled by the rate of change of V.

Similarly, many other comparisons of AE rate data and da/dN have been made and are shown in Table 1 for three fatigue crack growth specimens. Please be aware that the percent correlation determinations are a relative measure of the dependency of the two variables. They do not indicate the exact functional relationship.

Preliminary AE-da/dN correlations show that low amplitude AE event count signals of fast rise time provide the best measure of da/dN and that plastic zone volume appears to play a dominant role in the production of the low amplitude-fast rise time signals. These data are preliminary but the results are encouraging for using rate of change of AE signals over a period of time as a measure of flaw growth rate in a pressure vessel.

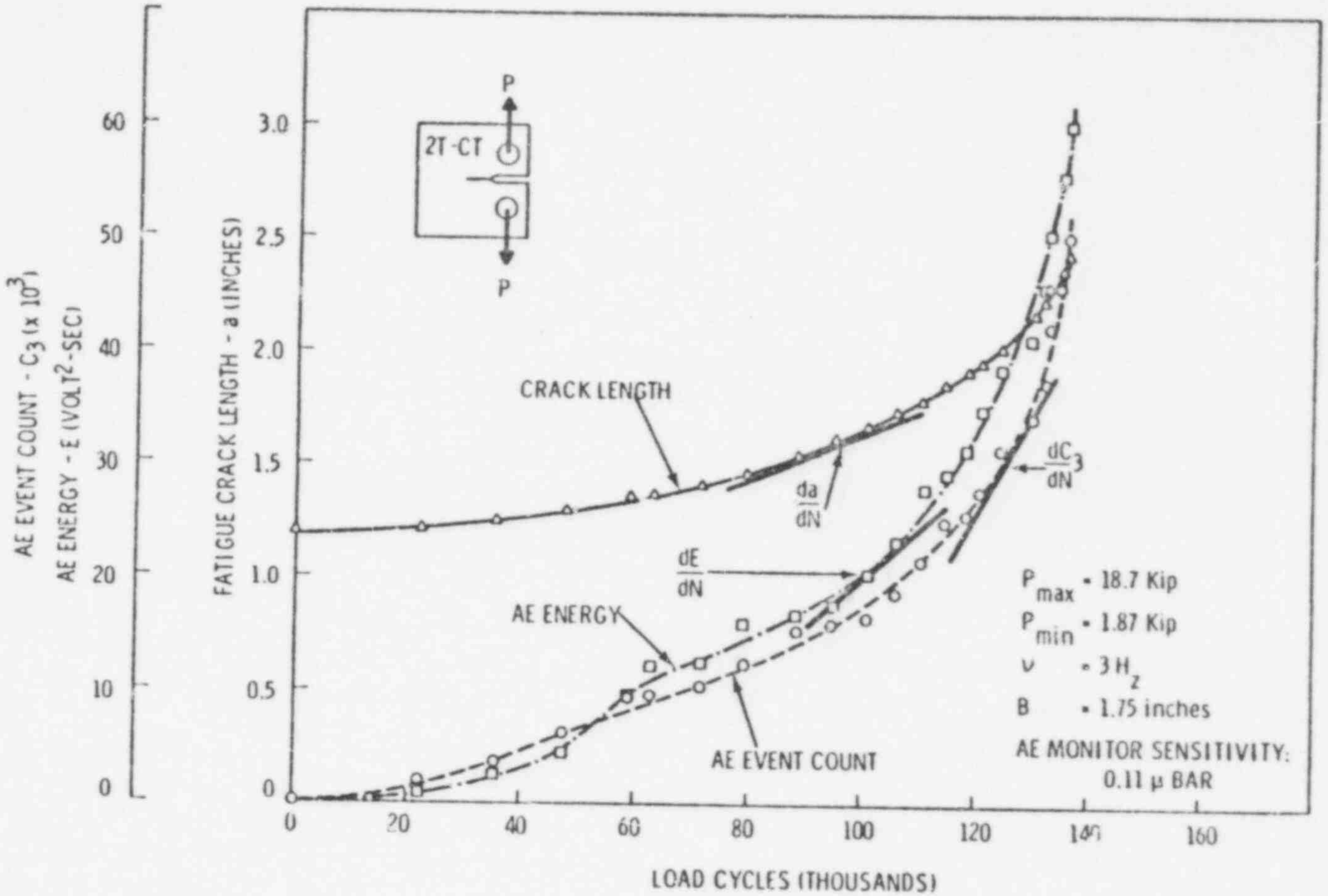

FIGURE 15. Fatigue Crack Length, AE Data vs Load Cycles: Size 2T-CT Compact Tension Specimen (B2-1R) Base Metal.

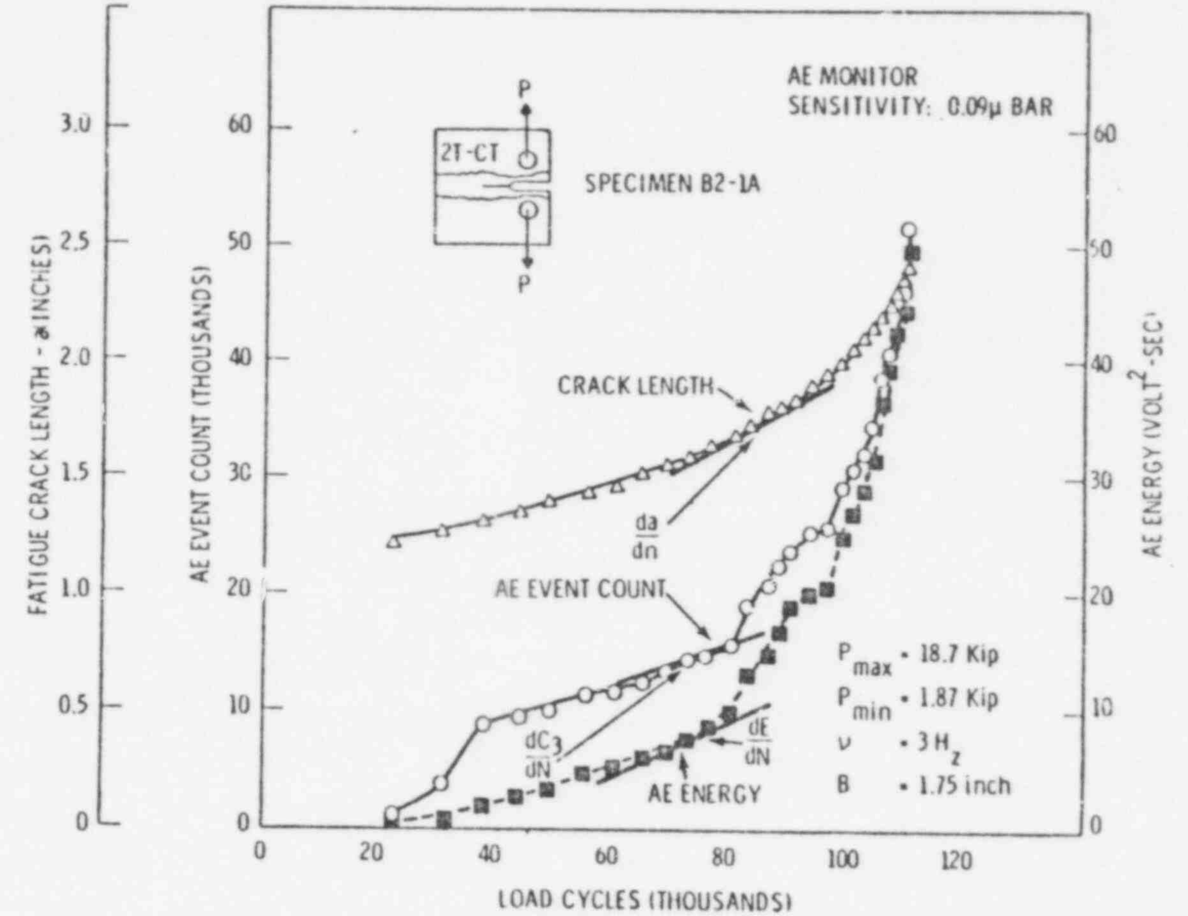

FIGURE 16. Fatigue Crack Length, AE Data vs Load Cycles, Size 2T Compact Tension Specimen (B2-1A), Weld Metal

815 216

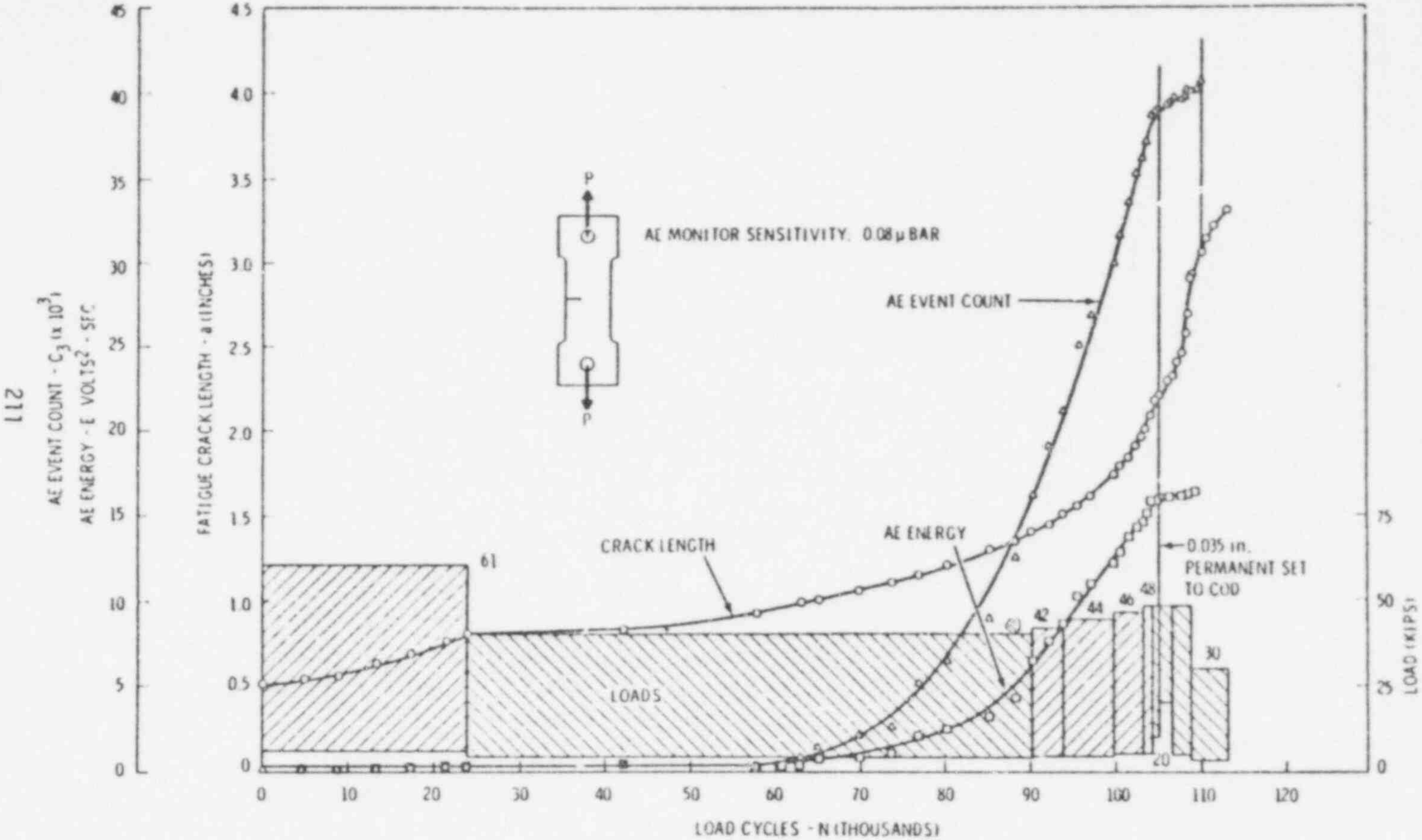

FIGURE 17. Fatigue Crack Length, AE Data, Fatigue Loads vs Cycles: Specimen 1-1A-2A, SEN Specimen.

POOR ORIGINAL

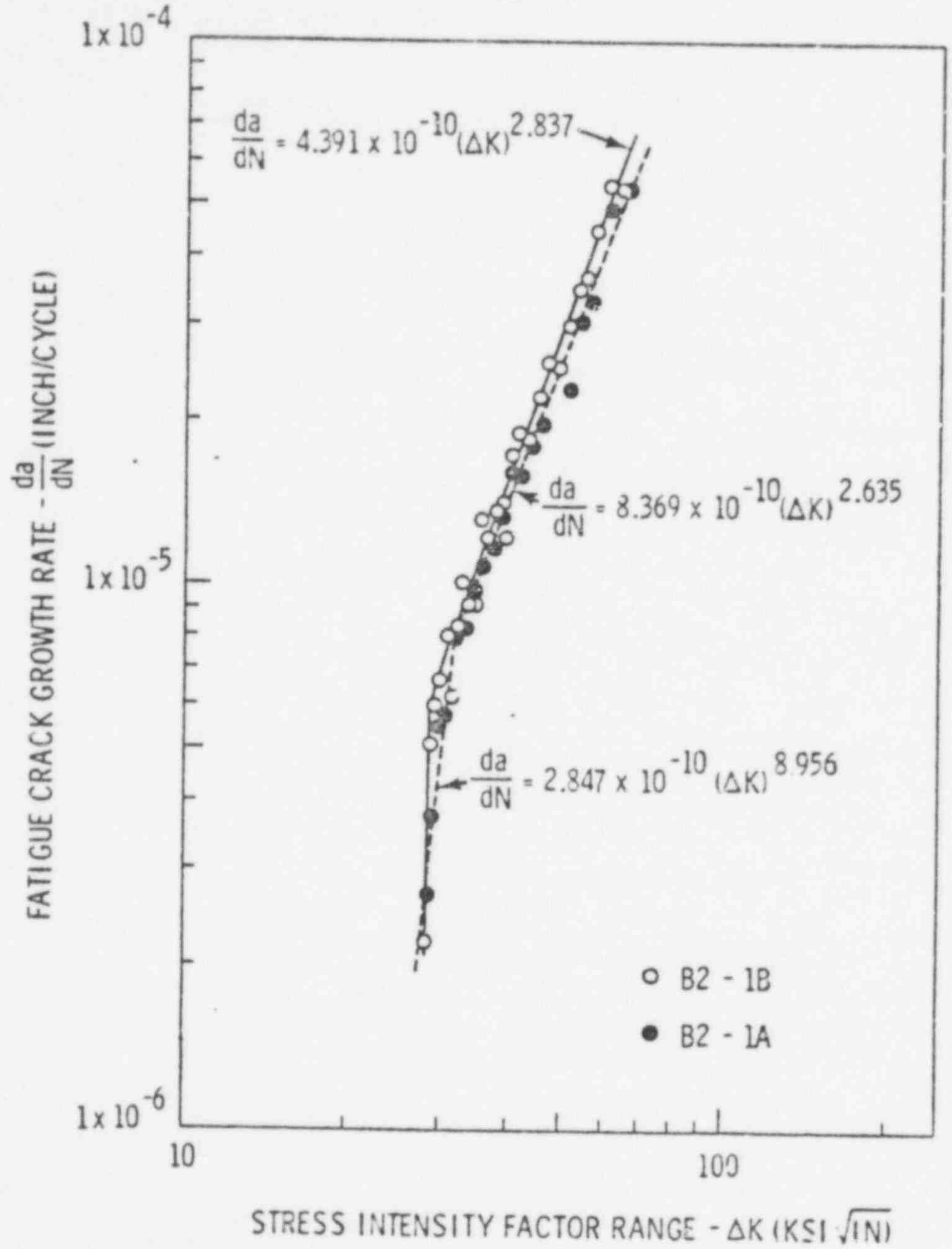

FIGURE 18. Fatigue Crack Growth Rate vs Stress Intensity Factor Range for 2T-CT Specimens B2-1A (Weld Metal) and B2-1B (Base Metal).

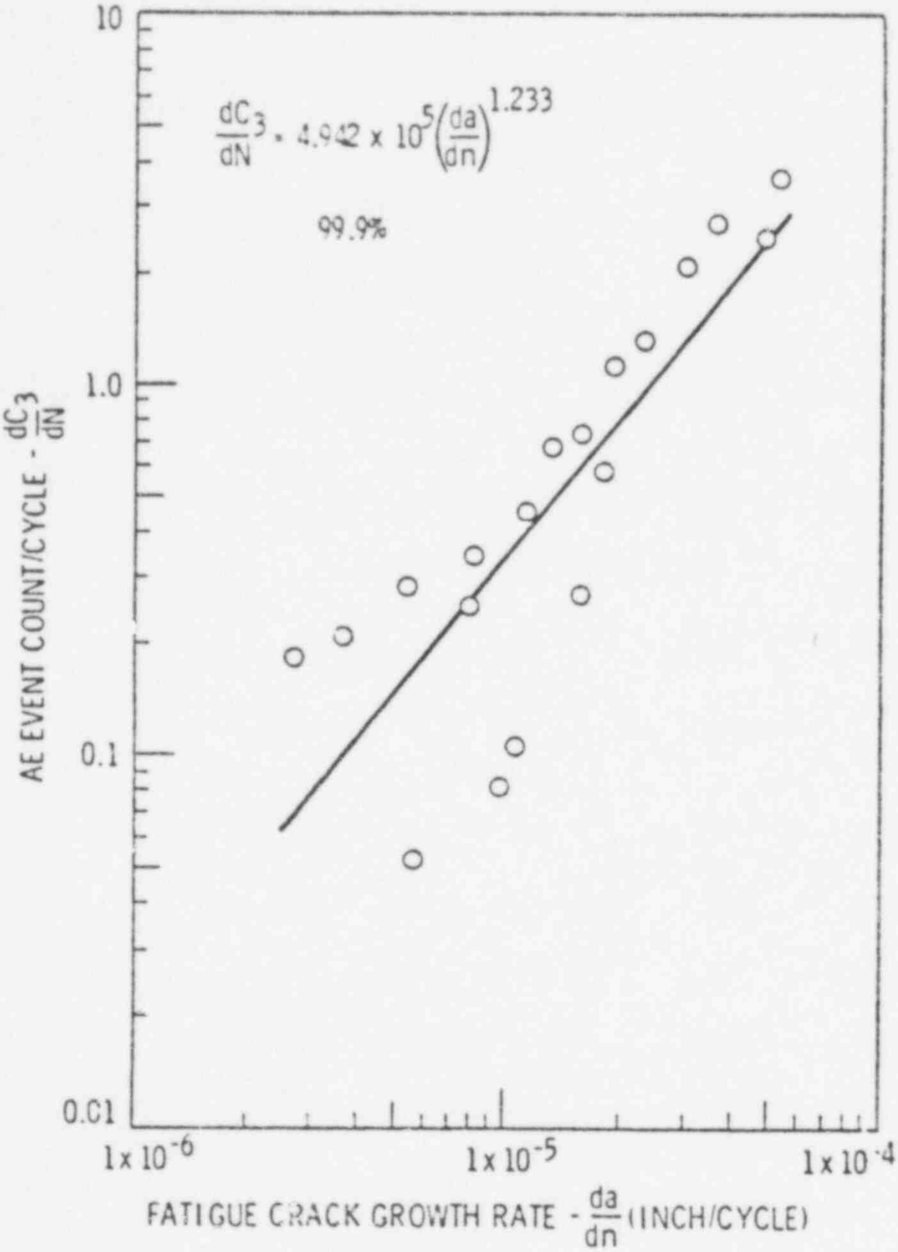

FIGURE 19. AE Event Count/Cycle vs Fatigue Crack Growth Rate for 2T-CT Specimen B2-1B (Base Metal)

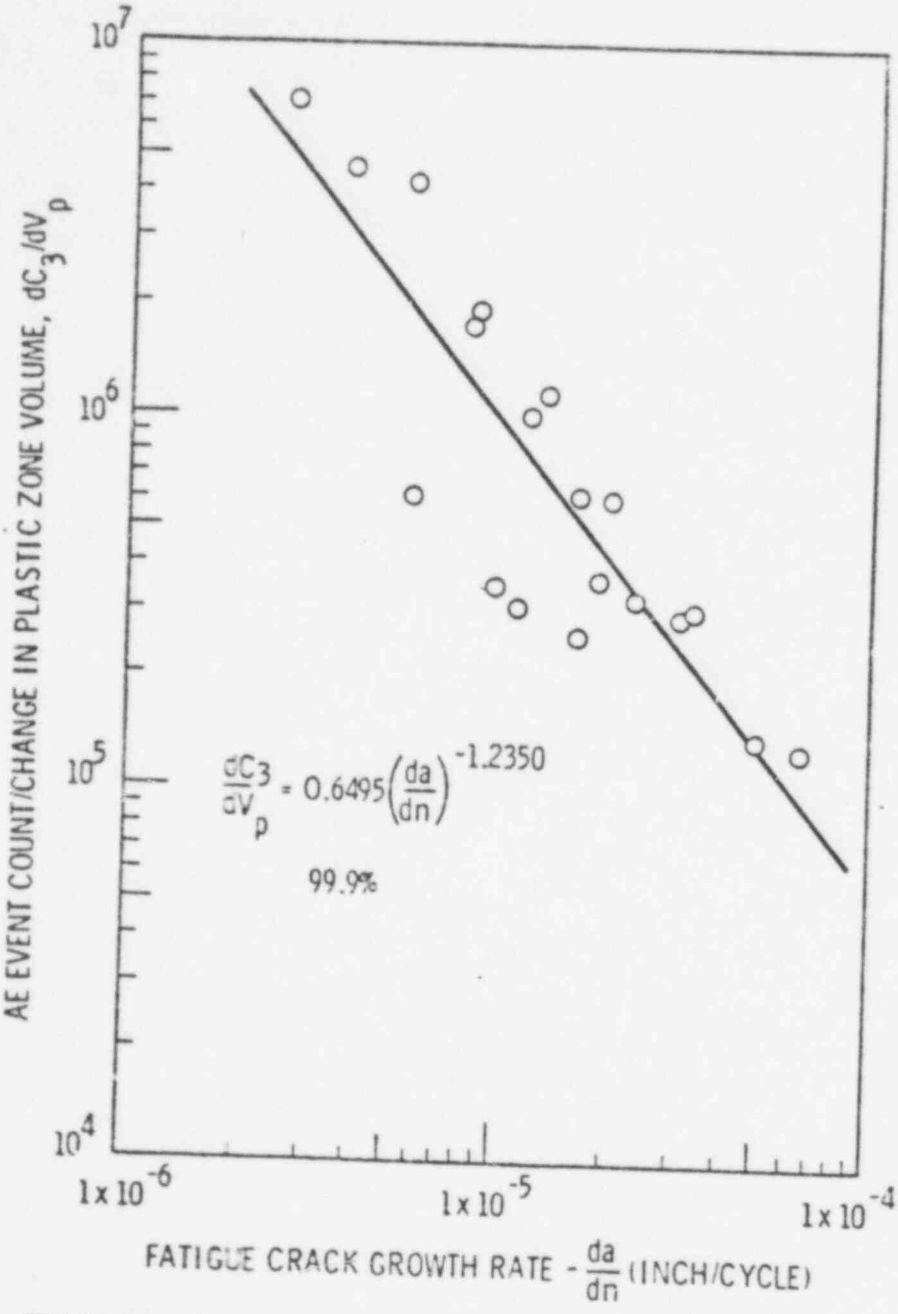

FIGURE 20. AE Event Count/Change in Plastic Zone Volume vs Fatigue Crack Growth Rate for 2T-CT Specimen B2-1B (Base Metal).

TABLE I

SUMMARY OF AE FUNCTIONS RELATED TO
FATIGUE CRACK GROWTH RATE (da/dN)
IN TERMS OF PERCENT CHANCE OF CORRELATION

	Test B2-1B Skin-Base Mat'l.	Test B2-1A Skin-Weld Mat'l.	Test 1-1A-2A Skin-Base, 3% Prestrain
dC/dN	>99.9	>99.9	>99.9
dC/dA	72.9	86.8	18.2
dC/dV	>99.9	97.52	>99.9
dE/dN	>99.9	>99.9	99.8
dE/dA	77.0	99.02	52.4
dE/dV	>99.9	96.25	>99.9
dH_1/dN	>99.5	>99.9	>99.9
dH_1/dA	99.87	88.2	54.1
dH_1/dV	98.45	98.42	>99.9
dH_4/dN	>99.9	99.74	1.8
dH_4/dA	99.79	87.5	94.4
dH_4/dV	27.8	7.9	>99.9
dR_1/dN	>99.9	>99.9	>99.9
dR_1/dA	79.5	94.82	14.6
dR_1/dV	>99.9	98.61	>99.9
dR_4/dN	97.8	>99.9	52.5
dR_4/dA	64.9	98.81	86.8
dR_4/dV	93.1	67.7	>99.9

Nomenclature

C - AE event count (<1.3 - >5.0 volts)
E - AE energy-volt^2-sec.
H_1 - Number of lowest amplitude events (<1.3 volts)
H_4 - Number of highest amplitude events (>5.0 volts)
R_1 - Number of fastest rise time events (<1μsec)
R_4 - Number of slowest rise time events (>10μsec)
a - Crack length
N - Number of load cycles
A - Crack area
V - Volume of the crack front plastic zone

Significance of Percent Numbers

This is based on a statistical evaluation with the following criteria:

>99.9% - highly significant
99.0 - 99.9% - significant
95.0 - 99.0 - marginal significance
<95.0 - insignificant

AE Characteristics

Investigation of unique characteristics of AE signals from flaw growth as opposed to signals from innocuous sources such as slag inclusion and oxide cracking has been limited during this report period. Work has concentrated on AE from flaws and for justifiable reasons, planned tests involving slag and oxide cracking were not completed. Some AE signal characteristics have been observed, however, which have potential significance:

- AE signals in these tests fall into three general categories - fast rise time with low amplitude, fast rise time with high amplitude, slow rise time with various amplitudes (Figure 21). As discussed previously, fast rise time, lower amplitude signals show the best correlation with crack growth parameters. This combination also offers a potential for screening out many noise signals.
- Observation of AE signal wave forms shows some evidence that they may characteristically start with a negative half cycle* (Figure 21).
- AE signal frequency spectra tend to maintain a level up to about 600 kHz while for noise signals the level drops with increasing frequency above about 200-300 kHz (Figure 21).

These characteristics are all subject to confirmation by further testing.

Fracture Mechanics Relationships and Application

Projecting to show how this type of analysis leads to relationships which may be used on a reactor, consider Figures 22 and 23. Each figure compares accumulated C3 or E as a function of K_{max} (or $\Delta K/1-R, R = .1$) on a linear scale for three specimens. The two 2T-CT specimen C3 data points fall upon each other and both show a "knee" at the same K level as the da/dN-ΔK curves.

The E vs K_{max} data behave similarly but do not appear to exhibit the change in slope at the ΔK level where the da/dN-AE curve changes slope.

*This assumes a fixed polarity of the sensing crystal.

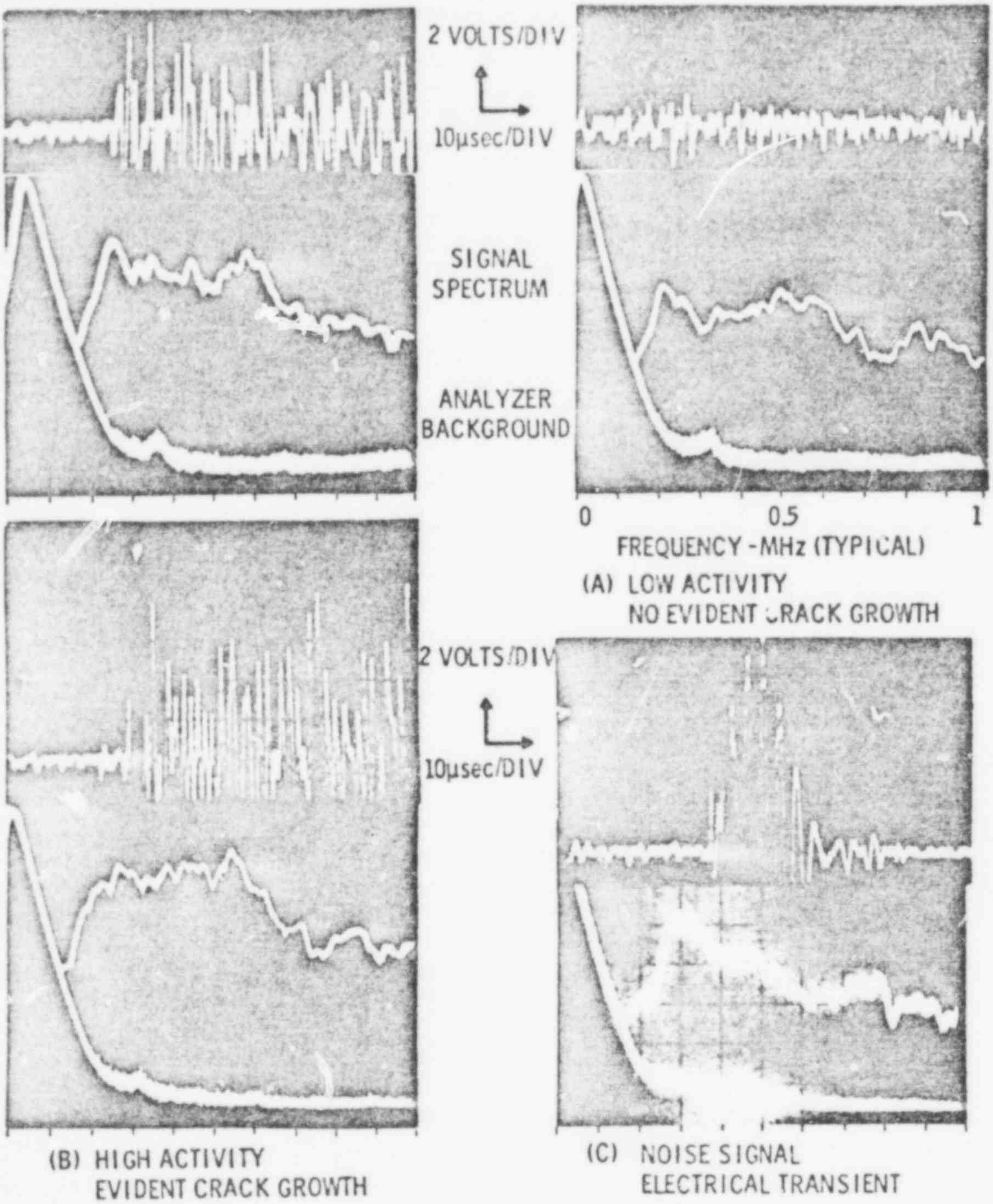

FIGURE 21. Samples of Different AE Signal Wave Forms
Fatigue Test B2-1B

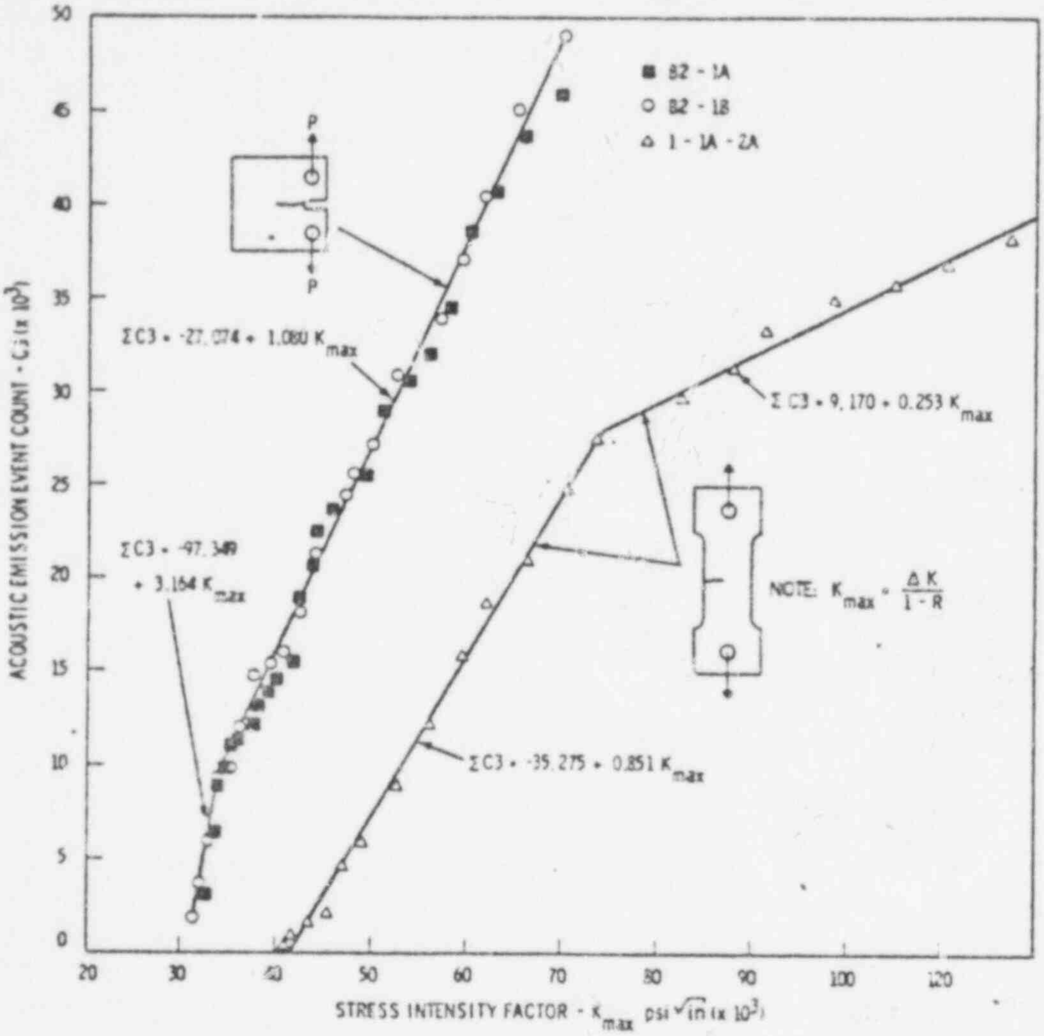

FIGURE 22. Summation AE Event Count vs Stress Intensity Factor for 2T-CT & SEN Specimens.

POOR ORIGINAL

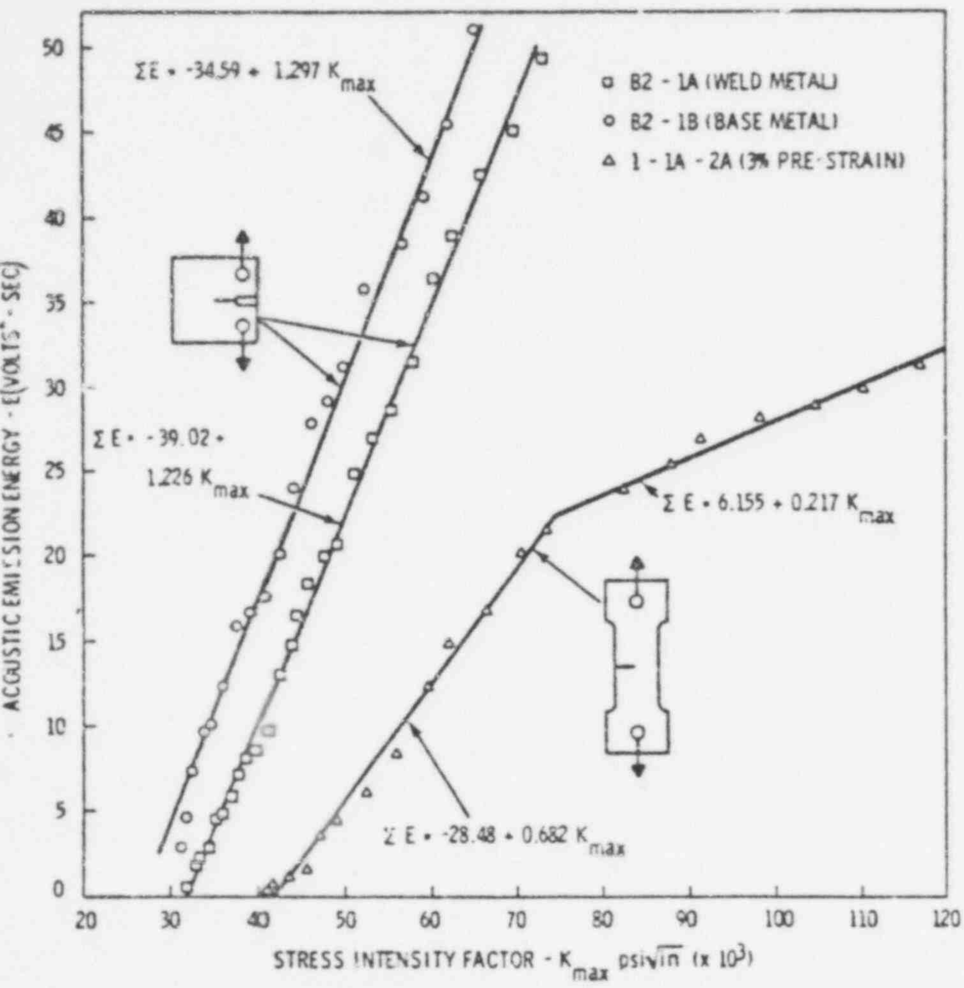

FIGURE 23. Summation AE Energy vs Stress Intensity Factor for 2T-CT and SEN Specimens.

The 3% prior prestrain specimen (SEN) data is displaced below the 2T-CT data. This could be due to starting the SEN specimens at a higher ΔK level or a decrease in AE sensitivity due to the 3% prestrain. The change in slope of the SEN C3-K_{max} appears real, interestingly it occurs at nearly the same K level where the 2T-CT specimen tests stopped.

Figure 24 compares calculated plastic zone volume, V_p with total AE event count. These curves follow the C3-K_{max} data based on the plastic zone volume being,

$$V_p = \pi r_p^2 B \text{ where } r_p = (K_{max}/\sigma_{ys})^2 \times 1/2\pi$$

Even though this calculation follows directly from the C3-K curve, this data suggests that partitioning plastic zone volume over a range of flaws that could exist in a finite volume in a vessel might allow another means of characterizing the damage level(s) in that vessel.

One obvious limitation at this point of the above relationships is the need to establish an initial flaw size. A possible solution may be to use both a rate and a summation interrogation of the AE data.

PLANS FOR ON-GOING RESEARCH

The overall research plan considers the following:

FY-78:

Based primarily on laboratory testing and considering a limited range of variables (material condition, environment, flaw growth mechanisms, etc.), demonstrate that a meaningful AE-flaw growth relationship for field application can be achieved.

FY-79:

Contingent on successful completion of the above, work in FY-79 would test the relationship against a full realistic range of variables and initiate transfer to a real structure to demonstrate that the technique can be applied for inservice flaw evaluation. This latter would probably extend into the following year.

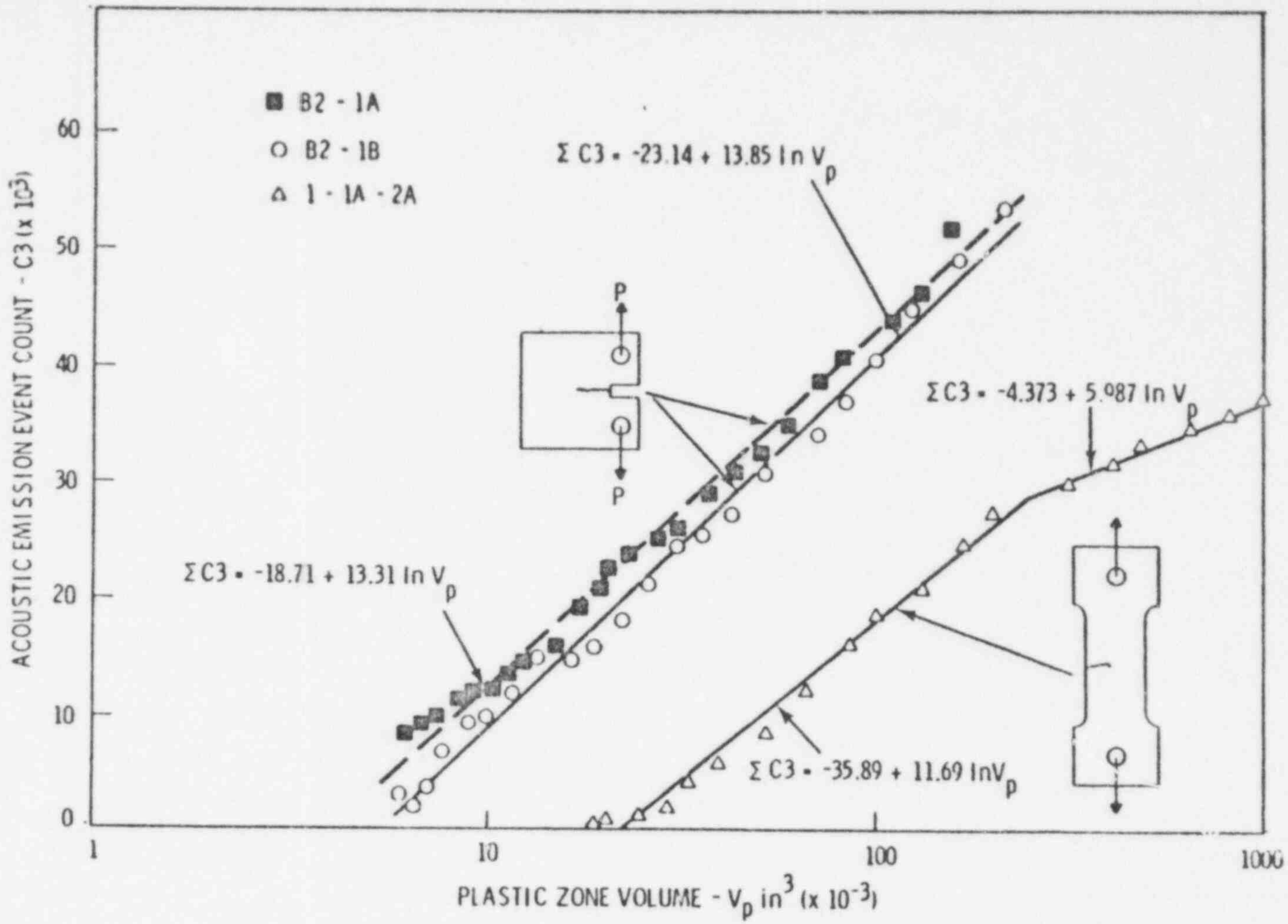

FIGURE 24. Summation AE Event Count vs Plastic Zone Volume for 2T-CT & SEN Specimens.

PUBLICATIONS

1. P.H. Hutton, E.B. Schwenk, Program to Develop Acoustic Emission-Flaw Relationships for Inservice Monitoring of Nuclear Pressure Vessels, Progress Report No. 1, July 1, 1976 to February 1, 1977, NUREG 0250-1, BNWL 2232-1, March 1977.
2. P.H. Hutton, E.B. Schwenk, Analysis Before Test - Program to Develop Acoustic Emission Characterization of Flaw Growth in A533B Pressure Vessel Steel, December 1976. Published as Appendix to report 1 above.
3. P.H. Hutton, E.B. Schwenk, Program to Develop Acoustic Emission-Flaw Relationship for Inservice Monitoring of Nuclear Pressure Vessels, Progress Report No. 2, February 1, 1977 to July 1, 1977, NUREG 0250-2, BNWL 2232-2, September 1977.

CREDITS

Several Battelle staff members deserve credit for their part in this work. Primary among these are J.R. Skorpik, C. Pavloff, R.J. Kurtz, J.F. Dawson, R.T. Lansiedel and G.O. Shearer.

INHIBITION OF INTERGRANULAR STRESS CORROSION CRACKING OF SENSITIZED TYPE 304 STAINLESS STEEL

The American University, Washington, DC 20016

Dr. B. F. Brown, Principal Investigator

Objective: The purpose of this project is to assess the effectiveness of modern corrosion inhibitors in mitigating intergranular stress corrosion cracking in sensitized Type 304 stainless steel. At present, the purity requirements for bulk BWR feedwater are stringent, yet cracking occurs. There are only three routes out of this problem: (1) Change the steel, (2) lower the stress, or (3) change the environment. The present project is an exploratory study of the third route involving the addition of small quantities of substances known as inhibitors, both evaluating the effectiveness of these substances and developing a better understanding of the mechanism(s) by which the more promising ones work.

FY 77 Scope: Finish evaluating candidate inhibitors added both singly and in combination. Analyze the mechanism by which the better inhibitors work by producing polarization curves, studying film breakdown kinetics with and without inhibitors, and studying repassivation kinetics of a scraped surface in the presence of a solution with and without inhibitors. The substance whose inhibitive mechanism(s) is (are) of primary interest is $CdSO_4$.

Summary of research activities and results: It is known that the concentration of solute species at the tips of growing stress corrosion cracks is grossly different from the bulk solution outside the cracks. The pH at the crack tip regions has been measured for high strength low alloy steels, titanium alloys, and aluminum alloys in salt water at room temperature, and for austenitic stainless steel in boiling saturated magnesium chloride at approximately 154°C. Neither the pH nor other measurements have been made on the solution inside cracks in BWR's, that is, on the solution which is driving the stress corrosion process. From a consideration of what is known about crevice corrosion and pitting corrosion of stainless steels, it is postulated that the solution in the crack tip is very acid, due to the hydrolysis of chromium. And if it is acid, there must be a high concentration of anions, probably chloride ions. For this reason we have arbitrarily selected 4 $\dot{M}$ NaCl acidified with HCl to pH 2.3 as our reference solution. Incidentally, the actual composition of the local solution bears only a very distant relation to the composition of the controlled values for the bulk BWR water, and the concept of a distribution relationship between the two is not a valid concept. Therefore one probably does not make any significant change in the solution chemistry within growing cracks by increasing the purity of the BWR bulk water, though what one may do by such a measure would be to decrease the probability of initiation of a local corrosion cell. It is this concentrated, local solution which we are seeking to inhibit.

It should be noted that since our reference solution is 4 M NaCl, any addition of, say, NaBr is reported as "bromide addition"; likewise the addition of, say, $CdCl_2$ (which would be done at constant chloride concentration) would be reported as a "cadmium addition."

The procedures used to evaluate candidate inhibitors of IGSCC in sensitized type 304 stainless steel have been described in a previous report (NUREG-0185), "Annual Report of Contract Research for the Metallurgy and Materials Research Branch, Division of Reactor Safety Research, Fiscal Year 1976", page 206.) Briefly, U-bend specimens are exposed to solution with and without selected candidate inhibitors, and the times for appearance of first cracks are noted. The experience in the present program with various types of inhibitors is summarized in chart form in Figures 1-7. In these charts the first column identifies the inhibitors, the central panel show graphically the time for first detection of cracks, the next column shows the electrode potential of the steel in that particular environment, and the final column provides brief remarks about the specimen appearance. In most cases the experiments on a given candidate inhibitor at a given concentration were run in triplicate. The concentration of the candidate inhibitor is 0.5 M unless shown otherwise.

The results with organic substances are shown in Figures 1 and 2. The propynol with the acetic acid (both at 0.5M) are the most effective of those studied, and even these permitted some reaction with the surface in addition to eventually permitting SCC. Quinoline (a standard inhibitor) was only moderately effective against cracking, and even so permitted general corrosion.

The results and observations with anionic inhibitors are shown in Figures 3 and 4. Figure 3 has only polyoxyanions. These were included in the program because some of them were thought reasonable candidates to help stabilize the protective oxide on the stainless steel. In fact, none of the polyoxyanions was appreciably effective in inhibiting SCC, and not surprisingly some of them (particularly sodium nitrite) promoted pitting.

There are two points of special interest in the data shown for the anionic inhibitors of Figure 4. First of all, there is a very modest inhibiting action displayed by the sulfate ion; we will come back later to

Organic Inhibitors

Inhibitor	Hours to SCC (0 20 40 60 80 100 120 140 160 180 200 220 240 260)	E_{sce}	Remarks
None		-0.360	No corrosion except SCC
1% Armco RC-910 (Commercial Imidizoline)		-0.369	Dull surface
0.002 M 2-(2,'4,'-Dihydroxyphenyl-azo)-phenylarsenic Acid		-	Yellow tint with SCC
0.5 M 2-Propyn-1-ol		-0.318	Dull surface
0.0025 M 1-Hexadecylpyridinium Chloride		-0.360	Brown area around pits (origin of SCC)
0.025 M 1-Hexadecyltrimethyl Ammonium Chloride		-0.362	Brown area around SCC)
Acetic Acid		-0.380	Dull surface

Key: no cracks ├──┤ cracks

Figure 1. Evaluation of one group of candidate organic inhibitors.

Organic Inhibitors

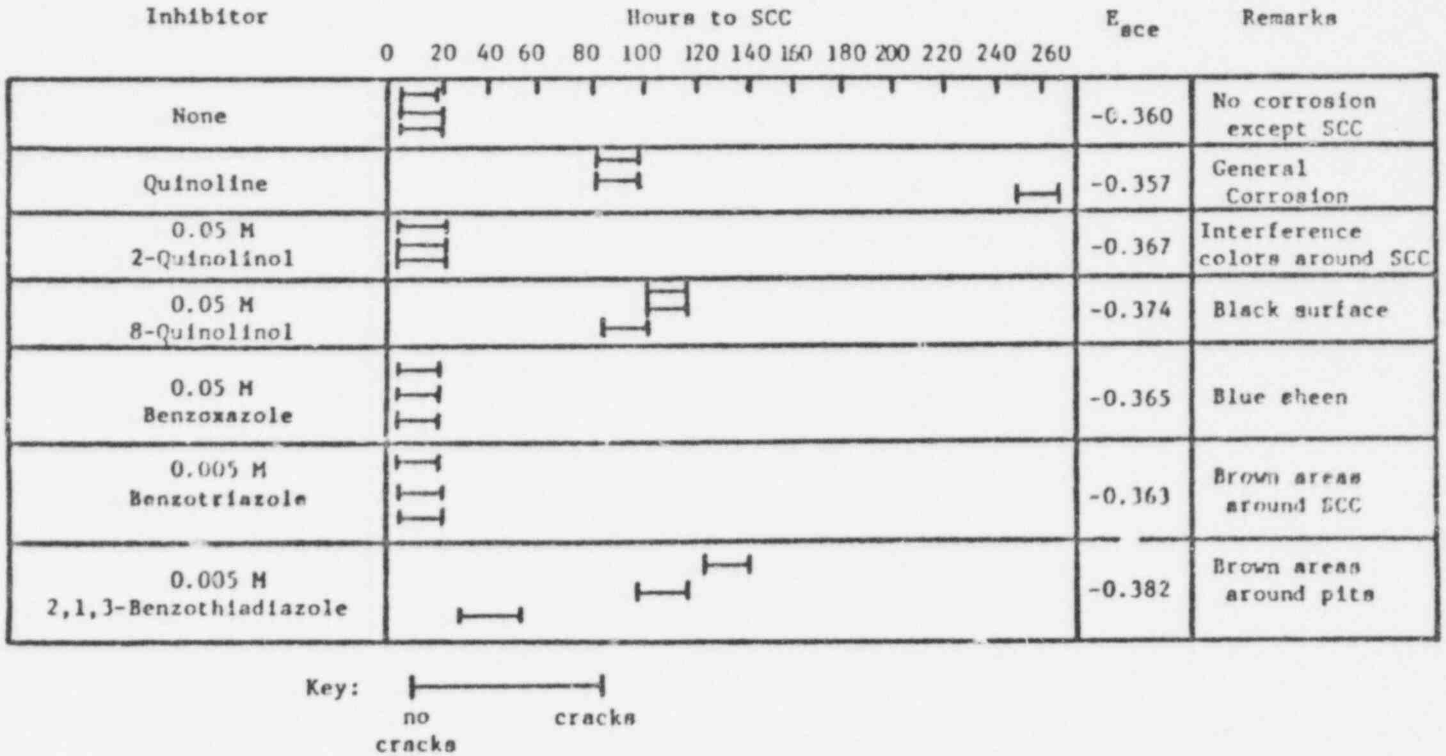

227

Figure 2 Evaluation of a further group of candidate organic inhibitors.

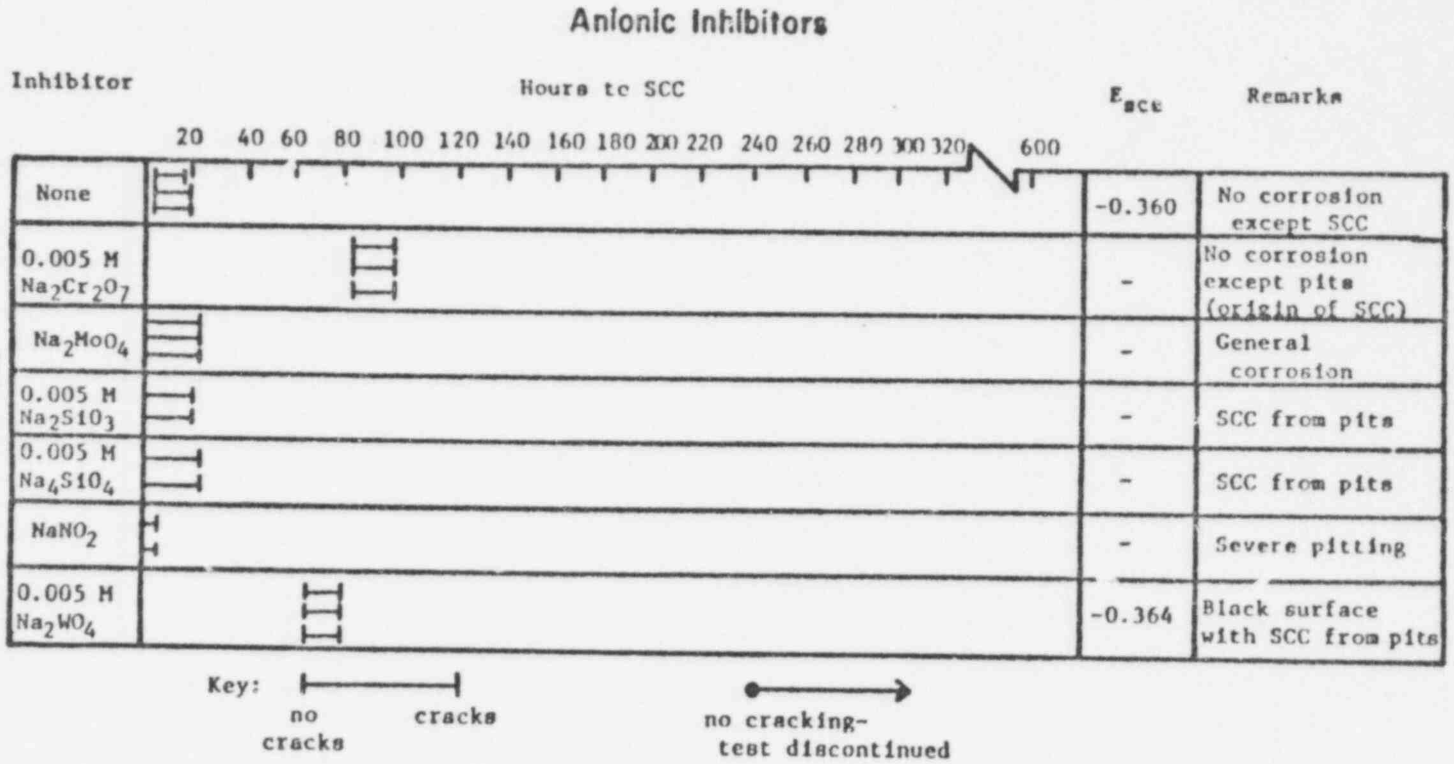

Figure 3. Evaluation of selected polyoxyionic anionic inhibitors.

Anionic Inhibitors

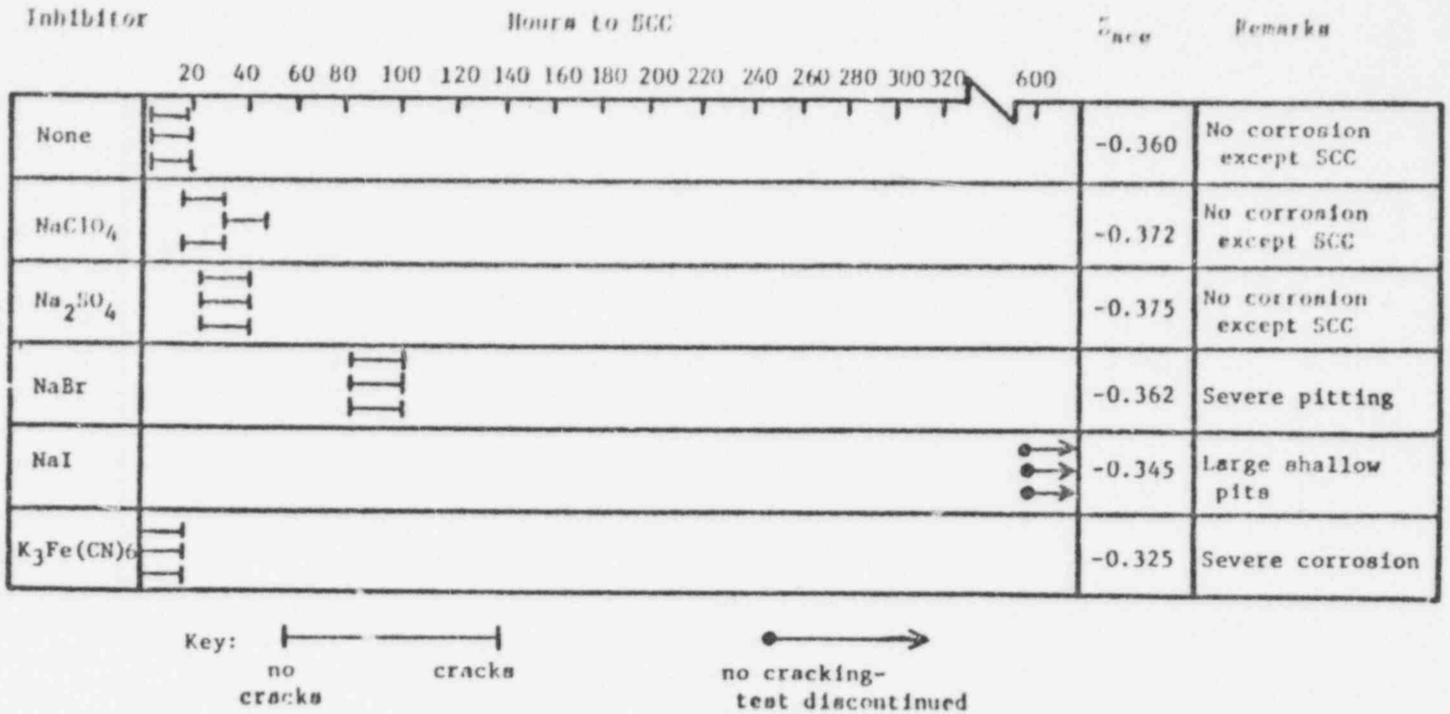

Figure 4. Evaluation of some miscellaneous anionic inhibitors.

229

815 235

this ion. Second, the iodide ion is very effective against SCC, in fact totally inhibiting that form of corrosion up to the termination of the experiments after 600 hours. The iodide, however, did not prevent the formation of large, shallow pits.

Figures 5 and 6 summarize the observations made with cationic inhibitors. There are three points of special interest in Figure 5. Calcium provides appreciable inhibition. This is of interest because cadmium, which will be seen in Figure 6 to be a comparable inhibitor, has approximately the same ionic size and identical valence as calcium. Cobalt added as the sulfate is also seen to have inhibitive powers, and it is further interesting to note that like calcium this simple ion also inhibits pitting. Ferric chloride is seen to prevent SCC altogether, but at the price of severe general corrosion. This is in harmony with the general observation that almost all (but not quite every one) of the combinations of environment and alloy which cause SCC are those in which much or even most of the alloy surface is passive, the corrosion being restricted to local cells.

Note in Figure 6 that zinc sulfate is a strong inhibitor, but that it does not totally inhibit SCC. Stannous and stannic ions completely inhibit SCC (as judged by our 600-hour test), but they permit some pitting and general corrosion, respectively.

Figure 7 summarizes the observations on combinations of simple cations and simple anions. The results with $CdCl_2$ and Na_2SO_4 from previous figures are repeated here for convenience in comparing them with results with $CdSO_4$. The sulfate ion remains of interest in possible combinations despite its relatively poor showing singly because of its reputed value in displacing more aggressive ions from metal surfaces. Note in Figure 7 that the effect of combining SO_4^{-2} and Cd^{+2} are not simply additive but genuinely synergistic.

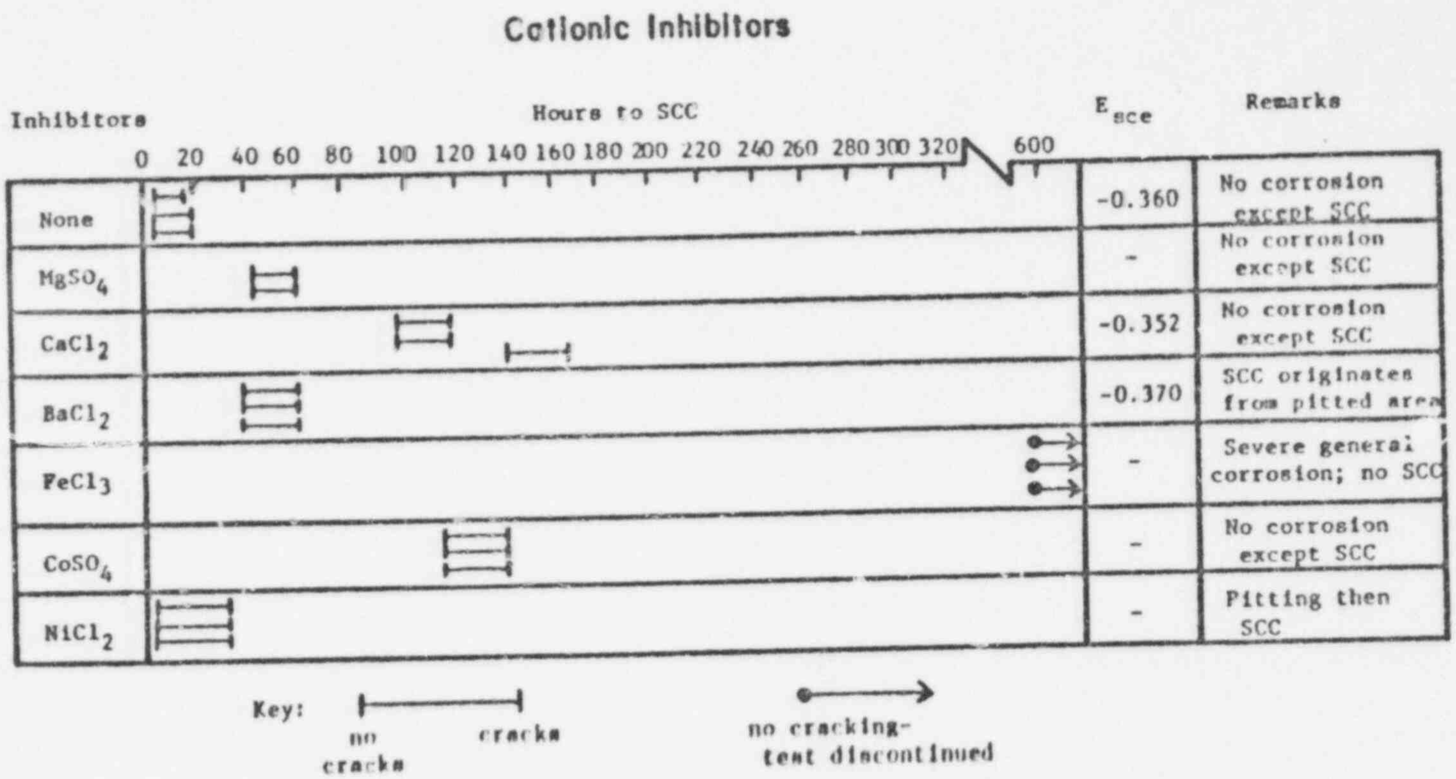

Figure 5. Evaluation of some selected cationic inhibitors.

231

Cationic Inhibitors

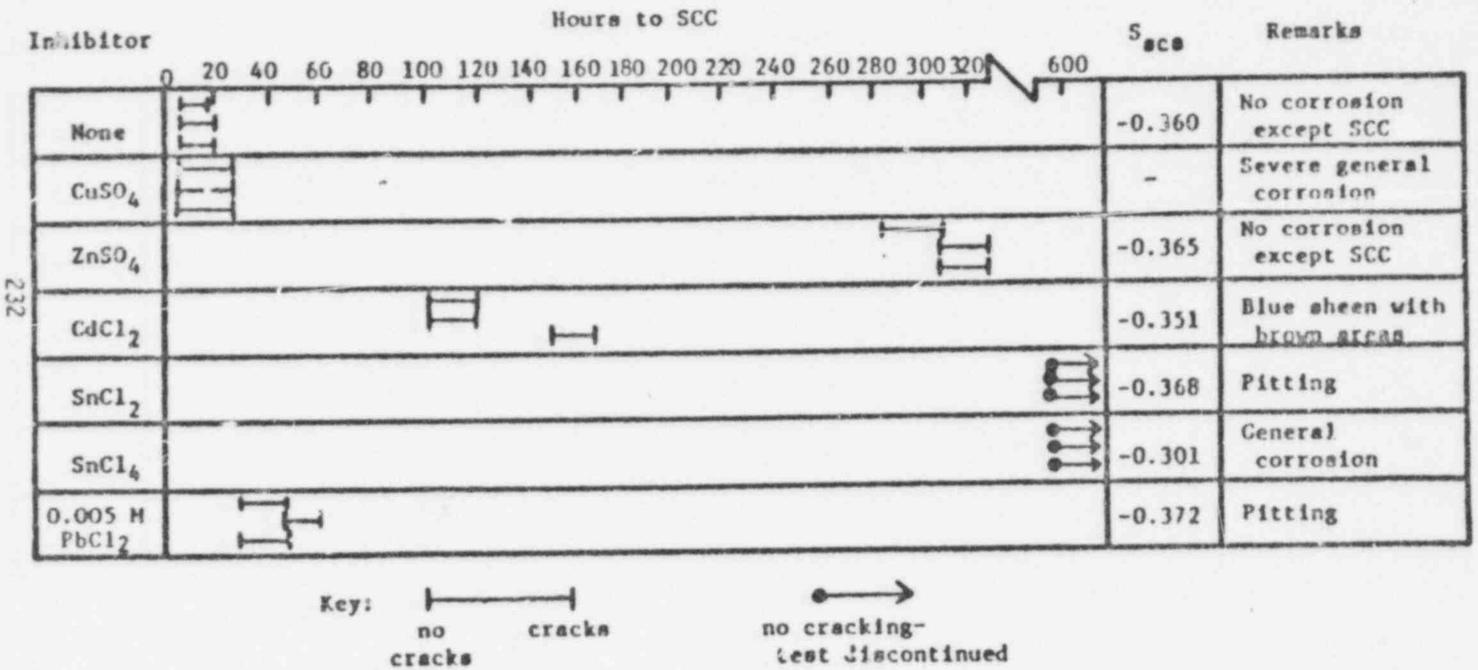

232

Figure 6. Evaluation of additional selected cationic inhibitors. Note that $CdCl_2$ behaves much like $CaCl_2$ (in Figure 5), possibly because the cations have similar sizes and identical valence.

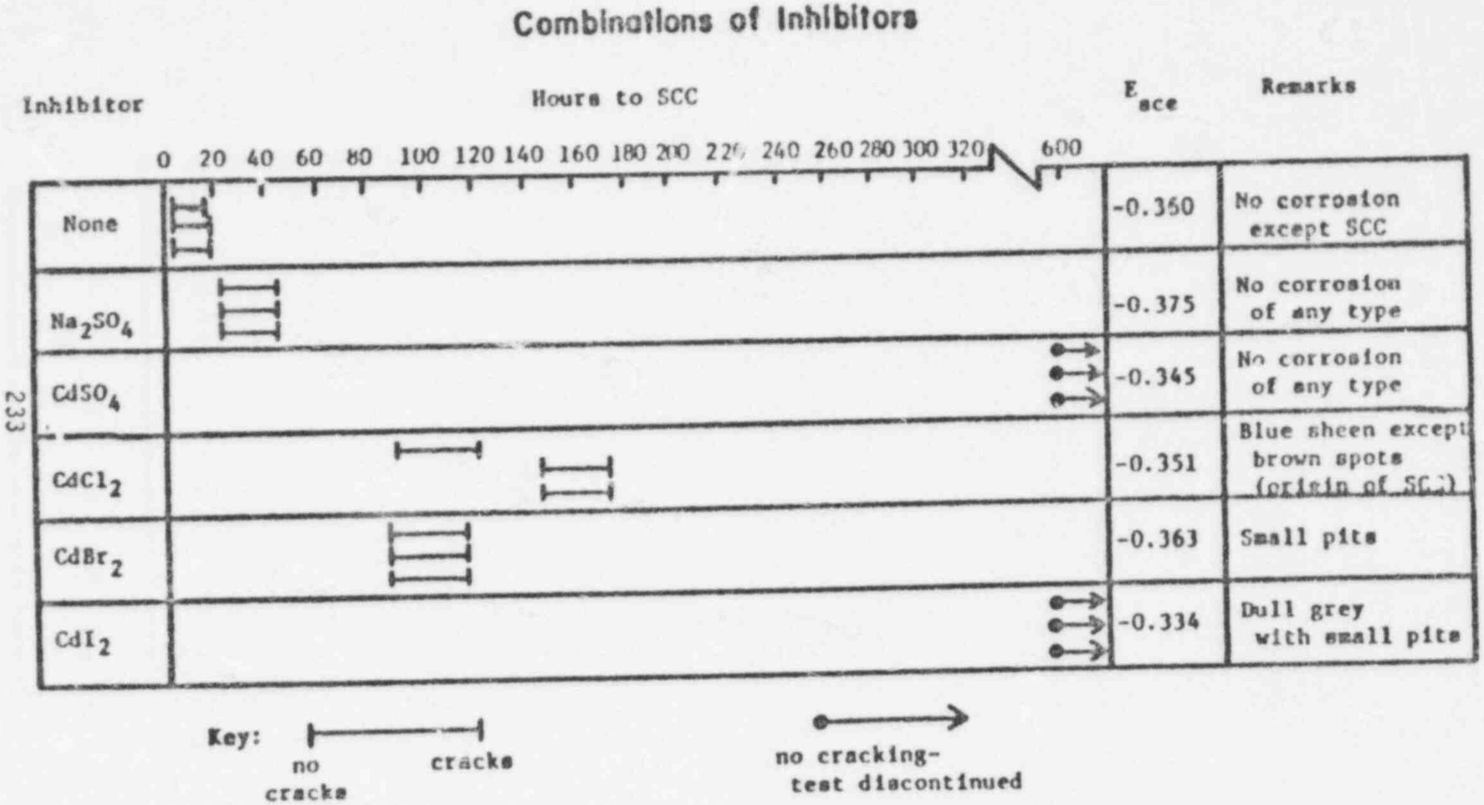

Figure 7. Evaluation of selected combinations of anions and cations, with $CdCl_2$ repeated for comparison. The combination of Ca^{++} and SO_4^{--} was not evaluated because of its extremely low solubility.

233

815 239

$CdSO_4$ has in fact continued to be the most successful inhibiting substance evaluated to date.

Referring further to Figure 7, it is noted that cadmium added to bromide confers no additional benefit with respect to SCC, although it does markedly reduce the pitting aggressivity of the solution. It will be recalled (Figure 4) that the iodide ion by itself conferred total immunity to SCC, but without preventing pitting. Figure 7 shows that the combination of iodide with cadmium continues to confer immunity to SCC, and with less pitting attack than with the cadmium-free addition.

In short, $CdSO_4$ was found to be an inhibitor of all forms of corrosion in the reference solution under our test conditions, and no other substance has yet been found to match its performance. Our interest has now been turned to an analysis of the reason for the performance of the $CdSO_4$, using thus far three techniques, as follows.

ELECTRODE POTENTIAL

There is a concept of a critical (minimum) potential for SCC which is valid for austenitic stainless steels, and anything which brings the electrode potential of the steel below the critical potential will prevent SCC ("below" in the Gibbs-Pourbaix-Stockholm convention). In most of our experiments the potential of the steel was monitored, with a clear-cut conclusion: Whatever the mechanism of inhibition by the effective substances, it is not attributable to the effect of the substances on potential.

FILM BREAKDOWN KINETICS

At this writing, the results of these film breakdown kinetics experiments cannot be expressed in a statistically rigorous manner because of reproducibility problems. It is hoped that these problems can be overcome in one way or other before the writing of the final technical report. It can be said on the basis of results to date, however, that $CdSO_4$ confers a stability to the protective film far beyond that experienced in the absence of the inhibitor. This observation is in harmony with the observation that the $CdSO_4$ protects against all forms of corrosion encountered in the uninhibited reference solution, including those which do not necessarily involve stress (pitting and crevice corrosion.)

POLARIZATION CHARACTERISTICS

Cathodic and anodic polarization curves have been developed using the standard ASTM procedure, both in the reference solution alone and with a large number of selected candidate inhibitors. All of the polarization curves will appear in the final report. Only four of the key curves will be shown here.

The first of these, Figure 8, shows polarization behavior in the reference solution. The lower branch of the curve is the cathodic branch. The upper branch of the curve shows first an active nose, then at higher potentials an approach to passivity, and at a still higher potential, breakaway behavior.

Figure 8 is to be compared with Figure 9, which shows the effects of sulfate ion. Note that the current density for the active nose is somewhat reduced, the current density for the passive region is greatly reduced, and the potential for breakaway behavior is raised.

Figure 10 shows that cadmium also reduces the current for the active nose, except even more than the sulfate, and it like the sulfate raises the breakaway potential.

Figure 11 shows that the combination of cadmium and sulfate essentially eliminates the active nose and vastly raises the breakaway potential.

236

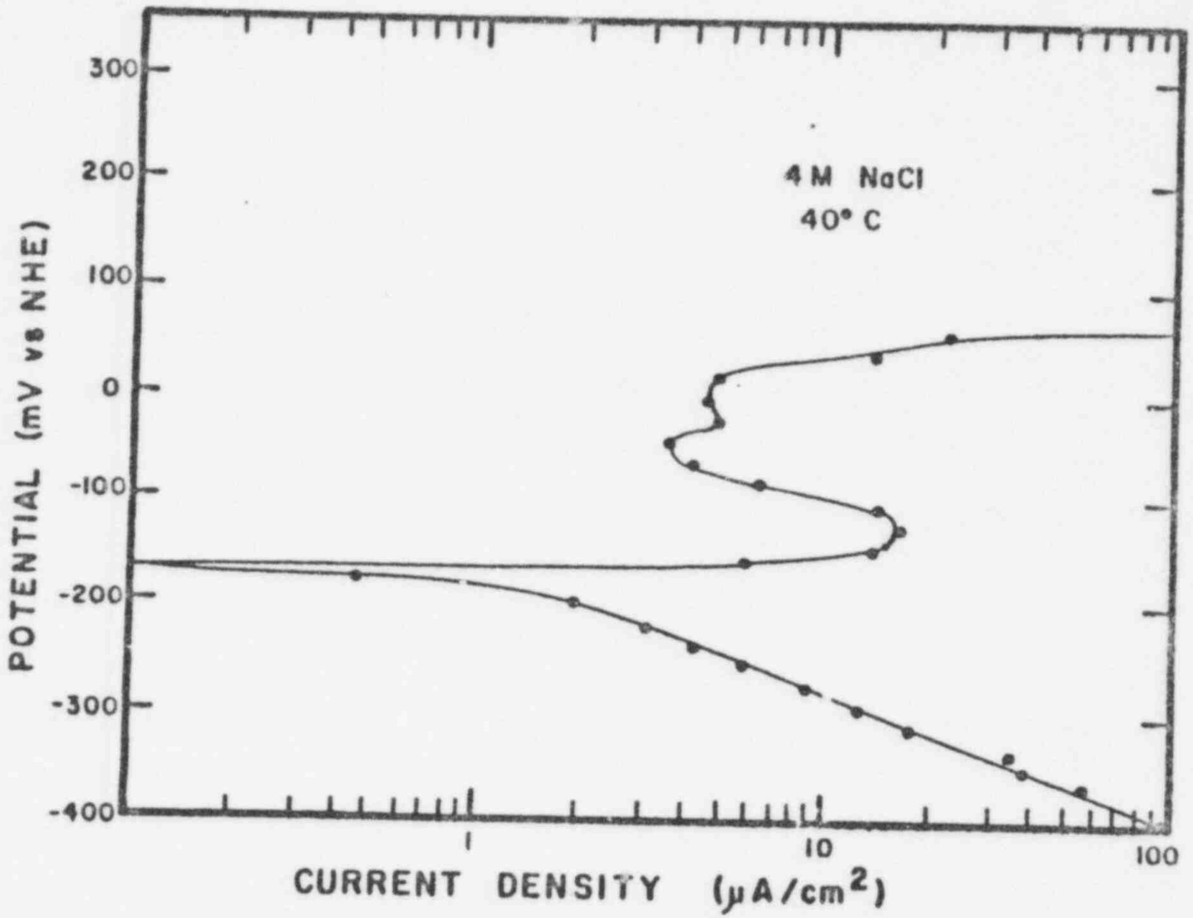

Figure 8. Polarization curves for Type 304 stainless steel in reference solution. Lower curve is for cathodic reaction, upper curve for anodic.

815 242

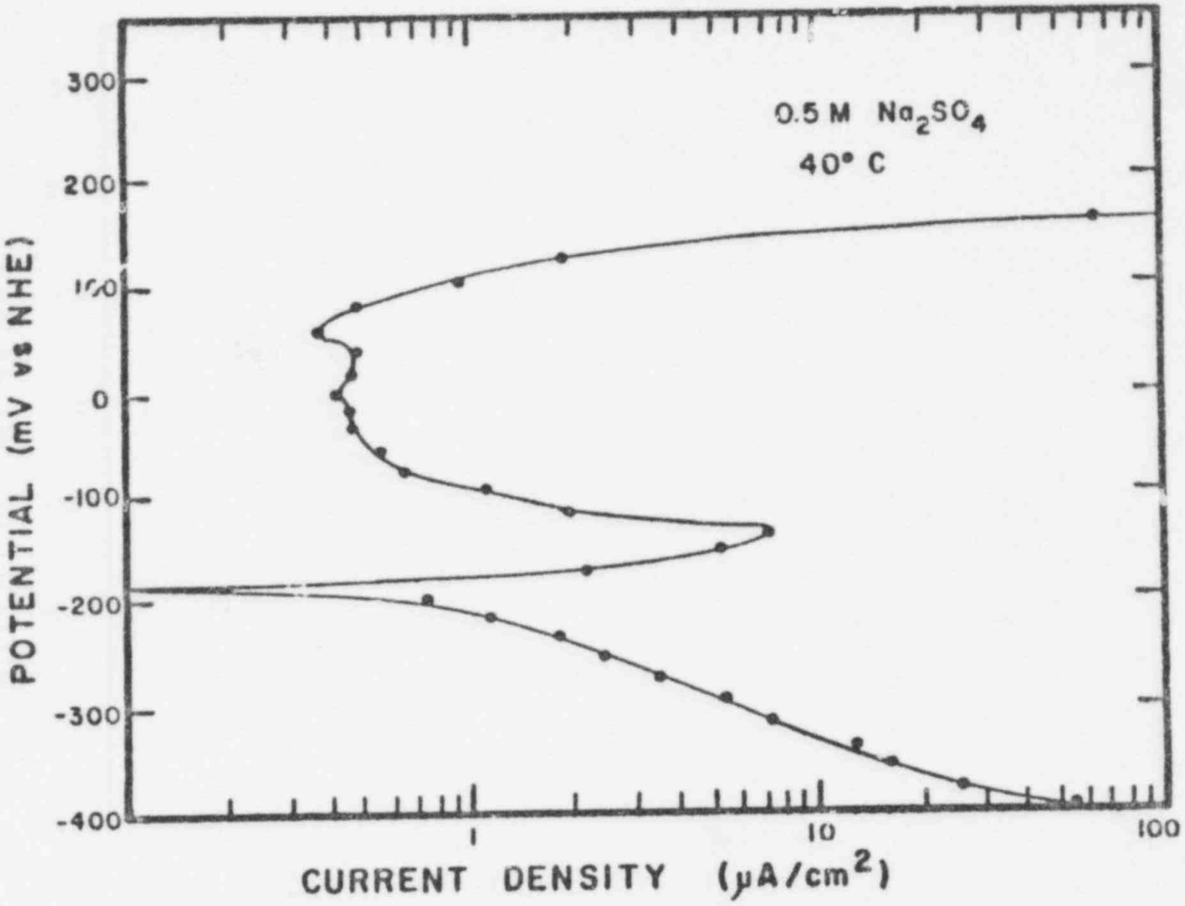

Figure 9. Same conditions as Figure 8 except with sulfate added. Note broadened passive bay.

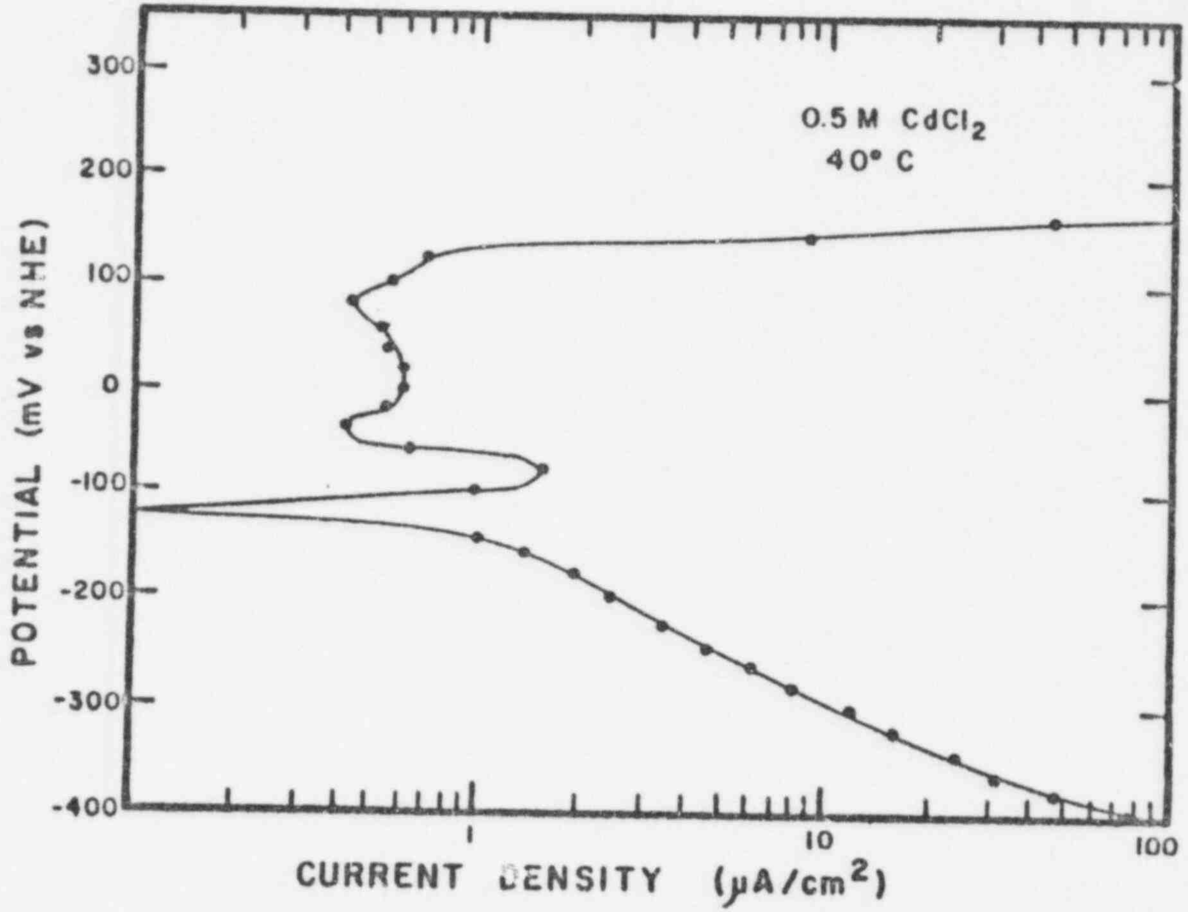

Figure 10. Same as Figure 8 except with added cadmium. Note that active nose is smaller and passive bay is larger than in Figure 8.

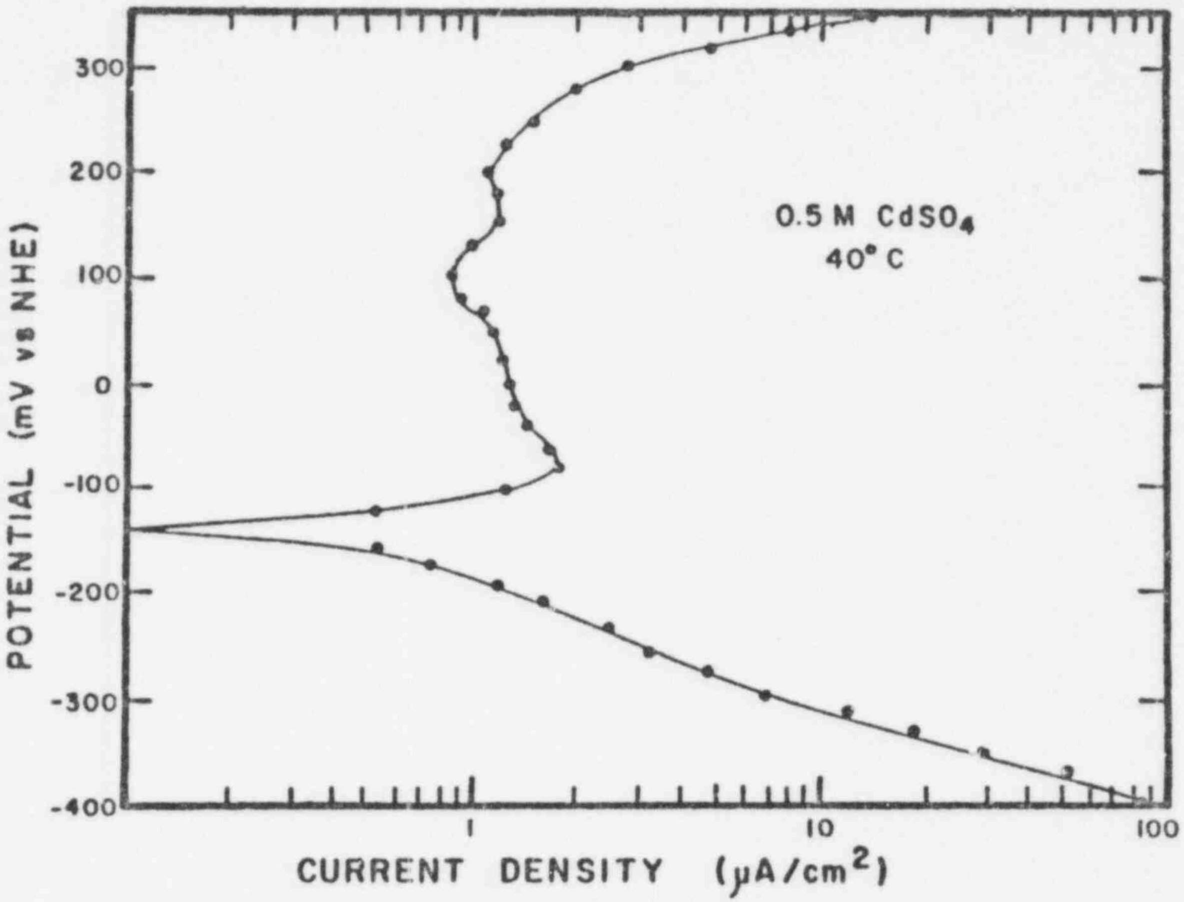

Figure 11. Same as Figure 8 except with $CdSO_4$. Note suppression of active nose and broadening of passive bay.

Thus the effective inhibitors are those which are interfering with the anodic reaction. They do not markedly affect the cathodic reaction.

CONCLUSIONS

1) The combination of cadmium and sulfate ions produces a synergistic effect in inhibiting all forms of corrosion seen in our tests of sensitized 304 stainless steel.
2) Although other substances have shown dramatic inhibiting effects on SCC, they have not matched the $CdSO_4$ in total inhibition.
3) All of the substances which appear possibly effective considering the total BWR environment, based on our present understanding of the fundamentals of the problem, have been evaluated without finding one of practical utility. This status does not exclude the possibility of finding such an inhibitor in the future.
4) Whatever the mechanism of the $CdSO_4$ inhibition, it does not depend on changes in electrode potential.
5) $CdSO_4$ enhances the stability of the protective film on stainless steel, though we cannot presently place a number to this enhancement.
6) $CdSO_4$ has its inhibitive effect on the anodic reaction, not the cathodic reaction.

PLAN OF RESEARCH FOR FUTURE YEARS

This work has progressed to the point of demonstrating that in principle the inhibitor route is a viable route for the prevention of intergranular stress corrosion cracking. Unfortunately the most satisfactory inhibitor found to date is not compatible with a nuclear environment. No way out of this problem has been foreseen to date and the present project will be concluded 14 December 1977. The vendor is planning some studies on the nature of local crevice corrodent in the BWR system; assuming these studies prove fruitful, the results may be useful in guiding research more accurately than the reference solution used in the present study which solution was formulated on the basis of imprecise analogs.

If the large number of studies on altered metallurgy, reduced residual stresses, and perhaps altered operating practice (particularly limitation of oxygen during shutdowns), all of which aspects are being investigated not only nationally but internationally, should prove incompletely effective, then it might be in order to resume the search for a compatible inhibitor based in part upon the new knowledge about localized crevice which would presumably then be available.

BIBLIOGRAPHY

1) C. S. O'Dell, B. F. Brown, and R. T. Foley, Abstract 128, pp. 354-356, The Electrochemical Society Extended Abstracts, Fall Meeting, October 9-14, 1977.

2) B. F. Brown, NUREG-0185, pp. 206-215, 1976.

Project Title

STEAM GENERATOR TUBE INTEGRITY PROGRAM

Contractor and Location

Battelle
Pacific Northwest Laboratories
Battelle Boulevard
Richland, Washington 99352

Principal Investigators

J. M. Alzheimer
R. A. Clark
C. J. Morris
M. Vagins

OBJECTIVES

The purpose of this program is the development of a large data base dealing with the integrity of defected PWR steam generator tubing. Major specific program objectives are:

- Tubing representative of tubes presently installed in PWR steam generators are defected using both mechanical and chemical means. Defects are to be similar to those expected in PWR steam generators.
- Using replication, eddy current and other nondestructive methodologies, characterize the defects as completely as possible.
- Carry out burst and collapse tests on defected tubes in environments chemically and thermally similar to those found in-service.
- Develop methodology for correlating the results of field defect determination with results of burst and collapse tests.

FY-77 SCOPE

The program scope for FY-77 included:

1. Procure Inconel 600 tubing representative of that presently in-service.
2. Procure a single-frequency eddy current testing (ECT) system.
3. Design and build burst, collapse, cyclic fatigue, leak rate and bulging facilities.
4. Perform baseline ultrasonic and eddy current inspection of all tubing.
5. Have carefully controlled defects representative of those expected in PWR steam generator machined into a selected number of tubing specimens.
6. Using several testing methods, including single-frequency eddy current inspection, fully characterize defect geometries.
7. Carry out burst and collapse tests in representative PWR environments.
8. Develop methodology for correlating the results of burst and collapse tests with the results of field inspection defect determination.
9. Develop criteria for estimating margins-of-safety to be applied to the evaluation of tubes in which flaws are found during in-service inspection of PWR steam generators.

SUMMARY

This report covers the period of November 1, 1976 to December 31, 1977. A brief review of major accomplishments includes:

- All needed Inconel tubing, eddy current inspection equipment and pressure testing equipment was purchased.
- Baseline eddy current and ultrasonic inspections of undefected tubing were completed.

- Hardness and tensile tests were performed to check tubing material properties.
- Approximately 540 specimens were prepared using selected defect geometries.
- Eddy current examinations were performed on defected tubing using standard field practice.
- Full matrix of burst tests were carried out.
- Initial bulging tests completed.
- Feasibility study of chemical defecting techniques was completed.

Results will be discussed under the following topics:

1. Tubing procurement and baseline characterization.
2. Defect preparation and characterization.
3. Pressure test facilities and test results.

TUBING PROCUREMENT AND BASELINE CHARACTERIZATION

Arrangements were made to obtain Inconel 600 steam generator tubing produced in a Westinghouse facility and fabricated to Westinghouse specifications. The four different sizes of tubing used are 0.875 x 0.050 in., 0.750 x 0.050 in., 0.750 x 0.043 in. and 0.625 x 0.034 in. Upon arrival, baseline ultrasonic and eddy current inspections were performed on all tubing. The ultrasonic inspection included a detailed survey of the dimensions of each tube. A helical scan of the entire tube length was performed for each 10-ft long tube. In addition, a complete survey was made of the entire tube circumference at selected locations. These locations are the place where defects were to be placed in the tubes. At each of these locations, maximum and minimum ID, OD and wall thickness, ID and OD ovality and eccentricity were precisely determined and recorded. At these locations, the spot of minimum wall thickness was marked on the tube. For the most part, the tubing was very uniform and of high quality. At a few locations, abnormal indications were detected in the ultrasonic signals. At these locations, small defects such as sanded spots, dents and scratches were found, and they were recorded. Baseline eddy current inspections were also performed on all 10-ft long tubes. Standard single-frequency inspection techniques were performed using the EM 3300 system, which is shown in Figure 1. Any abnormalities in the eddy current signals were recorded.

After baseline examinations of the tubing were completed, tubes were selected to be used for test specimens. Only tubes which showed no abnormal indications during baseline ultrasonic and eddy current inspections were used. Sufficient tubing was cut into 1-ft lengths for test specimens. In addition, 1-in. long rings were cut from each 1-ft long specimen. These were used for hardness and ring tensile tests for material properties characterization. Tube specimens were also selected for ASTM tube tensile tests. These tests show the Inconel 600 tubing very uniform from tube to tube within a heat.

DEFECT PREPARATION AND CHARACTERIZATION

Each 1-ft long specimen had been assigned an identification number. These numbers were assigned to specific defect geometries in the test matrix. Each specimen had a quality assurance sheet that contained baseline and defect information. The tubes were sent along with the data sheets to the vendor for defect fabrication. Seven basic types of defect geometries were used. They are EDM slots, elliptical wastage, elliptical wastage plus through wall slot, uniform thinning, denting, denting plus elliptical wastage and denting plus uniform thinning. Figures 2 through 7 show some of the basic geometry types. These defect geometries were selected because they are types of defects that might be found in PWR steam generators. Maximum defect depths were characteristically varied from 25% to 90%. Other varied parameters include defect length, cutter radius and wrap angle.

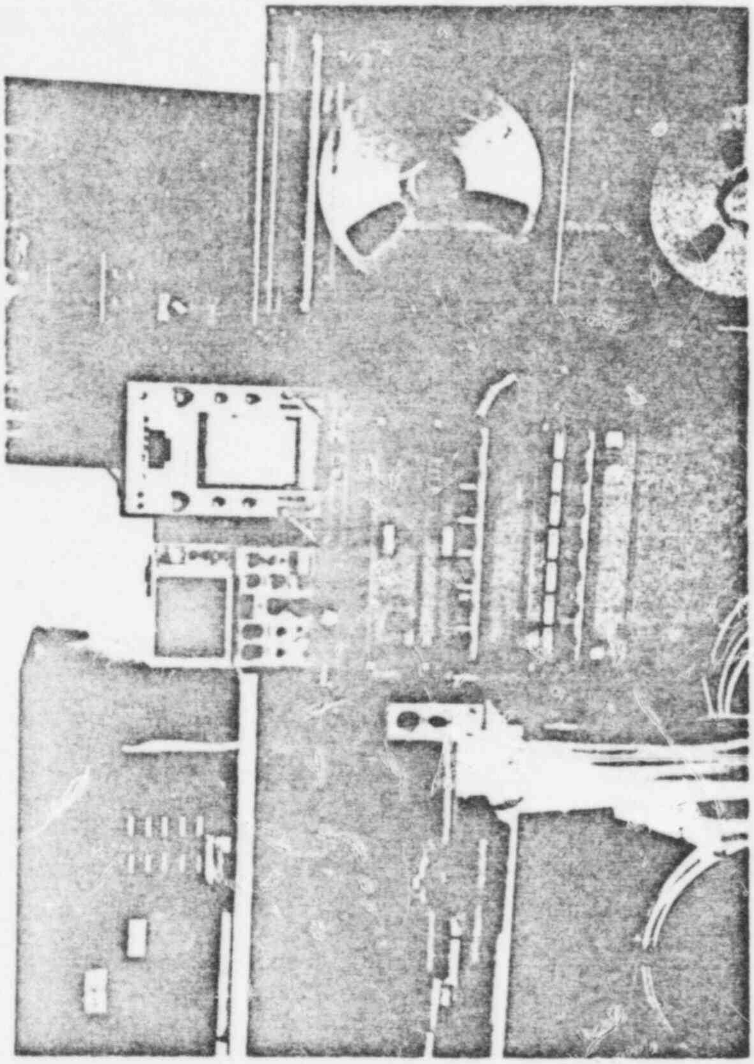

FIGURE 1. SINGLE FREQUENCY EDDY CURRENT INSPECTION SYSTEM

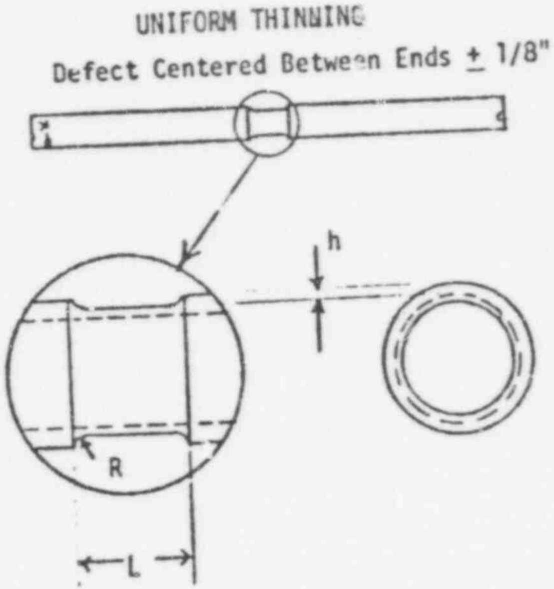

FIGURE 2. UNIFORM THINNING GEOMETRY

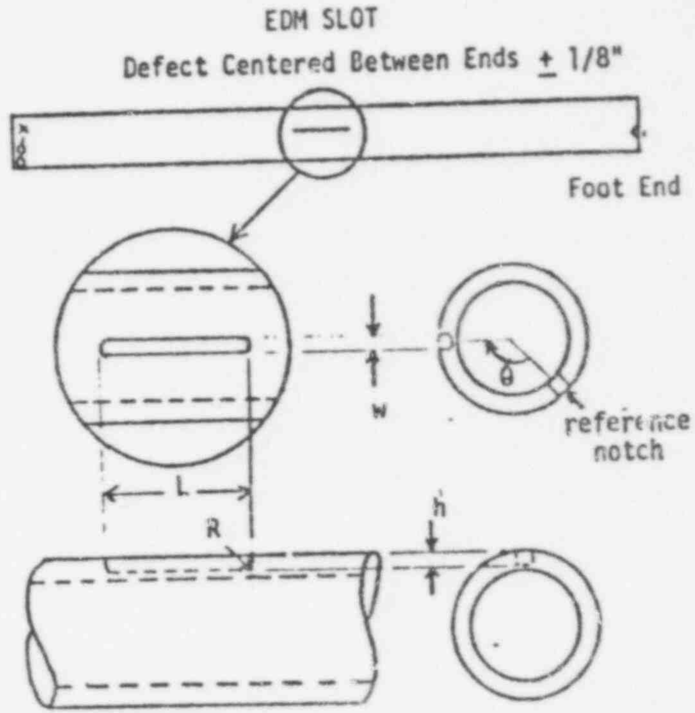

FIGURE 3. EDM SLOT GEOMETRY

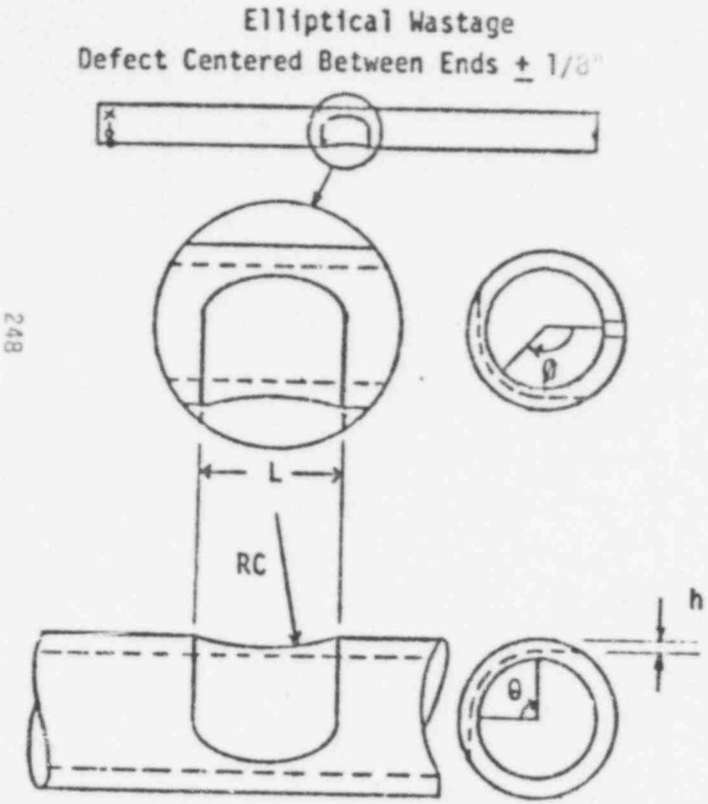

FIGURE 4. ELLIPTICAL WASTAGE ONLY

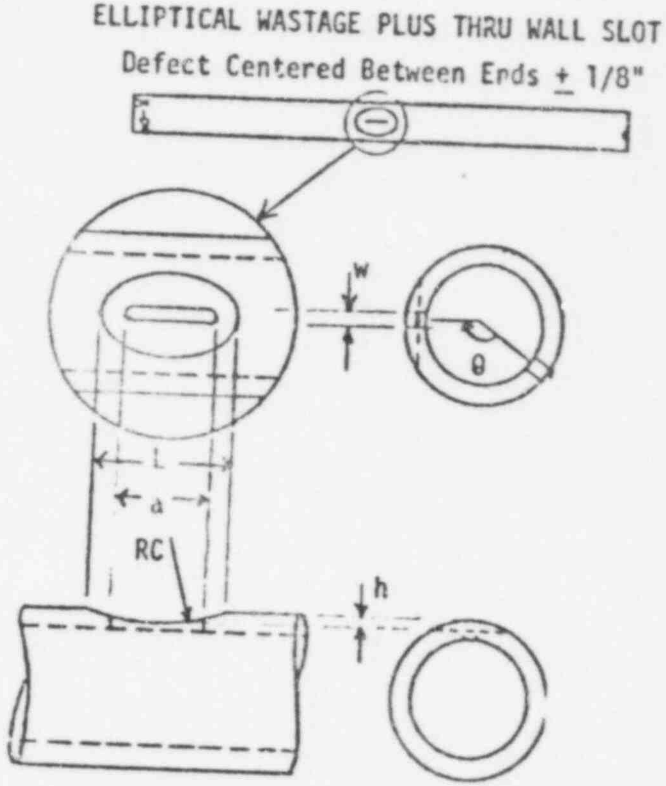

FIGURE 5. ELLIPTICAL WASTAGE PLUS THROUGH WALL SLOT

248

815 254

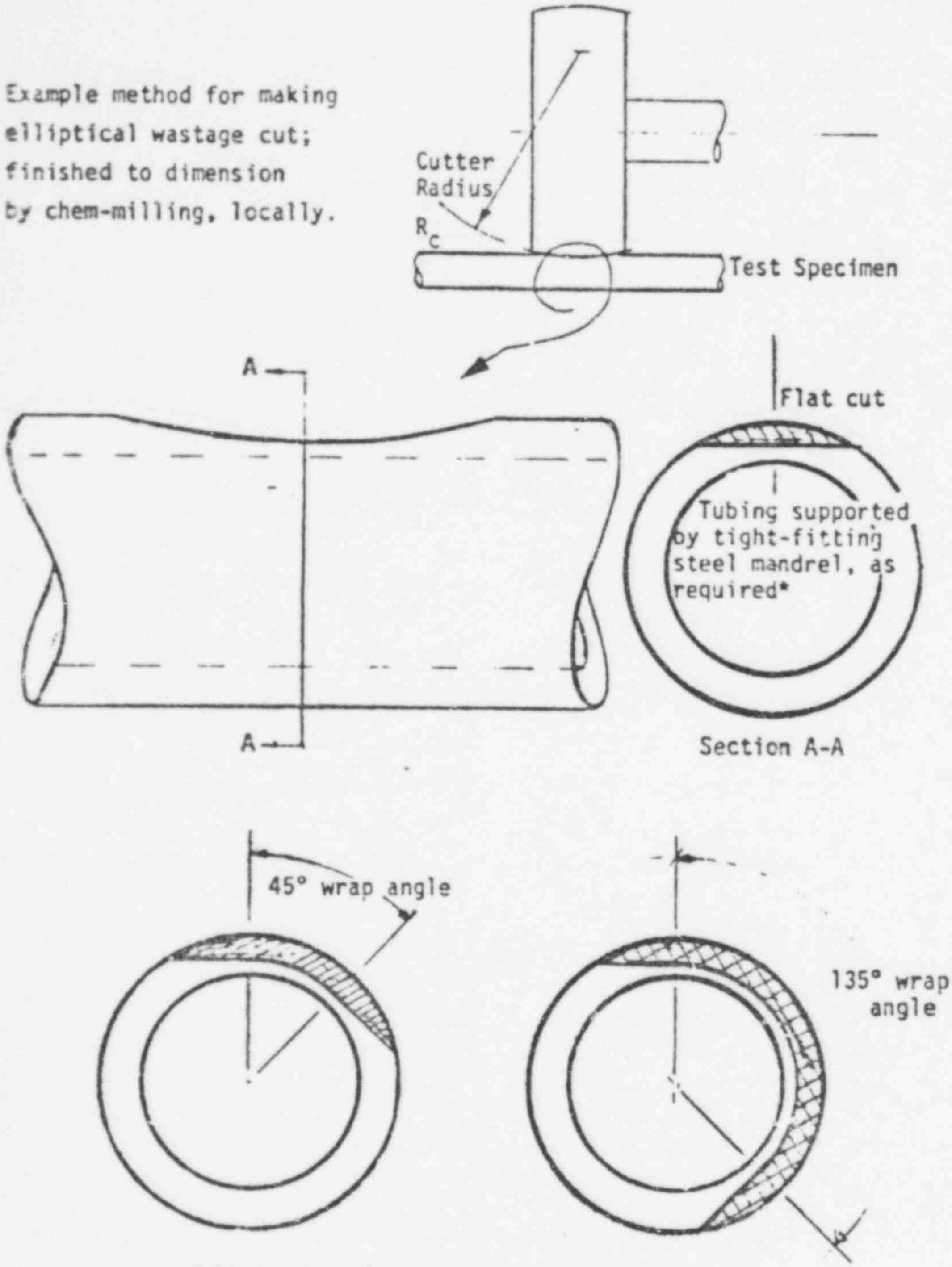

FIGURE 6. ELLIPTICAL WASTAGE DEFECT

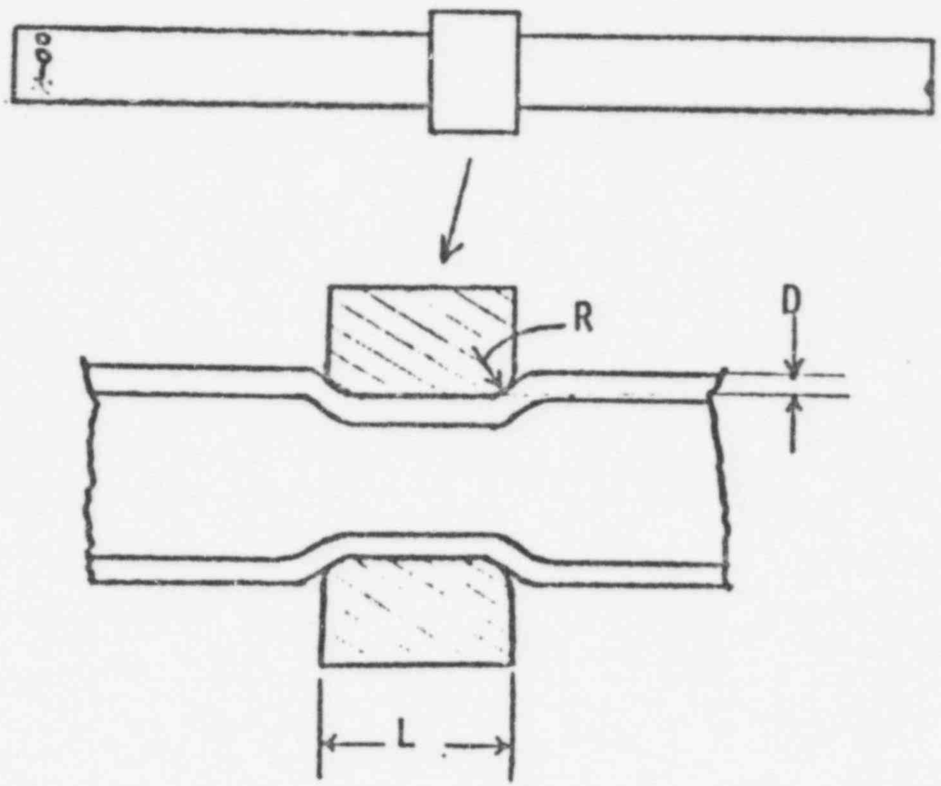

FIGURE 7. DENTING DEFECT GEOMETRY

Defects were placed at the locations of minimum wall thickness. Tolerances on defect dimensions were not made restrictively small, which would have added to the cost of machining. Instead, great care was taken to insure accurate characterization of defect dimension after they were machined. This insured that dimensional effects on pressure tests could be examined with the needed accuracy.

The primary method used for defect characterization was replication with a special silicone rubber. All pertinent dimensions were measured from the replicas. Since the defects were placed at the minimum wall locations and the maximum defect depth had been determined, the maximum percent degradation could be calculated for each specimen. This is one of the key parameters in the data correlation. It is the parameter currently used in plugging criteria and is the parameter the eddy current inspection technique tries to predict.

After the defects had been replicated, specimens were examined using standard single-frequency eddy current techniques. At present, all defects have been eddy current examined, but all these data have not been analyzed. Care was taken to insure that as much as possible the techniques used were the same as those currently used in the field. Figure 8 shows the type of trace that is obtained during the eddy current test. Figure 9 is a comparison of the ECT indicated percent degradation with the actual percent degradation for several of the first specimens tested. It is very obvious from this plot that the ECT method does not predict the actual degradation as well as would be hoped. The worst readings were obtained for EDM slots where the present degradation was consistently underpredicted. One specimen with a shallow defect even gave no indication at all. All indications for EDM slots were unconservative. This is disturbing, but is not as bad as might be imagined, as will be seen when ECT readings are compared to actual pressure test data. This will be discussed later in the report.

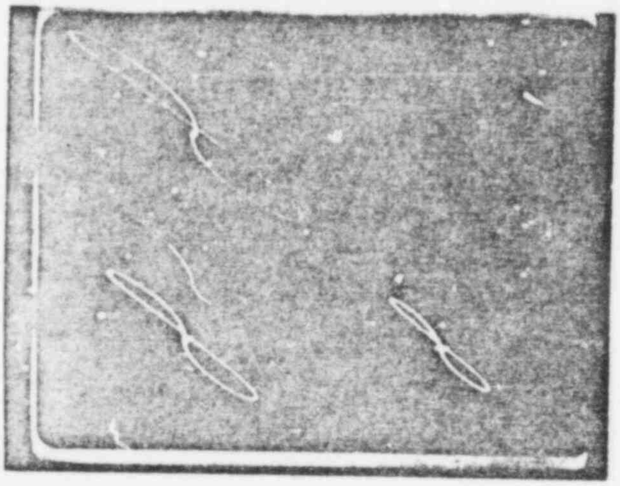

FIGURE 8. TYPICAL TRACE FROM CRT
OBTAINED IN ECT INSPECTION

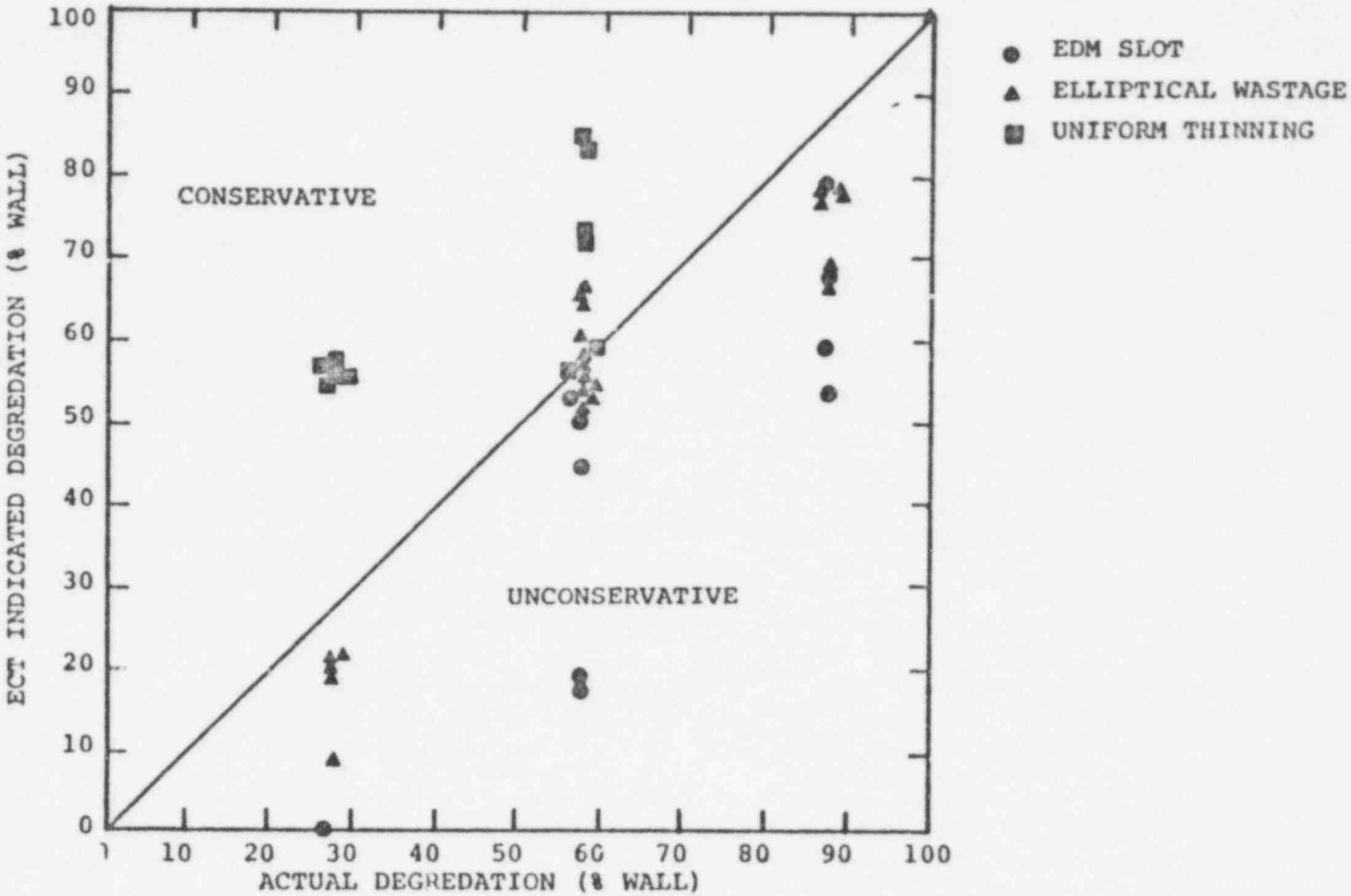

FIGURE 9. COMPARISON OF ECT RESULTS WITH ACTUAL DEGREDATION

Elliptical wastages were more accurately characterized by the ECT. Some readings are still unconservative, but are not as bad as the EDM slot data. The uniform thinning data are all conservative. It can be seen that the more material there was removed in producing a defect, the higher the indicated degradation for a given actual degradation. The uniform thinning removes the largest possible amount of material for a given depth, whereas only a small amount of material was removed to produce the EDM slots. The elliptical wastage removes an amount somewhere in between.

Obviously, there are deficiencies in the presently used ECT methods for defect characterization. When the remainder of ECT data is analyzed, it is hoped that more meaningful interpretations of the ECT data can be made. The present method of ECT signal interpretation uses only part of the data available in the signal and a more detailed interpretation of the signal may lead to much better defect characterization using the ECT method.

PRESSURE TEST FACILITIES AND TEST RESULTS

Five types of pressure tests are included as part of this program. These are burst tests, collapse tests, cyclic fatigue tests, leak rate tests and bulging tests. All of the facilities needed to conduct these tests have been built but, to date, only the burst tests have been completed. The remainder of the tests are in various stages of completion.

Burst tests are conducted in an autoclave assembly as shown in Figures 10 and 11. Conditions in the autoclave during burst tests are thermally and chemically similar to those found in PWR steam generators. Pressurization of both the tube (or primary side) and the autoclave (or secondary side) is with water chemically simulating PWR steam generator feed water. The chemistry is defined on the chart accompanying Figure 12. Initial water supply is tested by condensing on-plant steam, running through an anion-cation exchange bed, then through a sulfite deoxygenator. A total of approximately 300 specimens of all defect geometries were burst tested.

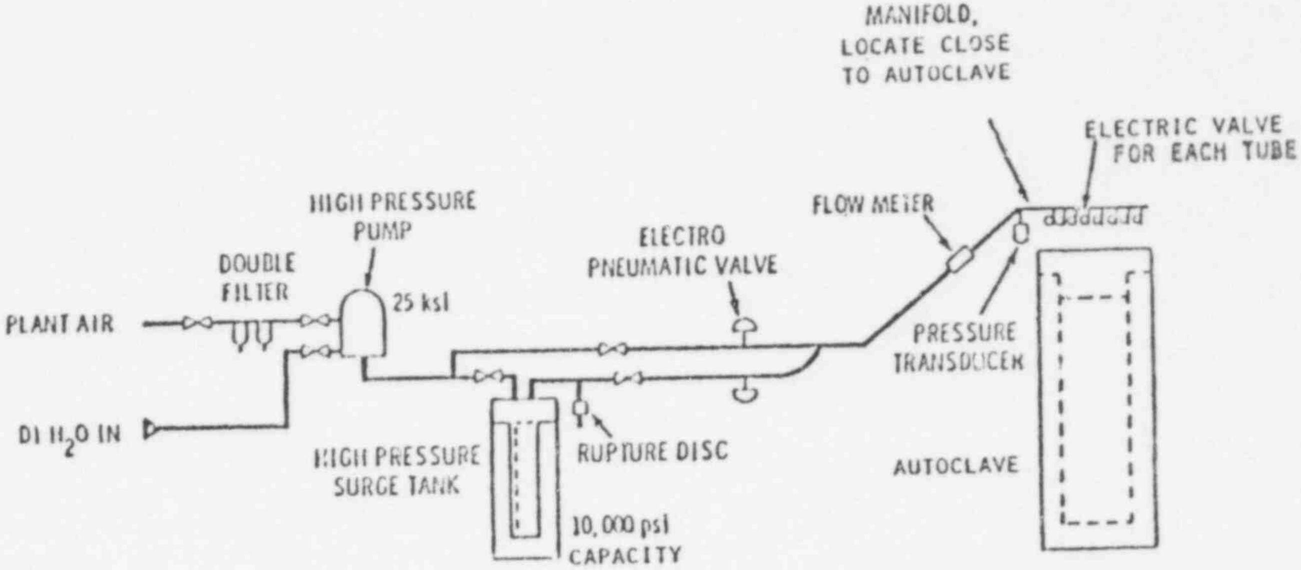

FIGURE 10. TUBING HIGH PRESSURE SYSTEM FOR BURST

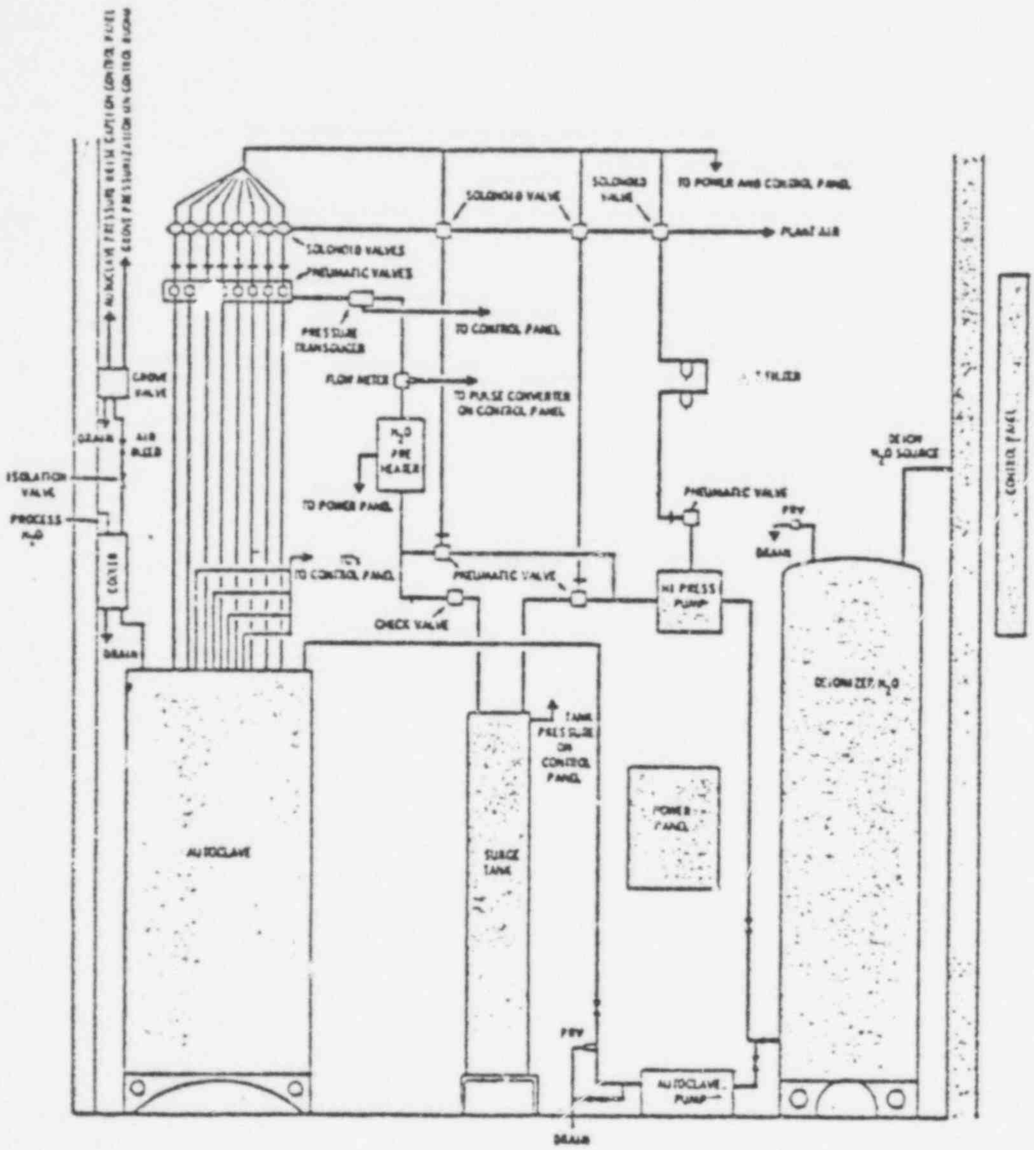

FIGURE 11. BURST FACILITY

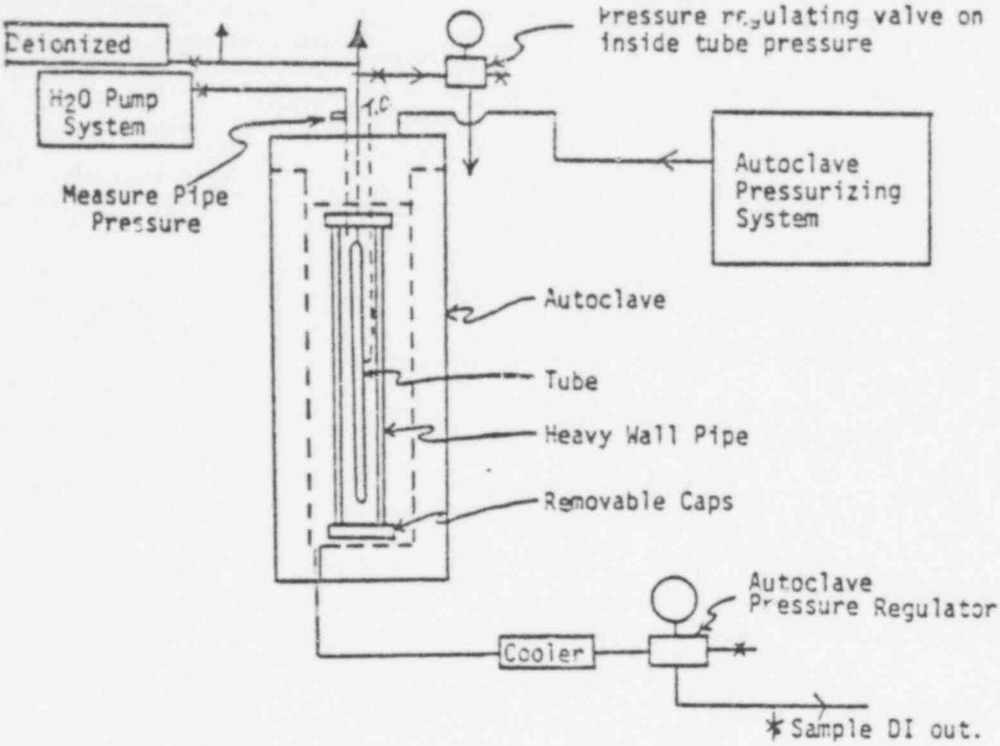

Several fully instrumented assemblies can be handled per autoclave run.

FIGURE 12. Collapse Test Set-Up.

Water Chemistry

Total Base H_2O Conductivity	10 mho/cm[a]
Hydrazine (for O_2 Control)	100 ppm[a]
O_2	20 ppb[b]
pH (Controlled With Ammonia)	8.5-9.5[a]
Cl^-	10 ppb[a]

(a) Feed water and tank chemistry.
(b) Measured at bleed end of test.

During burst tests, the autoclave and its load of tube specimens are simultaneously pressurized to 2250 psi, then heated to 600 F. This establishes the starting conditions for the test. Each specimen, in turn, is rapidly pressurized to bursting (1000 to 2000 psi/min). The primary and secondary pressures and temperatures are recorded on a data logger as a function of time. In addition, the burst pressure is shown on a Heise gauge.

Collapse tests are conducted in an autoclave assembly as shown in Figure 12. Some components of the collapse set-up are used in the burst set-up and, therefore, collapse tests can start only when burst tests are complete. Collapse tests start by pressurizing the tubes and surrounding pipe section to 2250 psi. The autoclave is then pressurized to 2250 psi and heated to 600 F, thus heating the test assembly. Upon commencement of the test, the tube-side pressure is then vented to ~1600 psig. The pipe (secondary) pressure is then increased at the rate of 1000 to 2000 psi/min until collapse occurs. Testing of companion tube/pipe systems will continue until all tubes in that autoclave load have collapsed. A total of about 160 collapse tests are planned.

The test set-up for the cyclic fatigue tests is shown in Figures 13 and 14. Specimens used for cyclic fatigue tests include dented specimens and dented plus elliptical wastage specimens. During cyclic fatigue tests, the specimens are subjected to thermal and pressure cycles simulating a typical PWR steam generator startup and shutdown. Each specimen will be subjected to a maximum of 400 cycles. A test will be terminated when a specimen starts to leak or 400 cycles have been completed.

Two types of leak rate tests are planned. The first of these will be in an autoclave, as shown in Figure 15. Both the primary and secondary sides of the specimens will be environments similar to those found in PWR steam generators. This means that both sides of the tubes will be liquid and at approximately 600 F. This will be a leak rate test from liquid to liquid. Specimens used will have through wall EDM slots. The secondary leak rate tests will be

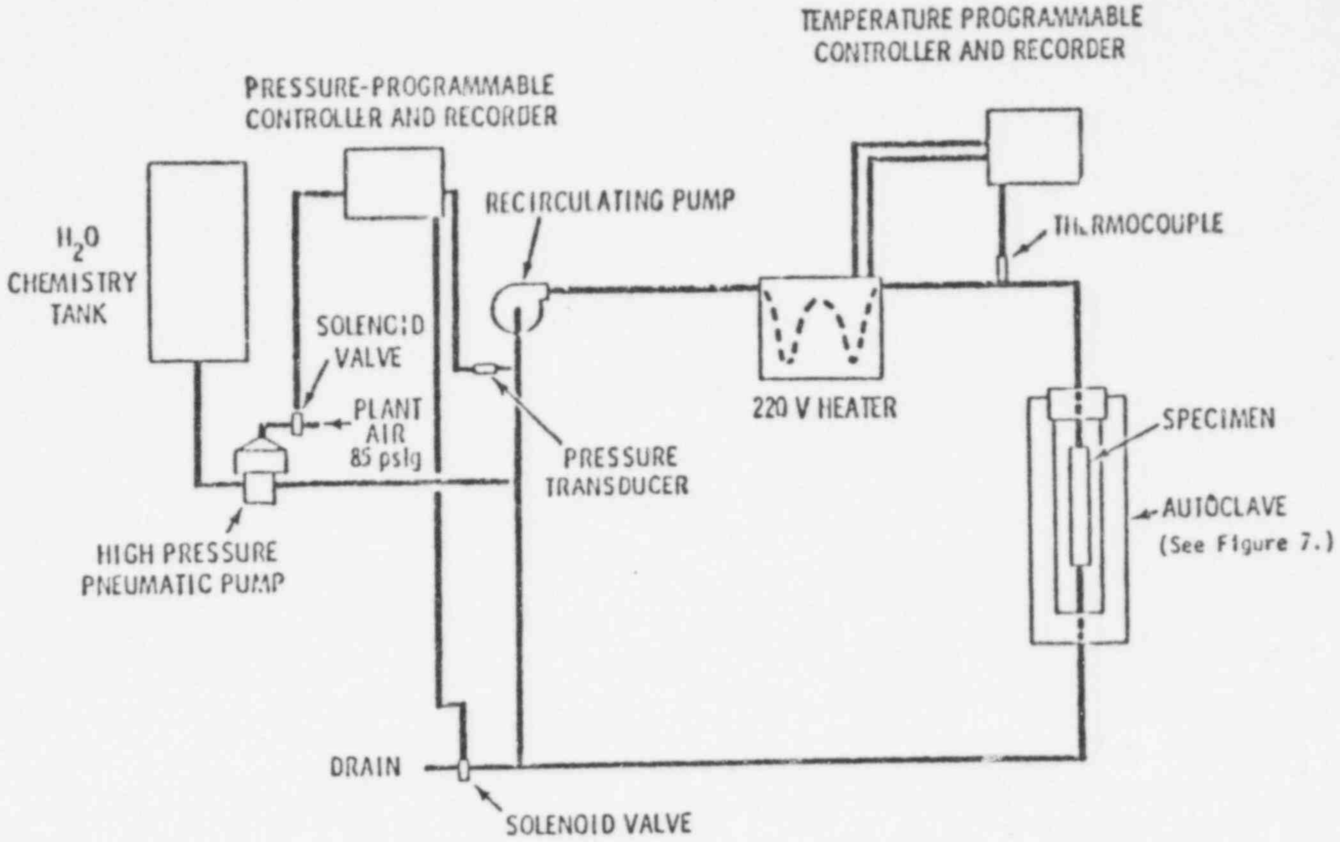

FIGURE 13. Fatigue Test Design/Instrumentation - Primary Loop

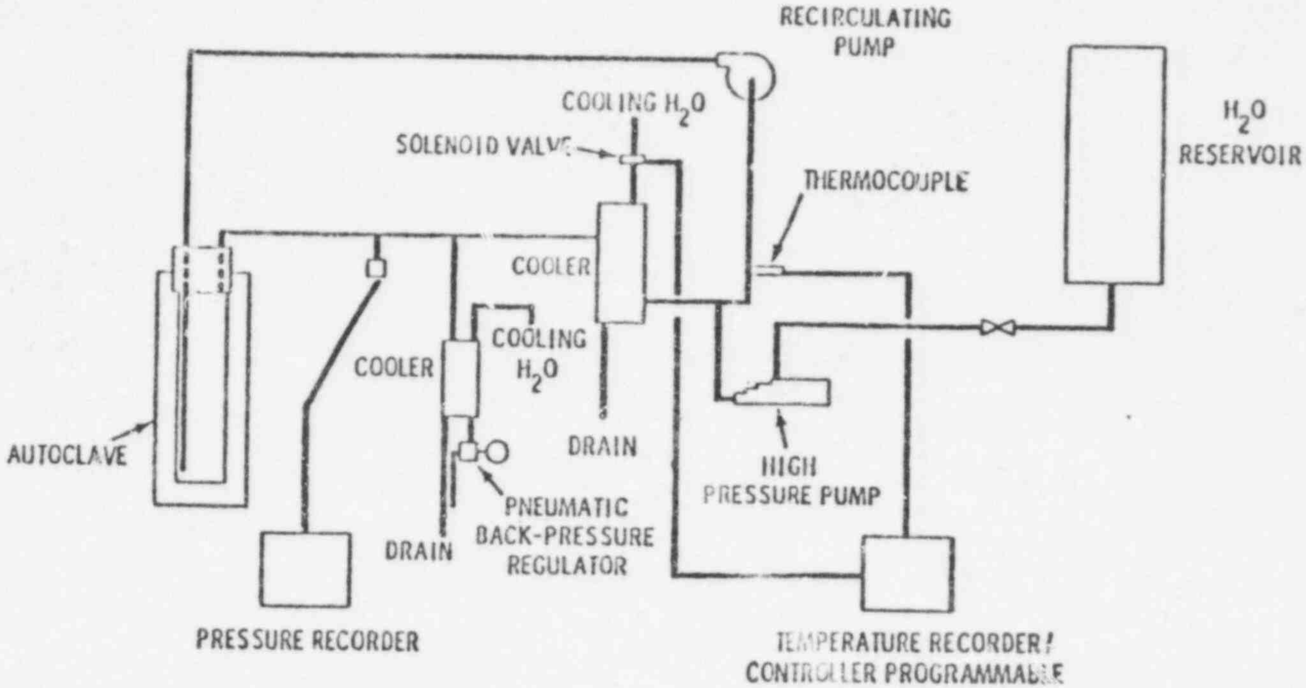

FIGURE 14. Fatigue Test Design/Instrumentation - Secondary Loop

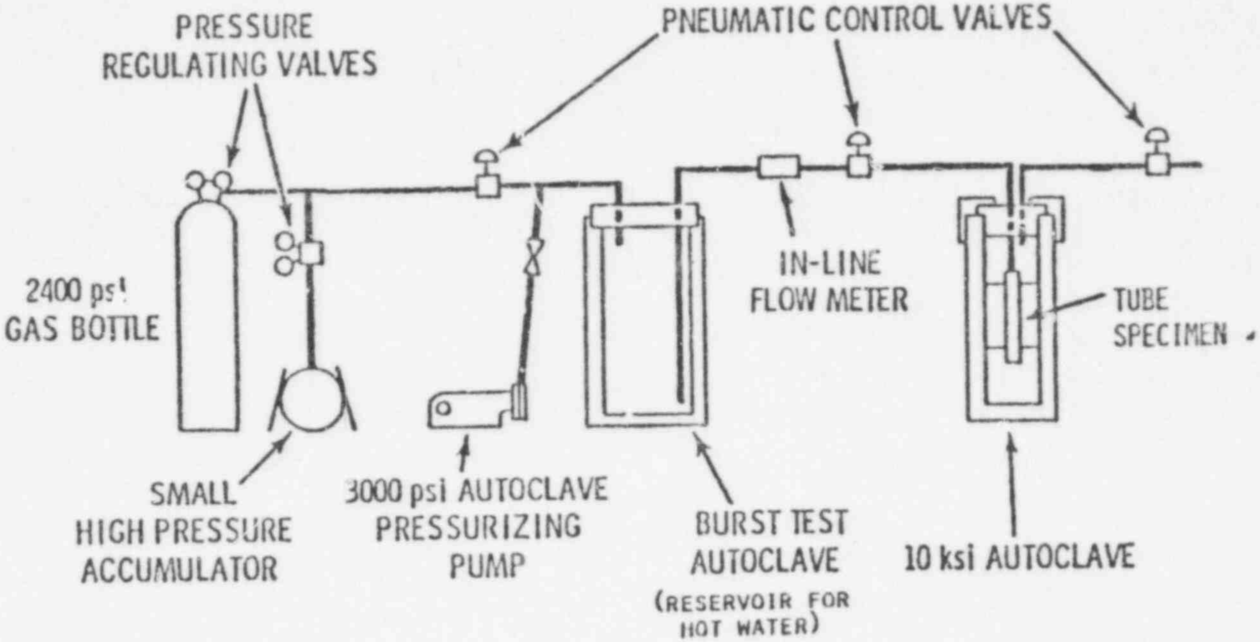

FIGURE 15. Controlled Secondary-Side Leak Rate Setup

conducted with the secondary side of the specimen at room temperature. This set-up is shown in Figure 16. Since components of these systems are used in the burst and collapse tests and leak rate tests, this set-up will not be available until the burst and collapse tests are completed.

Various bulging specimens have 1/4 in., 1/2 in. and 1 1/2 in. through wall slots. Neoprene bladders inside the tubes allow pressurization of the tubes. A grid is placed on the specimens using a photo emulsion that does not affect the tube properties. Specimens in ambient air are pressurized with room temperature water. The pressure is increased until the bladder extends through the slot and ruptures. Video tape pictures of the tests are taken which show time, tube pressure and the specimens. Initial tests using 0.750 x 0.043 in. size tubing and 1/2 in. long slots produced failure pressures in excess of 3200 psi.

To date, only the burst tests have been completed. Collapse tests are underway, as are the bulging and cyclic fatigue tests. Leak rate tests will start as soon as the collapse tests are finished. Data from the burst tests are currently being analyzed. Samples of burst data are shown in Figures 17, 18 and 19.

Operating margins-of-safety and accident margins-of-safety are defined as follows:

OMS = burst pressure divided by 1250 psi

AMS = burst pressure divided by 2300 psi.

The 1250 psi represents a fairly common operating pressure differential in PWR steam generators. The 2250 psi represents the worst credible accident condition.

As can be seen from Figure 17, the results of the burst tests for uniform thinning are very consistent with very little data scatter. Obviously, both length and depth of the uniform thinning have an effect on the burst pressure. Figure 18 shows results of the elliptical wastage data for one size of tubing. Again, the results are very consistent and show a small amount of scatter. Figure 19

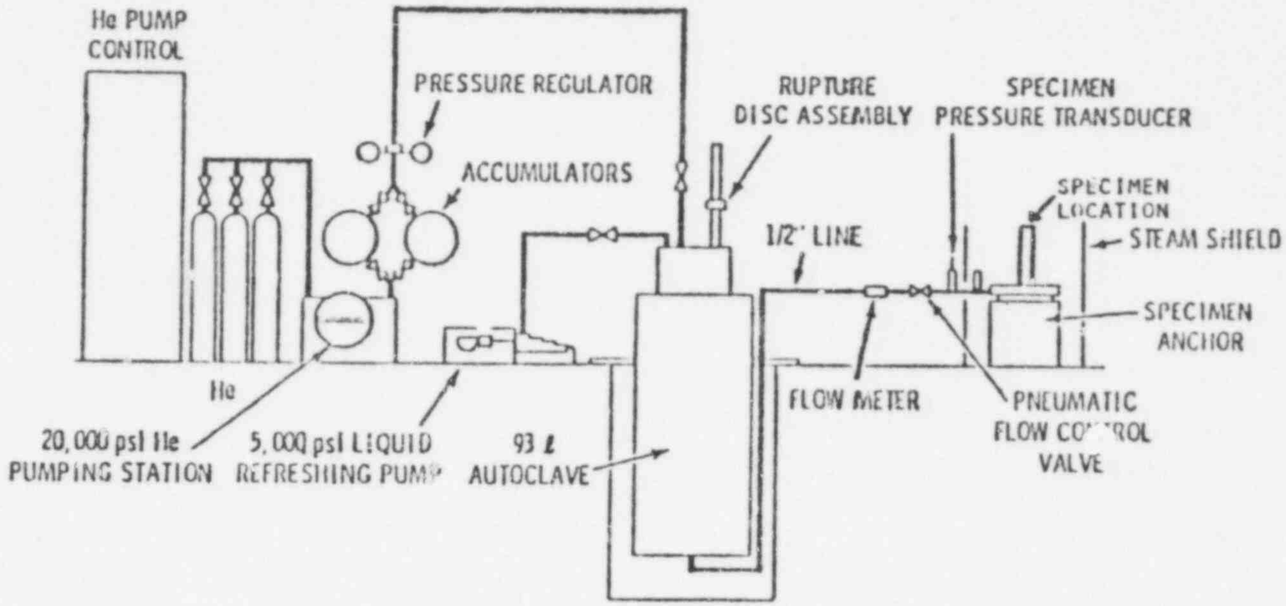

FIGURE 16. Experimental Setup for Leak Rate Tests into Ambient Pressure

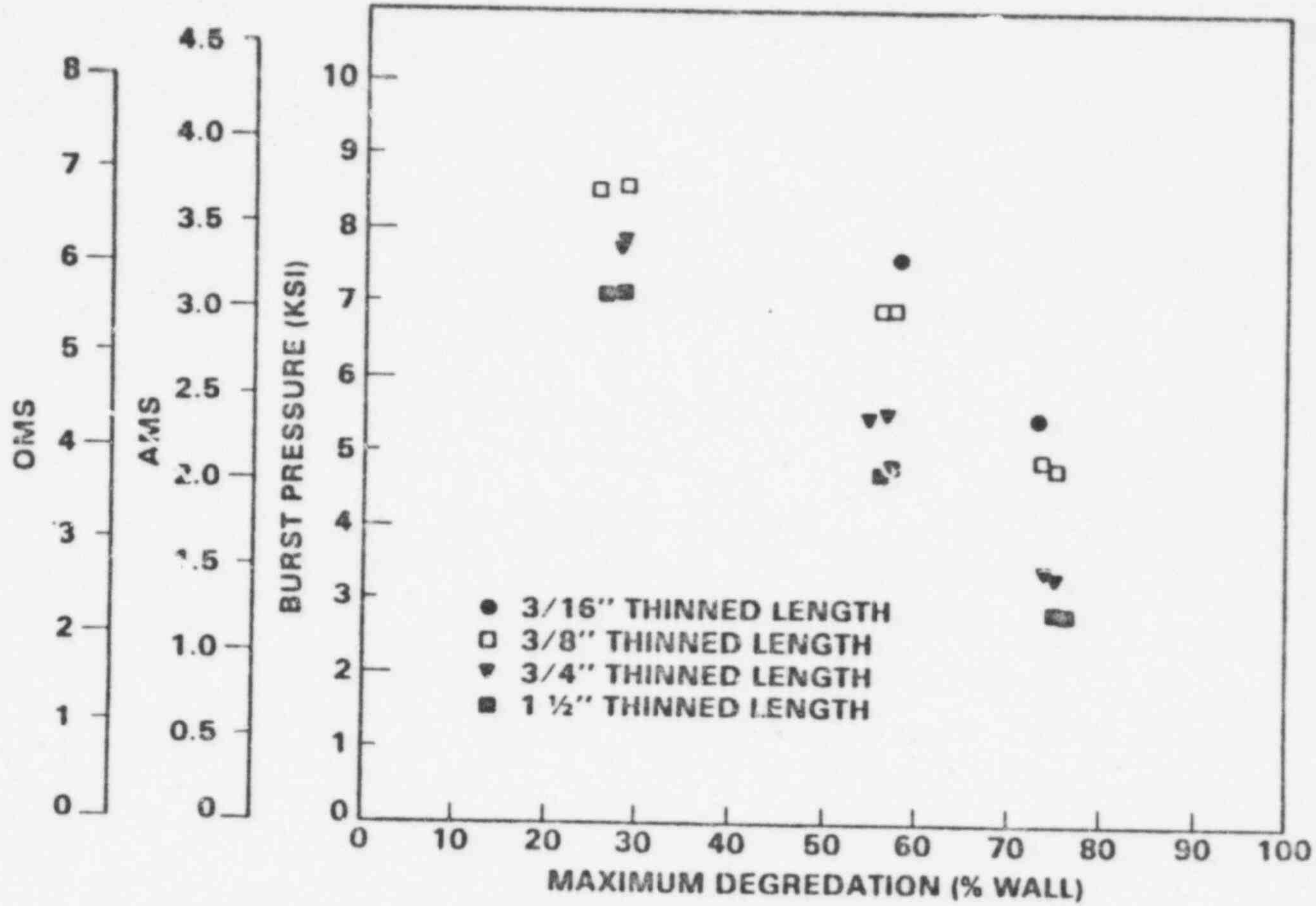

FIGUR. 17. BURST PRESSURES FOR .875 x .050 UNIFORM THINNING

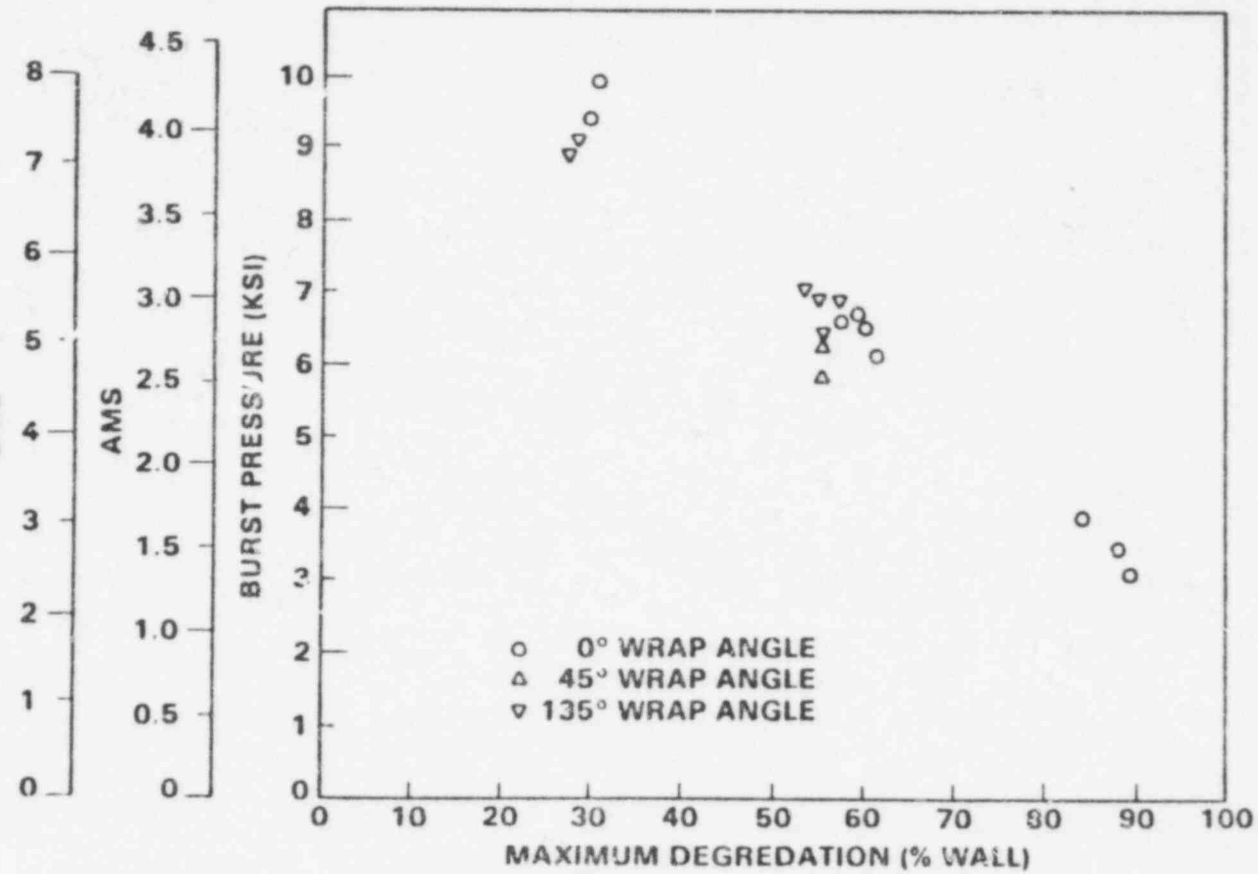

FIGURE 18. BURST PRESSURES FOR .750 x .050 ELLIPTICAL WASTAGE

265

815 271

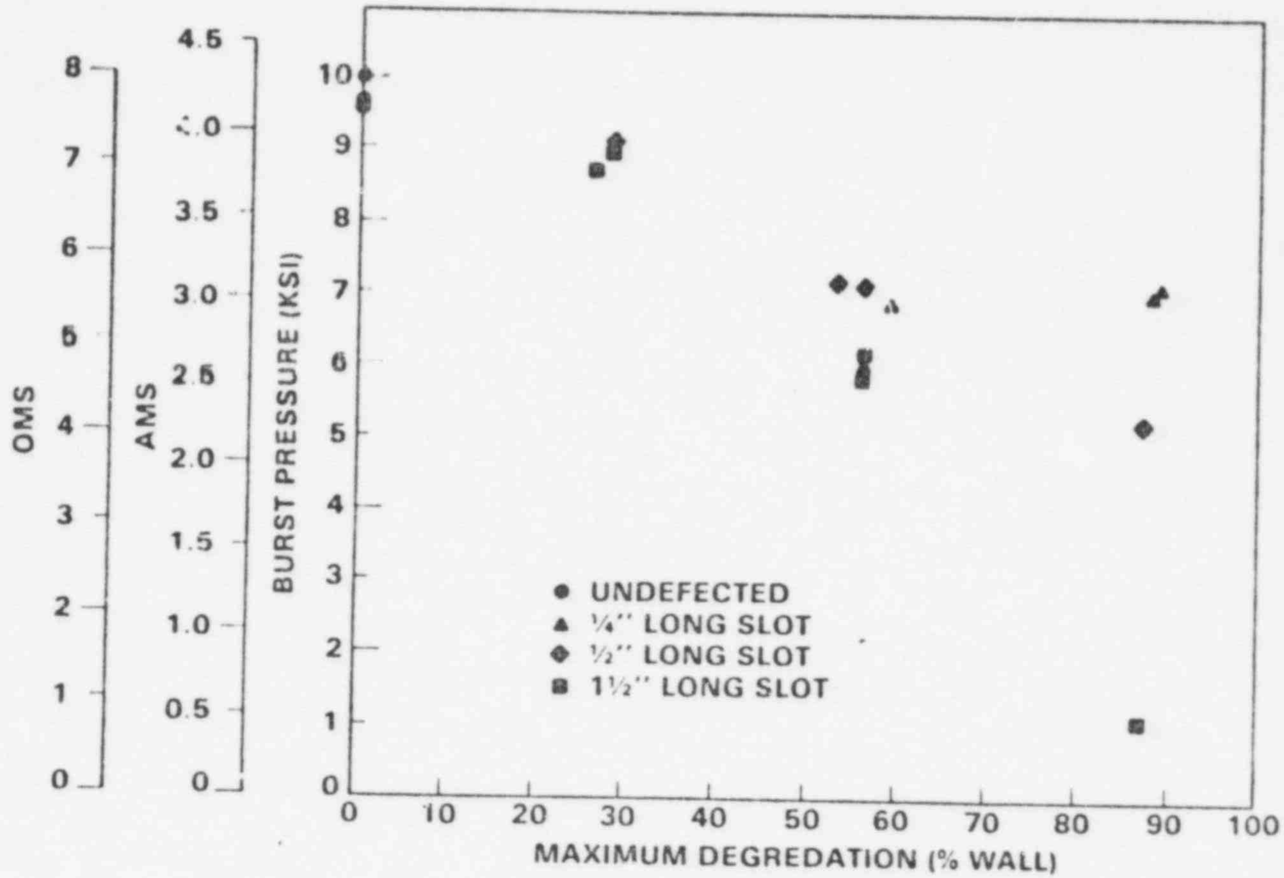

FIGURE 19. BURST PRESSURES FOR .750 x .043 EDM SLOTS

is a representative plot of EDM slot data. Here, the scatter in the data is somewhat larger, mainly due to the nature of the EDM slots. It was not possible to maintain a tight tolerance on the EDM slots as on the uniform thinning and elliptical wastage. A computer program is currently being developed to assist in the manipulation and plotting of the data. This is one of the primary tools used in the data analysis.

Figure 20 shows the results of the burst tests for the first specimens examined by ECT. Whereas it had previously been shown that the ECT did not accurately determine the magnitude of the defects, it can be seen from this figure that the criteria would have plugged all defects that had burst pressures less than 5000 psi, which is over twice the worst credible accident condition. Current plugging criteria calls for plugging of tubes that have indications of greater than 40%.

ONGOING RESEARCH

FY-78

Continue using chemically defected tubing method of mechanically defected tubing. Emphasis is on tight cracks.

FY-79

Continue using in-service defected tubing.

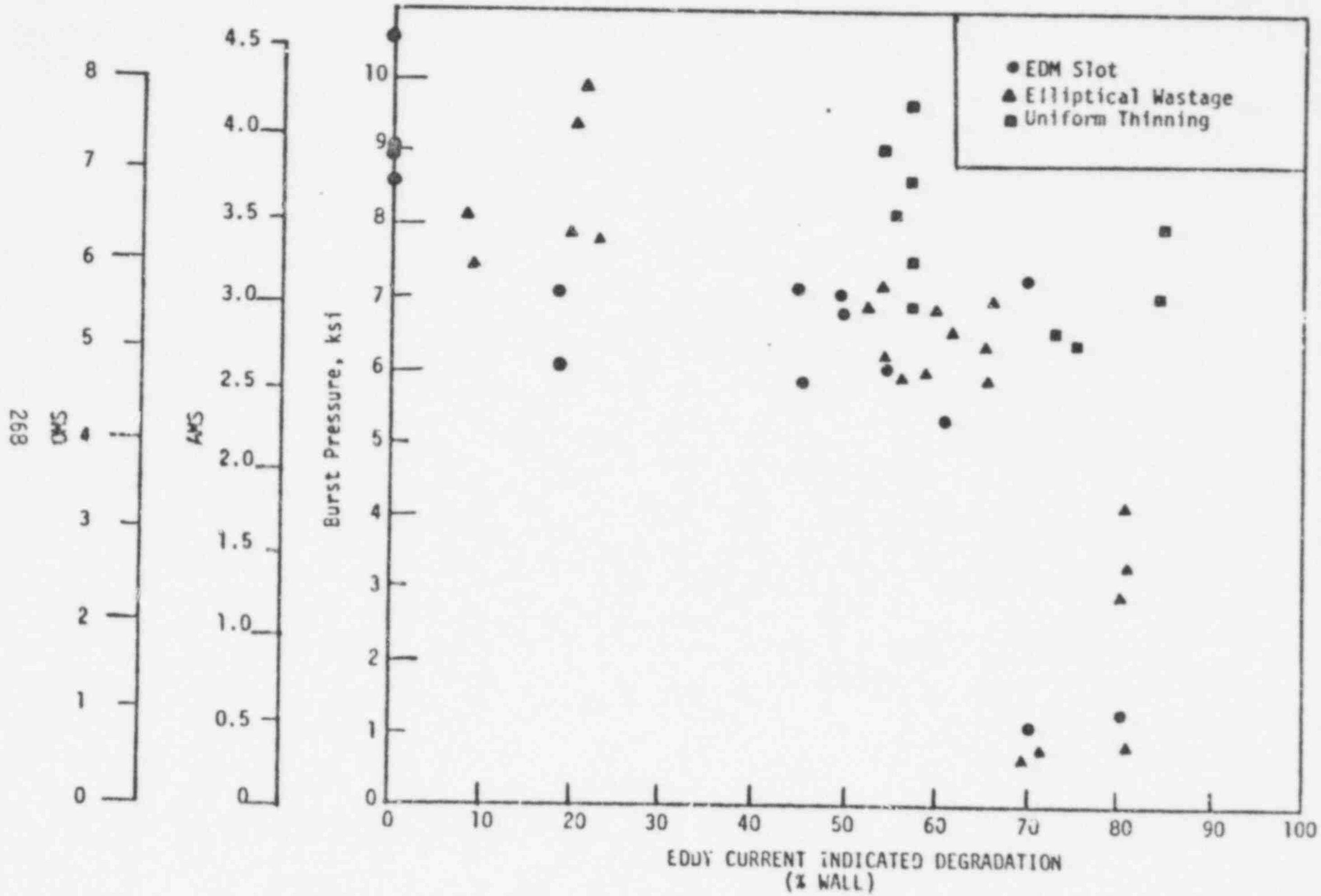

FIGURE 20. COMPARISON OF ECT RESULTS TO BURST PRESSURES

Contract — Primary Coolant Pipe Rupture Study, Task G, Method for Detecting Sensitization in Stainless Steel: AT(49-24)0202

Contractor — General Electric Company
Nuclear Energy Division
Boiling Water Reactor Systems Department
San Jose, CA

Principal Investigators — W. L. Clarke, Jr. and V. M. Romero

OBJECTIVES

Extend the development of a technique (EPR) for detecting sensitization in stainless steels to permit obtaining measurements on actual components in the fabrication shop and in the field. Design and fabricate a portable polarization system and electrochemical test cell so that quantitative degree of sensitization measurements can be obtained nondestructively. Qualify the portable system using a welded stainless steel pipe field mockup assembly. Perform laboratory experiments to increase the data base of the measurement technique, so that greater confidence is achieved in making judgments relative to stress corrosion cracking susceptibility based entirely on degree of sensitization.

FY 77 SCOPE

1. Complete a number of laboratory studies which were initiated during FY 76, and which are supportive to the total EPR development effort.

   a. Determine the effects of grain size on the sensitization values measured.

   b. The ten welded Type-304 stainless steel pipes used for the EPR development were retested using the test parameters optimized during FY 76.

   c. The pipe weld heat affected zones were profiled from the inside to the outside.

   d. One heat of pipe was tested to study the effects of sensitization temperatures and times-at-temperature.

   e. Long term constant load tests were continued to assess the intergranular stress corrosion cracking susceptibility of welded Type-304 stainless steel.

2. A portable polarization system was designed and fabrication initiated by a sub-contractor.

3. An electrochemical test cell for use with the portable polarization system in the field was designed and fabricated. Qualification of the field cell was completed using a welded Type-304 stainless steel pipe mockup assembly.

4. Procedures and specifications for obtaining degree of sensitization measurements using the EPR technique in the laboratory were prepared and published in the open literature.

5. Efforts were initiated to obtain ASTM adoption of the EPR technique as a standard practice for detecting sensitization in stainless steels.

6. A topical report summarizing all FY 76 activities was issued.

INTRODUCTION

A technique has been developed[1] for quantitatively measuring the degree of sensitization in thermally treated Types-304 and -304L stainless steels. The EPR test (Electrochemical Potentiokinetic Reactivation) was developed because of an industrial need for a rapid, nondestructive, quantitative field test which could be used for assessing sensitization in reactor components. All the tests used by the industry to detect sensitization are considered deficient,[2] and these deficiencies limit the use of these tests in shop-fabricated and field-constructed (welded) components. It was anticipated the results of the EPR measurements could be compared to results of stress corrosion tests on materials with a similar degree of sensitization in the environment of concern. Thus, a judgment could be made concerning the possibility of intergranular stress corrosion (IGSCC) occurring in the component in service. The development effort was originally divided into two phases. The feasibility of the EPR method to measure quantitatively the degree of sensitization was the objective of Phase I. The EPR technique was determined to be viable and superior to the present chemical method (ASTM Procedure A262-Practice E) for laboratory evaluation of welded and as-received conditions.

Phase II was devoted to conducting numerous tests to establish a data pool for correlating EPR determined degree of sensitization with stress corrosion resistance of welded Types-304 and -304L stainless steel piping. The parameters to be used for conducting the EPR test were also extensively investigated during Phase II. All the data developed during Phase I, and the major portion of the work accomplished under Phase II have been reported.[1] A few additional tests initiated during Phase II and completed during Phase III are included in this document (discussed next). Development efforts during Phase III were directed toward the fabrication and qualification of an EPR measurement unit capable of detecting sensitization nondestructively in stainless steel components in the field. This phase can be further divided into five tasks. The first task was concerned with completing testing initiated during Phase II and with studies useful for the application of the electrochemical cell used in the external field measurement of piping.

The major emphasis during Phase III was the design, fabrication, and qualification of an electrochemical cell needed for sensitization detection measurements in the field. These accomplishments were completed during Task 2; while Task 3 was devoted to completing the design, and making arrangements for, fabrication of a portable polarization system to be used with the EPR cell.

The procedures and General Electric Company specifications for conducting EPR measurements were completed during Task 4. Finally, Task 5, which is in progress, is concerned with obtaining ASTM adoption of the EPR test as a standard to be used by the metallurgical industry for the detection of sensitization in Types-304 and -304L stainless steels.

EXPERIMENTAL PROCEDURES

The bulk of studies during this reporting period was performed using a single heat (M7772) of Type-304 stainless steel piping (4-inch, Schedule-80 seamless). However, a number of tests were conducted using five heats of Type-304 and three heats of Type-304L seamless pipe (4-inch, Schedule-80), one heat of 10-inch seamless, and two heats of 26-inch rolled and welded Type-304 pipe.

The degree of sensitization was quantified using the recently developed EPR method. This method consists of developing potentiokinetic curves of a polarized sample obtained by controlled potential sweep from the passive to the active region (reactivation) in a specific electrolyte; details of the test technique have been reported.[1] The test conditions used for the EPR measurements are given in Table I.

Intergranular stress corrosion cracking (IGSCC) tests were conducted using two methods. Most of the samples (particularly the welded condition) were rapidly screened for IGSCC susceptibility using the Constant Extension Rate Test (CERT) method. In this test, the uniaxial tensile samples are slowly strained to failure at a controlled extension rate of 3.3×10^{-5} in./min in 289°C (550°F) high-purity water containing 8 ppm dissolved oxygen. Susceptible materials generally reveal shorter failure times, lower breaking stresses, and lower reduction-in-area values compared to similar tests performed in air or inert gas. In addition, the failure mode is documented by Scanning Electron Microscope (SEM) examination of the fractured samples.

In conjunction with the CERT tests, some samples were exposed to 289°C water with 8 ppm dissolved oxygen under constant load (60% ultimate tensile strength at 289°C). Again, all samples were examined metallographically and by SEM after testing to assess the failure mode.

RESULTS

COMPLETION OF EARLIER STUDIES

1. Grain Size Effect

Earlier studies indicated one heat (834264) of large-grained (ASTM 3.5) 26-inch rolled and welded pipe was very susceptible to IGSCC in the welded condition, but consistently yielded low degree of sensitization values after EPR testing. A second heat (17192) of large-grained (ASTM 1-4) 26-inch pipe was evaluated to determine if this lack of agreement between IGSCC susceptibility and sensitization was due to grain size, or unique to the processing history experienced by the rolled and welded pipe. Additionally, EPR spot checks were made on large-graine (ASTM 2-3) reactor hardware which was known to be IGSCC susceptible. The weld heat affected zone (HAZ) profiles for these pipes are shown in Figure 1, where the levels of sensitization for both heats are comparable. The degrees of sensitization for both welded pipes are considered quite low as P_a values between 4 to 40 C/cm^2 are common for IGSCC susceptible heats of as-welded Type-304 stainless steel.

Both heats were determined to be susceptible to IGSCC, which on a ranking basis, would rank these two heats among the least-resistant of the 11 piping heats evaluated. Similar tests conducted on IGSCC-susceptible reactor hardware revealed P_a values greater than 20 C/cm^2 for the welded large grained material. Therefore, it appears the low values of P_a obtained for the rolled and welded pipe is due to a processing history, or other effect unique to that type of product, i.e., the anomalous sensitization – IGSCC behavior cannot be expained solely by grain size.

2. Weld Retesting

Ten of the welded pipes were retested for degree of sensitization using the optimum EPR test parameters developed during the Phase II studies. These parameters were established to provide the greatest sensitivity possible when assessing sensitization in welded Type-304 stainless steel. Basically, the latter tests were conducted on inside weld HAZ planar samples using an electrolyte of 0.5*M* H_2SO_4 + 0.05*M* KSCN and a reactivation scan rate of 3 V/h, rather than the 0.01*M* KSCN and 6 V/h generally used (all other test conditions ramain the same).

The results of the weld retest are given in Table 2, and are compared to the earlier determined values using the original test conditions. Unquestionably, the greater KSCN concentration and slower reactivation scan rates produce greater sensitivity (higher P_a values). The rankings are somewhat different but these tests were conducted on single samples and probably reflect usual weld variability. However, the sensitivity obtained using the original test conditions is considered sufficient, particularly in view of the problems encountered in application with the higher concentration of KSCN. The 0.05*M* concentration is more unstable (can make the 0.01*M* solution in bulk and store for 1 month) and makes passivation more difficult during the EPR test. The additional time for passivation with the 0.05*M* electrolyte plus the extended reactivation time using a 3 V/h rate rather than 6 V/h results in a 30-minute test instead of 10 to 15 minutes. The shorter test time is desirable for production usage, and especially when conducting a field test *in-situ*.

3. Pipe Through-Wall Profiling

The successful application of a pipe exter[illegible] weld HAZ sensitization measurement, in terms of making judgments relative to [illegible] ide, require minimal change in degree of sensitization after welding from the inside to the outside surfaces. Welded samples from four of the pipes were analyzed by the EPR profiling technique[1] from the inside to the

815 279

outside until a significant change in degree of sensitization occurred. The results revealed the degree of sensitization for three heats dropped significantly (values decreased by 50 to 75% of inside surface measurements) for about the first 0.040 inch away from the inside (toward the outside diameter). After which, the levels of sensitization remained somewhat constant throughout the pipe wall. However, one heat showed little drop in the level of sensitization for the first 0.080 inch, but then decreased gradually toward the outside.

4. Time and Temperature Study

Future studies to develop the EPR field technique further will include pipe external surface heat treatments to identify potentially "bad" heats of material which sensitize readily. The time and temperature studies were conducted to provide advance information relative to the conditions required to obtain significant degrees of sensitization in Type-304 stainless steel pipe in short times. The heat of 4-inch seamless pipe (heat 7772) used for the EPR field cell qualification was also used for the time and temperature studies. Nonwelded samples were EPR tested after aging between 10 to 60 minutes at 620°C (1150°F) and 732°C (1350°F), and after 1-hour treatments between 482°C (900°F) to 704°C (1300°F). These studies indicate levels of sensitization comparable to those required to produce IGSCC susceptibility after welding can be obtained by aging 1-hour at 575°C (1050°F), 10 minutes at 620°C (1150°F), or for 2-minutes at 732°C (1350°F).

5. IGSCC Constant Load Tests

Welded samples from the Phase II studies were undergoing constant load testing for relative IGSCC susceptibility when the Phase III activities commenced. Because of the long times necessary for failure, if any, of welded Type-304 in the constant load test, these tests were continued through Phase III. The results of these tests are given in Table 3. These data are incomplete since many of the samples had not failed and continued under test at the time this report was prepared. To date, samples from five of the Type-304 heats have failed by IGSCC, while two heats of Type-304 (heats 2P6396 and 454659) and all three Type-304L heats are demonstrating good resistance. Analysis of the data for multiple samples of each heat confirms the variability in stress corrosion behavior of the welded condition for Type-304 stainless steel. For comparison, post weld, heat-treated (620°C/24-40 h) Type-304 samples would have failed by IGSCC in this test in times around 100 hours. The superiority of the welded condition over the furnace-sensitized condition relative to stress corrosion resistance based entirely on degree of sensitization is quite apparent. It is also apparent the Type-304L welded samples are far more resistant to stress corrosion than the regular grades of Type-304 in the accelerated BWR environmental test.

FIELD TEST DEVELOPMENT

1. External Cell Fabrication

An electrochemical cell was designed and fabricated, which could be attached to the outside of a pipe (or other component) for obtaining EPR measurements in the field. The components of the field cell include (Figure 2): the acrylic body, "O"-ring sealed end caps with curvatures corresponding to the diameter of various size pipes, a top cap with internal penetrations, a platinum counter electrode, a standard calomel reference electrode, a deaeration capillary which is also used for adding and removing the electrolyte, a spring-loaded working electrode, and adjustable stainless steel attachment straps. The assembled cell is shown attached to a 4-inch pipe in Figure 2b.

2. Portable Polarization System

Arrangements were made with an outside vendor for the fabrication of an automated, portable EPR polarization system to be used with the field cell. A schematic of the instrument is shown in Figure 3. With these two units (cell and polarization system), and a variety of small hardware pieces and supplies, a fully portable instrument will be available for conducting degree of sensitization measurements of Type-304 stainless steel in the field.

3. Field Cell Qualification

The field cell was qualified in this study by measuring sensitization in a number of pipe weld HAZs using a mockup section simulating an actual 4-inch, Schedule-80 reactor by-pass pipe. This mockup (Figure 4) was fabricated from Type-304 stainless steel (heat M7772) using weld procedures similar to those employed during shop and field fabrication.

After welding, the assembly was prepared for EPR field measurement by polishing approximately 1-inch diameter spots with one edge butted against the weld fusion line (Figure 5). The cell was attached to the pipe over the polished spot and an EPR measurement taken using the conventional laboratory polarization system (Figure 6).

After the external *in-situ* measurements were completed, the pipe was sectioned for conventional laboratory EPR testing and IGSCC characterization.

The conventional samples were taken through the same polished spot where the external measurements were obtained, and the IGSCC samples taken adjacent to the EPR samples. These conventional samples were taken from both the pipe inside diameter and outside diameter locations in the weld HAZ.

Typical EPR curves are shown in Figure 7 comparing the external outside diameter cell measurements to conventional inside diameter and outside diameter values. There is good agreement in the curves generated by both the external cell and conventional laboratory samples, indicating the field cell will measure degree of sensitization nondestructively. Both values show lower degrees of sensitization on the outside diameter compared to the inside diameter, which is generally the case, and is in good agreement with earlier studies.[1]

The results of measurements obtained for the 2G and 5G welds are given in Tables 4 and 5, respectively. Again, the levels of sensitization on the inside diameter are generally higher than on the outside diameter, although occasionally reverse behavior is noted, probably the result of heat input variability during the welding process. All the EPR values shown in Tables 4 and 5 for the 2-cm^2 area measurements are low. These low values result from an "averaging effect" in which the narrow HAZ (causes the current flow which is measured during the EPR test) passes through a relatively large nonthermally affected base metal sample (refer to Figure 5). Additionally, the field cell measurements are generally lower than the conventional laboratory sample. This latter effect is due to the lesser amount of HAZ in the areas of the round samples compared to the rectangular samples (Figure 5), and to the meandering nature of weld HAZs; not continuous through the edge of the round polished spots. A truer representation of the weld HAZ was obtained by sectioning a major portion of the base metal to test a 0.5-cm^2 sample (instead of 2 cm^2). This operation was conducted on a limited number of the rectangular conventional laboratory samples,the results are also given in Tables 4 and 5. Here, the degree of sensitization values are much higher as the HAZ is contained in much smaller samples, so that when the

P_a values are normalized to sample size, the "averaging effect" is less significant. The P_a values thus measured correspond to those obtained in earlier studies,[1] and account for the IGSCC susceptibility noted in the companion pipe samples. Therefore, it appears the external cell is capable of measuring degree of sensitization nondestructively on components in the field. Future cell designs will contain a narrow rectangular opening for measurement, rather than the 2-cm^2 round geometry used in the feasibility study.

4. ASTM Adoption

Efforts were initiated to obtain adoption of the EPR method as an ASTM standard for detecting sensitization in Type-304 stainless steel. Currently, a round robin test of General Electric Company prepared samples is being performed by a number of investigators throughout the United States. This round robin is being handled by the ASTM sub-committee G1-08 (Corrosion of Nuclear Materials). The samples were fabricated from one heat each of Types-304 and -304L stainless steel sheets, and heat treated to produce three levels of sensitization, plus the mill annealed condition. The baseline data was obtained in our laboratory using conventional laboratory testing techniques, after which they were transmitted to the first round robiin participating laboratory for testing.

PLAN OF RESEARCH FOR FUTURE YEARS

1. Investigate alternate methods for measuring degree of sensitization in the field using the EPR technique. This research would be necessary if it proves unfeasible to make judgments relative to IGSCC on the inside of a pipe weld HAZ based entirely on sensitization measurements obtained on the outside.

2. Establish fabrication shop and field procedures for obtaining degree of sensitization measurements using the portable EPR technique.

3. Continue to refine the EPR field hardware and measurement technique.

4. Enlarge the data pool for welded Type-304 stainless steel in terms of IGSCC susceptibility as influenced by varying degrees of sensitization as measured by EPR.

5. Attempt to establish safe limits of sensitization for welded Type-304 stainless steel in terms of IGSCC resistance using a more realistic simulated BWR coolant environment test.

REFERENCES

1. Clarke, W. L., Romero, V. M., and Danko, J. C., "Detection of Sensitization in Stainless Steels Using Electrochemical Techniques," General Electric Company, GEAP-21382, August 1976, and NACE Corrosion Conference Paper 180, March 1977, San Francisco, CA.

2. Clarke, W. L., Cowan, R. L., and Walker, W. L., "Comparative Methods for Measuring Degree of Sensitization in Stainless Steel," General Electric Company, NEDO-12669, May 1977, and ASTM STP from ASTM Symposium on Evaluation Criteria for Determining the Susceptibility of Stainless Steels to Intergranular Corrosion, Toronto, Ontario, May 2 and 3, 1977.

TABLE 1. EPR Test Conditions

Electrolyte	0.5M H_2SO_4 + 0.01M KSCN
Temperature	$30^{o}C$
Sample Surface Finish	1 μm (diamond paste)
Reactivation Sweep Rate	6 V/h (cathodic)
Passivation Potential/Time	+ 200 mV/2 min
Deareation	N_2
Polarization System	Hokuto-Denko with Princeton Applied Research Curve Integrator
Degree of Sensitization (Data Normalization)	P_a (C/cm^2) = Q(C)/GBA(cm^2)[a]

[a]GBA = Calculated Grain Boundary Area in Sample

TABLE 2. Degree of Sensitization in Type-304 Stainless Steel Pipe Weld HAZs (Inside Surface)

Alloy	Heat	0.05 KSCN 3 V/h	0.01 KSCN 6 V/h	IGSCC Susceptible[d]
304	M7616[a]	226.8	39.5	Yes
304	2P6396[a]	160.5	10.6	Yes
304	2P6424[a]	149.3	18.6	Yes
304	TH6656[b]	71.1	2.7	Yes
304	M7772[a]	54.8	4.8	Yes
304	454659[a]	22.0	1.5	No
304L	482038[a]	13.2	0.4	No
304	834264[c]	10.9	3.4	Yes
304L	00575[a]	6.1	0.2	No
304L	482135[a]	3.4	0.1	No

[a]4-in., Schedule-80 seamless

[b]10-in., Schedule-80 seamless

[c]26-in., Schedule-80 rolled and welded

[d]CERT in 289°C water with 8 ppm O_2

815 285

TABLE 3. Constant-Load IGSCC Test Results for Ten Welded Pipe Heats of Types-304 and -304L Stainless Steel ($288^\circ C$ Water, 8 ppm O_2, $\sigma = 60\%$ UTS $288^\circ C$)

Alloy	Heat	Applied Stress [ksi (MPa)]	Exposure Time[a] (h)
304	M7616	41.6 (287)	1,470 F
304	M7616	41.6 (287)	9,371
304	M7616	41.6 (287)	2,000 F
304	2P6424	39.6 (273)	3,602 F
304	2P6424	39.6 (273)	696 F
304	834264	39.7 (274)	464 F
304	834264	39.7 (274)	2,547 F
304	834264	39.7 (274)	2,000
304	TH6656	39.7 (274)	13,275
304	TH6656	39.7 (274)	12,405
304	TH6656	39.7 (274)	6,628 F
304	TH6656	39.7 (274)	2 000
304	2P6396	39.2 (270)	10,401
304	2P6396	39.2 (270)	2,000
304	M7772	41.8 (288)	8,666 F
304	M7772	41.8 (288)	12,344
304	M7772	41.8 (288)	2,000
304	454659	40.0 (276)	12,408
304	454659	40.0 (276)	12,422
304L	482135	37.8 (261)	12,408
304L	482038	35.2 (243)	10,409
304L	00575	40.4 (279)	10,387

[a]F = Failed by IGSCC

TABLE 4 Degree of Sensitization in Type-304 Pipe (Heat M7772) Weld HAZ (2G Position) $0.5M$ H_2SO_4 + $0.01M$ KSCN at $30^{o}C$ (P_a, C/cm^2)

Weldment Location	External Field Cell (2 cm^2 Area)	Conventional Laboratory Sample 2 cm^2 Area	0.5 cm^2 Area	IGSCC[a]
2G-1A				
i.d.	-	1.7	2.8	n.d.
o.d.	0.6	1.6	13.2	n.d.
2G-1B				
i.d.	-	0.6	4.3	Yes
o.d.	0.4	0.3	2.0	Yes
2G-1C				
i.d.	-	0.4	-	n.d.
o.d.	0.2	0.3	-	n.d.
2G-1D				
i.d.	-	0.2	-	Yes
o.d.	0.04	0.1	-	Yes
2G-2A				
i.d.	-	0.4	-	n.d.
o.d.	0.2	1.1	-	n.d.
2G-2C				
i.d.	-	0.4	-	n.d.
o.d.	0.04	0.1	-	n.d.

[a]CERT in $289^{o}C$ water with 8 ppm O_2; n.d. = not determined.

815 287

TABLE 5. Degree of Sensitization in Type-304 Pipe (Heat M7772) Weld HAZ (5G Position) 0.5M H_2SO_4 + 0.01M KSCN at 30°C (P_a, C/cm^2)

Weldment Location	External Field Cell (2 cm^2 Area)	Conventional Laboratory Sample 2 cm^2 Area	0.5 cm^2 Area	IGSCC[a]
5G-1A				
i.d.	-	0.5	-	Yes
o.d.	0.1	0.3	-	Yes
5G-1B				
i.d.	-	0.8	4.4	Yes
o.d.	0.1	0.7	4.6	Yes
5G-1D				
i.d.	-	0.4	-	n.d.
o.d.	0.2	0.2	-	n.d.
5G-2A				
i.d.	-	0.2	-	Yes
o.d.	0.04	0.2	-	No
5G-2C				
i.d.	-	0.4	-	n.d.
o.d.	0.1	0.1	-	n.d.

[a]CERT in 289°C water with 8 ppm O_2.

815 288

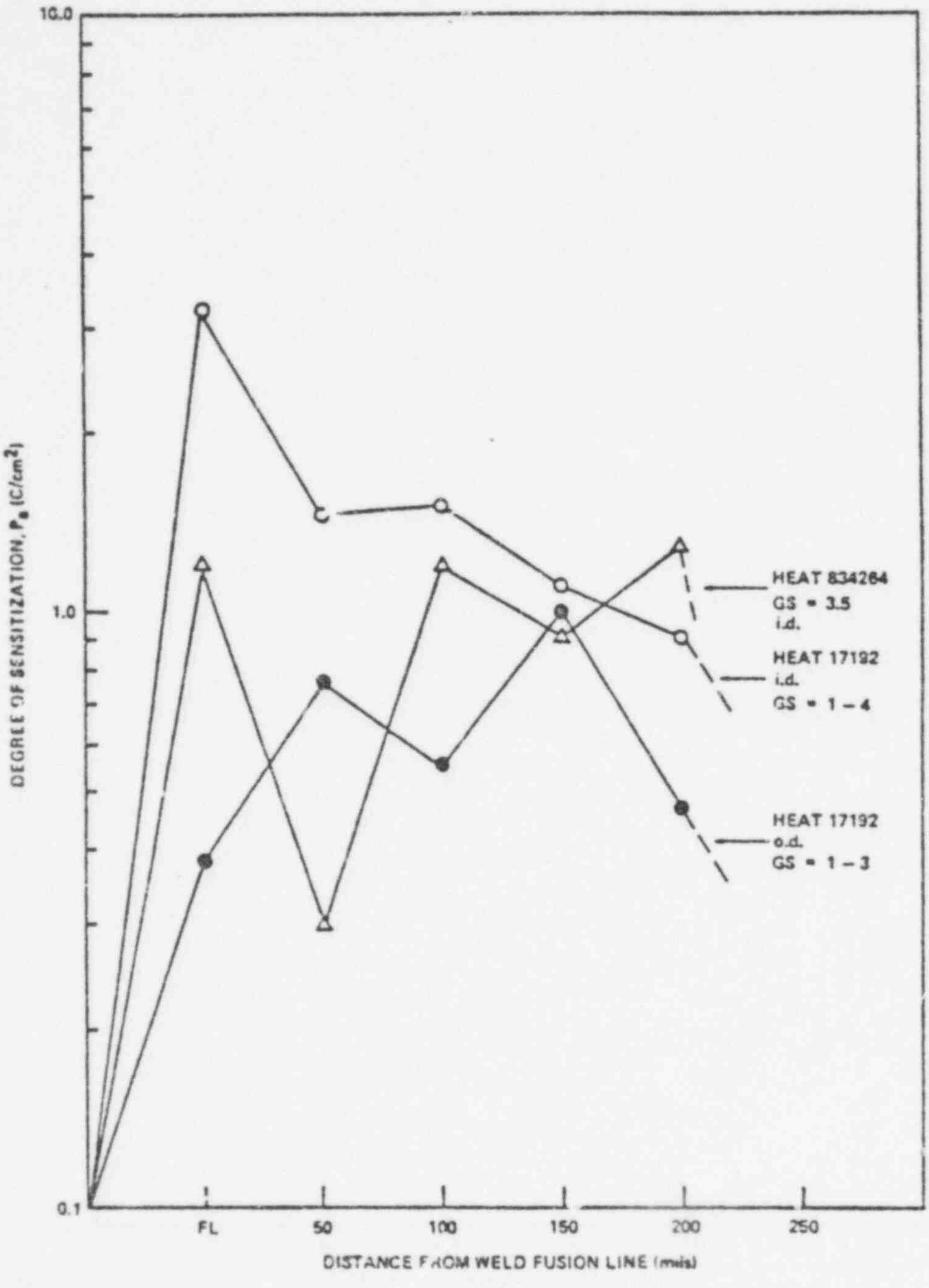

FIGURE 1. EPR HEAT AFFECTED ZONE WELD PROFILES
FOR 26-in. TYPE-304 ROLLED AND WELDED PIPE

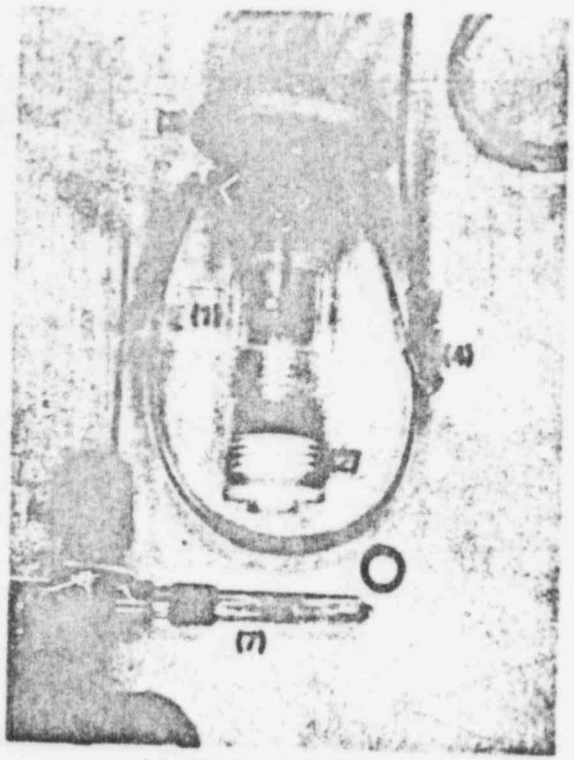

(a) DISASSEMBLED

(b) ASSEMBLED, ATTACHED TO PIPE

FIGURE 2. EXTERNAL CELL USED FOR CONDUCTING EPR MEASUREMENTS ON STAINLESS STEEL PIPING IN THE FIELD

THE COMPONENTS OF THE CELL INCLUDE:

1. BODY
2. END PIECE WITH "O"–RING SEAL
3. CAP
4. HOLD–DOWN STRAP
5. WORKING ELECTRODE CONNECTOR
6. PLATINUM COUNTER ELECTRODE
7. CALOMEL REFERENCE ELECTRODE
8. DEAERATION CAPILLARY

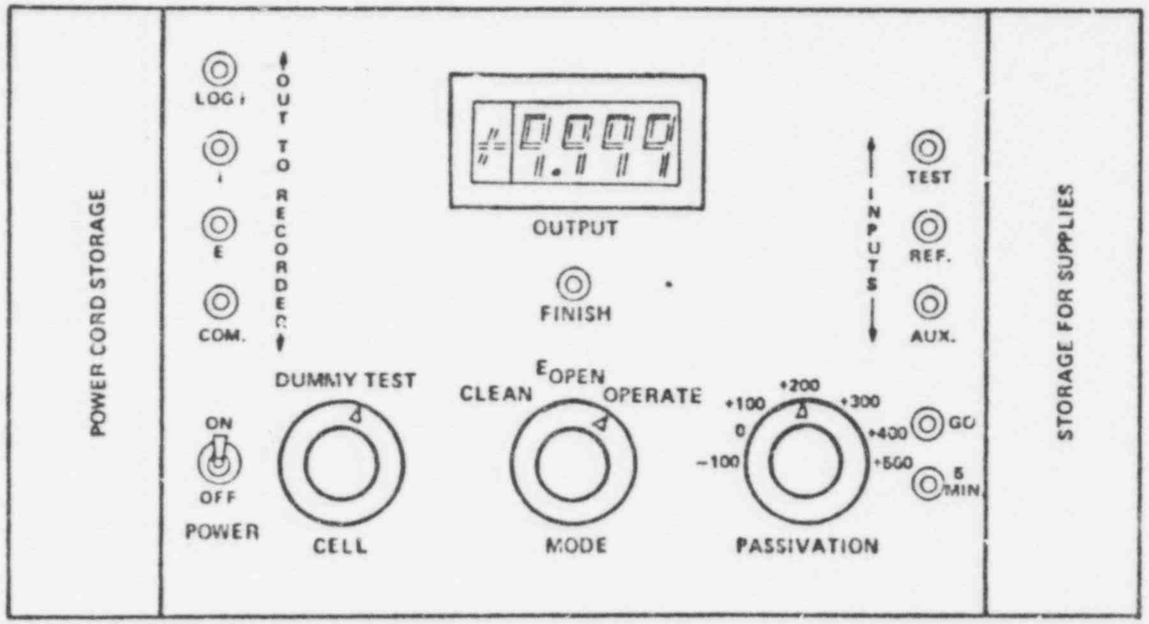

FIGURE 3. PORTABLE EPR POLARIZATION SYSTEM

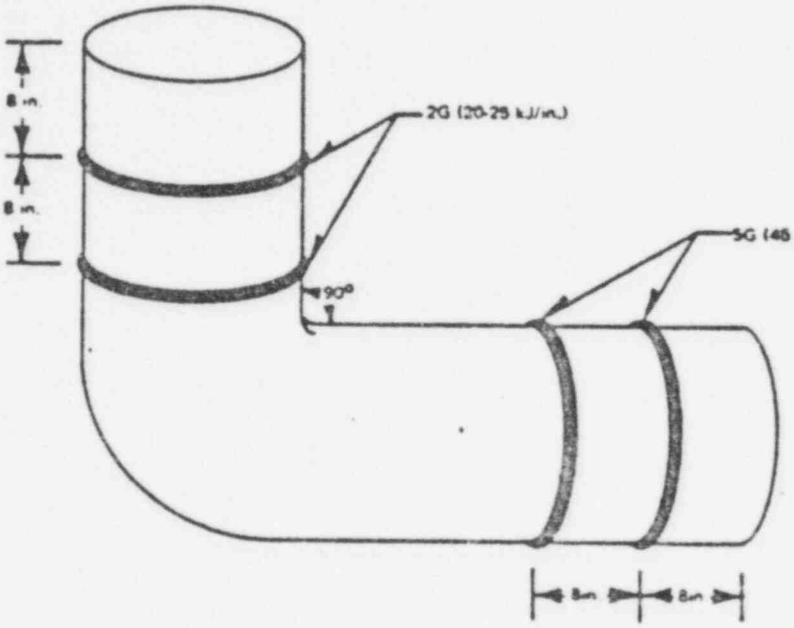

FIGURE 4. WELDED PIPE MOCKUP USED FOR EPR FIELD CELL LABORATORY QUALIFICATION (ELBOW FABRICATED FROM TYPE-304, HEAT 24.700; PIPING FROM HEAT M7772)

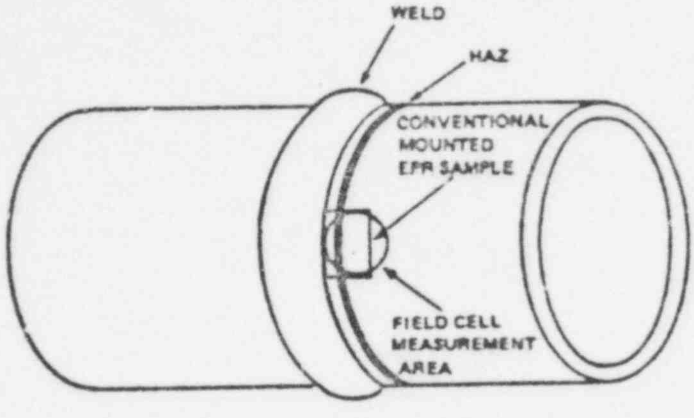

NOT TO SCALE

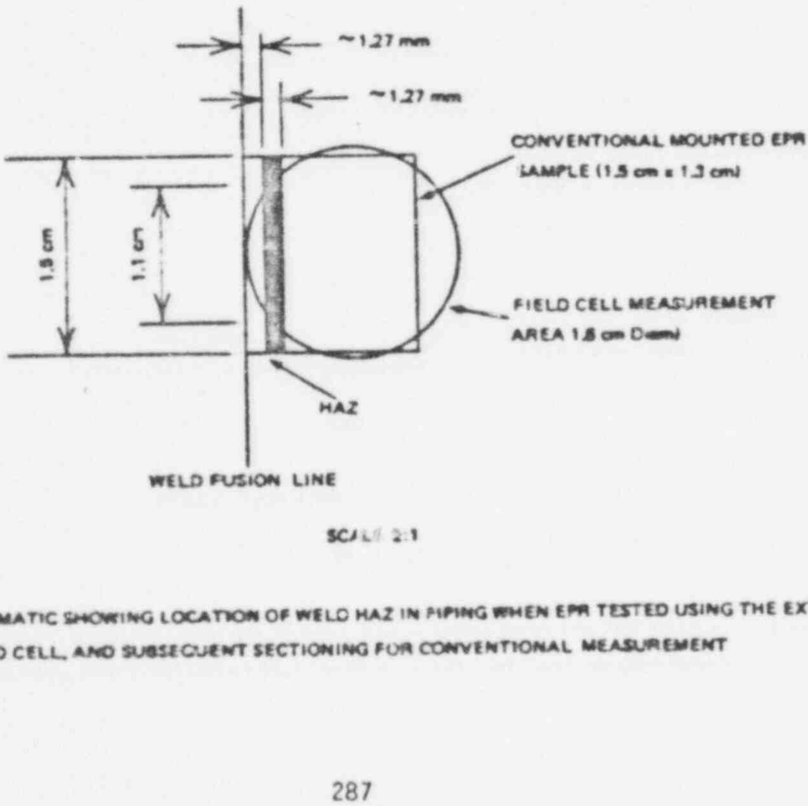

SCALE 2:1

FIGURE 5. SCHEMATIC SHOWING LOCATION OF WELD HAZ IN PIPING WHEN EPR TESTED USING THE EXTERNAL FIELD CELL, AND SUBSEQUENT SECTIONING FOR CONVENTIONAL MEASUREMENT

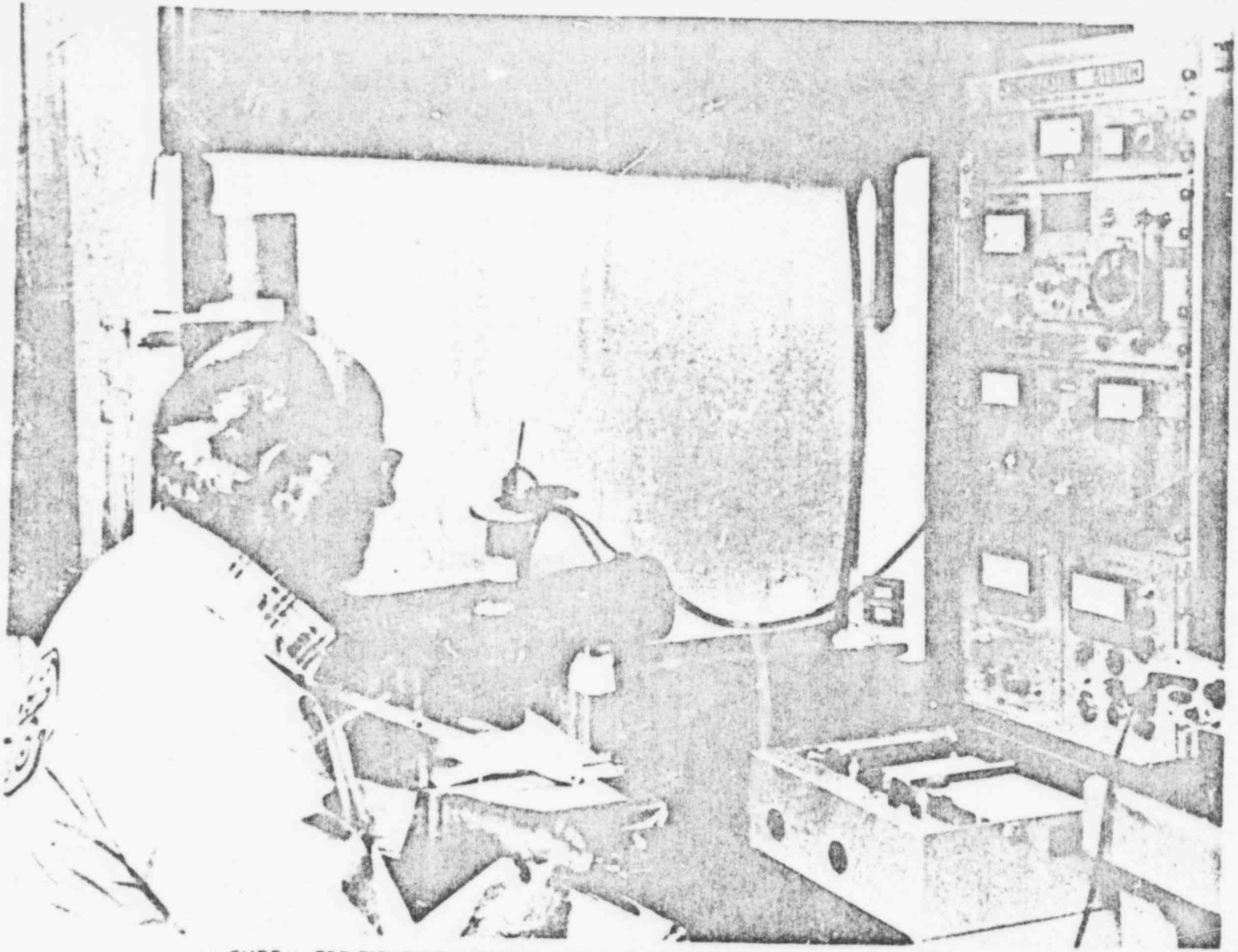

FIGURE 6. EPR FIELD CELL SHOWN ATTACHED TO STAINLESS STEEL WELDED PIPE AND CONNECTED TO LABORATORY POLARIZATION SYSTEM

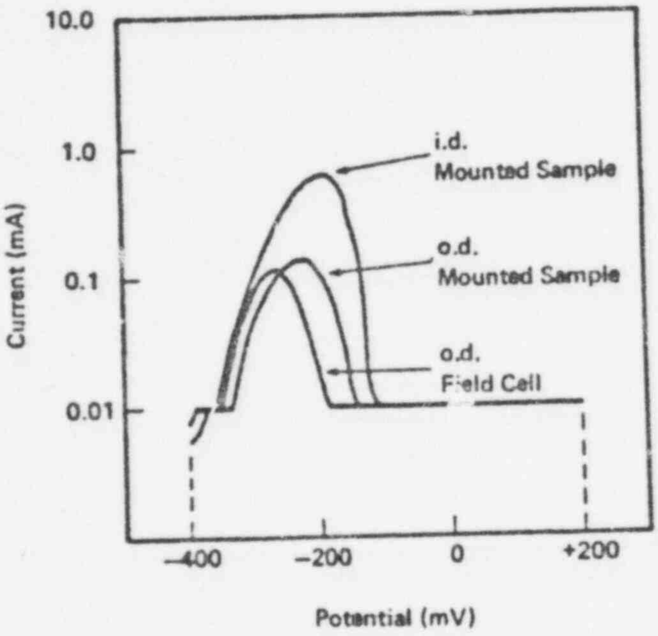

FIGURE 7. EPR CURVES FOR WELDED TYPE-304 (HEAT M7772) PIPE IN $0.5M\ H_2SO_4 + 0.01M$ KSCN AT 30^oC COMPARING THE EXTERNAL FIELD CELL MEASUREMENTS TO CONVENTIONAL LABORATORY MOUNTED SAMPLES

CONTRACT TITLE: Dosimetry Measurement Reference Data Base for LWR Pressure Vessel Irradiation Surveillance.

CONTRACTOR AND LOCATION: NBS, Gaithersburg, Maryland.

PRINCIPAL INVESTIGATORS: J. A. Grundl and E. D. McGarry

OBJECTIVE: Provide benchmark neutron field irradiations, a compendium of recommended neutron spectra, and associated reference data for benchmark testing of multiple-foil and other sensors employed in LWR pressure vessel dosimetry. Perform NBS fission chamber measurements in LWR-PV dosimetry benchmark fields. Participate in preparation of recommended practices for routine LWR-RPV dosimetry and surveillance which will include detector reference procedures and interpretation. Provide QA checked neutron fluence counting standards for round-robin testing of ASTM recommended practices. All of these activities provide traceable calibrations of LWR-PV surveillance dosimetry to NBS neutron standard fields and reaction rate measurement methods.

FY-77 SCOPE:

1. Begin investigation of calculated spectra and detector responses in LWR-PV neutron spectra.
2. Preliminary experiments with dosimetry sensors in operating power reactors.
3. Furnish certified nickel activation fluence dosimetry standards.

SUMMARY OF RESEARCH ACTIVITIES AND RESULTS:

Introduction. The assessment of radiation induced embrittlement of steel within reactor pressure vessels (RPV) involves neutron transport calculations and neutron fluence measurements in a variety of neutron environments. Appropriate field definitions are required for regions extending from the edge of reactor core to the outer boundry of the pressure vessel, for test regions in which pressure-vessel-steel sections are irradiated, and for benchmark neutron fields that provide detector calibration and measurement validation. The neutron exposures of vessel steels, obtained from such neutron-dosimetry activities, are interpreted in units of atom displacement appropriate for correlation with measured metallurgical property changes. The goal of the entire effort is to produce a set of ASTM Guides and/or Procedures that are fully validated and backed by an array of developed neutron sensors and benchmark fields, which are permanently available for measurement reference and sensor performance testing.

The responsibility of the National Bureau of Standards in this neutron-dosimetry improvement program includes: (1) application of existing benchmark fields at NBS to RPV dosimetry referencing; (2) preparation of a compendium that describes the RPV dosimetry benchmarks and test regions, including selected results of measurements performed in them; (3) assistance with investigations of dosimetry sensor performance in RPV test regions. Three activities associated with these responsibilities are summarized in the following paragraphs.

Certified Neutron Fluence Dosimetry Standards. In order to provide neutron fluence standards for surveillance dosimetry of the fast-neutron exposure of light water RPV's, the first of a series of neutron-fluence standards was distributed for the LWR-PV program in September 1977. The standards are nickel disks (12.5 mm dia.) that were exposed to a certified fission-spectrum fluence of 1.3 X 10^{13} n/cm^2.

Five neutron fluence standards were prepared by means of a certified irradiation of the nickel disks at the NBS ^{252}Cf Fission Neutron Indoor Irradiation Facility. Approximately 0.02 microcuries of the 71-day half-life ^{58}Co activity were generated by the $^{58}Ni(n,p)^{58}Co$ reaction. The fluence standards were distributed to five laboratories for activation counting. This is the first step in establishing traceable fluence calibrations for LWR-PV surveillance dosimetry. NBS will periodically issue more fluence standards of other types of dosimetry materials of interest to the program, and will evaluate the results reported by laboratories receiving the standards.

Fig. 1 shows fluence sensors mounted in light-weight aluminum holders at an accurately measured distance of 4.7 cm from the NBS Standard ^{252}Cf source in compensated flux geometry. This terminology refers to the practice of placing nearly identical sensors on opposite sides and equidistant from the source. The first-order distance error in the certified neutron flux is then associated with the separation of the detector pair and not the source-to-detector distance. Details of the minimum-mass, point source of ^{252}Cf are shown in Fig. 2.

Neutron field parameters for the irradiation, excluding neutron return from the environment are given in Table I. Neutron return from the environment, including irradiation support structures, and the resultant background are given in Table II.

Preliminary Experiments With Dosimetry Sensors in Operati[illegible] Power Reactors.

In an effort to obtain early in-situ experience with dosimetry measurements for LWR-PV environments, particularly those accompanied by metallurgical test specimens, opportunities to stimulate cooperative research with power reactor operators have been pursued on an international scale. To date, the significant accomplishments are as follows:

The Garigliano Reactor in Rome, Italy (a BWR, Dresden type) is operated by the ENEL, the Italian Atomic Power Authority. It provides an opportunity to place activation sensors and metallurgical specimens close to the inner surface of the pressure vessel and at an accelerated surveillance position near the thermal shield. Irradiation will be in progress during the power cycle that will end late in 1978. Two multi-sensor dosimetry capsules, sent to Italy in September 1977, contained the following HEDL fast-neutron dosimeters: ^{235}U, ^{238}U and ^{232}Th fission foils and a set of non-fission, threshold-type activation sensors including Fe, Ni, Sc, Ti and Al. This wide array of sensors should provide multiple integral-fluence measurements suitable for spectrum unfolding. The purpose of the Garigliano irradiations is to investigate the performance of a wide variety of sensor materials in a BWR-PV neutron environment and to obtain early measurements that can be compared with calculated RPV-related spectra.

NBS has negotiated through the University of Arkansas to obtain approval to place HEDL dosimetry capsules in the RPV cavity of the Arkansas Power and Light Company, Unit #1, PWR Reactor at Russelville, Arkansas. This experiment is a joint venture involving the plant staff, the University of Arkansas, NBS and HEDL. The dosimeters will be positioned in a detector well midway in the cavity outside of the pressure vessel for an irradiation of approximately four months. The foil packages provided by HEDL consist of twelve separate foils including Fe, ^{235}U, ^{238}U, Ti, Ni, Co, Mn, Sc, Cu, Ag/Al, S and Ta/Al. Presently, the irradiation is scheduled to start in mid-January 1978. The purpose of this experiment is to obtain some neutron field information in a RPV-related region almost untouched by measurement.

Dosimetry capsules were sent to Mol, Belgium via NBS for LWR-PV surveillance tests in the BR-3 Reactor this coming cycle, to begin late in 1977. These dosimeters represent a cooperative effort involving HEDL-GE dosimetery capsules, HEDL-Al capsules and individual HEDL dosimeters encapsulated in vanadium for insertion into a CEN/SEK outer capsule. An objective of the BR-3 irradiation is to intercompare multi-sensor results from the three different capsule designs and arrays of sensors.

Neutron Spectra and Integral Detector Response in RPV Radiation Environments. Collection and organization of information for a compendium of RPV-related neutron environments has begun. A preliminary set of integral sensor responses has been calculated in a straightforward and consistent manner. The relationship of these sensor responses to spectrum characteristics and to the fission neutron spectrum, taken as a reference, have been briefly evaluated.

Spectrum-averaged cross sections for six RPV-related neutron environments have been calculated using the DETAN code, which performs simple interpolations and extrapolations of the course-group output spectrum of neutron transport computations. As an example, spectrum calculations supplied by ENEL for the Garigliano BWR Reactor are shown in Fig. 3. Because of the course-group structure relative to the rapidly varying cross sections of threshold reactions, no meaningful threshold detector response can be predicted directly from such a computational output. A first-order, 620-group linear interpolation on a lethargy scale is performed with the DETAN code (see Fig. 4) and is the basis for evaluating spectrum-averaged cross sections. Table III presents conventional full-spectrum-averaged cross sections for the low-energy response sensors $^{239}Pu(n,f)$ and $^{235}U(n,f)$ and for the threshold reactions $^{238}U(n,f)$, $^{58}Ni(n,p)$ and $^{54}Fe(n,p)$. The energy-dependent cross sections employed in the DETAN code are from the ENDF/B-IV dosimetry file.

There is a wide variation in the ^{239}Pu and ^{235}U fission responses, reflecting strong spectral component differences in the intermediate and low-energy ranges. The threshold reactions also show a wide variation with no apparent pattern. However, such full-spectrum-averaged cross sections are not the most appropriate for threshold detectors since the flux integral is dominated by portions of the spectrum where the detectors do not respond. Detector response patterns are better indicated by truncated cross sections defined by

$$\bar{\sigma}(E>E_p) = \int_{E_p}^{\infty} \sigma(E)\phi(E)dE \Big/ \int_{E_p}^{\infty} \phi(E)dE$$

where E_p is the truncation energy above which a fraction, or percentile P, of the detector response occurs.

Table IV shows truncated cross section computed according to the above equation for the three common threshold reactions used in RPV neutron dosimetry. Included in the table are median response energies and energy response ranges for each detector. The truncation energy was set at P = 0.95; that is, the cross sections listed are spectrum averaged above the energy in each spectrum where 95% of the detector response occurs. The sensor response ranges given at the end of the table are little dependent upon spectrum shape and the nominal values listed are within a few tenths of an MeV of the specific values for each spectra.

The lowest threshold detector, $^{238}U(n,f)$, displays (with one exception) truncated cross sections for the inner PV wall spectra that depart by less than 3% from the average of the four values. The average value of 0.59 barn departs from the fission spectrum value of 0.54 barn by less than 10%. The higher threshold sensors Ni and Fe, with similar response ranges, show equivalent cross sections to within $\pm$ 6% for the same four inner wall spectra. The average value, however, departs from the fission spectrum values by more than 40%. Referring to Fig. 4, these simple comparisons can be seen as indexes of two characteristics of the four RPV inner wall spectra: a fission-spectrum-like slope from ~ 2 MeV to

~ 3.5 MeV and an interruption or shelf in this slope in the ~ 3.5 to 5 MeV energy range. The similarity of the ^{238}U truncated cross sections to the fission spectrum value of that cross section provides an index to the fission spectrum slope and the two threshold-sensor cross sections index the shelf component. These discernible connections between course-group calculations and the responses of integral detectors suggest that difficult and expensive reactor physics calculations may be quantitatively indexed by means of a small set of integral detectors whose responses are referenced against relevant benchmark neutron fields such as the fission spectrum. It is to be noted that these relationships are not apparent in the full-spectrum averaged cross sections of Table III.

Two PWR environments ("Westinghouse" and McGuire) present truncated cross sections differently related to the underlying fission spectrum values taken as a reference. These spectra must be examined further to understand the difference because RPV exposure fluences depend strongly on these spectrum shapes. For example, a fast-neutron fluence estimate for a reactor pressure vessel that would employ one or the other of the two PWR inner wall calculations (i.e., "Westinghouse" or "EPRI") to convert the common $^{54}Fe(n,p)$ ^{54}Mn response to fluence could differ by more than 20%. Because of much closer agreement among the other four spectra, for presumably equivalent environments, such a difference may be related to subtleties in the methods of calculation rather than real spectrum differences.

PLAN OF RESEARCH FOR FUTURE YEARS:

NBS will continue to provide certified-fluence irradiations in standard benchmark neutron fields, investigate and compile field-characterization data and dosimetry sensor-response data, and perform

NBS fission-chamber measurements to support the LWR-PV Surveillance Dosimetry Program. NBS will also continue to participate in the preparation of ASTM Standard Guides and Practices for routine surveillance of the neutron exposures of pressure vessels as required by this NRC program.

TABLE I. CALIFORNIUM-252 FISSION NEUTRON FIELD PARAMETERS AND UNCERTAINTIES FOR $^{58}Ni(n,p)^{58}Co$ NEUTRON FLUENCE DOSIMETRY STANDARDS

Free-field fission neutron flux (4.7cm source-detector distance)	1.8×10^{7} n/cm^2 sec
Free-field neutron fluence for 360 hr exposure	2.3×10^{13} n/cm^2
Specific activity for detector pair at end of irradiation	0.6×10^{-18} dps/nucl
Source decay during irradiation	0.5%
Source capsule scattering (inelastic plus net elastic inscatter)	1.1%
Error components for free-field fission neutron flux (1 σ)	
Source strength	± 1.1%
Distance measurements	± 0.6%
Source capsule and support scattering	± 0.7% (max.)
Total free-field flux error (rms sum)	± 1.4% (1 σ)

TABLE II. CORRECTIONS FOR IRRADIATION OF NICKEL FLUENCE STANDARDS IN THE INDOOR CALIFORNIUM-252 FISSION NEUTRON FIELD

Environmental return flux background above 0.4 eV for a distance to nearest background of 2.3 m	
Albedo from boundries	< 0.07%
Source and detector support structures	0.3 %
Air scatter	< 0.1 %

815 304

TABLE III. FULL-SPECTRUM AVERAGED CROSS SECTIONS CORRESPONDING TO SIX COMPUTED PRESSURE VESSEL SPECTRA

TEST REGIONS	$\bar{\sigma}(E>0.4eV)$ in barns				
	low-energy reactions		threshold reactions		
	$^{239}Pu(n,f)$	$^{235}U(n,f)$	$^{238}U(n,f)$	$^{58}Ni(n,p)$	$^{54}Fe(n,p)$
RPV inner wall					
BWR, EPRI	11.5	9.25	0.155	.0697	.0569
BWR, GARIGLIANO (ENEL).	6.88	6.21	0.183	.0795	.0640
BWR, BIG ROCK POINT . .	11.18	10.38	0.140	.0606	.0488
PWR, EPRI	12.9	10.4	0.129	.0531	.0428
PWR, WESTINGHOUSE . . . (near inner wall)	19.2	16.1	0.0477	.0136	.0101
mid-cavity outside RPV					
PWR, McGUIRE	11.92	10.12	0.0168	.00482	.00361
Energy response range (MeV)	---	---	(1.2 - 7.3)	(1.7 - 8.1)	(2.3 - 8.6)

TABLE IV. TRUNCATED THRESHOLD REACTION CROSS SECTIONS IN COMPUTED PRESSURE VESSEL SPECTRA

TEST REGIONS	$\bar{\sigma}(E > E_p)$ in barns, for P = 0.95		
	$^{238}U(n,f)$	$^{58}Ni(n,p)$	$^{54}Fe(n,p)$
PRV inner wall			
BWR, EPRI	0.61	0.39	0.37
BWR, GARIGLIANO (ENEL). .	0.58	0.35	0.33
BWR, BIG ROCK POINT . . .	0.58	0.35	0.33
PWR, EPRI	0.59	0.35	0.34
PWR, WESTINGHOUSE . . . . (near inner wall)	0.51	0.21	0.24
mid-cavity outside RPV			
PWR, McGUIRE	0.40	0.19	0.28
fission spectrum			
NBS segment fitted . . .	0.54	0.25	0.24
*energy response range (MeV)	1.2 - 7.3	1.7 - 8.4	2.3 - 8.6
median response energy	2.5	4.3	4.8

* 5% of detector response is below E_{min} and 5% above E_{max}; one half of the detector response is above the median response energy.

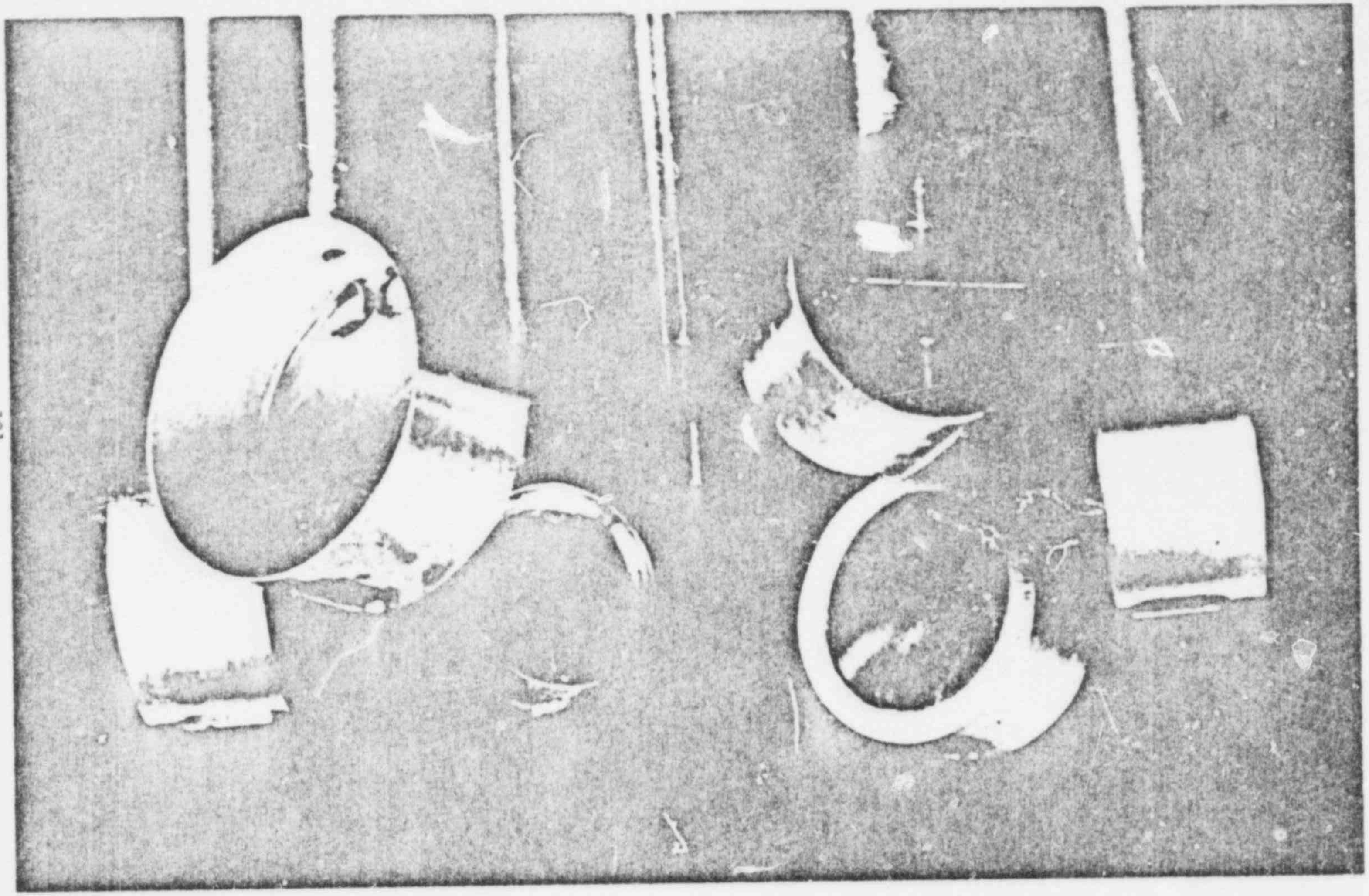

Fig. 1. Experimental arrangement of foils for a certified neutron irradiation to produce neutron fluence standards at the NBS Indoor Californium-252 Fission Neut: ı Irradiation Facility.

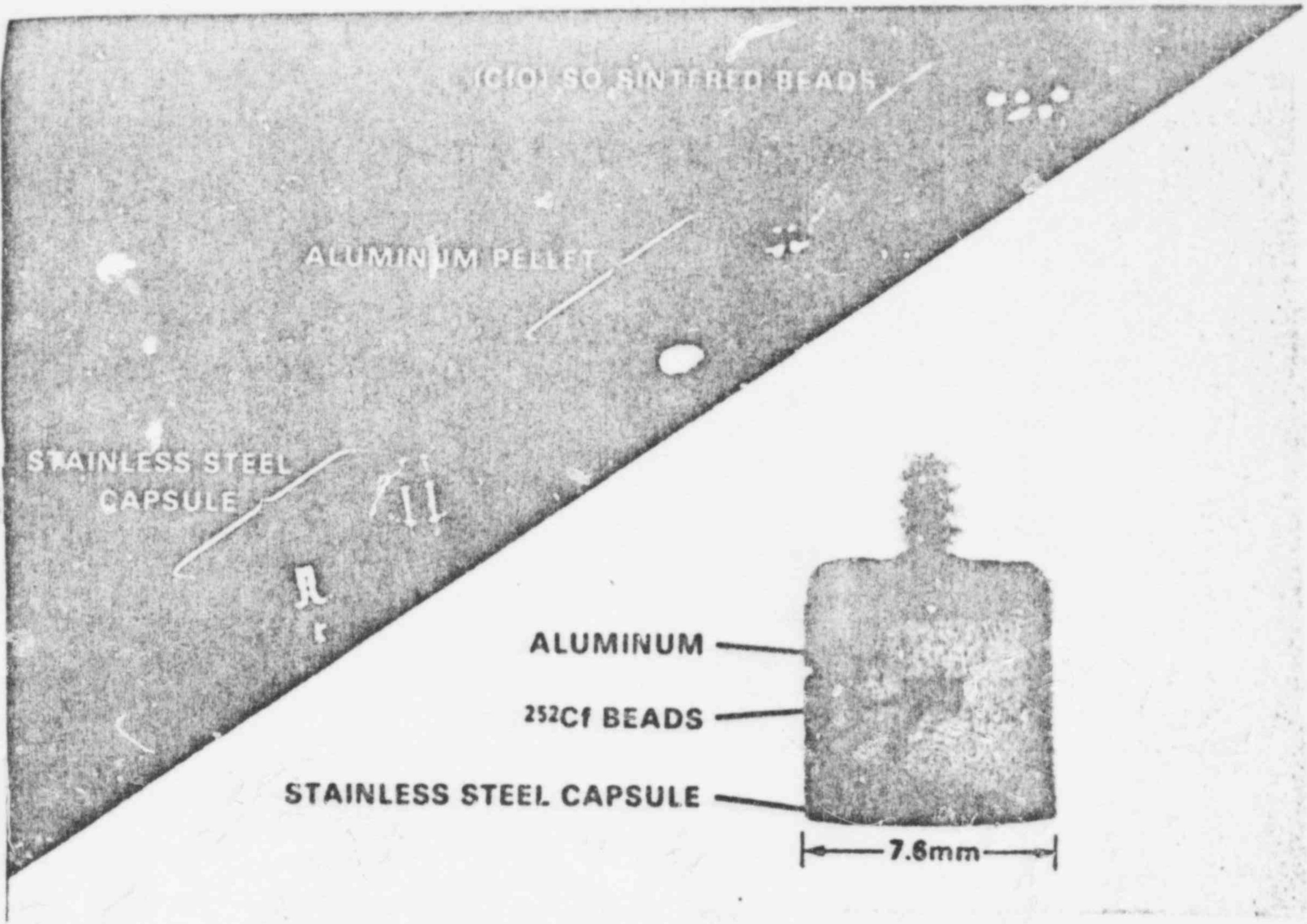

Fig. 2. NBS Standard Californium-252 Fission Neutron Source.

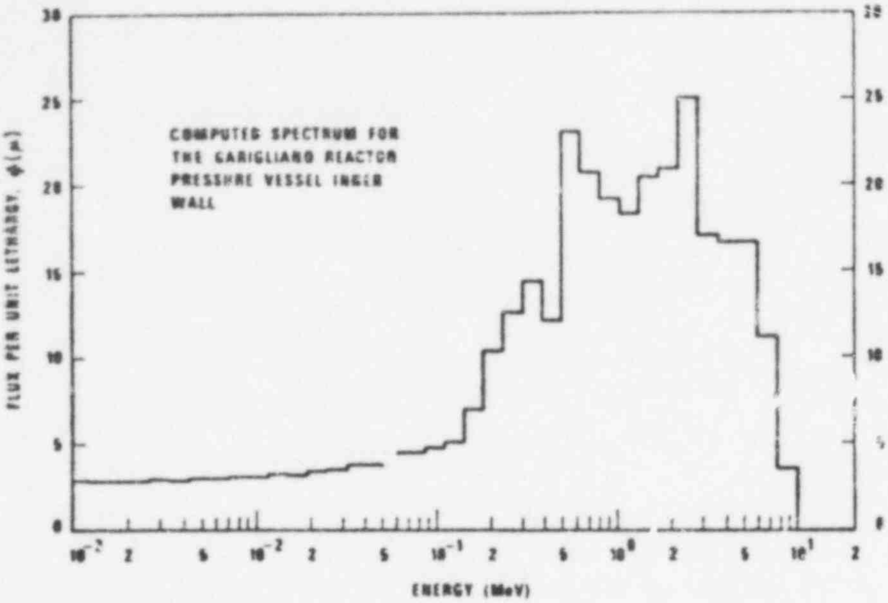

Fig. 3. Histogram of the calculated spectrum for the inner pressure vessel wall of the Garigliano, Dresden-type BWR.

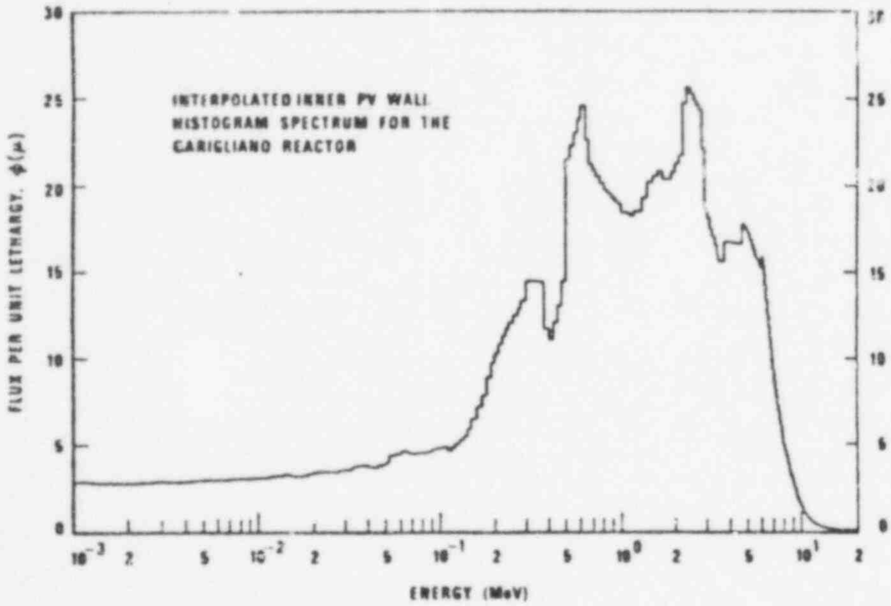

Fig. 4. Fine-group spectrum constructed by the DETAN code from the histogram shown in Fig. 3.

POOR ORIGINAL

Contract Title: LWR Pressure Vessel Irradiation Surveillance Dosimetry

Contractor and Location: HEDL, Richland, Washington

Principal Investigator(s): W. N. McElroy, R. Gold, G. L. Guthrie, and E. P. Lippincot
D. G. Doran, L. S. Kellogg, J. O. Schiffgens, F. H. Ruddy
and R. L. Simons are principal contributors.

OBJECTIVE:

Preparation of updated and improved ASTM Standards for LWR pressure vessel (PV) irradiation surveillance dosimetry. Make measurements in reactor "Standard, Reference, and Controlled Environment benchmark fields" and "test regions" for the validation/calibration of the recommended ASTM dosimetry techniques and associated damage exposure an correlation procedures.

FY 77 SCOPE:

A. Define completely the scope of the measurement program for each fiscal year, covering proposed irradiation, calibration, and validation studies in selected neutron fields. Include the scope in an "Analysis Before Test" document for NRC that also provides the technical approach, interfaces, experimental test plan, analyses, and outline of results for use by NRC.

B. Define required updated and improved LWR-PV surveillance dosimetry ASTM Standards and initiate writing of these standards.

C. Recommend and fabricate state-of-the-art passive LWR-PV surveillance dosimetry capsule sensor monitors:
Radiometric Monitors (RM); Solid State Track Recorder (SSTR) Monitors; Helium Accumulation Flux/Fluence Monitors (HAFM); Damage Monitors (DM); and Temperature Monitors (TM).

D. Recommend and fabricate passive multiple sensor monitor sets and capsules for irradiation in approved reactor "benchmark fields" and "test regions".

E. Define active and passive sensor measurement techniques to be used for validation, calibration studies in approved reactor "benchmark fields" and "test regions".

F. Initiate procurement, installation, check-out, and calibration of active and passive sensor measurement equipment associated with C, D, and E above.

SUMMARY OF RESEARCH ACTIVITIES AND RESULTS:

I. Background

The assessment of the radiation-induced degradation of material properties in a power reactor pressure vessel (RPV) requires accurate definition of the neutron field from the outer region of the reactor core to the outer boundaries of the pressure vessel [1-10]. The neutron flux and spectrum measurement problems are associated with two distinct components of RPV irradiation surveillance

815 310

procedures: (1) application of comprehensive calculational estimates of the neutron fluence delivered to the first half thickness of the vessel steel; and (2) relationship between metallurgical test specimens irradiated at accelerated neutron flux positions and the pressure vessel [1-7, 10].

The first component requires validation/calibration experiments in a variety of neutron irradiation test facilities including RPV mock-ups and related benchmark neutron fields. The benchmarks serve in particular as a permanent measurement reference for neutron flux detection techniques which are continually under development and widely applied by laboratories of quite different levels of capability [1-6, 9, 12-19]. The second component requires a serious extrapolation of an observed neutron-induced mechanical property change from the test specimen position to positions inside of the pressure vessel [1-4, 6-7, 10, 14, 20-21]. The neutron flux at the vessel is nearly one order of magnitude lower than at the specimen position and the neutron spectrum is substantially altered.

In order to meet the radiation monitoring requirements, a variety of neutron flux and fluence detectors are employed, most of which are passive [1-6, 10, 12, 14, 20-23]. Each detector must be validated for application to the RPV problem of low flux and degraded neutron spectrum. Required detectors must respond to neutrons of various energies in order to determine multigroup spectra well enough to provide adequate damage response estimates [2-4, 14, 18, 20, 21].

In orde to attack these measurement issues, a vigorous worldwide research program is underway with the following aims [1, 11, 12, 13, 15, 24-27]: (1) improve and review existing neutron dosimetric techniques; (2) perform high-quality measurements in operating commercial power reactor "test regions" and selected "benchmark fields"; and (3) establish proper measurement and calculational standards specifically for monitoring radiation effects on reactor pressure vessels. The goals of this strategy are to validate and calibrate dosimetry techniques as well as guide required neutron field calculations and to correlate changes in material properties with the characteristics of the neutron radiation field. The accepted accuracy goal for the flux/fluence integral parameters is set at $\pm(2\text{-}5)\%$ (1σ), although a higher upper bound uncertainty could become acceptable [2-4, 14, 15].

The results of this measurement-calculation strategy will be made available for the use of the nuclear industry as ASTM Standards. Federal Regulation Guide 10CFR50, Part 10, already calls for adherence to several ASTM Standards for incorporation of flux monitors and for post-irradiation evaluation. First drafts of revised and new standards, carefully structured to be up-to-date, flexible, and above all consistent, are in preparation [2].

In order to achieve the objectives of this NRC contract, strong operative links have been established with other national and international LWR pressure vessel surveillance program work. The strongest ties are those established with: The NRC LWR-PV and other programs at ORNL [2, 4, 9, 26-29]; the Center for Radiation Research Neutron Standards Programs at the National Bureau of Standards (NBS) [2, 4, 13, 17, 18, 30-34]; the Cross Section Evaluation Working Group (CSEWG) "ENDF/B - Special Applications Files" programs at the National Neutron Cross Section Center (BNL) [24]; EPRI programs [3, 4, 14, 15]; and the Centre d'Etude de l'Energie Nucleaire - Studiuentrum Voor Kern Energie (CEN/SCK) Standard Neutron Field programs at Mol, Belgium [3, 4, 16, 17, 19, 30, 35].

II. FY 1977 Accomplishments

A. The objectives, scope, and technical approach for this program were defined in an "Analysis Before Test" document and program management charts submitted to NRC. Three program subtasks were defined: A) Benchmark Fields; B) Recommended Practices and Procedures; and C) Damage Exposure and Correlation Procedures. Included were 1) expected results and applications of the program's three main subtasks, 2) a research plan and schedule for each of these subtasks, 3) interfaces with other national and international related program work, and 4) in the appendices, background information on programs and/or specific subjects that support the technical approach. The degree and success of the neutron field validation/calibration studies will determine what final program goal accuracies can be reasonably expected to be achieved on a routine basis by reactor designers and vendors, the utilities, and supporting research and/or service laboratories that will make use of the established ASTM Recommended Standards, see the Figures 1 and 2 Flow Charts.

As a part of the program definition phase, a foreign travel trip report was completed which documents HEDL, ORNL, and NRC efforts to exchange information and explore possible interlaboratory work which could be established with U. K., French and German laboratories performing LWR-PV research and development work.

B. With reference to Figures 1 and 2, the main result of this program will be the establishment of a new updated set of validated/calibrated ASTM Standard Recommended Guides and Practices and Standard Methods of Analysis [20] for LWR-PV irradiation test and surveillance programs. The initially identified standards include:

- METHODS OF SURVEILLANCE & CORRELATION

  Standard Recommended Practice for
  EXTRAPOLATING REACTOR VESSEL SURVEILLANCE DOSIMETRY RESULTS

  This practice will specify procedures for the extrapolation/interpolation of dosimetry and metallurgical surveillance data from test reactor and accelerated surveillance locations to the pressure vessel wall and different positions within the vessel, such as the 1/4 thickness.

  Standard Recommended Practice for
  CHARACTERIZING NEUTRON EXPOSURES IN FERRITIC STEELS IN TERMS OF DISPLACEMENTS PER ATOM, INCLUDING ASTM ENDF/A DPA FILE

  This displaced atom (dpa) exposure unit practice, including the specification of an ASTM ENDF/A file, will specify procedures for reporting metallurgical irradiation effects data on a common damage production exposure basis.

Standard Recommended Practice for
DAMAGE CORRELATION FOR REACTOR VESSEL SURVEILLANCE

The damage correlation practice will specify procedures to effect the best correlation between available metallurgical and dosimetry data. It may differ from the dpa practice by including flux, temperature, and possibly fluence (i.e. microstructural evolution) effects. That is, it will consider the separate or combined effects of irradiation variables (flux level, fluence, temperature, metallurgical state, etc.) on the development of embrittlement.

- SUPPORTING METHODOLOGY

Standard Recommended Guide for
APPLICATION OF MULTIPLE SENSOR FLUX-FLUENCE-SPECTRAL DETERMINATION CODES

This will contain descriptions and specifications for procedures and codes for unfolding multiple sensor data and associated error propagation. Selection criteria for dosimeter sets, cross section libraries, and input flux-spectra will be specified.

Standard Recommended Guide for
APPLICATION OF ASTM ENDF/A CROSS SECTION AND ERROR FILE

The procedures for using and establishing ASTM ENDF/A cross section and error data files for the analysis of single or multiple foil sensor measurements will be specified.

Standard Recommended Guide for
SENSOR SET DESIGN AND IRRADIATION FOR REACTOR VESSEL SURVEILLANCE

The selection, design and irradiation of dosimeter sensors and sets, covers, and capsules will be specified, including quality control of constituents and mass assay.

Standard Recommended Guide for
APPLICATION OF NEUTRON TRANSPORT METHODS FOR REACTOR VESSEL SURVEILLANCE

The principal aim is to use present "state-of-the-art" technology to arrive at consistent calculational tools and data sets which can be validated/calibrated against "benchmark field" integral experiments.

Standard Recommended Guide for
BENCHMARK TESTING OF REACTOR NEUTRON DOSIMETRY

Application of well-characterized neutron fields for the validation/calibration of individual sensors and multiple sensor sets will be described and evaluated in terms of LWR-PV requirements. Procedures for flux transfer, spectral index calibration, flux perturbation corrections, photofission corrections, and sensor self absorption and burn-in and -out corrections will be delineated. Selected results will be documented in a compendium of standard, reference, and controlled environment benchmark fields.

- SENSOR MEASUREMENTS

Standard Method for
ANALYSIS OF RADIOMETRIC MONITORS (RM) FOR REACTOR VESSEL SURVEILLANCE

Measurement procedures for RM monitors will be specified. Nondestructive and destructive radiochemistry methods for determining reactions and reaction rates will be covered including systematic effects such as interference from activation products, monitor selfshielding, branching ratios and fission yields. Proposed individual sensor monitors are identified in Table I.

Standard Method for
ANALYSIS OF SOLID STATE TRACK RECORDER (SSTR) MONITORS FOR REACTOR VESSEL SURVEILLANCE

Measurement procedures for SSTR monitors will be specified. Methods for determining reactions and reaction rates will be covered including associated systematic effects. Proposed individual sensor monitors are identified in Table I.

Standard Method for
ANALYSIS OF HELIUM ACCUMULATION FLUX/FLUENCE (HAFM) MONITORS FOR REACTOR VESSEL SURVEILLANCE

Measurement procedures for HAFM monitors will be specified. Methods for determining reactions and reaction rates will be covered including associated systematic effects. Proposed individual sensor monitors are identified in Table I.

Standard Method for
ANALYSIS OF DAMAGE MONITORS (DM) FOR REACTOR VESSEL SURVEILLANCE

Measurement procedures for DM monitors will be specified. Methods for determining exposure units will be covered including associated systematic effects. Proposed individual sensor monitors are identified in Table I.

Standard Method for
ANALYSIS OF TEMPERATURE MONITORS (TM) FOR REACTOR VESSEL SURVEILLANCE

Measurement procedures for TM monitors will be specified. Methods for determining temperature will be covered including associated systematic effects. Proposed individual sensor monitors are identified in Table I.

A steering committee for the development of the ASTM Standards has been established. The present membership is:

W. N. McElroy (Co-chairman) and G. L. Gutnrie (HEDL);
J. A. Grundl (Co-chairman) and E. D. McGarry (NBS);
F. B. K. Kam (ORNL); and A. Fabry (CEN/SCK).

Outlines for most of the standards have been prepared and a first draft of the "Standard Recommended Practice for Characterizing Neutron Exposures in Ferritic Steels in Terms of Displacements Per Atom" was completed by D. G. Doran of HEDL. An important review study related to the "Multiple Sensor Flux-Fluence-Spectral Determination Codes" was completed by C. A. Oster of BNW [36].

C. With Reference to Table I and Figure 2, a preliminary list of LWR-PV surveillance dosimetry sensor monitors has been recommended. The selection of these monitors was based on a study of: (1) available state-of-the-art sensor monitor reactions, including those in current use or measurable from metallurgical surveillance specimens, (2) sensor neutron energy response range, (3) sensor reaction products, very long half life and stable products are most desirable to minimize or eliminate the need to know the reactor power time history, (4) availability (present or planned) of sensor nuclear data on the ENDF/B - Special Application and Fission Yield Files, and (5) sensor monitor physical properties and state-of-the-art reaction product measurement capabilities.

Acquisition of an inventory of RM, SSTR, and HAFM sensor monitor materials was initiated and some preliminary QA work was completed. Most RM sensor monitors or materials are available through the Fast Reactor Material Dosimetry Center (FRMDC) at HEDL. Acquisition for those not available was started. SSTR fissionable deposit preparation for irradiation in the Browns Ferry (BWR) and McGuire (PWR) ex-vessel cavities was started at HEDL. A listing of the isotopes and deposit thicknesses is included in Table II. Figure 3 is a schematic representation of how a fissionable deposit and track recorder are assembled in the fabrication of a SSTR. A contract was let to Atomics International (AI) for the fabrication of encapsulated HAFM sensor monitors. H. Farrar IV of AI will be reponsible for the preparation and analysis of HAFMs. Figure 4 is a schematic representation of how a HAFM is fabricated. Presently, the DM and TM sensor monitors are being studied and evaluated as a joint effort between HEDL staff members, G. R. Odette of UCSB, and A. Fabry of CEN/SCK, but specific action to establish monitor inventories at HEDL was not initiated in FY 77.

D. Preparation and irradiation of passive individual and/or multiple sensor sets and capsules was initiated in a number of approved reactor "benchmark fields" and "test regions". The monitors or monitor sets used for these neutron fields and the status of the validation/calibration work are identified in Table III. Figures 5 and 6 show the as-built dosimetry for the BR-3 "test region" validation/calibration studies. A SSTR ($\sim$45 nanogram/cm^2 deposit of natural uranium on a stainless steel backing) was also included as a separate individual monitor for irradiation in the BR-3 ex-vessel cavity "test region". The HEDL—AI RM, HAFM, and SSTR sensor monitors will be irradiated with additional dosimetry provided by the CEN/SCK laboratory, which has the primary responsibility for the coordination of the BR-3 "test regions" validation/calibration studies.

E. The active and passive sensor measurement techniques selected for the validation/calibration studies in approved reactor "benchmark fields" and "test regions" are identified in Tables IV and V. Except for minor equipment needs, available measurement and data acquisition and analysis systems were determined to be adequate for RM, HAFM, DM, and TM sensor monitors. New equipment was determined to be needed, however, for the active neutron and gamma-ray spectrometry and passive SSTR measurement systems.

F. Required new active and passive sensor monitor measurement equipment is identified in Table VI.

SSTR specimens from LWR-PV irradiations will possess very high track densities. Specialized instrumentation is required, therefore, for quantitative track scanning. In the design of this instrumentation, the M/SP is a crucial interface used to control and process signals for the SEM track scanning system. Specifications for the M/SP were prepared and the component parts were ordered in FY 77. Such components as the digital-to-analog convertor (DAC's), analog-to-digital converter (ADC's), operational amplifier (OA's) and fast memory chips have been partially received.

The preparation of specifications for the "Dual Parameter Computer Based Pulse - Height Multichannel Analyzer" for the active spectrometry measurements was initiated in late FY 77 and was completed in early FY 78. Bids are expected in early CY 78 with equipment acquisition to follow soon thereafter.

III. FY 1977 Technical Meetings and Publications

HEDL and participating laboratory staff members helped organize and participated in a number of important and Professional Society, Consultants, Specialists, Workshops, and Task Group Meetings which focused on different aspects of the problems associated with the standardization of reactor dosimetry and damage analysis methods and data. Those meetings with most relevance to the current NRC LWR-PV Program are:

- November 1976 - IAEA Consultants' Meeting on Integral Cross Section Measurements in Standard Neutron Fields, IAEA, Vienna, Austria [15-18].
- November 1976 - IAEA Specialists' Meeting on Radiation Damage Units, Harwell, England [25].
- March 1977 - CSEWG Dosimetry Task Group Meeting, NBS, Washington D. C., U. S. A. [24].
- March 1977 - International Specialists' Symposium on Neutron Standards and Applications, NBS, Washington D. C., U. S. A. [13, 14].
- October 1977 - Second ASTM-Euratom Internation Symposium on Reactor Dosimetry, Palo Alto, California, U. S. A. [1-9, 22-24, 30-36].

- October 1977 - IAEA Technical Committee Meeting on Current Status of Neutron Spectrum Unfolding, Oak Ridge, Tennessee, U. S. A. [27].

IV. Plan of Research for Future Years

A contract was let to ORNL in late FY 77 for the design and fabrication of a PWR pressure vessel simulator benchmark for dosimetry validation/calibration studies. This PWR-PV mockup will be installed in the low flux level ORR-Pool Critical Assembly (PCA). A brief description of this facility as well as the complementary high flux level ORR-Pool Side Facility (PSF) mockup, which will be used for both dosimetry and damage exposure and correlation validation/calibration studies, is provided in Appendix A. NRC will provide direct contract support to ORNL for (1) the checkout and operation of the ORR-PCA and (2) the design of the ORR-PSF pressure vessel simulator in FY 78. Construction and operation of the ORR-PSF mockup are expected in FY 79 and FY 80, respectively.

HEDL will continue to be responsible for providing a major portion of the active and passive sensor monitors, new measurement equipment, and data acquisition and analysis systems required for the participating laboratories that will make dosimetry and materials damage measurements in the ORR-PCA, ORR-PSF and other approved neutron fields in FY 78 and beyond. The ORR-PCA and ORR-PSF PV mockups, Figure 1, will be the "key" U. S. "Controlled Environment benchmark field" facilities used for the validation/calibration of the recommended procedures. sensors, and associated nuclear data in the prepared ASTM Standards.

HEDL will have the contractual responsibility in FY 78 and beyond to prepare most of these Standards. ORNL and NBS are expected to have the primary contractual responsibility for the preparation of the "Standard Recommended Guide for Application of Neutron Transport Methods" and the "Standard Guide for Benchmark Testing of Reactor Neutron Dosimetry", respectively. CEN/SCK is expected to have the primary contractual responsibility for the preparation of the "Standard Method for Analysis of Damage Monitors" and the similar Standard for "Temperature Monitors".

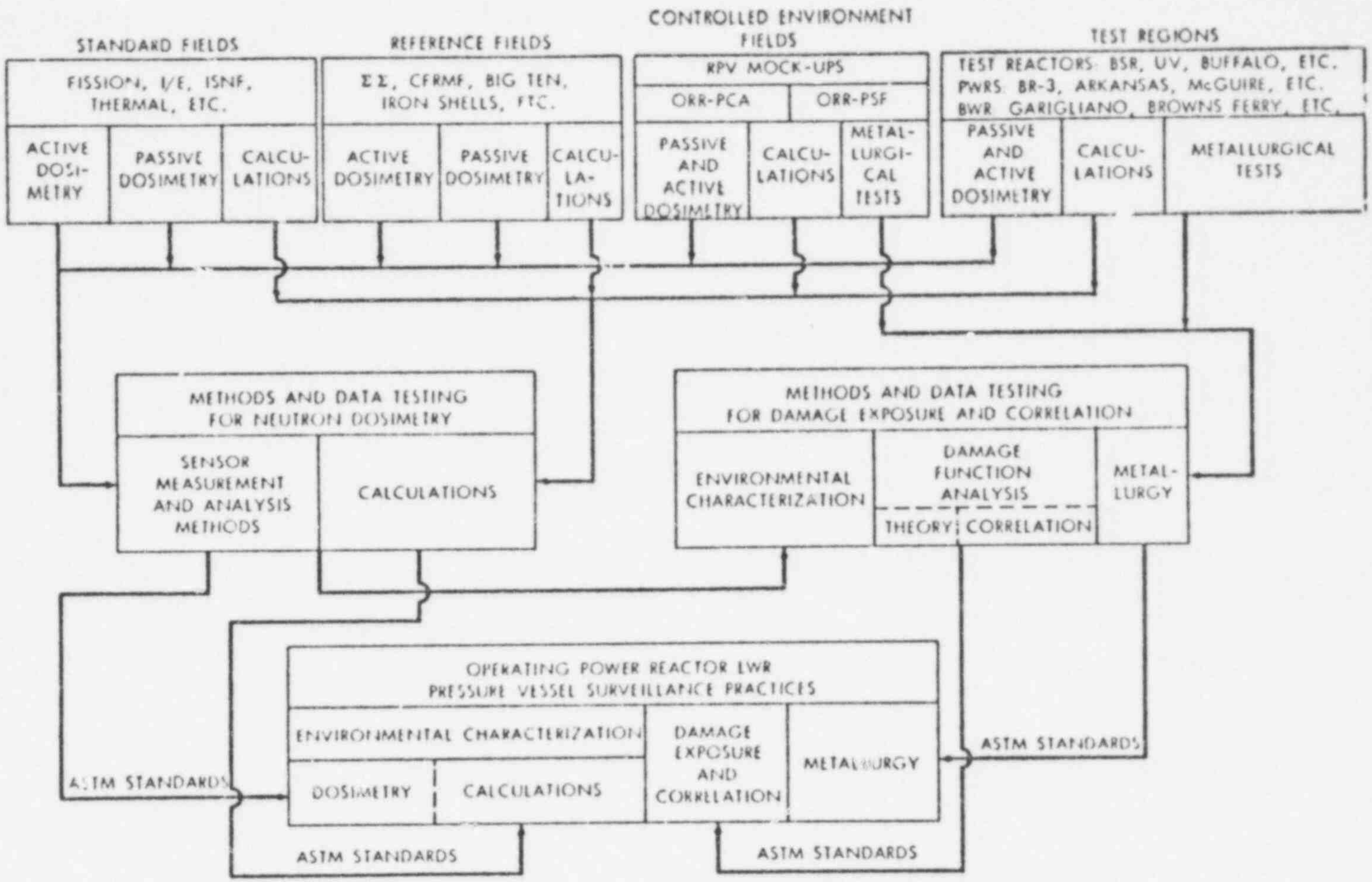

HEDL 7712-115.3

FIGURE 1. Flow Chart - Interrelationships of ASTM Standards Neutron Field Validation/Calibration Studies

815 318

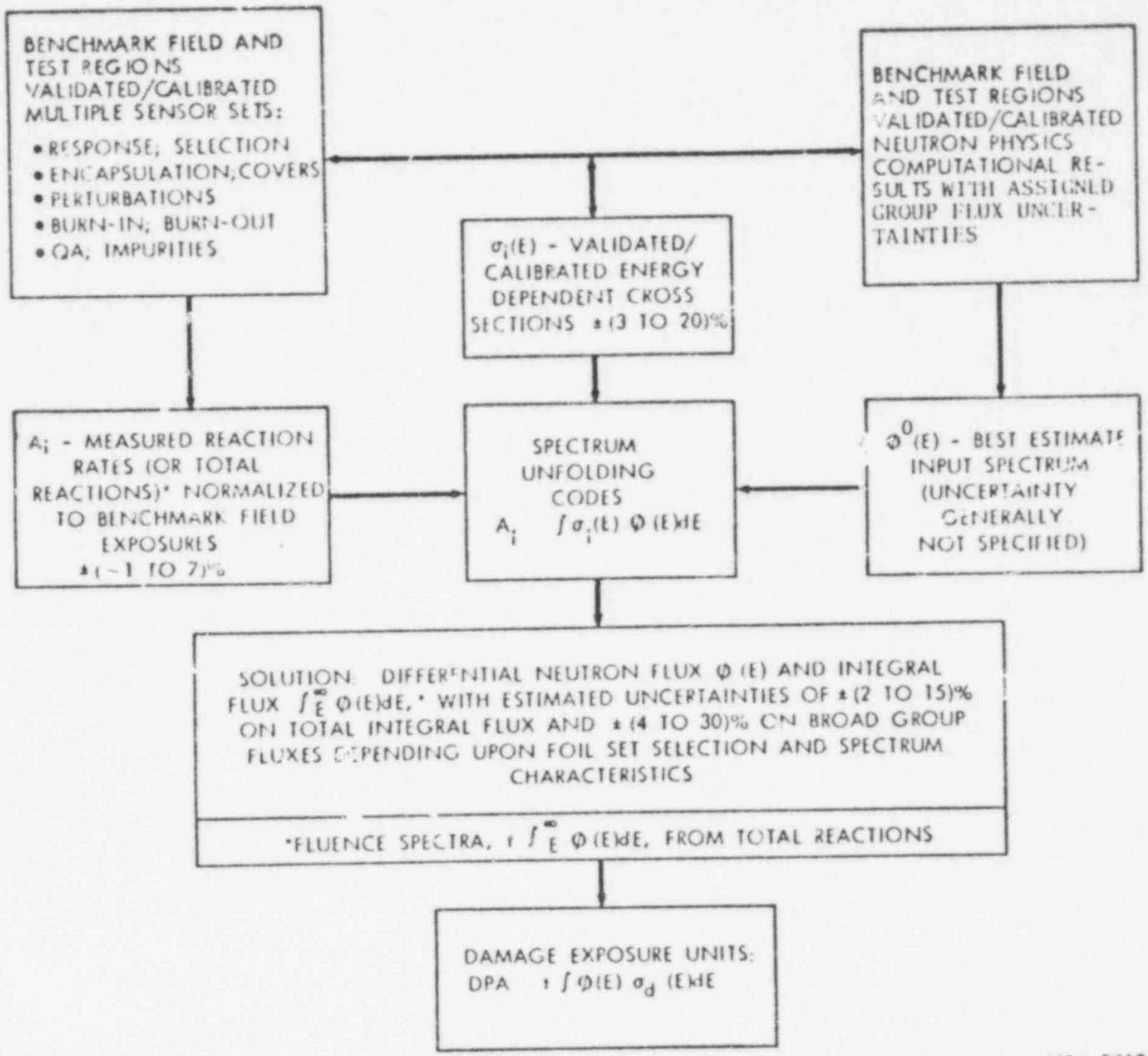

HEDL 7712-115.5

FIGURE 2. Flow Chart - Neutron Flux-Fluence Spectra and Exposure Unit Determination

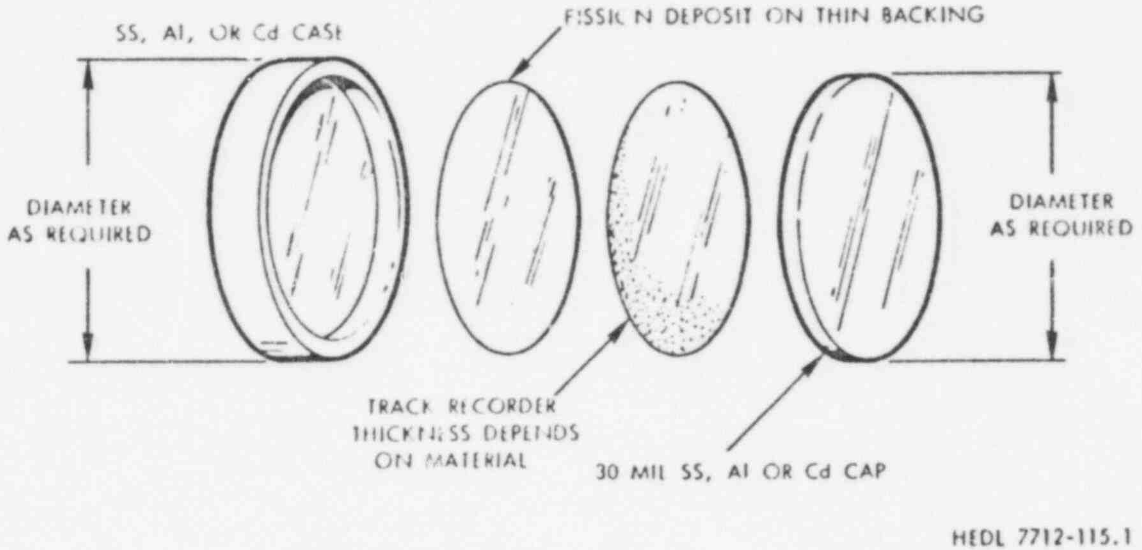

FIGURE 3. Conventional geometrical configuration used for SSTR Monitors

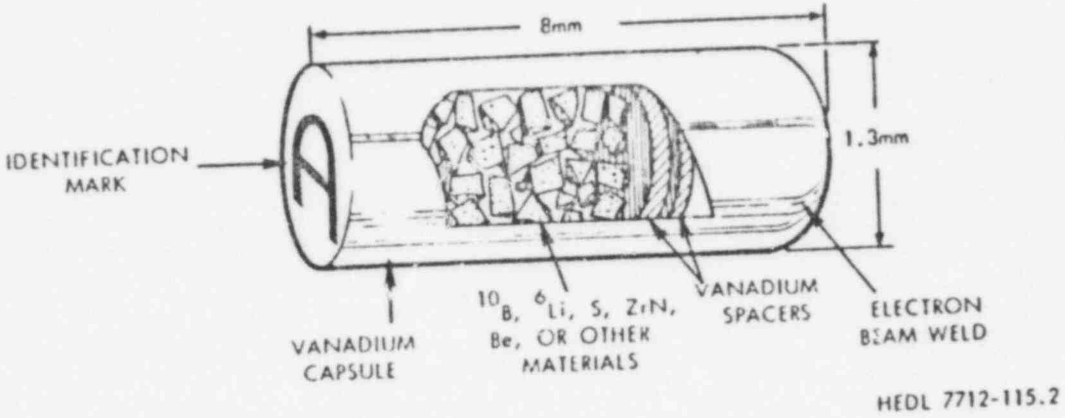

FIGURE 4 HELIUM ACCUMULATION FLUENCE MONITOR

BR-3 LOCATION	HF-4	LF-29	LF-63	I
HEDL-AI ID	3	29	63	I

FINAL LENGTH (INCHES)	1.968	1.966	1.964	0.229
DIAMETER	0.316	0.316	0.316	0.519
ENCAPSULATION MATERIAL	304 STAINLESS STEEL 3 CAPSULES			AL
HEDL ** ID	3G	29G	63G	IG

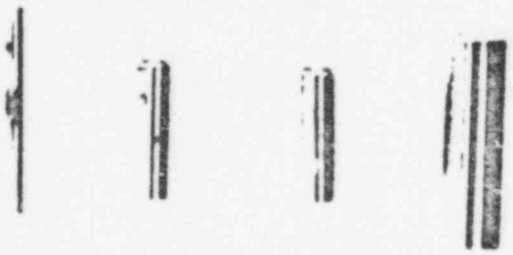

FINAL LENGTH (INCHES)	2.378	1.556	1.496	2.363
DIAMETER	0.300	0.466	0.466	0.781
ENCAPSULATION MATERIAL				

304 STAINLESS STEEL ALL CAPSULES

* INCLUDES HEDL AND ATOMICS INTERNATIONAL RM AND HAFM SENSOR MONITORS
** INCLUDES HEDL RM SENSOR MONITORS

HEDL 7710-212.3

FIGURE 5. BR-3 "Test Region" Completed Dosimetry Capsules

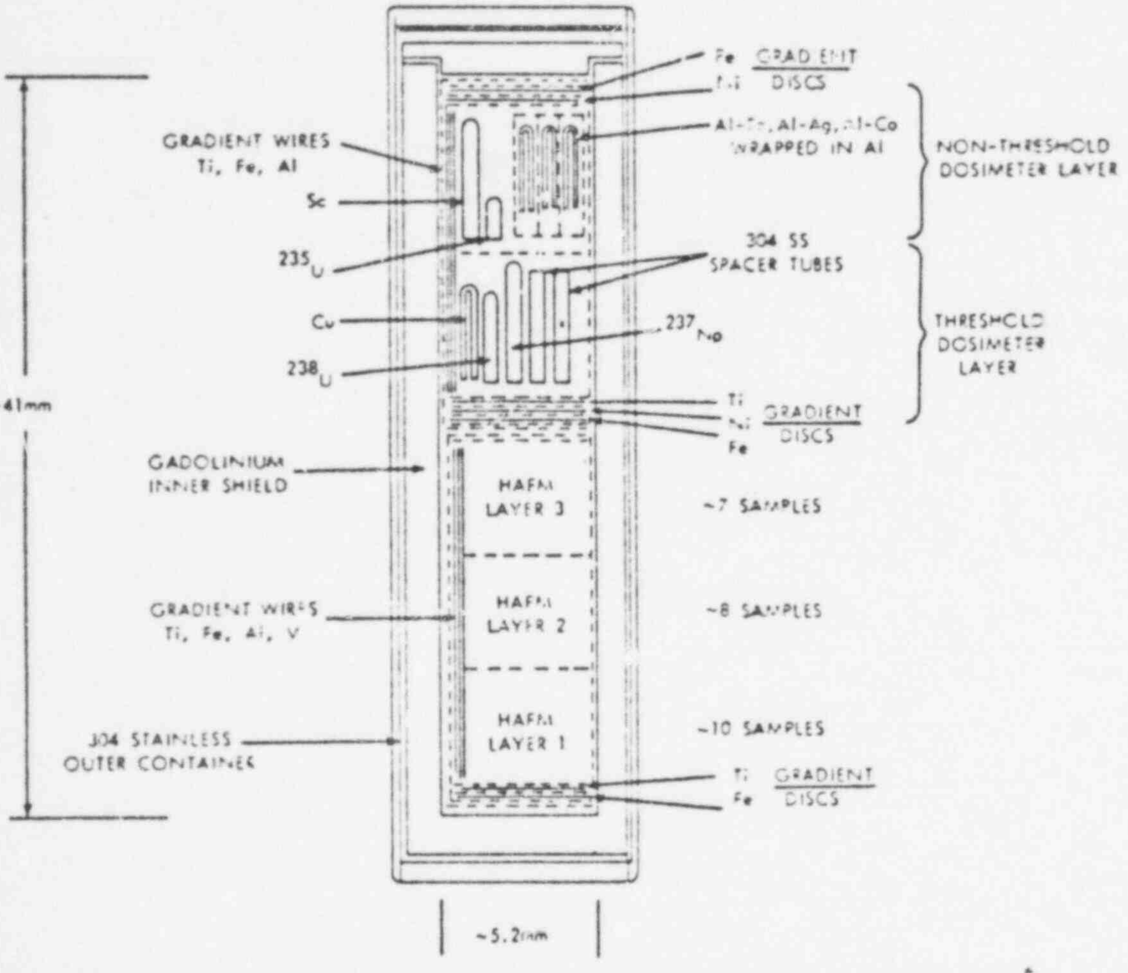

– – – Al FOILS 0.5 MIL THICK. HAFM HELIUM ACCUMULATION FLUENCE MONITORS. E.G. ^{6}Li, Li, B, ^{11}B, Be, ^{10}B-Al, ^{6}Li-Al, TiN, ZrN, Zr, Ti, Ni, Cu, Fe.

THE OUTER STAINLESS STEEL CONTAINER WAS WELDED IN AN ARGON ATMOSPHERE.

HEDL 7712-115.4

FIGURE 6 BR-3 "TEST REGION" HEDL-AI Dosimetry Capsules for BR-3 Irradiation Locations HF-4, LF-29, and LF-63

POOR ORIGINAL

TABLE I. SENSORS PROPOSED FOR LWR PRESSURE VESSEL SURVEILLANCE

DETECTION SCHEME	DETECTOR SENSOR* METHODS PLANNED FOR FY-78		DETECTOR SENSOR* METHODS PLANNED BEYOND FY-73	
RADIOMETRIC MONITORS (RM)	REACTION	(HALF LIFE)	REACTION	(HALF LIFE)
•Threshold response	$^{93}Nb(n,n')^{93m}Nb$	(~14 yr)	$^{232}Th(n,f)^{137}Cs$	(30 yr)
	$^{237}Np(n,f)^{137}Cs$	(30 yr)	$^{60}Ni(n,p)^{60}Co$	(5.3 yr)
	$^{238}U(n,f)^{137}Cs$	(30 yr)	$^{58}Ni(n,\alpha)^{55}Fe$	(2.7 yr)
	$^{54}Fe(n,p)^{54}Mn$	(313 d)	$^{55}Mn(n,2n)^{54}Mn$	(313 d)
	$^{58}Ni(n,p)^{58}Co$	(71 d)		
	$^{46}Ti(n,p)^{46}Sc$	(84 d)		
	$^{63}Cu(n,\alpha)^{60}Co$	(5.3 yr)		
•Non-threshold response	$^{109}Ag(n,\gamma)^{110m}Ag$	(~251 d)	$^{54}Fe(n,\gamma)^{55}Fe$	(2.7 yr)
	$^{181}Ta(n,\gamma)^{182}Ta$	(115 d)		
	$^{59}Co(n,\gamma)^{60}Co$	(5.3 yr)		
	$^{45}Sc(n,\gamma)^{46}Sc$	(84 d)		
	$^{58}Fe(n,\gamma)^{59}Fe$	(45 d)		
	$^{235}U(n,f)^{137}Cs$	(30 yr)		
	$^{239}Pu(n,f)^{137}Cs$	(30 yr)		

TABLE I. SENSORS PROPOSED FOR LWR PRESSURE VESSEL SURVEILLANCE (Continued)

DETECTION SCHEME	DETECTOR SENSOR* METHODS PLANNED FOR FY-78		DETECTOR SENSOR* METHODS PLANNED BEYOND FY-78	
HELIUM ACCUMULATION FLUX/ FLUENCE MONITORS (HAFM)	REACTION	(STABLE)	REACTION	(STABLE)
•Threshold response			S(n, Total Helium)	
			N(n, Total Helium)	
			Be(n, Total Helium)	
			Fe(n, Total Helium)	
•Non-threshold response	^{10}B(n, Total Helium)		Other Elements	
	^{6}Li(n, Total Helium)			
SOLID STATE TRACK RECORDER MONITORS (SSTR)	REACTION	(STABLE)	REACTION	(STABLE)
•Threshold response	^{237}Np(n,f)		^{238}Pu(n,f)	
	^{238}U(n,f)		^{232}Th(n,f)	
•Non-threshold response	^{235}U(n,f)		^{233}U(n,f)	
	^{239}Pu(n,f)		Other Elements	
DAMAGE MONITORS (DM)	Quartz		Metallurgical sensors	
TEMPERATURE MONITORS (TM)	Melt Wires		Thermal Expansion Detectors (TED's)	

* Many of these detectors will be used bare or with gadolinium or cadmium covers.

TABLE II

SSTR SENSOR MONITOR DEPOSITS FOR VALIDATION/CALIBRATION STUDIES IN PWR AND BWR POWER REACTOR "TEST REGIONS"

Nuclide	Thickness (ng/cm^2) (#)			
	McGuire I*		Browns Ferry 3**	
^{235}U	0.6	(4)†	0.1	(4)
	6.0	(2)	1.0	(2)
	60	(1)	10	(1)
^{238}U	30	(4)	5.0	(4)
	300	(2)	50	(2)
	3×10^3	(1)	500	(1)
^{239}Pu	0.6	(4)	0.1	(4)
	6.0	(2)	1.0	(2)
	60	(1)	10	(1)
^{237}Np	6	(4)	1.0	(4)
	60	(2)	10	(2)
	600	(1)	100	(1)
^{232}Th	120	(4)	20	(4)
	1.2×10^3	(2)	200	(2)
	12×10^3	(1)	2×10^3	(1)

* All deposits 0.250" diameter on 0.438" diameter, 5 mil Ni backing. Required date to begin QA testing 3/78. Required date for start of sensor irradiations 6/79.

** All deposits 0.250" diameter on 0.438" diameter, 5 mil Ni backing. Required date to begin QA testing 10/77. Required date for start of sensor irradiation 4/78.

† Number of deposits required.

TABLE III

REACTOR "BENCHMARK FIELD" AND "TEST REGION" VALIDATION/CALIBRATION STUDIES

Neutron Field*	Type of Dosimetry	Status
• Cf^{252} Fission (Standard Neutron Field at NBS)	Passive Nuclear Emulsions	Preliminary Irradiation Completed
• Σ Σ (Reference Neutron Field at CEN/SCK)	Passive Nuclear Emulsions and HAFM	Preliminary Irradiation Completed
• ^{235}U Fission (Reference Neutron Field at CEN/SCK)	HAFM	Preliminary Irradiation Completed
• BSR-HSST-Dosimetry Test (Test Reactor at ORNL)	RM	Irradiation Completed, Dosimetry Counting in Progress
• BR-3 (PWR Power Reactor at CEN/SCK)	RM, HAFM, SSTR, DM (Quartz), TM (Melt Wires)	Dosimetry at Sit - Ready for In- and Ex-Ve sel "Test Region" Irradiations
• Arkansas Power and Light Company, PWR Unit #1 (Russelville, Arkansas)	RM	Dosimetry at Site - Ready for Ex-Vessel "Test Region" Irradiation
• Garigliano Reactor (BWR Power Reactor at Rome, Italy)	RM	In-Vessel "Test Region" Irradiation in Progress

* See Figure 1

TABLE IV. SELECTED MEASUREMENT TECHNIQUES - DIFFERENTIAL METHODS

Method	E_L[a]	E_u[b]
1. Passive:		
• (n,p) Emulsions		
° Collimated Source	0.3	20
° Non-Collimated Source	0.3	10
2. Active:		
• (n,p) Proportional Counters	1×10^{-3}	2.5
• He^4 Proportional Counters	1	10
• $^6Li(n,t)^4He$ Proportional Counters	[illegible] $\times 10^{-2}$	6.5
• Si(Li) Gamma Compton Recoil Counters	0.2	2

a. Approximate lower energy limit of applicability, MeV.

b. Approximate upper energy limit of applicability, MeV.

TABLE V. SELECTED MEASUREMENT TECHNIQUES - INTEGRAL METHODS

I. Fission Monitors

- Radiometric (RM)
  - Ge(Li) Detectors
  - NaI (Tl) Detectors
- Solid State Track Recorders (SSTR)
  - Manual Optical Microscopy
  - Scanning Electron Microscopy
- Fission Chambers

II. Non-Fission Monitors

- Radiometric (RM)
  - Ge(Li)
  - Si(Li)
  - NaI(Tl)
  - Liquid Scintillation
- Helium Accumulation Flux/Fluence Monitors (HAFM)
  - Helium Mass Spectroscopy
- Solid State Track Recorders (SSTR)
  - Manual Optical Microscopy
  - Scanning Electron Microscopy

III. Damage Monitors (DM)

- Materials Property Changes

IV. Temperature Monitors (TM)

- Melt Wires
- Thermal Expansion Detectors (TED)

TABLE VI LWR-PV EQUIPMENT

1. Dual Parameter Computer Based Pulse-Height Multichannel Analyzer - for active dosimetry measurements. This system consists of the following components:

   - Analog to Digital Converter
   - ADC Interface
   - System Clocks
   - Spectrum Display
   - System Memory
   - Computer and Data Bus
   - Integral Printer (Optional)
   - System Disc & Controller
   - Pushbutton Control Panel
   - Integral NIM Slots
   - Integral Analog/Digital I/O Bin
   - Keyboard Printer
   - Cartridge Magnetic Tape (Optional)
   - Industry Compatible Magnetic Tape Transport & Controller

2. Scanning Electron Microscope (SEM) System - for counting high track density SSTR. This system consists of the following components:

   - SEM
   - Microcontroller/Signal Processor (M/SP)
   - Disc Memory and Controller
   - Vacuum Coating System

3. Optical Microscopy System - for manual scanning of SSTR.

4. Detectors and Pulse Processing Instrumentation - for active on-line neutron and gamma-ray spectrometry.

5. Miscellaneous Sensor Equipment - for passive monitor detection systems.

POOR ORIGINAL

REFERENCES

1. Proceedings of the Second International ASTM-Euratom Symposium on Reactor Dosimetry, Palo Alto, California, October 3-7, 1977.

2. W. N. McElroy, D. G. Doran, R. Gold, E. P. Lippincott, J. O. Schiffgens, R. L. Simons (HEDL); W. C. Morgan (BNW); J. A. Grundl and E. D. McGarry (NBS); F. B. K. Kam and J. H. Swank (ORNL); and G. R. Odette (UCSB); "Standardization of Dosimetry and Damage Analysis Work for U. S. LWR, FBR, and MFR Development Programs", Ibid.

3. G. R. Odette, N. D. Dudey, W. N. McElroy, R. Wulleart, and A. Fabry, "Application of Advanced Radiation Analysis Methods to LWR Pressure Vessel Test and Surveillance Programs", Ibid.

4. F. J. Rahn, C. Z. Serpan, A. Fabry, J. Debrue, W. N. McElroy, and J. A. Grundl, "Trends in Light Water Dosimetry Programs", Ibid.

5. G. C. Martin, Jr., "Dosimetry Method for Light Water Reactors", Ibid.

6. S. L. Anderson, "Characterization of the Neutron Environment for Commercial LWR Pressure Vessel Surveillance Programs", Ibid.

7. E. B. Norris and J. S. Perrin, "Determination and Evaluation of the Mechanical Properties of Specimens in Commercial LWR Pressure Vessel Surveillance Programs", Ibid.

8. A. D. Rossin, "Radiation Damage Outside the Reactor Vessel", Ibid.

9. F. B. K. Kam, J. H. Swanks and F. W. Stallman, "Dosimetry Experiment for Neutron Spectral Characterization of the Second NRC 4T-CT Irradiation Capsules at BSR", Ibid.

10. L. Steel, "Neutron Irradiation Embrittlement of Reactor Pressure Vessel Steels", IAEA Tech. Rept. Ser. #163, 1975.

11. M. F. Vlasov and C. L. Dunford, "Proceedings of a Consultants' Meeting on Nuclear Data for Reactor Neutron Dosimetry", Vienna, September 10-12, 1973, Report INDC (NDS)-56/U, IAEA (1973).

12. Proceedings of the First International ASTM-Euratom Symposium on Reactor Dosimetry, Petten, Netherlands, September 22-26, 1975, EUR 5667 e/f, Volumes I and II, 1977.

13. Proceedings of an "International Specialists' Symposium on Neutron Standards and Applications", National Bureau of Standards, March 28-31, 1977, NBS Special Publication 493, October 1977.

14. F. J. Rahn, K. E. Stahlkopf, T. V. Marston, R. Gold, and J. H. Roberts, "Standards for Dosimetry Beyond the Core", Ibid.

15. M. F. Vlasov, Editor, "IAEA Consultants' Meeting on Integral Cross-Section Measurements in Standard Neutron Fields - Summary Report, Conclusions, and Recommendations", Vienna, November 15-19, 1976, INDC(NDS)-81/L&M, March, 1977, and Meeting Papers and Proceedings.

16. W. N. McElroy, R. Gold, E. P. Lippincott, A. Fabry, and J. H. Roberts, "Spectral Characterization by Combining Neutron Spectroscopy, Analytical Calculations, and Integral Measurements", HEDL-SA 1149 (1976), in Reference 15.

17. A. Fabry, W. N. McElroy, L. S. Kellogg, E. P. Lippincott, J. A. Grundl, D. M. Gilliam, and G. E. Hansen, "Review of Microscopic Integral Cross Section Data in Fundamental Reactor Dosimetry Benchmark Neutron Fields", HEDL-SA 1148 (1976), in Reference 15.

18. J. A. Grundl and C. Eisenhauer, "Benchmark Neutron Fields for Reactor Dosimetry", NBS Report (1976), in Reference 15.

19. M. F. Vlasov, A. Fabry, and W. N. McElroy, "Status of Neutron Cross Sections for Reactor Dosimetry", HEDL-SA 890, Special Contributed Paper to 1976 International Conference on the Interactions of Neutrons with Nuclei, July 6-9, 1976, Lowell, Massachusetts (1976).

20. <u>1976 Annual Book of ASTM Standards, Part 45, Nuclear Standards</u>, American Society for Testing and Materials, 1916 Race St., Philadelphia, PA 19103.

21. Proceedings of a Minisymposium on "Neutron Dosimetry and Spectrum Analysis for Materials Applications", Journal of Testing and Evaluation <u>3</u> (1975).

22. H. Farrar IV and E. P. Lippincott, "Helium Production Measurements for Neutron Dosimetry and Damage Correlations", in Reference 1.

23. J. H. Roberts and R. Gold, "Solid State Track Recorder and Emulsion Techniques and Their Applications for FBR, LWR, and MFR Programs", in Reference 1.

24. L. Stewart, "Status of ENDF/B Special Applications Files", in Reference 1; and B. A. Magurno, "ENDF/B Dosimetry File for Version V", BNL Report (1976), in Reference 15.

25. Proceedings of the IAEA Consultants' Meeting on "Damage Units", Harwell, England, November, 1976.

26. D. K. Trubey, "A Review of Radiation Energy Spectra Unfolding, Proceedings of a Seminar-Workshop", ORNL/RSIC-40, October 1976.

27. F. B. K. Kam, G. L. Guthrie, and B. F. Maskewitz, IAEA Technical Committee Meeting on "Current Status of Neutron Spectrum Unfolding - Summary Report, Conclusions and Recommendations", Oak Ridge National Laboratory, November, 1977.

28. F. W. Stallmann and F. B. K. Kam, "Foil Activation Dosimetry at Energies Below 1 MeV", in Reference 1.

29. F. G. Perey, "Uncertainty Analysis of Dosimetry Spectrum Unfolding", in Reference 1.

30. A. Fabry, E. P. Lippincott, W. N. McElroy, J. A. Grundl, and H. Farrar IV, "Status Report: Benchmark Neutron Field Integral Data Testing and Adjustment of ENDF/B Files", in Reference 1.

31. C. M. Eisenhauer, D. M. Gilliam, J. A. Grundl, and V. Spiegel, "Utilization of NBS Standard Neutron Fields for Reactor Dosimetry", in Reference 1.

32. C. D. Bowman and D. M. Gilliam, "Photofission Effects in Reactor Dosimetry", in Reference 1.

33. D. M. Gilliam, J. A. Grundl, R. C. Greenwood, R. R. Heinrich, L. S. Kellogg, E. P. Lippincott and G. E. Hansen, "Reference and Standard Benchmark Field Consensus Fission Yields for U. S. Reactor Dosimetry Programs", in Reference 1.

34. V. Spiegel, C. M. Eisenhauer, J. A. Grundl (NBS), G. C. Martin, Jr. (GEVMC), "Reaction Rate Measurements and Integral Cross Sections Using the NBS ^{252}Cf Fission Neutron Indoor Irradiation Facility", in Reference 1.

35. G. DeLeeuw-Gierts and S. DeLeeuw, "Neutron Spectrometry for Reactor Dosimetry", in Reference 1.

36. C. A. Oster, "A Review of Unfolding Methods Used in the U. S. and Their Standardization for Dosimetry", in Reference 1.

APPENDIX A

BRIEF DESCRIPTION OF THE ORR-PCA AND ORR-PSF PV BENCHMARK FACILITIES

The planned U. S. Pressure Vessel Benchmark Facility will be built at Oak Ridge National Laboratory. It will consist of two complementary facilities - one at the low power Pool Critical Assembly (PCA) which will serve as a flux spectra characterization facility and the other at the Oak Ridge Research Reactor (ORR) which, due to its high flux, will be used as a facility in which irradiations of metallurgical specimens will be performed. Both facilities will be constructed in a manner which will provide the same physical arrangements and nuclear environment of the reactor core, thermal shield, and pressure vessel that exist in a typical pressurized water reactor. The general PCA layout is such as to provide an equivalent nuclear configuration as that employed at the ORR Pool Side Facility (PSF) so that accurate passive and active flux-fluence spectrum measurements can be done (see Figures A-1 and A-2); more specifically.

a) In the initial facility, for flux spectral characterization experiments with active detectors, the RPV simulator will be as "clean" as possible. The objective is to provide relevant experimental data to validate/calibrate reactor physics computations needed for extrapolation into the vessel of dosimetry observations in surveillance positions.

b) In a second series of experiments, the central part of the RPV simulator can be replaced by a mockup of the ORR-PSF metallurgical irradiation capsule.

The metallurgical specimen irradiations in PSF will be performed in instrumented irradiation capsules which will be heated to provide a uniform 550°F thermal environment. Arrays of metallurgical specimens will be located at four discrete positions. They are: 1) Behind the thermal shield in a position equivalent to an accelerated surveillance test position in a PWR, 2) at the H_2O - steel interface equivalent to the inside of the pressure vessel wall, 3) at the 1/4 T thickness (T: vessel overall thickness), and 4) at the 1/2 T thickness. The capsules will be irradiated until a neutron fluence of $\sim 5 \times 10^{18}$ neutrons/cm^2 (> 1 MeV) will be accumulated on the one at the 1/4 T thickness. Simultaneously the fluence accumulated at the 1/2 T position will be $\sim 2 - 3 \times 10^{18}$ neutrons/cm^2.

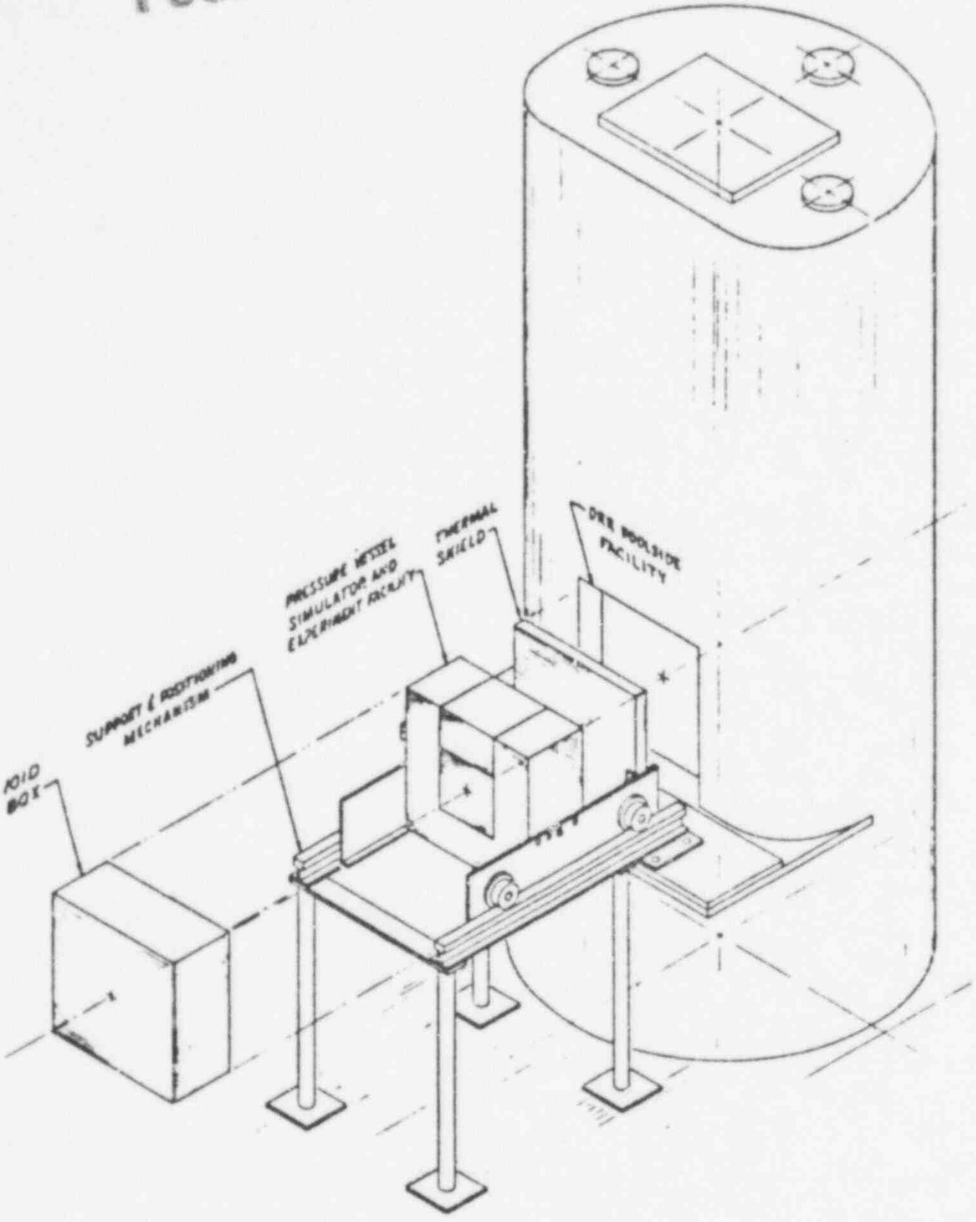

Figure A-1 ORR-PSF Pressure Vessel Benchmark Facility - Concept

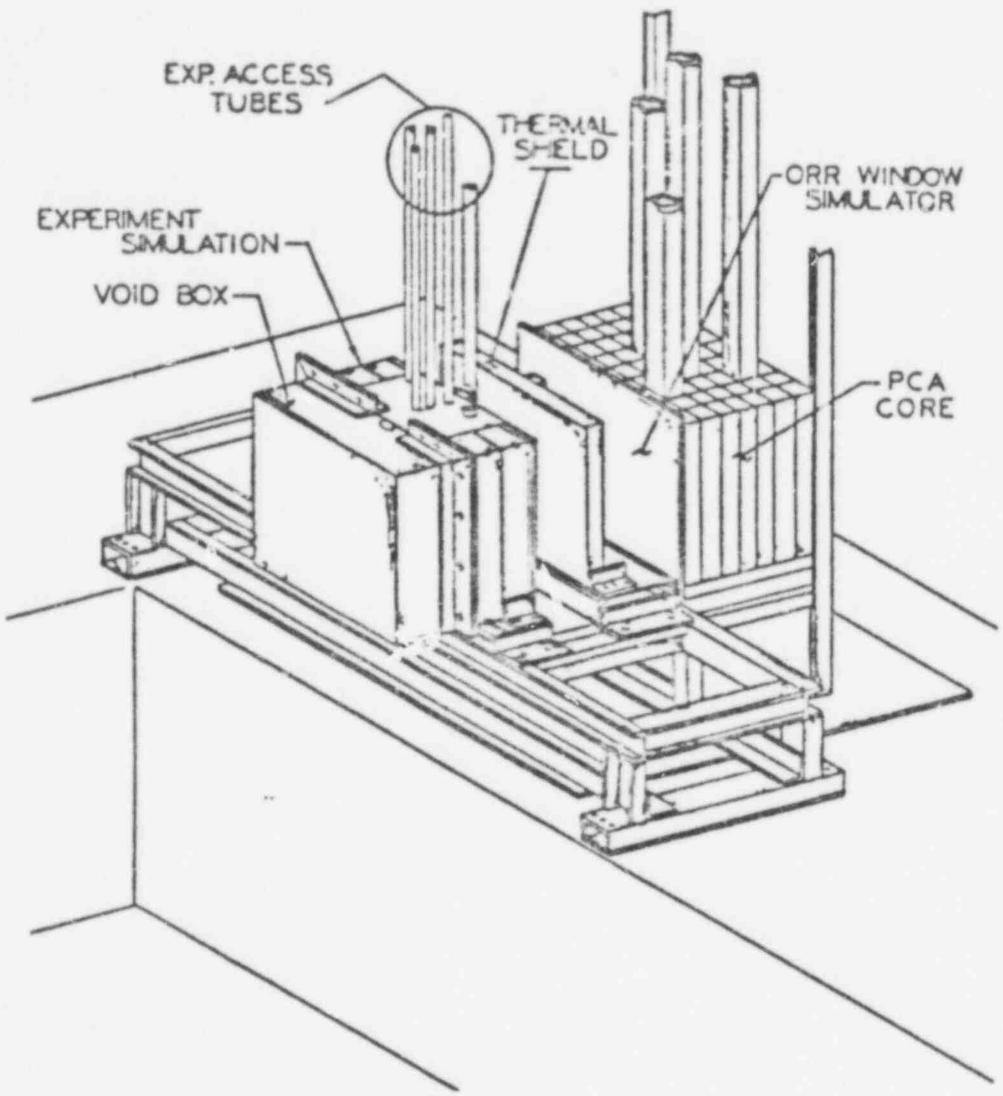

Figure A-2 ORR-PCA Pressure Vessel Benchmark Facility - Concept

DESIGN CRITERIA FOR PIPING AND NOZZLES PROGRAM

S. E. Moore J. W. Bryson

ABSTRACT

This report reviews the activities and accomplishments of the Design Criteria for Piping and Nozzles program being conducted by the Oak Ridge National Laboratory for the period October 1, 1976, to September 30, 1977. The objectives of the program are to conduct integrated experimental and analytical stress analysis studies of piping system components and isolated and closely-spaced pressure vessel nozzles — in order to conform and/or improve the adequacy of structural design criteria and analytical methods used to assure the safe design of nuclear power plants. Activities this year included the continued development and validation of finite element computer programs for analyzing cylindrical pressure vessels with isolated nozzles and with two or three closely spaced nozzles; finite element parameter studies of vessels with isolated nozzles; summary and evaluation of experimental studies on the elastic-response and fatigue failure of tees; an analytical study of flexibility factors for small branch connections; and the development and acceptance of manufacturing controls for butt-welding pipe fittings as well as a number of design qualification rules changes to the ASME Code.

Keywords: stress analysis, piping, pressure vessels, nozzles, elbows, tees, ASME Boiler and Pressure Vessel Code.

DESIGN CRITERIA FOR PIPING AND NOZZLES

Oak Ridge National Laboratory
Oak Ridge, Tennessee 37830

S. E. Moore J. W. Bryson

OBJECTIVE

To conduct integrated experimental and analytical stress analysis studies of piping system components and isolated and closely-spaced pressure vessel nozzles — in order to confirm and/or improve the adequacy of structural design criteria and analytical methods used to assure the safe design of nuclear power plants.

FY 77 SCOPE

This program is organized into eight major task areas which include program administration and PVRC and ASME Code committee work, and six tasks identified with the structural behavior of specific pressure vessel and piping system components. These include analytical studies of isolated and closely-spaced nozzles in cylindrical shells or pressure vessels ANSI standard piping tees and elbows (or curved pipe), and flanged or welded joints in straight pipe. In addition to participation in the assessment and/or improvement of design criteria and rules for Code use, the FY-77 work scope included:

1. the development of a finite element computer program (MULT-NOZZLE) for analyzing cylindrical pressure vessels with closely-spaced nozzles;
2. validation of a finite element computer program (CORTES) for analyzing ANSI standard piping tees, branch connections, and isolated nozzles in cylindrical vessels;
3. completion of a parameter study to determine the field of influence of single nozzles in cylindrical vessels under internal pressure loading, and assessment of Code rules based on the results;
4. completion of a summary report on the experimental stress analysis and fatigue-to-failure tests of ANSI B16.9 tees;

5. the development of proposed design qualification rules for flanged piping joints;
6. the development of dimensional and proof test controls for standard butt-welding pipe fittings; and
7. completion of a study of flexibility factors for small branch connections.

SUMMARY OF RESEARCH ACTIVITIES AND RESULTS

During fiscal year 1977 a substantial amount of work was done on each of the items listed above. The activities and results of this work are summarized below.

Nozzles in Cylindrical Pressure Vessels

Analytical finite element studies of the structural behavior of various ASME standard nozzle penetration designs for cylindrical pressure vessels are being conducted to provide detailed stress analysis data needed to assess the adequacy of current design qualification rules. These rules, given in Section NB-3330 of the Code* for designs which do not require a fatigue evaluation, and in NB-3200 for the more general case, govern the design and minimum spacings for both reinforced and unreinforced openings (nozzles) in Class 1 nuclear pressure vessels. The NB-3300 rules also provide stress indices for use in the analysis of nozzle designs which also meet the other requirements for use of the simplified design qualification procedures. Similar rules are contained in Section NC-3300 and ND-3300 for Class 2 and 3 vessels, respectively.

Earlier reports have shown clearly that these rules are in need of revision both with regard to spacing requirements[2] and stress indices.[3] For some design parameters a much closer spacing for reinforced nozzles should be acceptable than currently permitted, while for others the permitted spacings could result in undesirably high stresses. A similar situation also exists for the Code stress indices. For some parameters these are too high, while for others they are too low.

---

*The term "Code" as used here refers to the ASME Boiler and Pressure Vessel Code, Section III, Division 1 (Ref. 1).

In order to properly assess these rules, and to provide sufficient new information to develop suitable revisions and/or alternate rules, parametric finite element studies for both isolated and closely-spaced nozzle designs are being conducted. In both types of studies the Code specified standard nozzle reinforcement designs shown in Fig. 1 are being analyzed for various values of the dimensionless geometric parameters d/D, D/T, and d/t, where d and D are the inside diameters for the nozzle and vessel; and t and T are the corresponding wall thicknesses.

Isolated Nozzles

The rules of NB-3300 are generally based on the assumption that a given nozzle is sufficiently isolated from any other nozzle or structural discontinuity that their fields of influence do not interact. There is (was) not sufficient stress analysis data, however, to define "isolation" and consequently rules given in various paragraphs of NB-3300 for the design of reinforced openings appear to disagree. Moreover the stress index values given in NB-3338 for nozzles designed according to one set of rules differ from those given in NB-3339 for nozzles designed according to an alternate set of rules.

In order to provide the information needed to develop more consistent rules, parameter studies of isolated nozzles were (are being) conducted using the CORTES finite element computer codes developed earlier for us at the University of California.[4] This program, along with various modifications developed at Oak Ridge is an extremely efficient tool for analyzing pressure vessels with a single standard ASME reinforced or unreinforced nozzle.

Features of the program include automatic mesh generation (with options for manual setup or mesh modification), complete graphics for both pre- and post-processing, 8-node (modified) solid isoparametric elements, improved accuracy by bilinear Gauss point extrapolation, and improved computer efficiency using a compacted matrix equation solution algorithm. Loading capabilities include internal pressure, external force and moment loadings on the nozzle, and thermal stresses. The program is fully validated and available to U.S. citizens through the Argonne Code Center, Argonne National Laboratory, 9700 Cass Ave., Argonne, IL 60439.

ORNL-DWG 77-19051R

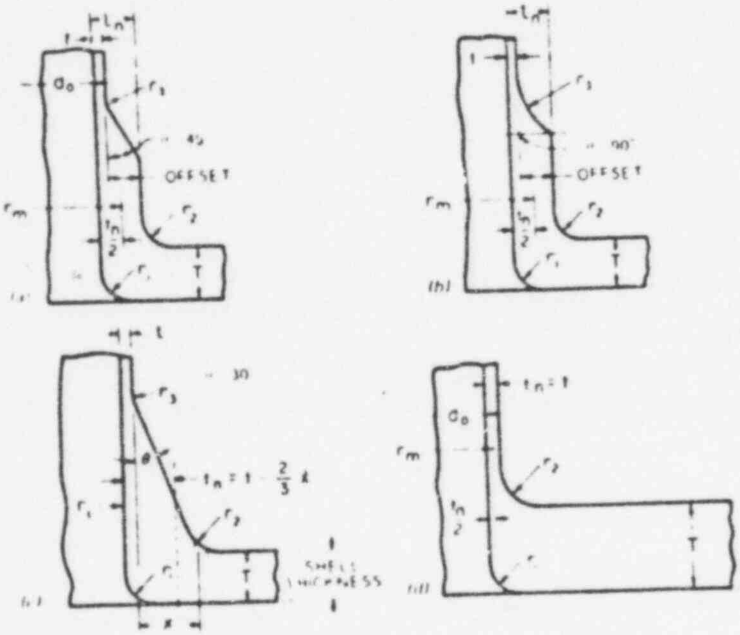

Fig. 1. Nozzle reinforcement details for ASME standard designs.

CORTES-SA (the elastic analysis program) was fully validated[5] during the past year by comparison analyses of six models for which experimental stress analysis data were available for internal pressure loading. This set included two thin-walled cylinder-to-cylinder models without transition fillets: ORNL-1 (Ref. 6) and ORNL-3 (Ref. 7); an ANSI B16.9 tee, ORNL-T8 (Ref. 8); a thick-walled steel pressure vessel: HSST-ITV9 (Ref. 9); and two photoelastic pressure vessel models tested at Westinghouse: WC-12D and WC-100D (Ref. 10). This group of models cover the parameter ranges for diameter-to-thickness ratios of $4.5 \leq D/T \leq 100$, and nozzle-to-vessel diameter ratios of $0.1 \leq d/D \leq 0.51$. Comparisons between the experimental photoelastic data and finite element results for WC-12D are shown in Fig. 2 for internal pressure loading ($p = 153.9$ psi).

During the past year CORTES-SA was used to conduct a study of 25 reinforced nozzle cylindrical vessel models with dimensionless parameters within the ranges $0.08 \leq d/D \leq 0.5$ and $10 \leq D/T \leq 100$ for internal pressure loading. Six of the models were essentially unreinforced except for the fillet reinforcement shown in Fig. 1(d) while the other 19 models were fully reinforced (100% area replacement) in the nozzle: fourteen with the so-called "standard" reinforcement like the detail shown in Fig. 1(a) and 5 with 30° pad reinforcement like the detail shown in Fig. 1(c). Complete sets of results are given in Ref 11 with tabulated summaries of maximum stresses in the body of the text and nodal point coordinates, principal stresses and their direction cosines, stress intensities, and displacements for each nodal point on the outer and inner surfaces of each of the models given on microfiche at the end of the report.

Maximum stresses from the parameter study, normalized to the stress index formulation of the Code are shown in Fig. 3, along with the current Code value (3.3) as a function of the dimensionless parameter $\psi = \rho(10^{2\chi})(D/T)^{-\chi}$ where $\rho = d/D\sqrt{DT}$, and $\chi = 0, 1$ depending on whether the nozzle is unreinforced or 100% reinforced. Triangular data points are for the unreinforced models, square data points are for the 30° pad reinforced models, and open circles are for the "standard" reinforced models. These results show that the Code index value (NB-3338) is conservative for nozzles with 100% of the required reinforcement in the nozzle wall, but unconservative for designs with all of the required reinforcement in the

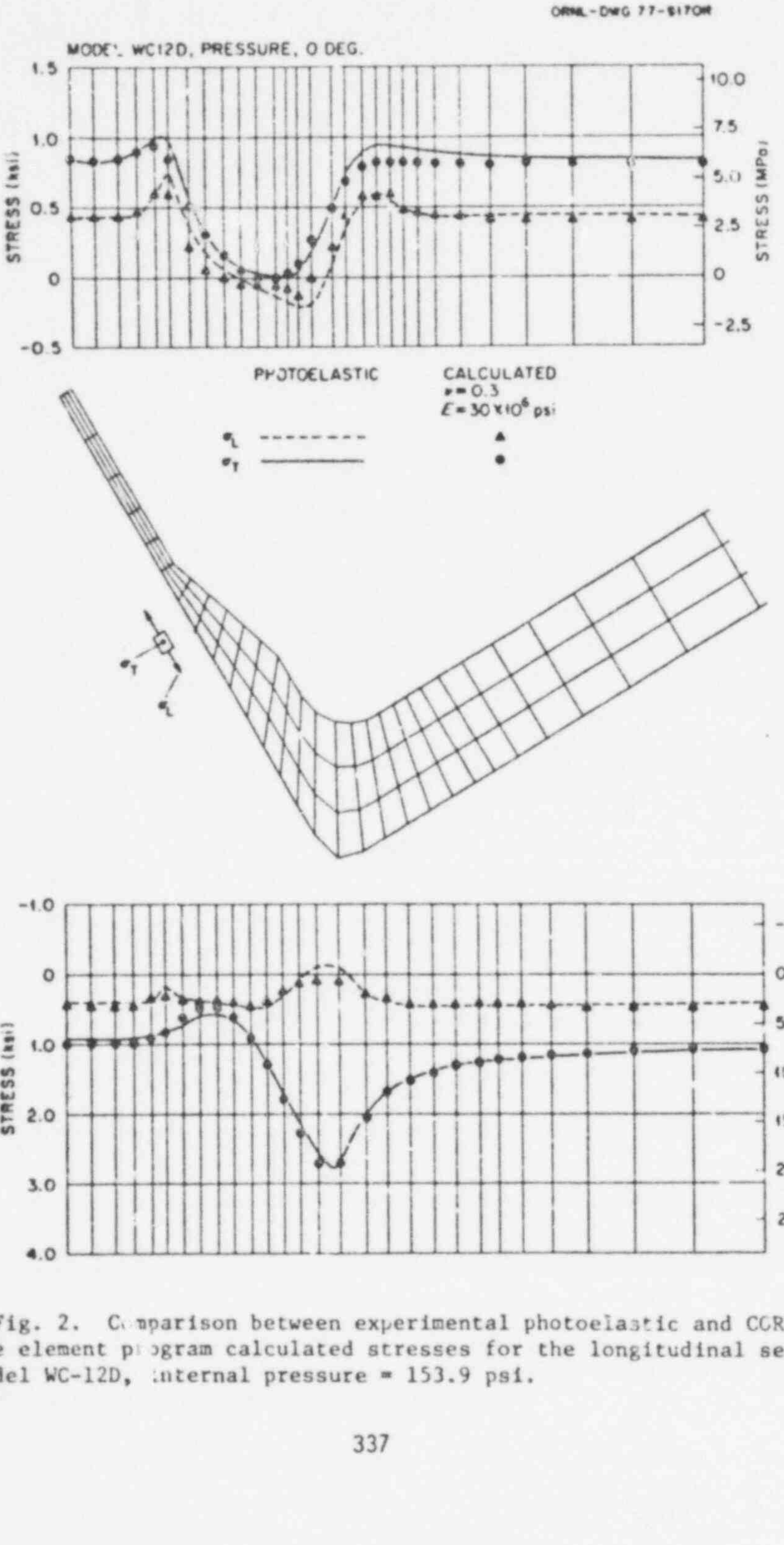

Fig. 2. Comparison between experimental photoelastic and CORTES-SA finite element program calculated stresses for the longitudinal section of model WC-12D, internal pressure = 153.9 psi.

POOR ORIGINAL

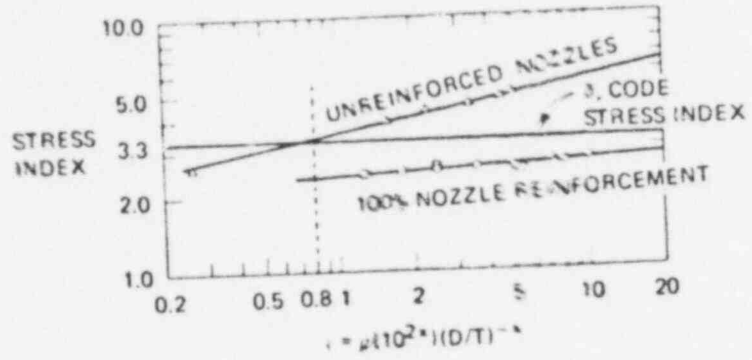

Fig. 3. Correlation of calculated maximum stress intensities (stress indices) for isolated pressure vessel nozzles under internal pressure loads.

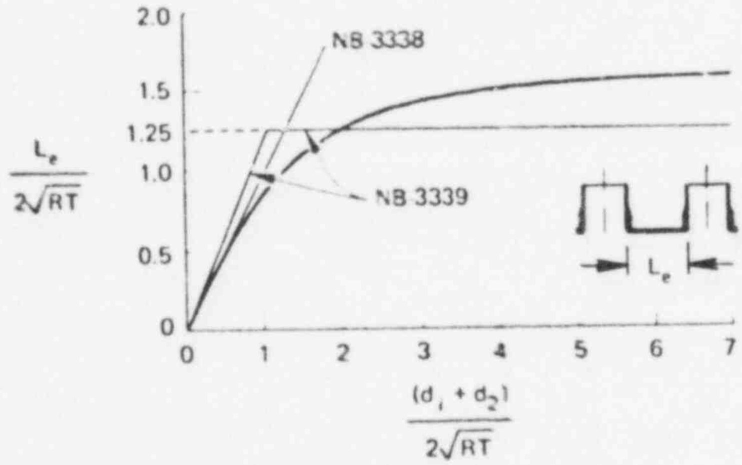

Fig. 4. Comparison of ASME Code rules for nozzle spacing with calculated local membrane stress attenuation distance.

vessel wall and a value of ψ greater than 0.8. A revision to the Code rules restricting the use of the current indices to ψ values less than 0.8 or for designs with 100% of the required reinforcement in the nozzle wall has been accepted by the ASME Boiler and Pressure Vessel Code Committee. The essential wording of the Code revision is given in Ref. 3.

Additional studies for moment loadings on the nozzles, and for nozzle-vessel designs with part of the required reinforcement in the nozzle wall and part in the vessel wall are currently underway. Results from these studies will be reported later.

Calculated membrane stress data from the parameter study were also used to assess the current Code requirements for nozzle spacing. (Required for use of the simplified procedure of NB-3300.) The results are shown in Fig. 4 where the normalized distance between the inside edges of adjacent nozzles, $Le/2\sqrt{RT}$, that is required for the local membrane stress to damp out to a value equal to 1.1 times the nominal membrane stress, is shown as a function of the sum of the normalized nozzle diameters, $(d_1 + d_2)/2\sqrt{RT}$; R and T are the inside radius and wall thickness of the vessel respectively. Also shown for comparison are the Code requirements for nozzle spacing from NB-3338 and from NB-3339. These results indicate that the Code rules are probably conservative for small diameter nozzles, i.e., $(d_1 + d_2)/2\sqrt{RT} < 2$ but probably unconservative for larger nozzles. Further work, however, is required before these results can be verified or alternate rules developed. F4

Closely-Spaced Nozzles

During the past year we have continued the development of the finite element computer program MULT-NOZZLE[12] to enable us to efficiently conduct parameter studies for cylindrical pressure vessels with two or three closely spaced nozzles under internal pressure and/or external force and moment loadings on the nozzle(s). The program includes a pre-processer (FEMG) that will automatically setup a finite element model for vessels with a single reinforced nozzle; with two identical reinforced nozzles that are placed arbitrarily close together in either a longitudinal plane (along the length) or in a transverse plane (around the circumference) of the vessel; or with three (or four) reinforced nozzles. Figure 5 shows a typical finite element model for two nozzles in a transverse plane of the vessel. The model is setup with symmetric (or antisymmetric) boundary conditions along the plane midway between the two nozzles so that only an eighth-section of the vessel needs to be considered. Figure 6 shows a typical finite element model for vessels with three (or four) nozzles. In this case the modeled section of the vessel is assumed to have two nonidentical nozzles, one of which is in a transverse plane, with the other in a longitudinal plane. Either nozzle may be the larger, and may be reinforced (or unreinforced) according to the details given in Fig. 1.

F5

F6

The main frame (SAP3M) of MULT-NOZZLE is a modified version of the SAP3 finite element program with the addition of an 8 to 21 node solid isoparametric element, bilinear Gauss point stress extrapolation, and compacted matrix equation solver. Boundary conditions for any of the desired loading conditions are setup automatically, partly by FEMG and partly by SAP3M. Both pre- and post-processing graphics are also available.

MULT-NOZZLE was completely validated for the analysis of vessels with two closely spaced nozzles under internal pressure loading this year,[12] and extended to analyze two nozzle vessels with force and/or moment loadings and three nozzle vessels with internal pressure. Validation studies included finite element analyses of several classical theoretical problems (beams and thick walled rings) and analyses of four experimental models that were tested with internal pressure loadings. The finite-element solutions to the classical problems generally agreed with the theoretical solutions to within about 1% with a few cases being in error about 2%. The experimental models that were analyzed include two photoelastic models[10] each with two identical nozzles in a longitudinal plane (WC-12DD and WC-100DD), one photoelastic model[13] with two nozzles in a transverse plane (SH-23DD), and one steel model[9] with an isolated nozzle (HSST-ITV9). The agreement between the finite-element and experimental maximum stresses was within 10% for all four models. Details of the study as well as a rather complete description of the MULT-NOZZLE program are given in Ref. 12.

ORNL-DWG 77-12931

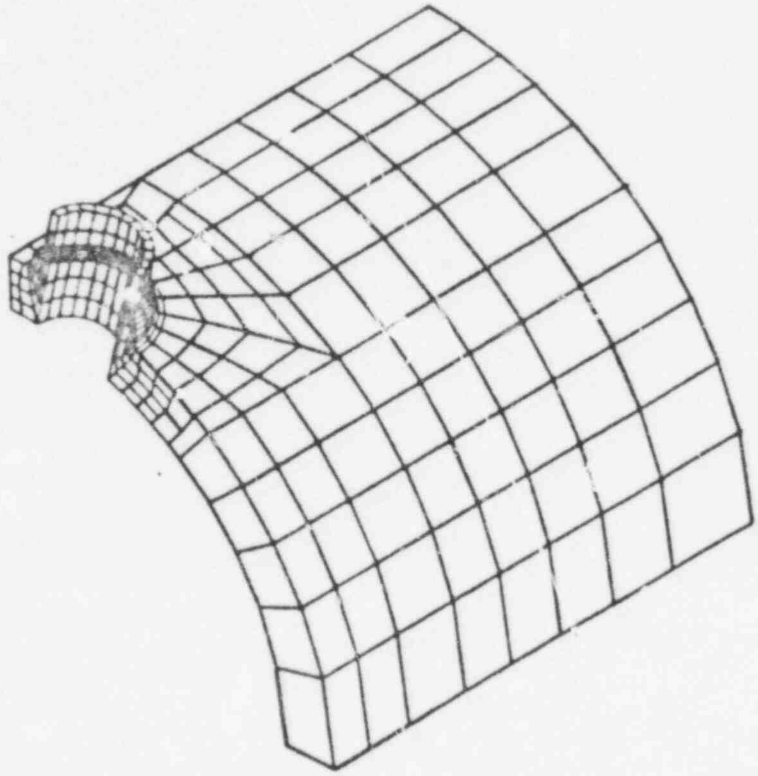

Fig. 5. Isometric view of the MULT-NOZZLE finite element mesh for the experimental photoelastic model SH-23DD.

815 347

ORNL–DWG 77–19054R

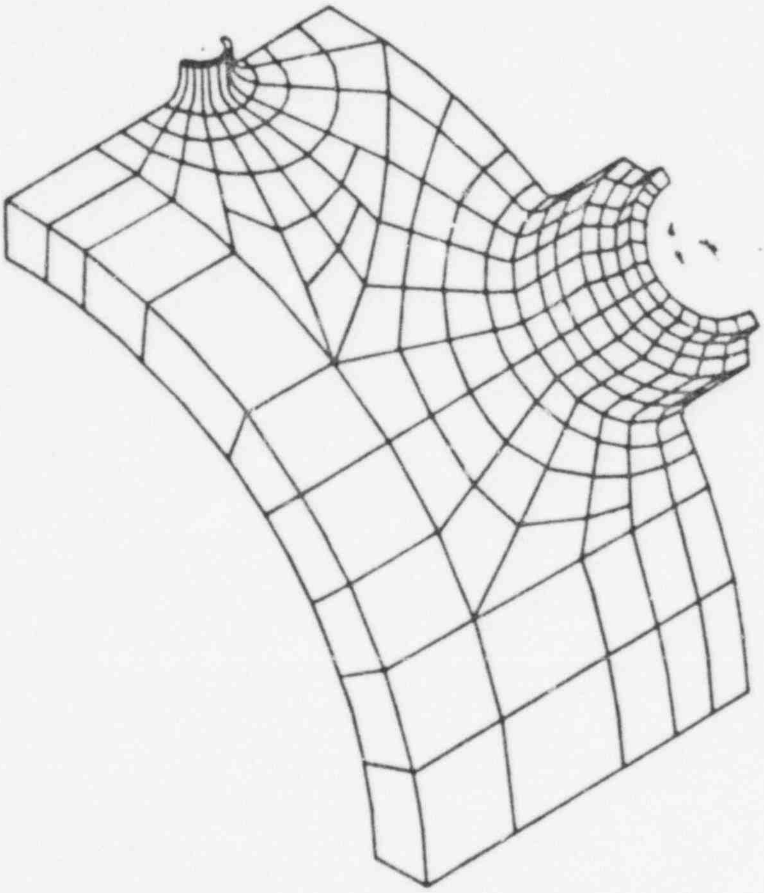

Fig. 6. Typical mesh generated by MULT-NOZZLE for a vessel with three closely-spaced nozzles.

Piping System Components

In contrast with the vessel design sections of the ASME Code, the piping design sections (NB-3600, NC-3600, and ND-3600) contain a negligible amount of discussion concerning stress categories, allowable stress values, and design criteria, but instead contain detailed design rules, stress indices, flexibility factors, and equations for calculating stresses which must be satisfied to qualify a given piping system design. For several years we have been working to provide the technical data needed to test and confirm the adequacy of the piping system design rules and formulas. Most of the remaining work is on the behavior of elbows, tees, fabricated branch connections, and welded or flanged joints in straight pipe. The year-end status of our piping system work is described below.

ANSI Standard Piping Tees

Over the past several years we have conducted rather extensive elastic-response and fatigue-to-failure tests on ANSI Standard B16.9 tees to provide experimental verification for the detailed design rules for Class 1 and Class 2 piping system tees. To date ten tees have been tested. One series of five 12-in. tees was tested under subcontract at Southwest Research Institute (SwRI) and a second series of five 24-in. tees was tested at Combustion Engineering, Inc. (CE) at Chattanooga.

Each of the ten tees was instrumented with between 225 and 240 three-gage strain rosettes located in two quadrants of the tee on both the inside and outside surfaces. Pipe extensions were welded to each of the three outlets, and each tee was tested under elastic-response conditions for 13 different loading conditions: internal pressure; six moments (in-plane, out-of-plane, and torsion on both the branch and run pipe extensions); and six direct forces (axial thrust, and in-plane and out-of-plane shear). During the elastic response tests strain-gage readings and pipe extension displacements were recorded as a function of the applied load. These data were then reduced to stresses, stress indices, and flexibility factors. Figure 7 shows a view of one of the 24 × 10 in. tee test

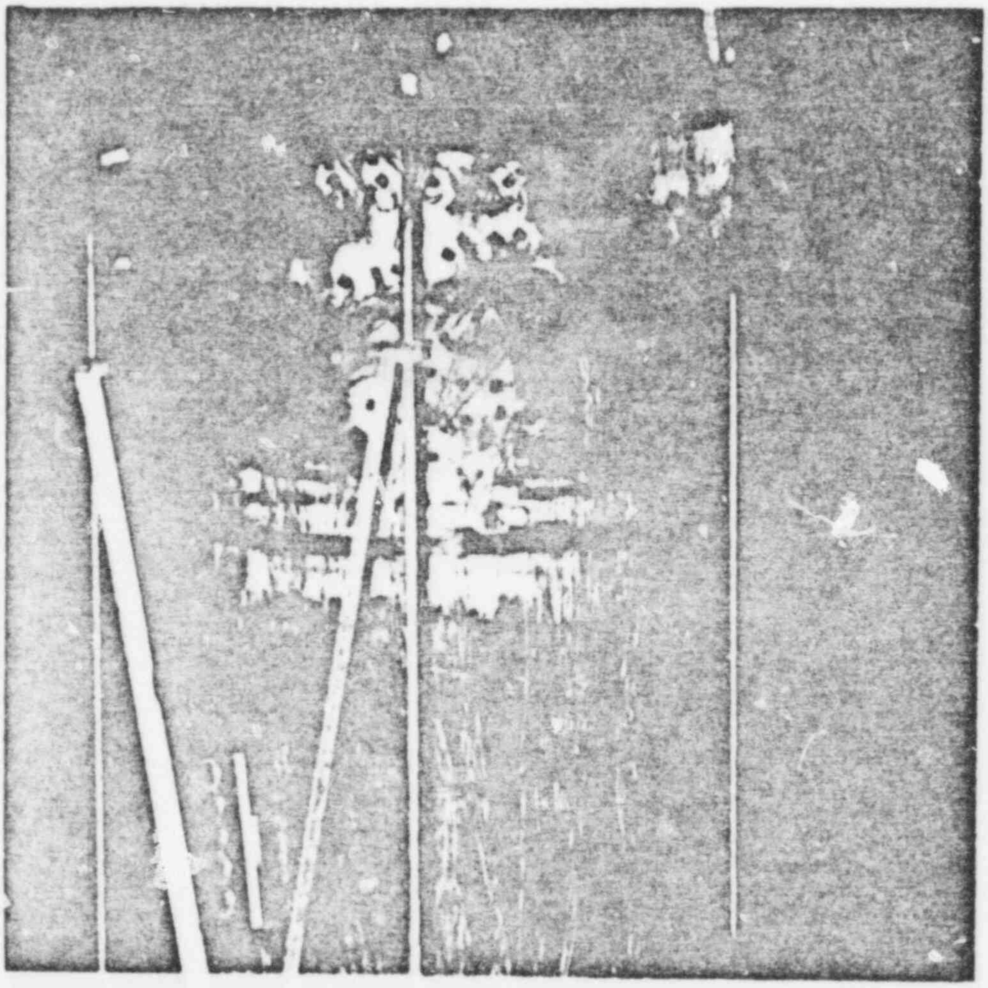

Fig. 7. View of a 24 × 10-in. ANSI B16.9 tee test assembly with strain gage and LVDT instrumentation.

assemblies with the attached strain gages and LVDT hardware for measureing the strains and displacements.

After the elastic response tests were completed each of the tees was fatigue-tested to failure with either an alternating moment load on the branch (displacement controlled) or a cyclic internal pressure. Results from the 24-in. tees tested at Combustion Engineering, Inc., have been summarized and compared with analytical predictions based on current Code rules in an ASME paper.[14] The comparisons show that, in general, the Code rules are conserva ive, but in need of minor revisions to conform better with the experimental evidence.

Summary reports which will include more complete evaluations of the experimental data from all of the tees, and proposed Code revisions based on these data are planned for next fiscal year.

Flanged Piping System Joints

A series of analytical studies on the structural behavior of flanged pipe joints[15, 16, 17] published in 1976 culminated during the past year in a number of significant changes in the ASME Code rules. In Ref. 17 we developed a complete new set of proposed design rules for flanged piping joints that use flanges, bolting, and gasket materials specified in the ANSI B16.5 (1968) standard with the added stipulation that the bolting material have a minimum design strength (S_m) of 20,000 psi at 100°F. These new rules are considerably less complicated to use than the old rules and at the same time effectively prohibit the use of the lighter weight flanges and weaker bolting material.

Early thi year the proposed new rules were accepted by the ASME Code committee for Class 1 piping and published in the Summer Addenda to the Boiler and Pressure Vessel Code. The proposed rules for Class 2 lass 3 piping, however, wer rejected. The primary objection to the proposed rules was that the requirement for stronger bolting materials and higher fit up forces would seriously effect the design of many low temperature water lines in Class 2 and 3 nuclear plant piping systems. Several options were therefore added to the proposed rules that will allow the use of current design analysis methods when they are adequate for the intended service. When current methods are not adequate for the intended service the designer will be required to specify the higher strength bolting materials and use the proposed rules. We expect ASME to adopt these modified rules for Class 2 and 3 flanged piping joints during the coming year.

Dimensional Control for Buttwelding Fittings

Early this year we completed and published a study[18] of the dimensional requirements and manufacturing practice for butt welding pipe fittings made according to the ANSI B16.9 and ANSI B16.28 standards. Fittings studied included short- and long-radius elbows, tees, concentric reducers, and pipe caps. The major conclusion of the study was that the requirements of the standards were not adequate to meet the intent of the design qualification rules of the Code for Class 1 nuclear piping, although they were probably adequate for Class 2 and 3 piping. As a result we developed a preposed supplementary standard for fittings to be used in nuclear Class 1 piping systems that required (1) additional controls and records for design qualification proof tests, (2) additional shape controls for elbows, tees, reducers, and caps, and (3) new dimensional information for fittings needed by designers to calculate numerical values for the stress indices given in the ASME Code. The proposed supplementary standard is included as an appendix in Ref. 18.

Reference 18 was approved by both PVRC and the Working Group on Piping of the ASME Code committee and referred to the Manufacturers Standards Society of the Valve and Fittings Industry, who, in turn, drafted a new standard for buttwelding fittings for nuclear Class 1 piping applications. This new standard, MSS-SP-87 (Ref. 19) incorporates essentially all the recommendations made in our report and proposed supplementary standard. In addition SP-87 requires more strict dimensional controls on wall thickness for a given nominal size fitting than was required under the ANSI standards. (We had recommended weight controls as being potentially easier, but actually prefer the wall thickness control.) MSS-SP-87 was approved by the ASME Working Group on Piping, and is expected to be published by the Manufacturers Standards Society in November.

Small Branch Connections

We also completed and published a study on flexibility factors for small, i.e., d/D < 1/3, fabricated branch connections under external moment loadings,[20] during FY-1977. The study is primarily a reevaluation of "old" information on the flexibility and displacements of piping branch connections in view of the changing needs for better piping system analyses. The report does include, however, some data which were not available when then current Code flexibility factors (NB-3687.5) were formulated in about 1969. These additional data establish quite firmly that the only significant flexibility factors for small branch connections are the two associated with bending the branch in the in-plane or out-of-plane directions. (Theoretically there could be as many as 36 flexibility factors different from zero for a branch connection or tee.)

The study shows that the two flexibility factors (k_{X3} and k_{z3}) which are currently in the Code are in reasonably good agreement with the available data, but they apparently do not properly include the effects of some types of local reinforcing. The "error" in the Code formulations would tend to underestimate the flexibility of branch connections with local reinforcing, and thus to overestimate the bending moments obtained from a piping system flexibility analysis. This error is toward the conservative side for static system behavior but could be nonconservative for dynamic system behavior. An improved formulation is presented in the report which is believed to be more accurate. Additional data, however, are needed to confirm this formulation before the new flexibility factors are presented to the Code for adoption. We expect to obtain these data from a finite element parameter study of isolated nozzles under external moment loadings to be conducted during FY-1978.

PLAN OF RESEARCH FOR FUTURE YEARS

Our plans for the near-term future (FY-1978, FY-1979) include completion and publication of twenty-four topical reports on various studies related to the structural behavior of reinforced nozzle penetrations in pressure vessels and piping system components, and the assessment and confirmation or improvement in the criteria and rules which govern the design of nuclear power plants. An important part of this work will be to complete the development of analytical tools and computer programs for calculating stresses in isolated and closely-spaced nozzles in cylindrical pressure vessels, and to conduct the needed parameter studies to support the development of improved design rules. We will also continue our close association with PVRC and the ASME Boiler and Pressure Vessel Code Committee as one of the more successful means for implementing needed changes in the Codes and Standards.

REFERENCES

1. *ASME Boiler and Pressure Vessel Code, Section III, Division I, Nuclear Power Plant Components*, American Society of Mechanical Engineers, New York, 1974.

2. J. L. Mershon and E. C. Rodabaugh, *Preliminary Evaluation of Closely Spaced Reinforced Openings in a Cylindrical Pressure Vessel Under Internal Pressure Loading*, ORNL/Sub/3131-10, June 30, 1975.

3. E. C. Rodabaugh, *Appropriate Nominal Stresses for Use with ASME Code Pressure-Loading Stress Indices for Nozzles*, ORNL/Sub/2913-2, June 1976.

4. A. N. Gantayat and G. H. Powell, *Stress Analysis of Tee Joints by the Finite Element Method*, Report UC-SESM 73-6, Structural Engineering Laboratory, University of California, Berkeley (February 1973).

5. B. R. Bass, J. W. Bryson, and S. E. Moore, "Validation of the Finite Element Stress Analysis Computer Program CORTES-SA for Analyzing Piping Tees and Pressure Vessel Nozzles," ASME Petroleum and Mechnical Engineering Conference, Houston, Texas (Sept. 18-22, 1977).

6. J. M. Corum et al., *Theoretical and Experimental Stress Analysis of ORNL Thin-Shell Cylinder-to-Cylinder Model No. 1*, ORNL-4553 (October 1972).

7. R. C. Gwaltney et al., *Theoretical and Experimental Stress Analyses of ORNL Thin-Shell Cylinder-to-Cylinder Model 3*, ORNL-5020 (June 1975).

8. S. E. Moore, R. A. Weed, and S. C. Grigory, *Experimental Stress Analysis and Fatigue Tests of Five 12-in. ANSI Standard B16.9 Tees*, ORNL/NUREG-3 (to be published).

9. J. G. Merkle et al., *Test of 6-in.-Thick Pressure Vessels. Series 4: Intermediate Test Vessels V-5 and V-9 with Inside Nozzle Corner Cracks*, ORNL/NUREG-7 (August 1977).

10. M. M. Leven, *Stress Distribution at Two Closely-Spaced Reinforced Openings in a Pressurized Cylinder*, Research Report 71-9E7-PHOTO-R1, Westinghouse Research Laboratories (April 1971).

11. J. W. Bryson, W. G. Johnson, and B. R. Bass, *Stresses in Reinforced Nozzle-Cylinder Attachments Under Internal Pressure Loading Analyzed by the Finite-Element Method — A Parameter Study*, ORNL/NUREG-4 (October 1977).

12. F. K. W. Tso et al., *Stress Analysis of Cylindrical Pressure Vessels with Closely Spaced Nozzles by the Finite-Element Method, Vol. 1. Stress Analysis of Vessels with Two Closely Spaced Nozzles Under Internal Pressure*, ORNL/NUREG-18/VI (November 1977).

13. R. M. Stone and S. Hochschild, "The Effect of Nozzle Spacing on the Pressure Stresses at the Intersection of Cylindrical Nozzles and Shells," *Trans. ASME*, Series A. pp. 360-68, July 1967.

14. J. K. Hayes and S. E. Moore, "Experimental Stress Analysis for Four 24-in. ANSI Standard B16.9 Tees," *Trans. ASME*, 99, 4, Series J, pp. 537-52, November 1977.

15. E. C. Rodabaugh, F. M. O'Hara, Jr., and S. E. Moore, *FLANGE: A Computer Program for the Analysis of Flanged Joints with Ring-Type Gaskets*, ORNL-5035, January 1976.

16. E. C. Rodabaugh and S. E. Moore, *Flanged Joints with Contact Outside the Bolt Circle — ASME Part B Design Rules*, ORNL/Sub/2913-1, Battelle-Columbus Laboratories, May 1976.

17. E. C. Rodabaugh and S. E. Moore, *Evaluation of the Bolting and Flanges of ANSI B16.5 Flanged Joints — ASME Part A Design Rules*, ORNL/Sub/2913-3, Battelle-Columbus Laboratories, September 1976.

18. E. C. Rodabaugh, S. E. Moore, and J. N. Robinson, *Dimensional Control of Butt-Welding Pipe Fittings for Nuclear Power Plants Class 1 Piping Systems*, ORNL/Sub-2913-5, Battelle-Columbus Laboratories, December 1976.

19. MSS Standard Practice SP-87, 1977 edition, "Factory-Made Butt-Welding Fittings for Class 1 Nuclear Piping Applications," Manufacturers Standardization Society of the Valve and Fittings Industry, Inc., November 1977.

20. E. C. Rodabaugh and S. E. Moore, *Flexibility Factors for Small (d/D < 1/3) Branch Connections with External Loadings*, ORNL/Sub/2913-6, Battelle-Columbus Laboratories, March 1977.